Journal of African Earth Sciences 61 (2011) 167–232

Contents lists available at SciVerse ScienceDirect

Journal of African Earth Sciences

journal homepage: www.elsevier.com/locate/jafrearsci

Late Cryogenian–Ediacaran history of the Arabian–Nubian Shield: A review of depositional, plutonic, structural, and tectonic events in the closing stages of the northern East African Orogen

P.R. Johnson [a,*], A. Andresen [b], A.S. Collins [c], A.R. Fowler [d], H. Fritz [e], W. Ghebreab [f], T. Kusky [g], R.J. Stern [h]

[a] 6016 SW Haines Street, Portland, OR 97219, USA
[b] Department of Geosciences, University of Oslo, P.O. Box 1047, Blindern 0316, Oslo, Norway
[c] Tectonics Resources and Exploration (TRaX), Geology and Geophysics, School of Earth and Environmental Sciences, The University of Adelaide, Adelaide, SA 5005, Australia
[d] Geology Department, Faculty of Sciences, United Arab Emirates University, P.O. Box 17551, Al-Ain, Abu Dhabi, United Arab Emirates
[e] Department of Earth Sciences, University of Graz, Heinrichstraße 26, A-8010 Graz, Austria
[f] Columbus State Community College, Department of Physical Sciences NH425, 550 East Spring Street, Columbus, OH 43215, USA
[g] State Key Laboratory of Geological Processes and Mineral Resources, Three Gorges Research Center for Geohazards, China University of Geosciences, Wuhan, China
[h] Geosciences Department, University of Texas at Dallas, Richardson, TX 75080-0688, USA

ARTICLE INFO

Article history:
Received 15 February 2011
Received in revised form 1 July 2011
Accepted 9 July 2011
Available online 23 July 2011

Keywords:
Arabian–Nubian Shield
Cryogenian
Ediacaran
Tectonics
Magmatism
Deposition

ABSTRACT

During the late Cryogenian–Ediacaran (650–542 Ma), the Arabian–Nubian Shield (ANS) underwent final assembly and accretion to the Saharan Metacraton concurrent with the assembly of eastern and western Gondwana. At the end of the Precambrian it lay at one end of the East African Orogen, with its northern margin (present coordinates) forming a low-relief stable shelf facing an open ocean; to the south the ANS transitioned into the Mozambique Belt. The geologic history of the ANS during this period provides insight into the closing developmental stages of one of the world's largest accretionary orogens. Following a 680–640 Ma orogenic event reflecting amalgamation of a core grouping of island-arc terranes (the proto-Arabian–Nubian Shield; pANS), the region underwent extensive exhumation, erosion, and subsidence. Depositional basins formed in the northern and eastern pANS, with those in the east below sea level and connected to an ocean. Periodic basin closure and formation of new basins in other parts of the ANS followed. Many basins were filled by terrestrial, molasse-type sediments interfingering with subordinate to predominant amounts of volcanic rocks. Magmatism was extensive throughout the period, initially characterized by tonalite–trondhjemite–granodiorite (TTG) and granite (monzogranite, syenogranite), but also characterized, from ~610 Ma on, by increasing amounts of alkali-feldspar granite and alkali granite. The plutons are largely undeformed, except where cut by brittle–ductile shear zones. The magma sources of the late Cryogenian–Ediacaran granitoids were dominated by juvenile crust and(or) depleted mantle and magmas mostly originated in anorogenic, post-collisional, commonly extensional, settings. They were derived by melting and fractionation of anhydrous high-grade metamorphosed lower crust, mafic- to intermediate calc-alkaline crust, and(or) subduction-modified mantle wedges associated with slab break-off or delamination.

By ~630 Ma, the region was affected by oblique (transpressional) convergence of continental blocks that formed eastern and western Gondwana—the pANS was approaching the Saharan Metacraton; north-trending shear and shortening zones developed in the southern ANS; and northwest-trending strike-slip shear zones of the Najd fault system dominated farther north. In the northwestern ANS, convergence and Najd transpression buckled the crust causing structural highs with domes of gneissic infracrust overlain by supracrust composed of ophiolitic and volcanosedimentary assemblages dating from the Tonian–middle Cryogenian period of island-arc activity. The supracrust was extensively translated to the northwest above a high-strain zone. Extension and tectonic escape augmented exhumation of the gneissic infracrust particularly between ~620–580 Ma. In the northeastern ANS, linear belts of gneiss formed from reworked older intrusive bodies or syntectonic intrusions that were emplaced along Najd faults. By ~620 Ma a marine basin on the eastern margin of the pANS (present coordinates) was beginning to close. A thick sedimentary assemblage (Abt formation) in this basin underwent metamorphism and folding, and subduction-related magmatism and volcanism farther into this basin (Al Amar arc; >690–615 Ma) was coming to an end. Amalgamation of the Abt formation, Al Amar arc, and the pANS

* Corresponding author.
E-mail address: petergeo@earthlink.net (P.R. Johnson).

doi:10.1016/j.jafrearsci.2011.07.003

occurred between ~620 and ~605 Ma, and terminal collision between the pANS and the Saharan Metacraton was complete by ~580 Ma. At this time, the ANS was fully assembled. Granite magmatism continued until ~565–560 Ma and orogeny ceased by ~550 Ma. During these terminal events, the region underwent strong chemical weathering and became a vast low-relief surface on which Lower Paleozoic sandstone was eventually deposited.

1. Introduction and geologic setting

This paper reviews the closing 100 million years of crustal growth in the Arabian–Nubian Shield (ANS), covering the period between 650 Ma and 542 Ma, and describes the late Cryogenian–Ediacaran depositional, structural, metamorphic, intrusive, and mineralization events involved in the final stages of the development of the northern part of the East African Orogen (EAO). The ANS is a collage of Neoproterozoic juvenile arcs, younger sedimentary and volcanic basins, voluminous granitoid intrusions, and enclaves of pre-Neoproterozoic crust that crop out in the western Arabian Plate and the northeastern African Plate (Fig. 1) at the northern end of the EAO (Stern, 1994; Kusky et al., 2003; Johnson and Woldehaimanot, 2003) (Fig. 2). Differences in the orientation of structural trends divide the shield into southern and northern parts. Prior to Red Sea-Gulf of Aden opening (beginning ~25 Ma), the Arabian and Nubian Shields were conjoined as one of the largest tracts of juvenile Neoproterozoic crust on Earth. The review period is bracketed by (1) the Tonian–middle Cryogenian development and amalgamation of island-arc terranes to form the core of what is now the ANS, and (2) the end-Precambrian conversion of the ANS into stable shield and its superimposition by a vast Lower Paleozoic siliciclastic blanket deposited above a regional unconformity developed on the newly created shield.

In a larger context, the events reviewed here are part of an orogenic cycle extending from the breakup of Rodinia (870–800 Ma) (Li et al., 2007) to the final amalgamation of Gondwana (Fig. 3) in the Cambrian (Li and Powell, 1993; Collins and Pisarevsky, 2005; Pisarevsky et al., 2008). Topics considered include: (1) the deposition of volcanosedimentary sequences in post-amalgamation basins unconformable on newly amalgamated island-arc rocks; (2) the emplacement of large volumes of granitic rock in the newly amalgamated island-arc terranes and the post-amalgamation basins; (3) the effects of transpression, transtension, uplift, and exhumation associated with orogenic collapse and tectonic escape, reflecting an interplay between compression and extension related to far-field movements of crustal blocks involved in the coalescence of Gondwana; and (4) periods of major erosion. Many of the late Cryogenian–Ediacaran events in this cycle have been individually described and interpreted in the geologic literature. Our aim in this contribution is to present an integrated geologic history, describing interrelated features during an important tectonic period in Earth history.

During the late Cryogenian and Ediacaran, the Earth was affected by major climatic changes evidenced by glaciation and isotopic excursions (Hoffman et al., 1998; Halverson et al., 2010; Fike et al., 2006; Hurtgen et al., 2006). It underwent a dramatic development of multicellular organisms augmenting a biosphere that, until the Ediacaran, was dominated by single-celled organisms best preserved as stromatolites, and it witnessed the growth of the longest-lived supercontinent of all time–Gondwana—that resulted from the assembly of crustal blocks derived from the earlier break-up of the Rodinia supercontinent and other independent continental blocks and the closure of the Mozambique and other oceans (Meert, 2002; Boger and Miller, 2004; Collins and Pisarevsky, 2005; Li et al., 2007; Meert and Lieberman, 2008; Pisarevsky et al., 2008). The ANS is a key part of this larger history having originated by subduction and island-arc development in the Mozambique Ocean, and ending as part of an orogenic belt caught up between converging Gondwanan blocks.

1.1. East African Orogen and the margins of ANS

The EAO (Stern, 1994; Kusky et al., 2003) (Fig. 2) consists of deformed and metamorphosed rocks of the ANS in the north and higher grade and more strongly deformed rocks of East Africa and Madagascar in the south. A southern continuation, through Mozambique into Antarctica, proposed by Jacobs and Thomas (2004), was challenged by Collins and Pisarevsky (2005). Here we use the original definition of the orogen and limit its southern extent to the northern Mozambique/Madagascar region where a western arm links with the Zambezi Belt (Johnson et al., 2005) and an eastern arm heads through southern India and Sri Lanka to enter East Antarctica in the region of Lutzow-Holm Bay (Collins and Pisarevsky, 2005). The geology of the East African part of the EAO is the subject of a forthcoming review by Fritz and colleagues.

The EAO is an extensive Neoproterozoic accretionary orogen and collisional zone within Gondwana (Stern, 1994; Collins and Windley, 2002; Cawood et al., 2009). Following the determination of a U–Pb age of 652 ± 10 Ma for zircons in garnet-bearing two-pyroxene granulite in Tanzania (Coolen et al., 1982), it was realized that high-grade metamorphism in East Africa was a Neoproterozoic, not an older event, despite the Mesoproterozoic to Archean protolith ages of some of the rocks caught up in the orogen (see geochronologic reviews by Möller et al. (1998), and Tenczer et al. (2006)). Greenwood et al. (1980) extended the Mozambique Belt northward into the ANS and Berhe (1990) described ANS-type ophiolite-decorated north-trending shear zones extending S into central Kenya, confirming that the Mozambique Belt and the Arabian–Nubian Shield are correlatives. Profound differences in lithology, structure, metamorphic grade, and tectonic history make detailed correlation challenging and intervening cover interrupts direct continuity. However, the link between the two regions is evidenced between southern Ethiopia and southern Kenya (Fig. 2). In southern Ethiopia, low-grade Neoproterozoic basement rocks of the Arabian–Nubian Shield structurally overly high-grade granitic migmatite of the Mozambique Belt (Yihunie and Tesfaye, 2002). Similar juxtaposition of high- and low-grade rocks is found in the Bulbul Belt, southern Ethiopia as a SE-dipping, top-to-the-SE, low-angle shear zone that developed during regional gravitational tectonic collapse (Tsige and Abdelsalam, 2005). In southern Kenya Neoproterozoic volcanic and sedimentary rocks occur between prominent ophiolite-decorated shear zones. The northwest-trending sinistral Aswa shear zone in the west contains the Seker ophiolite; the north-trending dextral Barsaloi shear zone in the center contains the Barsaloi ophiolite; and the curved, north-trending dextral Mutito shear zone in the east, contains the Moyale ophiolite.

In contrast to the ANS, the orogen in East Africa and Madagascar includes large amounts of Archean to Mesoproterozoic rocks that were reworked during Neoproterozoic metamorphism and anatexis, as well as subordinate amounts of juvenile Neoproterozoic igneous rocks. End-Precambrian extension and exhumation was intense in the S and the EAO exposures in East Africa are commonly

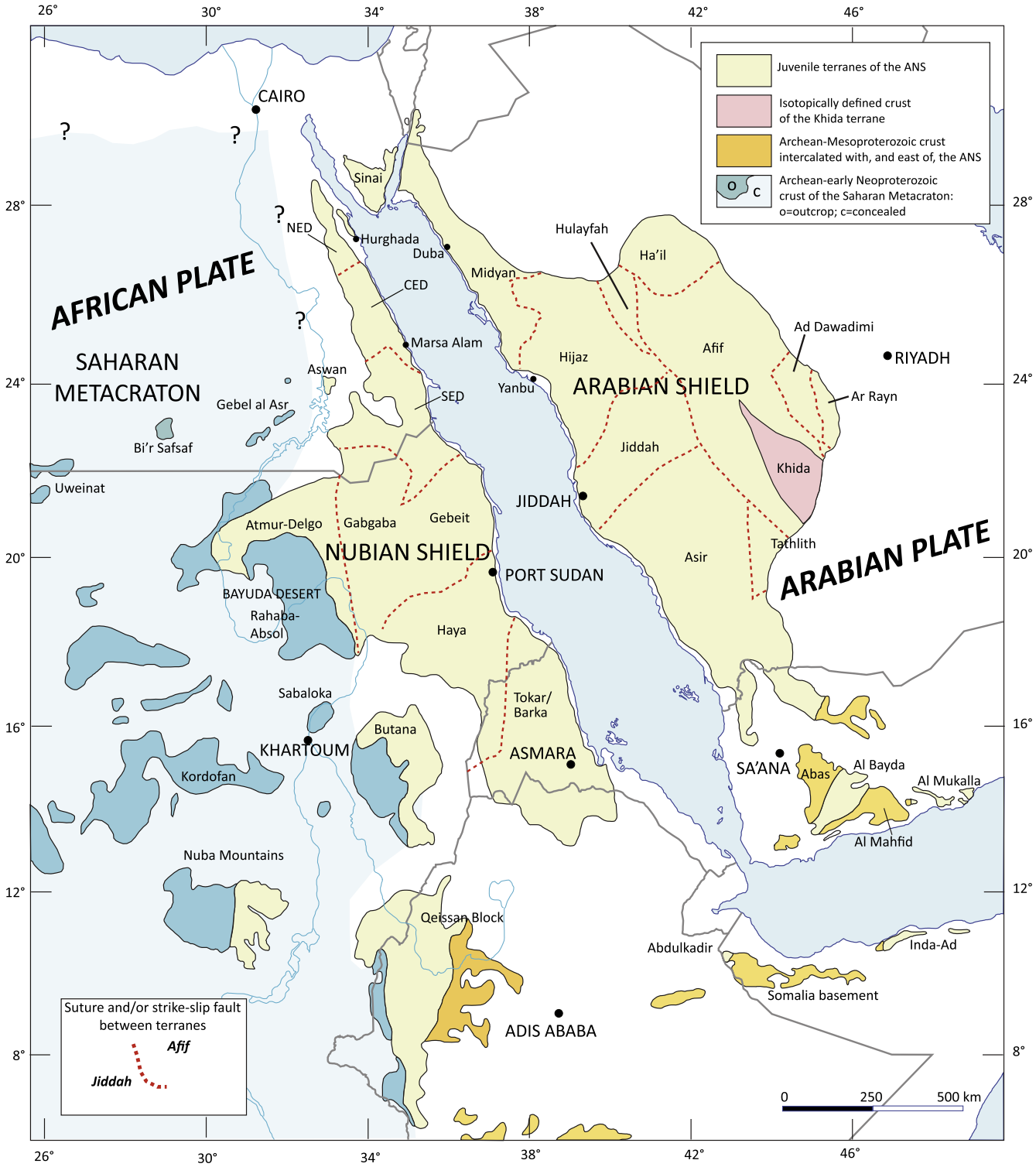

Fig. 1. The Arabian–Nubian Shield (ANS), showing its relationship to adjacent areas of older continental crust. The border with the Saharan Metacraton, on the west, is the effective contact between ANS and West Gondwana: a border, on the east, with putative East Gondwanan crust, is not certain. NED = North Eastern Desert; CED = Central Eastern Desert; SED = South Eastern Desert. In this and other figures, Tokar/Barka is a composite term for terranes in Eritrea (see Drury and de Souza Filho, 1998).

amphibolite- and granulite-facies schists and gneisses in contrast to the greenschist-facies rocks prevalent in the ANS, implying greater uplift and erosion southward. Another difference is that orogeny persisted longer in the south than in the north and continued into the early Cambrian (Bingen et al., 2009). Nonetheless, both regions are parts of a common orogenic belt affected by periods of E–W directed shortening generated by the closure of the Mozambique Ocean and the ultimate collision of Neoproterozoic India with the Congo–Tanzania–Bangweulu Block (in the south) and the Sahara Metacraton (in the north). The entire orogen remained intact until the dispersal of Gondwana in the Early to Middle Jurassic, and is now represented by fragments of Neoproterozoic–Cambrian deformed and metamorphosed rocks preserved in the Arabian, African, Madagascan, and Indian Plates.

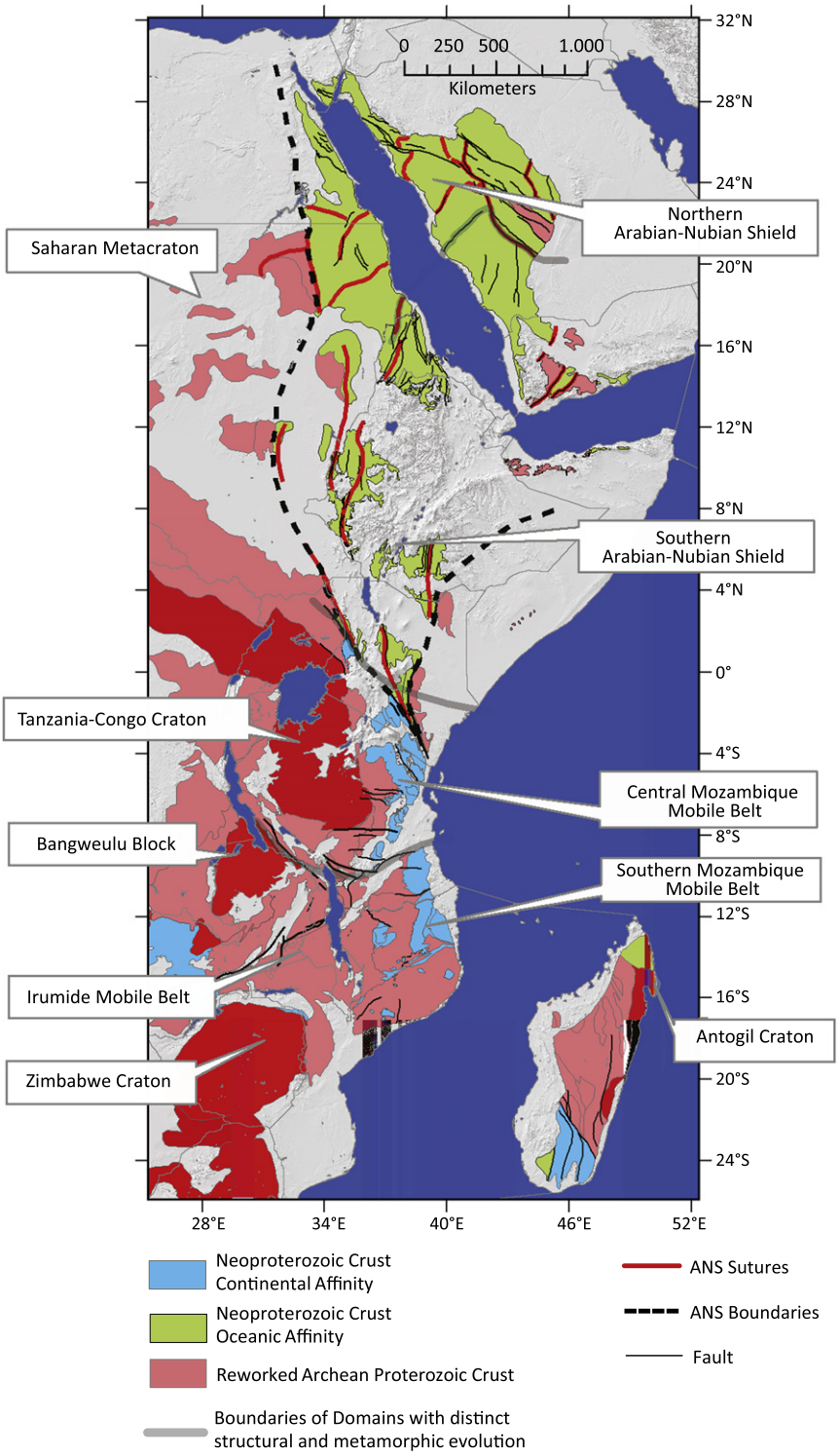

Fig. 2. The Arabian–Nubian Shield in relation to East Africa as component parts of the East African Orogen. Although the Arabian–Nubian Shield extends as far south as southern Kenya, the geographic focus of this review is on the ANS between northern Ethiopia and Sinai and Jordan.

Contemporary Neoproterozoic orogenic belts were present in other parts of greater Gondwana at the end of the Precambrian as the result of similar events of crustal accretion (e.g., Grunow, 1999; Abdelsalam et al., 2003; Collins and Pisarevsky, 2005; Brito Neves and Cordani, 1991).

For the purpose of this review, the margins of the ANS are defined as the limits of Neoproterozoic juvenile rocks of the type exposed on the Shield. The western margin is reasonably well delineated in northern Sudan (Figs. 1 and 2) where >900 Ma biotite–muscovite gneiss, biotite–garnet schist, and mica schist, amphibolite, and hornblende gneiss are overthrust from the north and east by low-grade rocks of ANS affinity belonging to the Atmur–Delgo belt exposed in the Rahaba–Absol terrane (Schandelmeier et al., 1994; Harms et al., 1994; Abdelsalam et al., 1995, 1998, 2002), and by 800–900 Ma high-grade metamorphic rocks in the east (Küster and Liégeois, 2001; Küster et al., 2008).

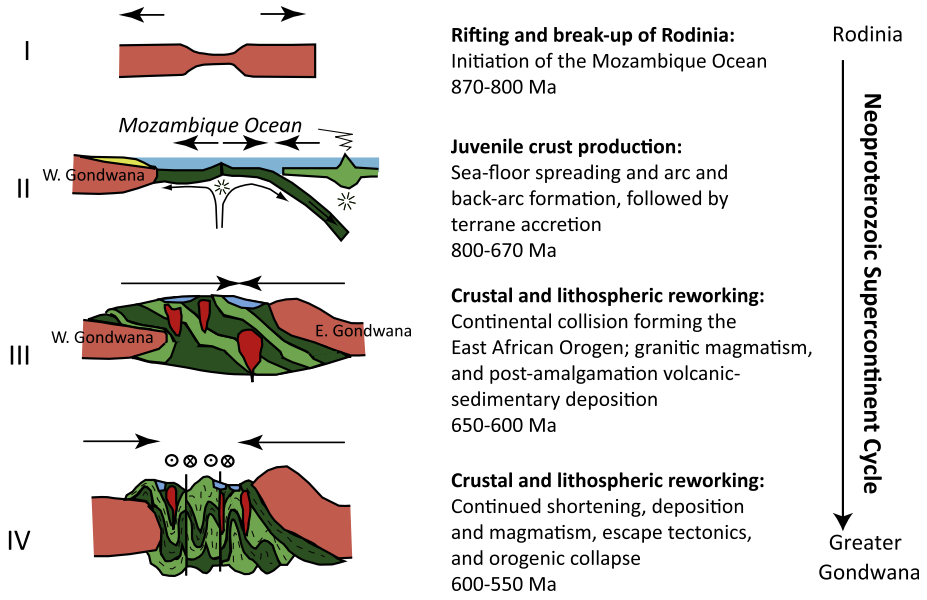

Fig. 3. Schematic illustration of stages in the development of ANS showing its setting in the supercontinent cycle bracketed by the break-up of Rodinia and the assembly of Gondwana. After Stern and Johnson (2010).

Deformation and nappe emplacement along the Atmur–Delgo belt were completed before 700 Ma (Abdelsalam et al., 1995). The Keraf suture, a north-trending belt of deformation at the eastern margin of the Bayuda Desert coincident with the contact between the ANS and the Saharan Metacraton was active between 640 and 560 Ma (Abdelsalam et al., 1998; Bailo et al., 2003). The contact is inferred to extend north into the area immediately west of the Ediacaran granites of Aswan and farther north into the area west of the Eastern Desert of Egypt.

The eastern margin of the ANS is much more ambiguous. Contacts between ~1820 and ~1400 Ma metasedimentary and metaplutonic rocks and younger Neoproterozoic supracrustal deposits (Inda-Ad and Abdulkadir complexes) are exposed in northern Somalia (Kröner and Sassi, 1996), but Neoproterozoic rocks extend across northern Somalia as far as the Indian Ocean and there is no sign of a limit to the ANS. The contact region in Yemen comprises structurally juxtaposed low-grade island-arc Neoproterozoic terranes (Al Bayda and Al Mukalla) and gneissic terranes (Abas and Al Mahfid). The gneissic terranes yield negative initial ε_{Nd} (−5.0 to −39.8), and have late Archean Nd model ages (~2.7–3.0 Ga) and U–Pb ion-microprobe zircon-core ages as old as 2.5 Ga indicating Archean–Paleoproterozoic origins, but were reworked during the Neoproterozoic (Whitehouse et al., 1998, 2001; Windley et al., 1996). The region is interpreted as an alternation of early Precambrian gneissic domains and Neoproterozoic island-arc domains that coalesced to form an arc-gneiss collage contemporaneous with accretionary events in the main part of the ANS.

Paleoproterozoic rocks also crop out in the Khida terrane (Stacey and Agar, 1985; Stoeser and Stacey, 1988; Stoeser et al., 2001), part of the Afif composite terrane, at the eastern margin of the Arabian Shield in Saudi Arabia. The Khida terrane was defined originally on the basis of evolved lead isotopes indicating a component of old continental lead in contrast to juvenile oceanic lead obtained from feldspar and galena samples elsewhere in the Arabian Shield (Stacey et al., 1980; Stoeser and Stacey, 1988) and on the basis of a U–Pb age of 1628 ± 200 Ma (Stacey and Hedge, 1984: Sample Z-103). The age of Z-103 has since been demonstrated to be 750 Ma (Whitehouse et al., 2001), but intact Paleoproterozoic rock has been discovered in adjacent exposures (Whitehouse et al., 2001; Stoeser et al., 2001) and the areal extent of evolved Pb isotopes has been increased (Fig. 4). Most exposed rocks in the Khida terrane are Cryogenian arc assemblages and late Cryogenian to Ediacaran granites, in terms of their crystallization ages, but their negative initial ε_{Nd}, Paleoproterozoic Nd model ages, and evolved Sr and O isotopic signatures (Whitehouse et al., 2001; Stoeser and Frost, 2006) imply the presence of older continental material in the subsurface. Similarities exist between the Khida terrane and the continental terranes in Yemen (Windley et al., 1996; Whitehouse et al., 1998, 2001) and Stoeser and Frost (2006) propose that the Khida terrane is the northwesternmost portion of an "Arabian Craton" underlying the central and southern part of the Arabian Peninsula that was part of the East Gondwana continent. Collins and Pisarevsky (2005) and Raharimahefa and Kusky (2006) treat the same rocks as part of a belt of Archean and Paleoproterozoic crust referred to as "Azania" extending along the eastern margin of the East African Orogen between Madagascar and Arabia. The character of the Arabian Plate basement farther east is uncertain because of Phanerozoic cover as much as 14 km thick. A crustal boundary mapped on the basis of magnetic and gravity data extends north from the Ar Rayn and Ad Dawadimi terranes through central and northern Arabia (Johnson and Stewart, 1995; Sharland et al., 2001; Stern and Johnson, 2010). The crust east of this boundary—the Rayn microplate of Al-Husseini (2000)—contains magnetic highs suggesting the presence of buried arc terranes (Johnson and Stewart, 1995) but the age of the crust and whether it is an extension of the ANS or a crustal block of different provenance are not currently known. Crystalline basement farther east in Oman contains juvenile Neoproterozoic plutonic, metamorphic, and sedimentary rocks similar to those of the ANS, although the timing of magmatism and sedimentation suggests that the Oman crust has a different history to the ANS. Stern and Johnson (2010) reviewed available rock ages and detrital zircons from the Huqf Group to conclude that the crust beneath the Arabian Platform was Cryogenian.

There is evidence from Sinai that ~1 Ga crust flanks the ANS to the north, although actual rock of this age has not yet been identified. Be'eri-Shlevin et al. (2009a) reported abundant 1.0 Ga detrital zircons from Sa'al Group metasedimentary rocks, and concluded that crust of this age must be nearby. Stern et al. (2010a) found that the Zaghra conglomerate contained concordant zircons with

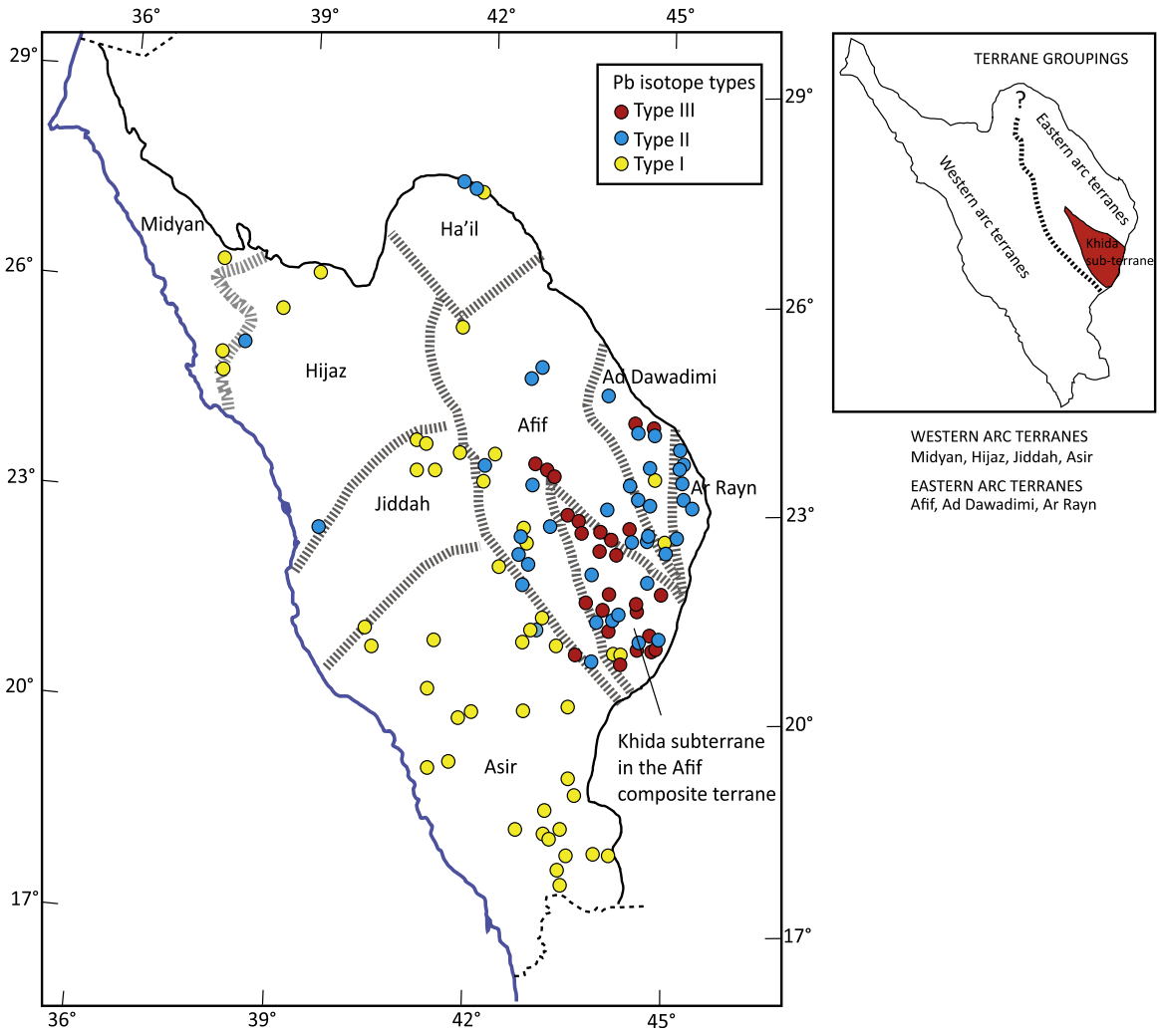

Fig. 4. Distribution of Pb isotope types in the Arabian Shield in Saudi Arabia (after Stoeser and Frost (2006) and Hargrove et al. (2006)), showing a tripartite division of the Arabian Shield into: (1) western intraoceanic juvenile arcs; (2) eastern arcs with continental contributions; and (3) the Khida terrane with highly evolved Pb isotopes indicating a significant contribution from older basement.

two groups of $^{206}Pb/^{238}U$ ages: 931 ± 14 Ma and 606 ± 10 Ma, and plotted a U–Pb discordia for the Zaghra metaconglomerate that has an upper intercept of 1045 ± 55 Ma and lower intercept of 569 ± 55 Ma. Bea et al. (2009), furthermore, found three zircon grains in the 844 Ma Abu Moneiga quartz diorite, located within the Katherine ring-complex in central Sinai, that have inherited cores of 1045 ± 13 Ma, 1046 ± 13 Ma, and 1025 ± 13 Ma, implying that the magmatic source of the Moneiga quartz-diorites involved ~1045 Ma to ~1025 Ma rocks. In this context it is interesting that Nd–Sr–Hf–O isotope data confirm that early crustal evolution in Sinai involved some crustal contamination by pre-ANS material (Be'eri-Shlevin et al., 2010). Isotopic provinciality is shown by post-collisional calc-alkaline and alkaline igneous rocks for ~635–570 Ma across Sinai, with silicic rocks in the northwest having lower $\varepsilon_{Nd}(T)$–$\varepsilon_{Hf}(T)$ and higher Sr_i and $\delta^{18}O$ than those to the southwest.

1.2. Pre-650 Ma arc-magmatism and terranes

Most pre-650 Ma rocks in the ANS are parts of Tonian–middle Cryogenian island-arc terranes (Fig. 5A) that developed in the Mozambique Ocean between rifted blocks of the Rodinia supercontinent and other cratons (Stoeser and Camp, 1985; Genna et al., 2002; Johnson and Woldehaimanot, 2003; Stoeser and Frost, 2006). They typically have crystallization ages close to their Nd model ages, and constitute juvenile additions to the crust (Stern, 2002). The terranes converged and amalgamated as a result of intraoceanic subduction-driven arc–arc and ultimately arc–continent collisions. Most terrane boundaries are high-strain shear zones that commonly contain dismembered ophiolites (Berhe, 1990) and refolded recumbent folds. The shear zones are widely interpreted as sutures that formed at the time of terrane amalgamation, although identification of the shears zones as sutures has been challenged (Church, 1991) and some shear zones are younger strike-slip shear zones that modified or reworked original sutures (e.g., Kusky and Matsah, 2003).

The oldest Neoproterozoic crust is in the Tokar/Barka–Asir terrane (the hyphen here indicating correlation across the Red Sea), the Jiddah–Haya terrane, and the Hijaz–Gebeit terrane. Although the crust in Eritrea is divided by many workers into many individually named domains (Drury and De Souza Filho, 1998), the composite term "Tokar/Barka terrane" is used here for convenience. The terranes converged and amalgamated during the middle Cryogenian along the Barka and Bir' Umq–Nakasib sutures (780–750 Ma) (Fig. 5B), resulting in a core grouping of terranes. By 700 Ma, the Midyan–Eastern Desert terrane had collided and amalgamated with the core group of terranes along the Yanbu and Sol Hamid–Allaqi–Heiani sutures, comprising a geologic entity

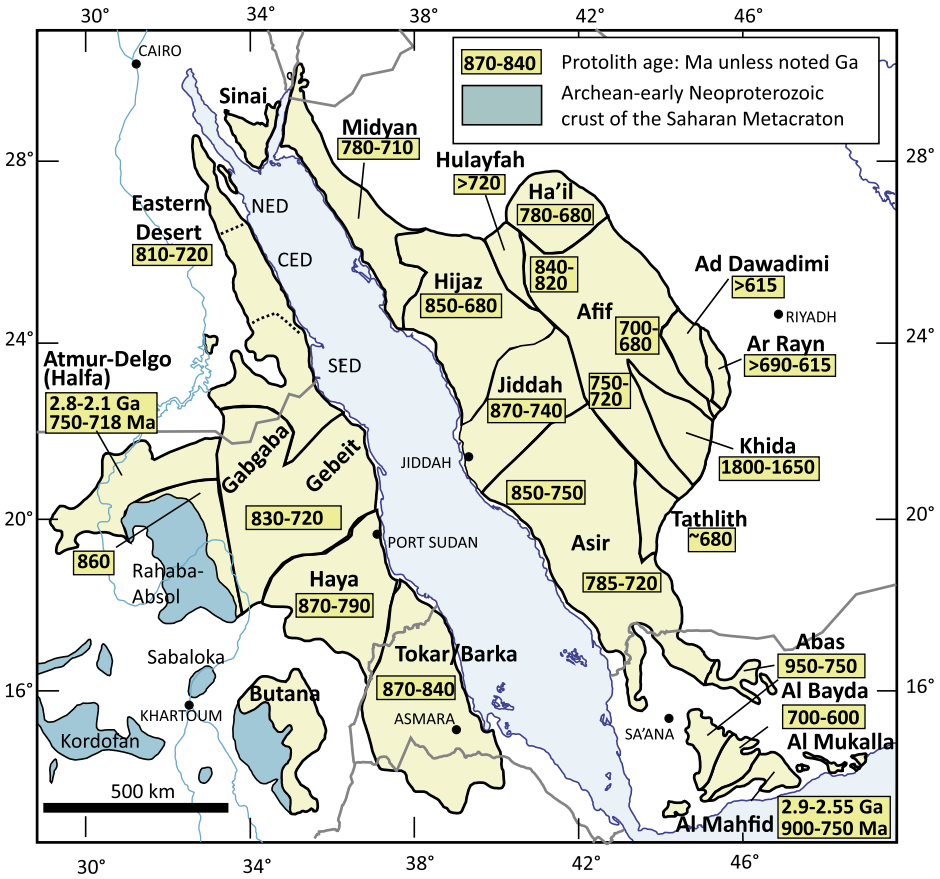

Fig. 5A. ANS tectonostratigraphic terranes, showing protolith ages. NED = North Eastern Desert; CED = Central Eastern Desert; SED = Southern Eastern Desert.

commonly referred to as the "western arc or oceanic terranes" of the ANS (e.g., Stoeser and Frost, 2006).

The Sol Hamid–Allaqi–Heiani suture (Stern et al., 1989; Stern, 1994; Abdelsalam and Stern, 1996) separates the South Eastern Desert (SED) (Gerf) terrane on the north (Kröner et al., 1987; Greiling et al., 1994; Shackleton, 1994; Abdelsalam and Stern, 1996; Kusky and Ramadan, 2002) from the 830–700 Ma Gebeit and Gabgaga terranes on the south. It strikes roughly east, but swings to the south in its middle section as it merges with and is overprinted by the NNE-trending Hamisana shear zone (de Wall et al., 2001). Relatively high-grade gneissic rocks of the SED terrane are interpreted as island-arc and ophiolitic nappes uplifted as they were thrust south over the Gebeit and Gabgaba terranes (Greiling et al., 1994; Kusky and Ramadan, 2002). The Gabgaba terrane contains an island arc assemblage (El-Nisr, 1997), including metavolcanic rocks and bands of marble, interpreted as deformed shallow-water carbonates that originally fringed the arc volcanics (Greiling et al., 1994).

The core group of ANS terranes subsequently collided and amalgamated between about 680 Ma and 640 Ma with the Afif and Tathlith terranes, creating a neocontinental crustal block referred to here as the proto-Arabian–Nubian Shield (pANS). The 680–640 Ma assembly of the pANS was associated with metamorphic, deformational, and intrusive events that, in the Arabian Shield, are referred to as the "Nabitah orogeny" (680–640 Ma) (Stoeser and Stacey, 1988). The orogeny is named after the Nabitah fault, the suture between the Asir and Tathlith terranes and a ductile shear zone within the Asir terrane. The fault gives its name to the Nabitah mobile belt (Stoeser and Stacey, 1988) (Fig. 5B), a broad zone of deformation and metamorphism that trends N–S across the Arabian Shield. The mobile belt encompasses the suture between the Afif terrane and western oceanic terranes and the suture between the Asir and Tathlith terranes. The Afif terrane is a composite tectonostratigraphic unit comprising the Paleoproterozoic Khida terrane (or subterrane) and three Neoproterozoic arc assemblages of about 840–820 Ma, 750–720 Ma, and 700–680 Ma (Fig. 5A). The Afif terrane and the western oceanic terranes were fully amalgamated by about 640 Ma. The youngest terranes in the ANS, with upper Cryogenian to Ediacaran protoliths, are the Ad Dawadimi and Ar Rayn terranes in the easternmost Arabian Shield. The history of these terranes is not fully established but is critical to our understanding of the tectonic evolution of the ANS (Cox et al., 2011) and is further described below. A suturing event along the eastern margin of the Afif terrane is marked by formation of the Halaban ophiolite at ~680–670 Ma (Al-Saleh et al., 1998). However, deposition of the Abt group, which makes up most of the Ad Dawadimi terrane, continued until ~620 Ma, when it was metamorphosed to greenschist and lower amphibolite facies (Cox et al., 2011) and when the Ad Dawadimi and Ar Rayn terranes amalgamated with the western oceanic terranes. This event was broadly contemporary with accretion of the entire ANS to the East Saharan craton along the arc–continent Keraf suture (~650–560 Ma) (Abdelsalam et al., 1998; Bailo et al., 2003), a sinistral transpressional suturing event that was one of the principal tectonic elements in the final assembly of Gondwana. The accretion of the ANS to the Saharan Metacraton is analogous to the proposed ~650–630 Ma collision of Azania with the East African margin in the southern Mozambique Belt (Collins and Windley, 2002; Collins and Pisarevsky, 2005; Collins, 2006; Collins et al., 2010). Collins and

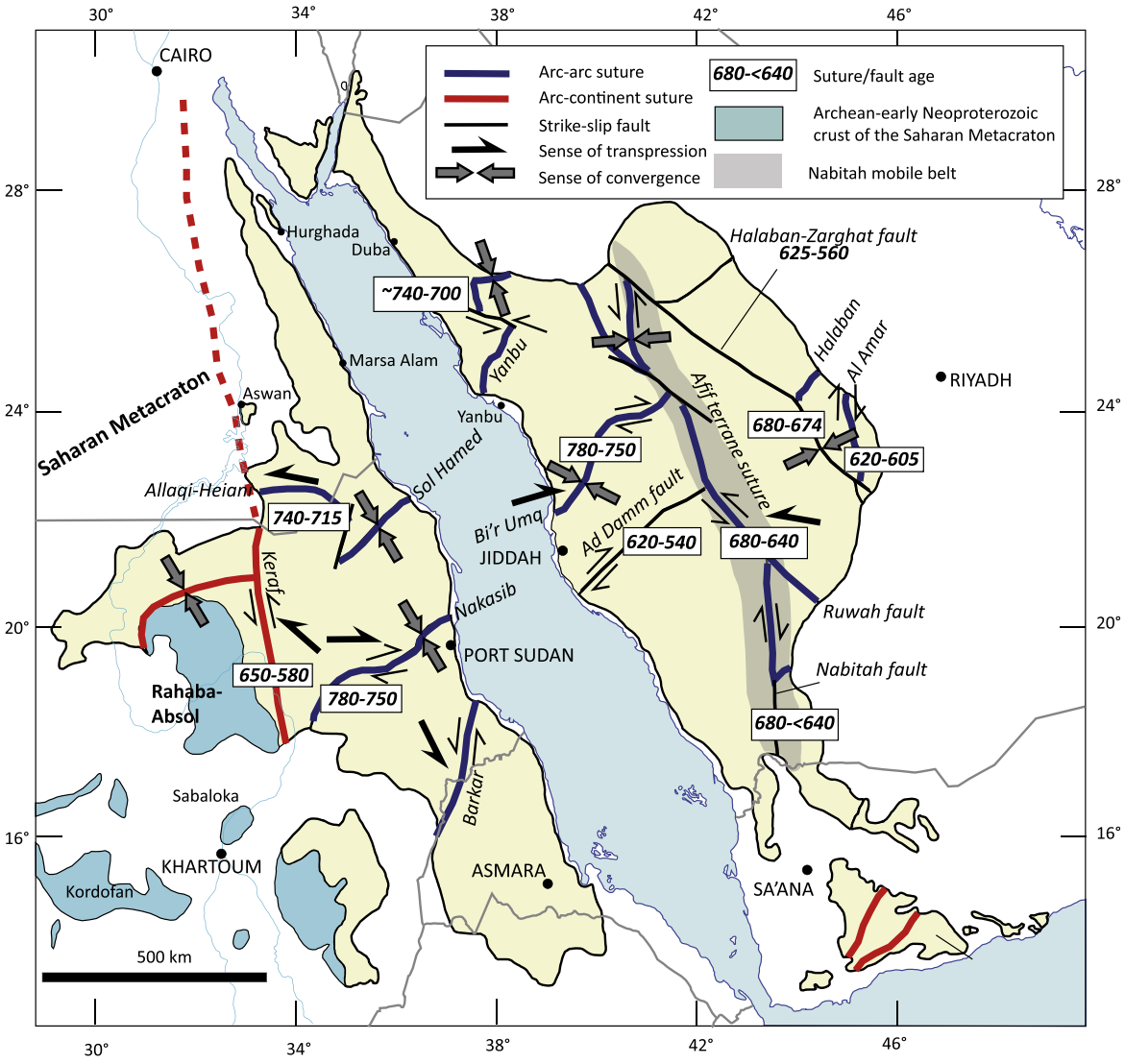

Fig. 5B. Terrane assembly in the ANS showing inferred ages of suturing and fault movements, and trajectories of amalgamation.

Pisarevsky (2005) suggested that the term the "East African Orogeny" be restricted to this event.

Terranes in the southern part of the ANS are widely disrupted by north-trending shears and shortening zones (Abdelsalam and Stern, 1996). Farther north, terranes are disrupted by northwest-trending shears belonging to the Najd fault system, although the amount of displacement and extent of deformation associated with the Najd system is controversial (e.g., Sultan et al., 1988; Andre, 1989; Sengör and Natalin, 1996; Smith et al., 1998; Kusky and Matsah, 2000, 2003; Johnson et al., 2004).

2. Late Cryogenian–Ediacaran geochronologic data base

The timing of 650–542 Ma events in the ANS is constrained by an extensive U–Pb, Pb–Pb, Rb–Sr, and Sm–Nd geochronologic database (Appendix A). The locations of the samples dated are plotted on Fig. 6. There are, of course, many age dates in the ANS for the period >650 Ma, but they are not shown on this figure because they are outside the time frame of our review (see Johnson and Kattan, 2007 for data about the Arabian Penninsula and Stern et al., 2010b for information about U–Pb and Pb–Pb ages in both the Arabian and Nubian Shields). $^{40}Ar/^{39}Ar$ measurements are not as numerous, but the results provide important constraints on metamorphic and exhumation events; they are separately listed in Table 1.

A frequency histogram of robust crystallization ages (Fig. 7A) shows peaks suggesting surges in magmatic activity in the ANS at 635 Ma, 610 Ma, 600 Ma, and 580 Ma. Bias must be taken into account when interpreting this histogram since most geochronologic data in the ANS have been obtained from granitoids, and somewhat different plots result from dividing the data according to broad rock type (Fig. 7B–E). Extrusive volcanic rocks in the ANS are commonly difficult to date because they yield fewer zircons than intrusive rocks: in addition, they contain more xenocrystic zircons (Stern et al., 2010b). As a consequence, ANS volcanic events are not as well constrained as intrusive events.

The growing number of ion microprobe zircon ages in the ANS has revealed that a small, but significant, number of ANS igneous rocks contain zircons that are significantly older than the crystallization ages of the host rocks (Küster et al., 2008; Be'eri-Shlevin et al., 2009c; Stern et al., 2010b). Inheritance in the Arabian Shield was first indicated by a report of zircons dating 1986 ± 200 Ma (Calvez et al., 1985) in Neoproterozoic plagiogranite immediately west of the Al Amar fault. A recent compilation (Stern et al., 2010b) shows that about 5% of individually dated zircons from ANS Neoproterozoic igneous rocks have ages older than 880 Ma,

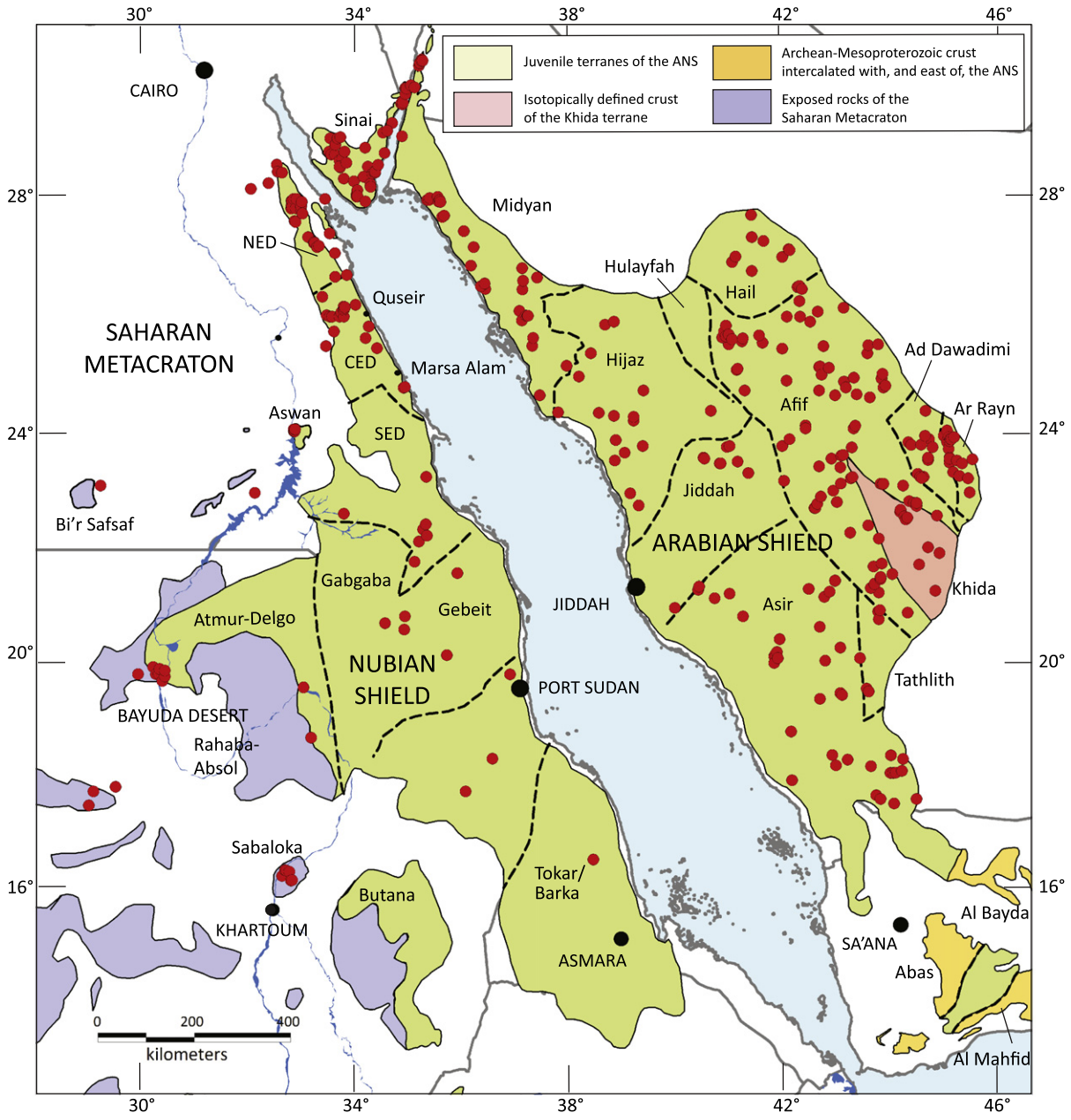

Fig. 6. Map of the Arabian–Nubian Shield showing the locations of rock samples with late Cryogenian–Ediacaran U–Pb, Sm–Nd, and Rb–Sr ages in the range 650–542 Ma. Details of the samples are given in Appendix A.

with concentrations in the Tonian–Mesoproterozoic (0.9–1.15 Ga); late Paleoproterozoic (1.7–2.1 Ga); Paleoproterozoic–Neoarchean (2.4–2.8 Ga); and early Archean (>3.2 Ga). Explanations for inheritance include: (1) contamination during processing; (2) assimilation from cryptic early Neoproterozoic to Archean basement; (3) assimilation of terrigenous sediment shed from nearby passive margins transported by rivers or glaciers; and (4) inheritance from a mantle source (Stern et al., 2010b).

3. Post-amalgamation basins

Deposition in the ANS prior to 650 Ma was dominated by volcanosedimentary assemblages in volcanic arcs; after 650 Ma, deposition changed to volcanosedimentary assemblages in post-amalgamation basins overlying newly amalgamated arc terranes. In contrast to the arc assemblages, the post-amalgamation-basin successions have unconformable basal contacts, indicating that they are autochthonous, in place at their site of deposition. The basal contacts vary from angular unconformities to nonconformities, in places grading from *in situ* weathered rubble on plutonic substrates up into conglomerate, sandstone, and siltstone. The post-amalgamation deposits occur throughout the ANS, but are mostly developed in the north and northeast (Figs. 8 and 9). Some deposits are as old as 660–650 Ma, but most are late Cryogenian to Ediacaran (Table 2). The basin deposits are variably deformed with gentle to vertical dips, and open-to-tight folds. Cleavage and lineations are common and some deposits are affected by ductile shearing and mylonitization. Most deposits are only weakly to moderately metamorphosed, apart from exceptions such as the Atura formation (<650 to >640 Ma), in the southern part of the Arabian Shield, which is at amphibolite grade (Fairer, 1985). The basins vary in

Table 1
Late Cryogenian–Ediacaran $^{40}Ar/^{39}Ar$ age dates from the Arabian–Nubian shield.

Sample	Plateau age	Isochron age	Laser fusion	Geologic unit	Lithology	Mineral dated	MSWD	Comment	Reference
Sibai 6	623.6 ± 0.2			Abu Markhat gneiss, Sibai dome	Hornblende-rich gneiss	Horblende		Interpreted as cooling below 500 °C; protolith age ~645 Ma	Fritz et al. (2002)
Ar-24	616 ± 3	625 ± 88	799	Shahmon Metabasite	Undeformed gabbro	Amphibolite		Disturbed $^{40}Ar/^{39}Ar$ spectra	Cosca et al. (1999)
S08-17	616 ± 2.8	617.52 ± 5.25		Metasedimentary siltstone (Abt formation)	Biotite–muscovite–chlorite schist	Muscovite	0.63	Interpreted as metamorphic muscovite with result giving the age of metamorphism	Lewis (2009)
S08-15	613 ± 5.9 618 ± 6*	615.51 ± 6.42 621 ± 4*		Metasedimentary siltstone (Abt formation)	Biotite–muscovite–chlorite schist	Muscovite	1.6	Interpreted as metamorphic muscovite with result giving the age of metamorphism. * = ages recalculate using decay constants revised by Renne et al., 2010	Lewis (2009)
RD-3	612 ± 3	612 ± 2		Ar Ridaniyah ophiolite melange	Metagabbro	Hornblende	0.8	Records time of cooling below blocking temperature of hornblende. Interpreted as 'uplift age' evidencing Ediacaran tectonic activity associated with rejuvenation of Ar Ridaniyah thrust fault after obduction of ophiolite 60 Ma earlier	Al-Saleh and Boyle (2001)
RD-9	611 ± 8	617 ± 6		Ar Ridaniyah ophiolite melange	Metagabbro	Hornblende	11.7	Records time of cooling below blocking temperature of hornblende. Interpreted as 'uplift age' evidencing Ediacaran tectonic activity associated with rejuvenation of Ar Ridaniyah thrust fault after obduction of ophiolite 60 Ma earlier	Al-Saleh and Boyle (2001)
RD-2	610 ± 2	612 ± 2		Ar Ridaniyah ophiolite melange	Amphibolite	Hornblende	0.5	Records time of cooling below blocking temperature of hornblende. Interpreted as 'uplift age' evidencing Ediacaran tectonic activity associated with rejuvenation of Ar Ridaniyah thrust fault after obduction of ophiolite 60 Ma earlier	Al-Saleh and Boyle (2001)
AD 24-25.4	609 ± 1.3		611 ± 1	Ad Duwayhi gold-bearing quartz vein	Quartz veins	Sericite		Inferred to be age of a post-mineralization thermal event, perhaps associated with late intrusions in the Haml batholith	Doebrich et al. (2004)
Sibai 5	606.7 ± 0.2			Pre-intrusive amphibolitic lens, Sibai dome	Amphibolitic lens	Hornblende		Interpreted as a possible second phase of cooling ~ 20 million years after onset of cooling (623 Ma) associated with denudation or cooling after advecive heating by granitoid intrusion	Fritz et al. (2002)
AD24-81.6	603 ± 1		608 ± 1	Ad Duwayhi gold-bearing quartz vein	Quartz veins	Sericite		Inferred to be age of a post-mineralization thermal event, perhaps associated with late intrusions in the Haml batholith	Doebrich et al. (2004)
Ar-12	601.4 ± 2.0		594	Taba tonalite gneiss		Biotite		Interpreted as age of regional metamorphic cooling, not a resetting event	Cosca et al. (1999)
HF 50	601 ± 4	599 ± 3		At Tari Structural Window	Migmatite	Hornblende		Closeness of both biotite and hornblende ages from the At Tari window suggst rapid uplift and cooling of the window	Al-Saleh et al. (1998)
Ar-31	598.4 ± 1.4		599	Elat Schist	Garnetiferous leucosome	Muscovite		Muscovite obtained from a late granitoid dike in Elat Schist. Interpreted as age of regional metamorphic cooling, not a resetting event	Cosca et al. (1999)
HC-60	597 ± 4	601 ± 5		Halaban sub-ophiolite complex	Amphibolite	Hornblende		Perhaps reset during emplacement of Abu Isnun pluton	Al-Saleh et al. (1998)
HF 54	597 ± 2	598 ± 3		At Tari Structural Window	Garnet–biotite schist	Biotite		Closeness of both biotite and hornblende ages from the At Tari window suggst rapid uplift and cooling of the window	Al-Saleh et al. (1998)
Ar-18	597.0 ± 1.4		597	Elat granite	Undeformed late- to post-kinematic granite	Biotite		Interpreted as age of regional metamorphic cooling, not a resetting event	Cosca et al. (1999)
RD-7	596 ± 6	602 ± 2		Ar Ridaniyah ophiolite melange	Metagabbro	Hornblende	1.5	Records time of cooling below blocking temperature of hornblende. Interpreted as 'uplift age' evidencing Ediacaran tectonic activity associated with rejuvenation of Ar Ridaniyah thrust fault after obduction of ophiolite 60 Ma earlier	Al-Saleh and Boyle (2001)
Meatiq 2	595.9 ± 0.5			Meatiq dome, southern low-angle normal fault	Shear-zone rock	Muscovite		Metamorphic age of muscovite forming at expense of feldspar during shearing; is similar to cooling ages and is consistent with interpretation that exhumation within the Meatiq dome was contemporary with shearing and extension on the margins	Fritz et al. (1996)
E98	594 ± 6			Ghedem terrane mylonitized gneiss	Titanite–amphibole gneiss and amphibolite	Hornblende		Cooling age after peak metamorphism at about 593 Ma; time of exhumation associated with orogenic collapse	Ghebreab et al. (2005)
Ar-16	592 ± 4	591 ± 9	575	Elat granite gneiss		Biotite		Interpreted as age of regional metamorphic cooling, not a resetting event	Cosca et al. (1999)
Meatiq 1	588.2 ± 0.3			Meatiq dome, western shear zone	Shear-zone rock	Muscovite		Metamorphic age of muscovite forming at expense of feldspar during shearing; is similar to cooling ages and is consistent with	Fritz et al. (1996)

							interpretation that exhumation within the Meatiq dome was contemporary with shearing and extension on the margins
Meati2 2	587.3 ± 0.2			Um Baanib gneiss, Meatiq Dome	Amphibolitic schollen	Hornblende	Interpreted as post-metamorphic cooling below 500 °C. Age is similar to that of muscovite (582 Ma) suggesting rapid cooling and exhumation	Fritz et al. (2002)
G2A	586 ± 6			Ghedem terrane mylonitized gneiss	Titanite–amphibole gneiss and amphibolite	Hornblende	Cooling age after peak metamorphism at about 593 Ma; time of exhumation associated with orogenic collapse	Ghebreab et al. (2005)
Hafafit 7	586.1 ± 0.3			Orthogneiss, Hafafit dome	Orthogneiss	Hornblende	Interpreted as cooling age below 500 °C associated with exhumation of Hafafit dome along NE-trending extensional faults. Protolith ages of granitoid gneiss are 682 Ma, 689 Ma, and 700 Ma	Fritz et al. (2002)
Hafafit 8	584.2 ± 0.2			Orthogneiss, Hafafit dome	Orthogneiss	Hornblende	Interpreted as cooling age below 500 °C associated with exhumation of Hafafit dome along NE-trending extensional faults. Protolith ages of granitoid gneiss are 682 Ma, 689 Ma, and 700 Ma	Fritz et al. (2002)
E99	583 ± 5			Ghedem terrane mylonitized gneiss	Titanite–amphibole gneiss and amphibolite	Hornblende	Cooling age after peak metamorphism at about 593 Ma; time of exhumation associated with orogenic collapse	Ghebreab et al. (2005)
Meatiq 4	583.9 ± 0.2			Um Baanib gneiss, Meatiq Dome	Amphibolitic schollen	Hornblende	Interpreted as post-metamorphic cooling below 500 °C. Age is similar to that of muscovite (582 Ma) suggesting rapid cooling and exhumation	Fritz et al. (2002)
Meatiq 9	582.3 ± 0.2			Garnet kyanite schist, Meatiq dome	Garnet–kyanite schist	Muscovite	Interpreted as cooling below ~375–400 °C (blocking temperature for muscovite). Result is similar to that for hornblende (587–579 Ma) suggesting rapid cooling and exhumation	Fritz et al. (2002)
Meatiq 1	580.3 ± 0.3			Um Baanib gneiss, Meatiq Dome	Amphibolitic schollen	Hornblende	Interpreted as post-metamorphic cooling below 500 °C. Age is similar to that of muscovite (582 Ma) suggesting rapid cooling and exhumation	Fritz et al. (2002)
E9B	579 ± 5			Ghedem terrane mylonitized gneiss	Titanite–amphibole gneiss and amphibolite	Hornblende	Cooling age after peak metamorphism at about 593 Ma; time of exhumation associated with orogenic collapse	Ghebreab et al. (2005)
Meatiq 3	579.1 ± 0.2			Um Baanib gneiss, Meatiq Dome	Amphibolitic schollen	Hornblende	Interpreted as post-metamorphic cooling below 500 °C. Age is similar to that of muscovite (582 Ma) suggesting rapid cooling and exhumation	Fritz et al. (2002)
K95-5-3	577 ± 5			Granite: Abu Hamed shear zone	Highly deformed granite	Biotite	Cooling age; dates cessation of ductile deformation on Abu Hamed shear zone and sinistral transpression on Keraf suture at ~577 Ma	Abdelsalam et al. (1998)
K95-5-3	577 ± 2			Granite: Abu Hamed shear zone	Highly deformed granite	Biotite	Cooling age; dates cessation of ductile deformation on Abu Hamed shear zone and sinistral transpression on Keraf suture at ~577 Ma	Abdelsalam et al. (1998)
K95-5-3	577 ± 2			Granite: Abu Hamed shear zone	Highly deformed granite	Hornblende	Cooling age; dates cessation of ductile deformation on Abu Hamed shear zone and sinistral transpression on Keraf suture at ~577 Ma	Abdelsalam et al. (1998)
G26	576 ± 6			Ghedem terrane mylonitized gneiss	Quartz-feldspar gneiss	Muscovite	Cooling age after peak metamorphism at about 593 Ma; time of exhumation associated with orogenic collapse	Ghebreab et al. (2005)
E9A	572 ± 7			Ghedem terrane mylonitized gneiss	Titanite–amphibole gneiss and amphibolite	Hornblende	Cooling age after peak metamorphism at about 593 Ma; time of exhumation associated with orogenic collapse	Ghebreab et al. (2005)
G26H	572 ± 6			Ghedem terrane mylonitized gneiss	Titanite–amphibole gneiss and amphibolite	Hornblende	Cooling age after peak metamorphism at about 593 Ma; time of exhumation associated with orogenic collapse	Ghebreab et al. (2005)
E97	566 ± 5			Ghedem terrane mylonitized gneiss	Quartz-feldspar gneiss	Muscovite	Cooling age after peak metamorphism at about 593 Ma; time of exhumation associated with orogenic collapse	Ghebreab et al. (2005)
G2C	565 ± 7			Ghedem terrane mylonitized gneiss	Titanite–amphibole gneiss and amphibolite	Hornblende	Cooling age after peak metamorphism at about 593 Ma; time of exhumation associated with orogenic collapse	Ghebreab et al. (2005)
E27	564 ± 5			Ghedem terrane mylonitized gneiss	Quartz-feldspar gneiss	Muscovite	Cooling age after peak metamorphism at about 593 Ma; time of exhumation associated with orogenic collapse	Ghebreab et al. (2005)
E2B	563 ± 5			Ghedem terrane mylonitized gneiss	Quartz-feldspar gneiss	Muscovite	Cooling age after peak metamorphism at about 593 Ma; time of exhumation associated with orogenic collapse	Ghebreab et al. (2005)
Ar-16			607	Elat granite gneiss		Biotite	Interpreted as age of regional metamorphic cooling, not a resetting event	Cosca et al. (1999)
AR-24			595	Shahmon Metabasite	Undeformed gabbro	Phlogopite	Interpreted as age of regional metamorphic cooling, not a resetting event	Cosca et al. (1999)
K-1		557 ± 15		Kirsh gneiss belt	Biotite paragneiss	Biotite	Interpreted as cooling age and minimum age of development of Kirsh gneiss belt. Broadly coeval with Rb–Sr w.r. isochron of 535 Ma and K–Ar hornblende age of 588 Ma for foliated granitoid between Ruwah and Ar Rika fault zones	Al-Saleh (2010)

surface area from as much as about 72,000 km^2 for the largest, the Murdama basin in the northeastern ANS, to small isolated basins of 200 km^2 (e.g., Johnson, 2003; Matsah and Kusky, 1999, 2001; Willis et al., 1988; Abdeen and Greiling, 2005; Eliwa et al., 2006, 2010). The deposits may be entirely or largely volcanic or volcaniclastic in origin; many include volcanic, volcaniclastic, and epiclastic rocks; others are dominantly or entirely sedimentary. The depositional environments range from terrestrial to shallow marine and include scarp front and alluvial settings as well as marine basins or basins connected to an ocean. Rocks deposited in terrestrial settings are characterized by red–maroon coloration stained by ferric iron and, in some cases, show rain-prints or mudcracks (Abdeen et al., 1997). Marine settings are indicated by a prevalent gray–green coloration of epiclastic rocks, and the presence of limestone formations up to several hundred meters thick, containing stromatolitic bioherms, undulose algal bedding, suspect multicellular organisms, and isotopes of marine affinity. The evolution of isotopic systems in ancient sedimentary rocks is now well established for the Neoproterozoic (Halverson et al., 2010) and conspicuous perturbations are recognized during the Cryogenian and Ediacaran that are linked with the concept of Snowball Earth and periodic glaciations. The world's largest δC excursion is recorded in Ediacaran sediments in Oman associated with the ~630 Ma Marinoan glaciation (Le Guerroué et al., 2006). A similar, but less extreme, negative anomaly has recently been recorded in the Antaq Basin (Nettle, 2009), but no isotopic evidence of glaciation has been found in any other post-amalgamation basin in the ANS. However, diamictite in some of the Jibalah group basins (Miller et al., 2008) suggests that further evidence may be forthcoming.

Marine post-amalgamation basins, typified by the Murdama, Bani Ghayy, Fatima, and Ablah groups, are prominent in the eastern part of the ANS. They began to be deposited during and soon after the Nabitah orogeny (680–640 Ma) that marked suturing of the Afif terrane with oceanic ANS terranes to the west. The Murdama basin, the largest in the ANS, was deposited on the eastern flank of the Nabitah mobile belt and appears to be a foreland basin. The Bani Ghayy group, similar in age to the Murdama, was deposited in extensional rift basins closer to the axis of the Nabitah mobile belt. The Fatima and Ablah groups were deposited west of the axis of the Nabitah mobile belt. *Terrestrial basins* are chiefly located in the northwestern part of the ANS, in the northern Arabian Shield, in Sinai, and in the Eastern Desert. Small basins occur in Sudan (Amaki formation) at the contact between the ANS and Saharan Metacraton. They include foreland basins, intermontane molasse basins, and strike-slip pull-apart basins not connected to any ocean. Conglomerate is abundant, limestone lacking, and volcanic assemblages extensive. *Mixed terrestrial–shallow marine basins* are present throughout the northern part of the ANS. They contain clastic rocks indicative of subaerial deposition, limestone of marine or possible marine origin, and varying amounts of volcanic rocks. Diamictite and possible dropstones suggest deposition coincident with glaciation. The basins are characterized by the Jibalah group (~590–560 Ma) and appear to have a more restricted time frame than other types of post-amalgamation basins in the ANS.

Despite their abundance and, locally, great thickness, relatively little is known about the development and depositional environments of the post-amalgamation basin in the ANS. Fundamental unanswered questions concern (1) the causes of subsidence that created the basins, whether thermal contraction, loading or flexure downwarping, or extension and pull-apart development in strike-slip systems; (2) the apparent genetic relationships between basin formation and local and regional structures such as strike-slip faulting and mantle doming; (3) the relationship between basin formation and granitoid magmatism; (4) the extent to which some of the basins were originally interconnected; (5) which basins were marine or connected to a late Cryogenian–Ediacaran ocean; and (6) whether any basins contain unequivocal Ediacaran multicellular fossils.

The sedimentary formations in many of the post-amalgamation basins in the ANS are referred to as "molasse" (e.g. Shalaby et al., 2006; Abd El-Wahed, 2009; Genna et al., 2002), implying deposition in front of a rising mountain belt synchronous with orogeny or in intermontane basins in the internal part of a mountain belt as it collapsed and underwent extensional and strike-slip faulting. The abundance of post-amalgamation basins, and the presence of marine deposits in some, implies that large areas of the ANS were depressed during the late Cryogenian and Ediacaran so as to accommodate thick sequences of sedimentary and volcanic rocks and significant parts were below sea level. It is pertinent to question therefore whether the EAO during its formation was a continuous or discontinuous, broken-up mountain belt, whether it was high above sea level and far from oceanic influences, or whether it was deeply penetrated by seaways along valleys and depressions.

3.1. Marine basins

The *Murdama basin* is the largest post-amalgamation basin in the ANS, more than 600 km long and 120 km wide. It crops out at the eastern margin of the Afif terrane and beneath Phanerozoic cover to the southeast (Johnson, 2003). The basin contains the Afif formation, a thin volcanic unit of calc-alkaline to alkaline rhyolite, dacite, andesite, and basalt at the base in the west, and the Murdama group, a thick sandstone, conglomerate, limestone, and subordinate volcanic succession above. In the east, the Murdama group unconformably overlies greenschist- to amphibolite- and, locally, granulite-facies metavolcanic and plutonic rocks of the Afif terrane, a relationship that suggests as much as 15–20 km uplift and erosion prior to Murdama deposition.

The Murdama group is estimated to have been deposited between ~650 and 620 Ma, toward the end of and after the 680–640 Ma Nabitah orogeny. It is dated by U–Pb SHRIMP ages of 630–624 Ma obtained from rhyolite in the southern part of the basin (Kennedy et al., 2010) and by a conventional U–Pb zircon age of 625 ± 4 Ma obtained from volcanic rocks to the northwest (Kusky and Matsah, 2003); in the north, the group may be as old as 650 Ma (Cole and Hedge, 1986). The group is intruded by ~650–570 Ma granitoid plutons (Cole and Hedge, 1986), and by ~630 Ma rhyolite sills (Kennedy et al., 2004).

The Murdama group is dominantly well-bedded fine- to medium-grained gray–green lithic (volcanic) arenite and arkosic arenite, with planar cross bedding, ripple cross lamination, planar lamination, grading, and scour-and-fill features. Upward-fining cycles of sandstone, siltstone, and shale less than 1 to several meters thick are locally present (Wallace, 1986). Polymict conglomerate, in part filling channels, is common at the base of the Murdama group and higher in the sequence. Limestone units, 10 to more than 1000 m thick and commonly stromatolitic, crop out at the base of the group along the eastern margin of the basin. An overall marine environment is clearly identified by the limestone, but in detail the basin appears to grade from a volcanic–plutonic terrain in the west to a marine and shallow-marine basin in the east. Deltaic environments are suggested by Greene (1993) and Cole (1988), whereas Wallace (1986) describes a near-shore mud-flat and broad-channel environment with lagoonal, lacustrine, or shallow-marine carbonate mud and algal buildups in the northern part of the basin. Gently plunging, open, upright, north-trending folds with locally vertical limbs are pervasive, indicating bulk E–W shortening, in part associated with sinistral shearing on transcurrent Najd faults (Moore, 1979; Johnson, 2003).

Smaller marine basins are represented by the Bani Ghayy and Fatima groups. The Bani Ghayy group, about 6000 m thick (Agar,

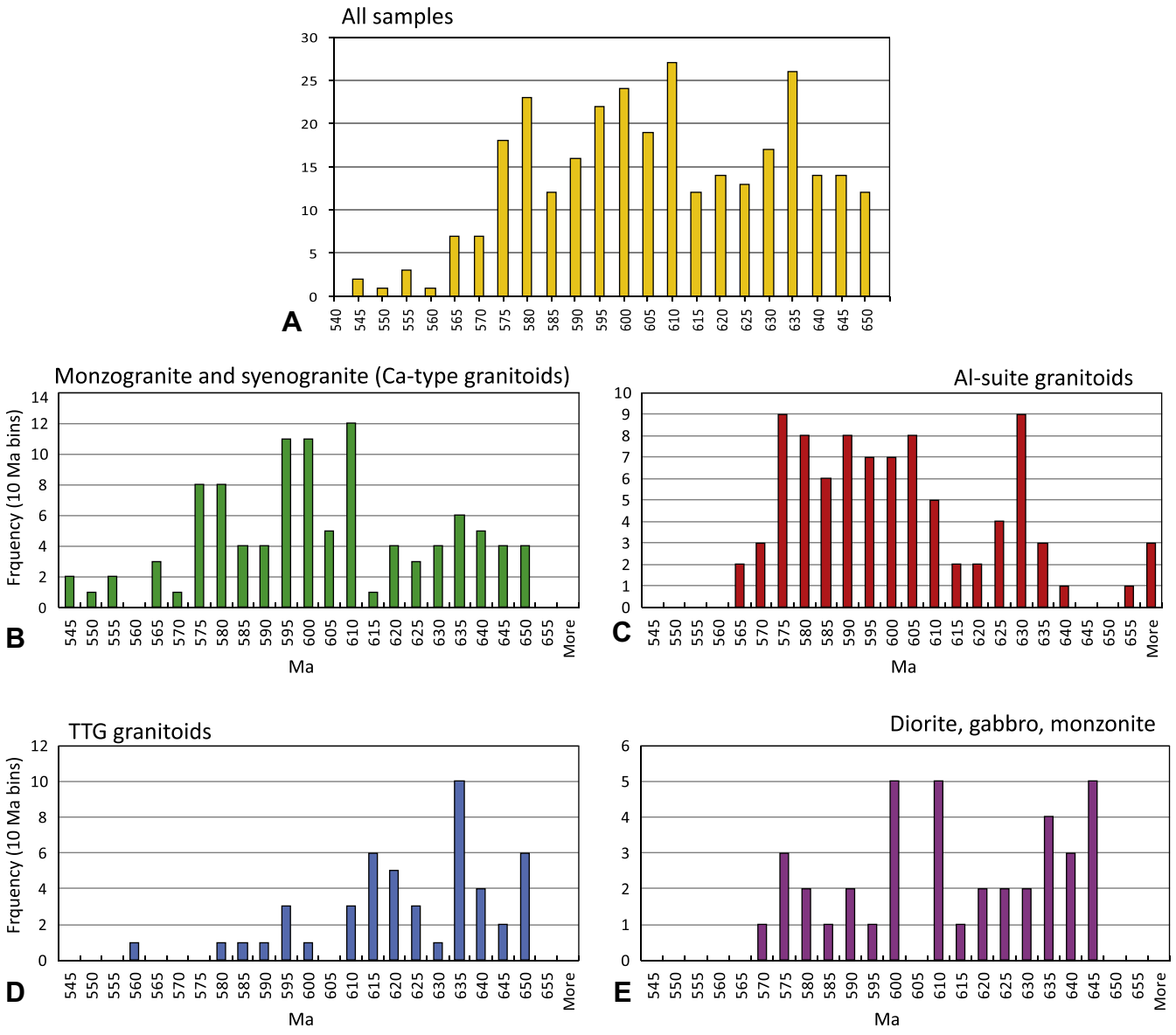

Fig. 7. Frequency plot of crystallization ages for selected groups of late Cryogenian–Ediacaran plutonic rocks in the ANS. Histograms plotted from U–Pb conventional, U–Pb ion-probe, and Rb–Sr whole rock crystallization ages listed in Appendix A. (A) All the data. (B) Chiefly monzogranite and syenogranite samples although some sampled plutons are composite and include granodiorite. (C) Chiefly alkali-feldspar and alkali-granite, but includes some syenogranite samples. (D) Chiefly trondhjemite, tonalite, and granodiorite samples, but includes some monzogranite. (E) Diorite, gabbro, and monzonite samples. The data are biased in favor of granite samples as being the most productive rocks for zircons and a deliberate focus of research interest, but the histograms are consistent with geologic observation that granite dominates late Cryogenian–Ediacaran magmatism in the ANS. The data also suggest an increase in the abundance of Al-type granitoids after about 610 Ma and a decrease in the abundance of Ca-type granitoids. The abundance of TTG samples reflects arc-type magmatism in the Ar Rayn terrane. Note the presence of diorite, gabbro, and monzonite throughout the period.

1986), crops out in a series of basins, 20–50 km wide, that are offset by as much as 50 km from each other by Najd faults. Prior to faulting, they probably formed a north-trending continuous basin more than 600 km long. The Bani Ghayy group is dated at ~620 Ma (Stacey and Agar, 1985, conventional U–Pb zircon age in rhyolite; Fleck et al., 1980, Rb–Sr whole-rock andesite age), although the group is intruded by quartz porphyry dated at 646 ± 11 Ma (Doebrich et al., 2004), which suggests that the maximum deposition age may be older than indicated by the direct dating; the group is listed in Table 2 as ~650–620 Ma. In places, the Bani Ghayy and Murdama groups are in virtual juxtaposition, and not all workers accept that they represent separate distinct lithostratigraphic units, referring to both as "Murdama group" (Brown et al., 1989). At issue is the extent to which the different lithologic compositions and depositional environments of the Murdama and Bani Ghayy groups warrant using separate lithostratigraphic names, a question that requires future assessment by stratigraphers.

The Bani Ghayy group contains polymict conglomerate, tuffaceous wacke, siltstone, limestone as much as 1000 m thick, and a bimodal sequence of porphyritic rhyolite, basalt, and andesite flows and tuffs as much as 1000 m thick (Pellaton, 1985; Agar, 1986; Kattan and Harire, 2000). Agar (1986) interprets the Bani Ghayy basin to be a fault-bounded graben. One of the bounding faults is exposed as a steeply, east-dipping serpentinite-decorated reverse fault (the Bi'r Tawilah fault shown on Fig. 15B) that is currently being explored for orogenic gold. Folds in the Bani Ghayy group indicate E–W shortening similar to that implied by folding in the Murdama basins.

The *Fatima group* crops out in a northeast-trending basin in the Jiddah terrane (Fig. 7). It contains conglomerate, sandstone, rhyolite, and basalt, and a considerable amount of limestone

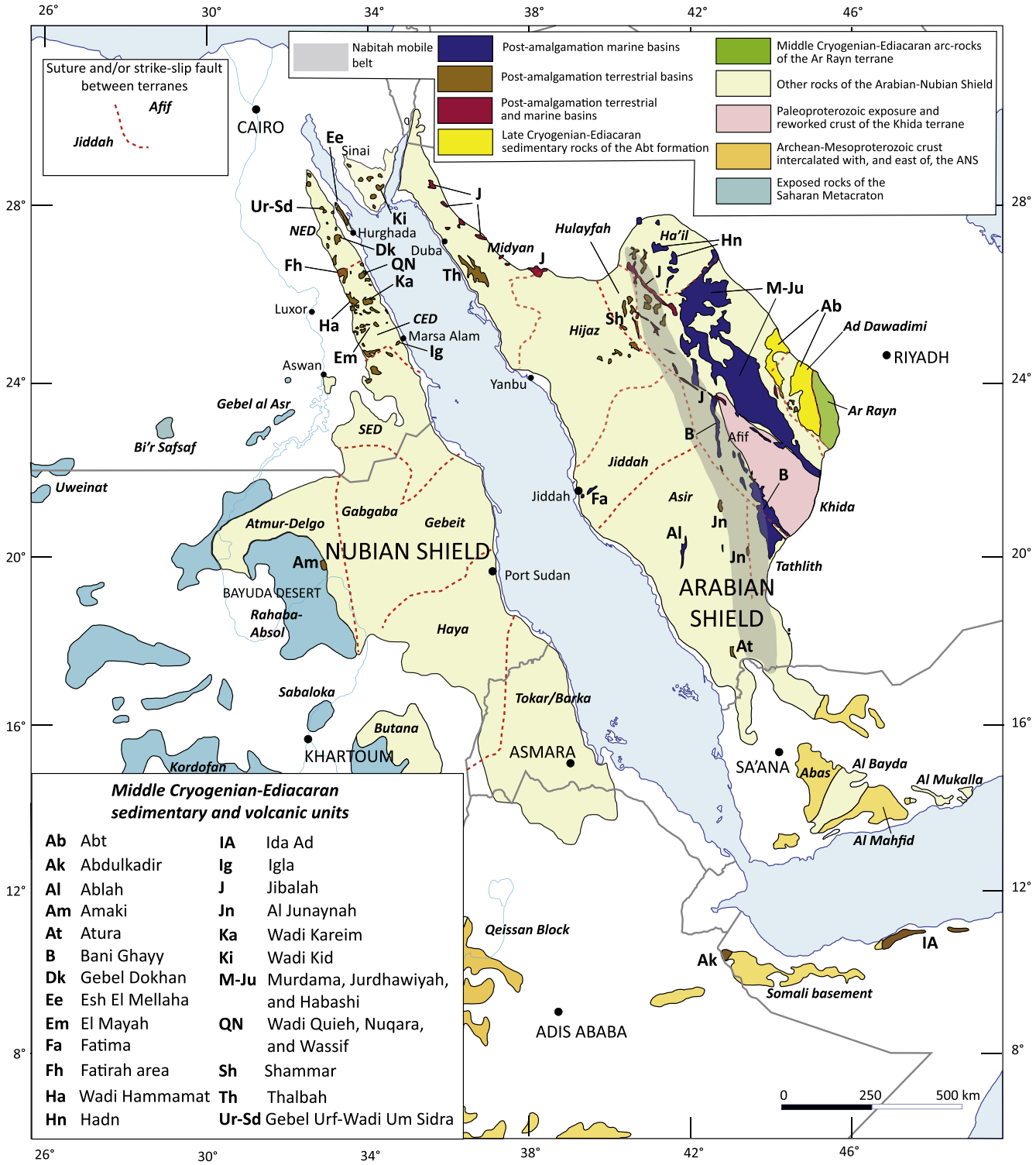

Fig. 8. Middle Cryogenian–Ediacaran sedimentary and volcanic assemblages in the Arabian–Nubian Shield. These assemblages mostly crop out in post-amalgamation basins, unconformable on newly amalgamated arc terranes. Exceptions are the Abt formation (Ab) and the arc rocks of the Ar Rayn terrane, which are treated as late Cryogenian–Ediacaran terranes rather than post-amalgamation basins. The figure includes some post-amalgamation assemblages that are middle Cryogenian (680–650 Ma) and older than the time period of this review, but are shown here for completeness.

with abundant crypalgalaminates, stromatolites, and archeocyathid biomicrites that may have been deposited in a stable shallow littoral-marine platform (Basahel et al., 1984). On the basis of Rb–Sr whole-rock ages from basalt, andesite, and rhyolite, the group is inferred to be about 685 Ma (Darbyshire et al., 1983), but Basahel et al. (1984) argue that its organic remains imply a Lower Cambrian age. From what is now known about the youngest rocks of the shield elsewhere, this seems unlikely. It is possible that the Fatima group correlates with the Jibalah (580–560 Ma), but this needs to be substantiated. The Fatima group is folded and was down faulted along the Fatima shear zone.

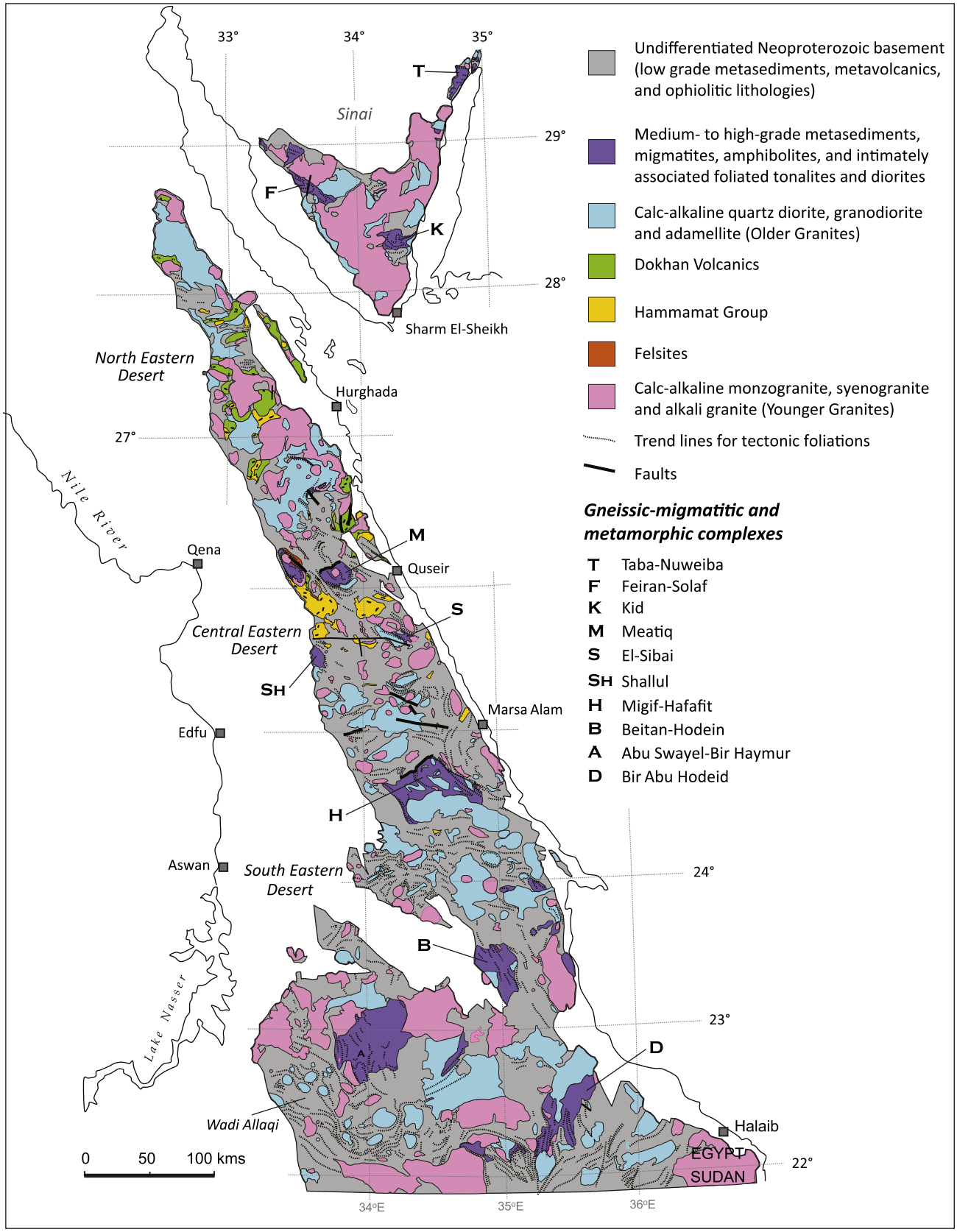

Fig. 9. Geologic map of the Eastern Desert and Sinai showing the distribution of the main geologic units and broad structural trends. Notice also the location of gneisses. Compiled and edited by A. Fowler from EGPC/CONOC Coral (1987) and Geological Survey of Egypt (EGSMA) 1:250,000 Geological Map series, 1992 to 2001.

Table 2
Middle Cryogenian–Ediacaran (650–542 Ma) sedimentary and volcanic successions in the Arabian–Nubian Shield. Apart from the Abt formation, these rocks occupy post-amalgamation basins. The basins are generally named after the deposit that fills them except for basins in the Eastern Desert, Egypt, which are individually named (see Fig. 7).

Name	Age/age range(Ma)	Comment	Depositional environment	Reference
Thalbah group	660–620	Not directly dated; unconformable on Zaam group and Imdan complex (660 ± 4 Ma) and intruded by Liban complex (621 ± 7 Ma)	Terrestrial: post-amalgamation basin	Davies (1985)
Afif formation and Murdama group	650–625	Minimum age reasonably well constrained; maximum age uncertain. Comprise largest post-amalgamation basin in ANS	Marine: post-amalgamation basin	Cole (1988), Cole and Hedge (1986), Greene (1993), Wallace (1986) and Kennedy et al. (2010)
Atura formation	<650 to >640	Not directly dated; small, strongly deformed and metamorphosed basin in the Asir terrane	Terrestrial: post-amalgamation basin	Fairer (1985)
Bani Ghayy group	~650–620	Depositional age weakly constrained	Marine: post-amalgamation basin	Agar (1986), Doebrich et al. (2004)
Ablah group	640–615	Directly dated at 641 ± 4 Ma and 613 ± 7 Ma	Marine: post-amalgamation basin	Genna et al. (1999) and Johnson et al. (2001)
Al Junaynah group	<640	Unconformable on Asir terrane supracrustals and ~640 Ma granites along Nabitah fault zone; small north-trending basins along the Nabitah and adjacent shear zones	Terrestrial: post-amalgamation basin	Not directly dated
Hibshi formation	632 ± 5	Unconformable on the Hail terrane; in fault contact with Murdama group; directly dated at 632 ± 5 Ma	Terrestrial: post-amalgamation basin	Cole and Hedge (1986) and Williams et al. (1986)
Shammar group	630–625	Unconformable on Nuqrah assemblage (~820 Ma) and intruded by granites (~630 Ma)	Terrestrial: post-amalgamation basin	Calvez and Kemp (1987) and Kemp (1996, 1998)
Amaki Series	Uncertain	Pull apart associated with transpression–transtension on the Keraf suture	Terrestrial: post-amalgamation basin	Ries et al. (1985) and Abdelsalam and Stern (1996)
Abt formation	$\gtrsim$ 620	Stratigraphic base and top unknown; intruded by granite plutons 605–565 Ma: sedimentary sequence comprising the Ad Dawadimi terrane	Marine: tectonic setting debated, possibly forearc basin with respect to the Al Amar arc	Delfour (1982), Kennedy et al. (2005, 2011), Lewis (2009) and Cox et al. (2011)
Hadn formation	~614–600	Unconformable on crystalline rocks of the Ha'il terrane and intruded by plutons of the Idah suite (620–615 Ma): epiclastic and calc-alkaline volcanic rocks	Terrestrial: post-amalgamation basin	Cole and Hedge (1986), Johnson (2006) and Kennedy et al. (2010)
Jurdhawiyah group	612–594	Unconformable on Murdama group; directly dated in the An Nir basin. Terrigenous clastic and volcanic deposit	Terrestrial: post-amalgamation basin	Cole (1988), Cole and Hedge (1986) and Kennedy et al. (2004, 2005)
Dokhan Volcanics and Hammamat Group	616–585	Unconformable on Older Metavolcanics and Older Granite; intruded by or synchronous with Younger Granites	Terrestrial: post-amalgamation basin	Willis et al. (1988), Wilde and Youssef (2000) and Breitkreuz et al. (2010)
Jibalah group	~590–560	Age well constrained by direct dating of zircon clasts and igneous (tuffaceous) grains. Southeast of Al 'Ula, is unconformably overlain by the newly recognized Kurayshah group, the youngest Ediacaran succession on the Arabian Shield	Terrestrial–marine: post-amalgamation basin	Delfour (1970), Matsah and Kusky (1999), Nicholson et al. (2008), Vickers-Rich et al. (2010), Miller et al. (2008) and Nettle (2009)
Saramuj Conglomerate, Haiyala Volcaniclastic Formation, Wadi Araba volcanic suite, and Wadi Abu Barqa Formation	~555–550	Age constrained by Rb–Sr whole rock isochron for alkali-feldspar rhyolite in the Wadi Araba volcanic suite (553 ± 11 Ma) and trachybasalt (545 ± 13 Ma) and andesite (550 ± 13) dikes that intrude the layered rocks	Terrestrial; locally shallow marine	Jarrar et al. (1992)

3.2. Terrestrial basins

Post-amalgamation basins in the northwestern part of the ANS are terrestrial suggesting a location more elevated and(or) farther from the sea than the marine basins in the east. One of the oldest and largest is the *Thalbah basin* (100 km by 45 km), occupied by the Thalbah group (Davies, 1985), in the Midyan terrane in the northwestern part of the Arabian Shield. The Thalbah is entirely epiclastic; other terrestrial basins contain volcanic and epiclastic sequences, such as the Dokhan Volcanics and the Hammamat Group of Egypt.

The Thalbah group (>5000 m) comprises polymict conglomerate, sandstone, and siltstone. Neither limestone nor volcanic rocks are present. The group is unconformable on the arc-related Zaam group and Imdan plutonic complex (660 ± 4 Ma) and intruded by the Liban complex (621 ± 7 Ma), which brackets deposition between 660 Ma and 620 Ma. The rocks are moderately folded, with bedding dips between <10° and 70°. Cleavage is well developed, but the rocks are barely metamorphosed except along the Qazaz shear zone where conglomerate clasts are stretched and the rock is changed to paragneiss, with foliation and mineral/stretching lineations conformable with those in orthogneiss in the shear zone. The Thalbah group reflects rapid deposition of rudaceous and arenaceous sediment interrupted by quieter intervals of fine grained sedimentation close to an emerging and strongly eroded mountainous hinterland (Genna et al., 2002). Massive conglomerates suggest mass flow deposition; bedded conglomerates and sandstones indicate fluvial deposition.

The *Dokhan Volcanics* and *Hammamat Group* crop out in small terrestrial post-amalgamation basins in the Eastern Desert; limestone is absent. They have been recognized in the Eastern Desert for many years (Akkad and El Ramly, 1958; El Ramly, 1972) and are described by an extensive literature. The Dokhan Volcanics succession varies in thickness from basin to basin, ranging from a few tens of meters to 1300 m (Eliwa et al., 2006). The Hammamat Group ranges from about 4000 m thick along Wadi Hammamat

in the type Hammamat basin (Abd El-Wahed, 2009) to about 7500 m in the Kareim basin (Fritz and Messner, 1999).

The proportions of volcanic and sedimentary rocks vary from basin to basin. Some contain only volcanic rocks, for example, the type Dokhan Volcanics basin; others are entirely sedimentary, such as the type Hammamat Group basin; yet other basins contain both volcanic and sedimentary rocks. Because of the varied distributions of these volcanic and sedimentary rocks and different relationships in basins where both rock types occur, the stratigraphy of the Dokhan Volcanics and Hammamat Group is debated. Some workers consider that the Hammamat Group underlies the Dokhan Volcanics (e.g., Stern and Hedge, 1985; Willis et al., 1988); others believe that the Hammamat overlies the Dokhan (e.g., Dardir and Abu Zeid, 1972; El Ramly, 1972; Akkad and Noweir, 1980; Ries et al., 1983; Hassan and Hashad, 1990); yet others infer that the two interfinger and are essentially contemporaneous (Ressetar and Monrad, 1983; Stern et al., 1984; El-Gaby et al., 1989; Eliwa et al., 2010). A problem is that the Hammamat Group and Dokhan Volcanics are defined on the basis of facies, whereas deposition took place in a dynamic setting around isolated volcanic centers and basin systems with different structural controls and different ages (Breitkreuz et al., 2010), so that the two facies should not be expected to occur in the same relative stratigraphic position in every basin.

Both units are Ediacaran. Recent SHRIMP U–Pb dating of zircons from ignimbrite and subvolcanic rhyolite (Breitkreuz et al., 2010) and previous Rb–Sr whole-rock ages (Stern, 1979; Abdel-Rahman and Doig, 1987), U–Pb conventional zircon ages (Stern and Hedge, 1985), and SHRIMP zircon ages (Wilde and Youssef, 2000) establish that the Dokhan Volcanics erupted between ~630 and ~592 Ma. An older weighted U–Pb SHRIMP age of uncertain significance is reported by Wilde and Youssef (2000) (685 ± 16 Ma) from a zircon core. Detrital zircons from the base of the Hammamat succession in the Gebel Um Tawat area, northern Eastern Desert, Egypt, yield a U–Pb SHRIMP age of about 585 Ma, and Wilde and Youssef (2000) infer that the group overall was deposited between about 593 and 579 Ma.

Wilde and Youssef (2002) suggest that the Hammamat Group was deposited in a major fluvial system of continental proportions that linked the various basins, and possibly linked to similar successions in Sinai and Jordan; other workers infer that the group was deposited in isolated, fault-bounded basins (Grothaus et al., 1979; Abdeen and Greiling, 2005). These are variously classified as a foreland basin, in the case of the type Hammamat basin (Fritz et al., 1996), intermontane basins in the cases of the Kareim, Queih, and Igla basins, for example (Abd El-Wahed, 2009), a strike-slip pull-apart basin, in the case of the El Mayah basin (Shalaby et al., 2006), and fault-bounded basins (Abdeen and Greiling, 2005). The range of inferred structural controls included thrusting, normal faulting, strike-slip faulting, N–S to NW–SE extension, and magmatic doming. In the type Hammamat basin, the Hammamat Group was deformed and metamorphosed and thrust over younger Dokhan Volcanics, perhaps as a result of deposition in a piggy-back foreland basin in front of a SW-propagating thrust front (Andresen et al., 2009). Both Hammamat and Dokhan units were affected by rapid hinterland uplift at about 595–588 Ma (Fritz et al., 1996; Loizenbauer et al., 2001) and subsequently intruded by the 596 Ma Um Had granite (Andresen et al., 2009). Initial subsidence of the Hammamat Group in the Kareim basin was associated with the formation of strike-slip faults around the Sibai gneiss dome as this was beginning to be exhumed (~650 Ma) (Bregar, 1996; Bregar et al., 2002) and terminal fanglomerate deposition was associated with the intrusion of young granite at about 580 Ma (Hassan and Hashad, 1990; Fritz and Messner, 1999). The El Mayah basin (Shalaby et al., 2006) was initiated as a fault-bounded half-graben and later evolved into a pull-apart basin at a prominent bend in a sinistral shear system of the Najd fault (see the location of the basin shown in Fig. 16).

The Hammamat Group typically comprises greenish-gray siltstone, lithic sandstone, and polymict conglomerate containing pebble-sized clasts of quartz, foliated granite, purple Dokhan type andesite, felsic volcanic rock, basalt, quartz porphyry, and undeformed pink granites. The Gebel El Urf basin, which contains both Hammamat and Dokhan facies, comprises alluvial-fan deposits, fluvial braided flood-plain deposits, deep lacustrine deposits, lacustrine-delta deposits, andesitic phreatomagmatic volcanic deposits, explosive pyroclastic deposits, and coherent bodies of lava flows, sills, and dikes (Eliwa et al., 2010). It is inferred that the rocks accumulated in a structurally controlled intermontane basin, beginning with alluvial-fan conglomerates and sandstone eroded from flanking high mountains, followed by the development of a deep lake, perhaps as a result of down faulting. Shrinkage of the lake is marked by a return of high-energy arenaceous and rudaceous sedimentation concurrent with the onset of silica-rich and silica-poor volcanic centers leading to the formation of volcanogenic mass flow deposits, hyaloclastic deposits, and lavas. The terminal history of the basin was marked by at least two large ignimbrite-forming caldera eruptions. The original margins of the basin are unknown. The succession has been folded into a broad E-trending syncline, the southern limb of which is metamorphosed in its basal part.

The Dokhan Volcanics typically include basaltic andesite, andesite, dacite, and rhyolite that some consider to be a bimodal suite (Stern and Gottfried, 1986; Mohamed et al., 2000) although this conclusion has been challenged (Eliwa et al., 2006). The rocks are enriched in LILEs (Rb, Ba, K, Th, Ce) relative to high field strength elements (Nb, Zr, P, Ti) and show strong affinity to calc-alkaline subduction-related rocks. However, their undeformed character, their temporal and spatial association with posttectonic A-type granite, and their high Zr/Y suggest that their emplacement followed the cessation of subduction in the Eastern Desert in an extensional, within-plate setting. Equivalent felsic volcanic rocks in the Wadi Kid area, Sinai, have strong high-K calc-alkaline affinity, with relative enrichment in total alkalis, Ba, Y, Zr and total REEs, depletion in Sr, and a LREE-enriched REE patterns with significant negative Eu anomalies. On the basis of these geochemical characteristics, which are compatible with both orogenic arc-type and anorogenic within-plate environments, El-Bialy (2010) suggests that they were erupted in a transitional "post-collisional tectonic setting". Mohamed et al. (2000) argue that their major and trace-element variations are consistent with their formation by partial melting of an enriched subcontinental lithospheric mantle followed by a limited amount of low-pressure fractional crystallization of olivine and pyroxene prior to eruption. In contrast, Eliwa et al. (2006) concluded that the trace element compositions of Dokhan alkali basalt, calc-alkaline, and adakitic lavas indicated that Dokhan magmas reflected melting of hot oceanic crust due to subduction of a hot oceanic ridge.

3.3. Mixed terrestrial–marine basins

This type of post-amalgamation basin in the ANS is typified by the *Jibalah group* (Delfour, 1970) (alternative spellings: J'balah, Jubaylah). The group crops out in small, isolated synclinorial basins adjacent to northwest-trending Najd faults in the northern part of the Arabian Shield (Fig. 10). The Jibalah rocks are folded and bedding dips may be steep but the group is barely metamorphosed. Disharmonic, en-echelon, and S- and Z-shaped asymmetric folds in some basins probably formed under conditions of sinistral and dextral simple shear (Kusky and Matsah, 2003). Matsah and Kusky (2001) and Kusky and Matsah (2003) suggested that some of these basins, such as the Jifn Basin along the Halaban-Zarghat fault,

formed as pull-apart basins during early dextral stages of motion along the Najd faults, and were then cut by structures related to a later sinistral motion along the faults.

The Jibalah group, the recently recognized Kurayshah Group (Nicholson et al., 2008), which overlies the Jibalah group in the Al 'Ula area of Saudi Arabia, and the broadly coeval Saramuj Conglomerate, Haiyala Volcaniclastics, Wadi Araba volcanic rocks (Jarrar et al., 1992), and the Wadi Abu Barqa Formation (Bandel and Shinaq, 2003) in Jordan are the youngest depositional units in the ANS. They unconformably overlie all other rocks in the Shield, with the exception of some posttectonic dikes, and are unconformably overlain by Lower Cambrian sandstone. Zircons from tuff beds in the Jibalah group yield ages of 560 ± 4 Ma (Vickers-Rich et al., 2010), 599 ± 5 Ma (core) and 570 ± 5 Ma (rim) (Kennedy et al., 2011), 588–600 Ma (Nicholson et al., 2008), and 568–585 Ma (Nettle, 2009) suggesting deposition between ~590 and 560 Ma. The minimum deposition age for Jibalah rocks in the north-central part of the Arabian Shield is constrained by a felsite dike dated at 577 ± 6 Ma that intrudes the group (Kusky and Matsah, 2003).

The group is characterized by maroon and purple sandstone, siltstone, and polymict conglomerate, cherty and siliceous stromatolitic limestone and calcareous argillite, dacite and rhyolite. In some basins, thick fanglomerates along the faulted sides of the basins suggest deposition during active faulting (Kusky and Matsah, 2003). Volcanic rocks and limestone are absent from some Jibalah-group basins, but the clastic deposits are always present. The purple-brown coloration of many of the Jibalah rocks, the algal-mat and stromatolitic biohermal carbonates, and sedimentary structures including ripple marks, graded bedding, and cross lamination indicate deposition in shallow water.

At Jabal Jibalah in the north-central part of the Arabian Shield (Fig. 10), the group is more than 3300 m thick; in the Antaq basin, a half graben or pull-apart basin 45 km by 10 km in extent, the group is as much as 2000 m thick (Nettle, 2009). Small Jibalah group basins in the northwestern Arabian Shield are similar (Hadley, 1974; Nicholson et al., 2008; Miller et al., 2008; Grainger and Hanif, 1989; Vickers-Rich et al., 2010). Recent work has identified matrix-supported boulders, cobbles, and possible dropstones in conglomeratic sandstone in some of the basins that may represent glaciogenic diamictite although most conglomeratic units are fanglomerate (Kusky and Matsah, 2003; Miller et al., 2008; Vickers-Rich et al., 2010).

The appearance of carbonates in the Jibalah basins marks a gradual change from a restricted non-marine environment to an increasingly marine environment. Microbial-mat structures in the carbonates are widespread, and the group has been recently searched for Ediacaran macrofossils (Miller et al., 2008; Vickers-Rich et al., 2010; Nettle, 2009). Exposures in basins in the northwestern Arabian Shield contain *Beltanelloides*-like structures that may represent algae or metazoans; a possible *Pteridinium* imprint and possible trails or burrows (Miller et al., 2008); and helically coiled tubular filaments of *Obruchevella parva* and the conical stromatolite *Conophyton* (Cloud et al., 1979). More recently, a fragment of *Charniodiscus* sp. and three possible specimens of *Aspidella* sp. have been reported from the Jibalah group in the Antaq basin in the far eastern Arabian Shield (Nettle, 2009). Cyanobacterial mats extensively developed during deposition of the Wadi Abu Barqa Formation in Jordan, which is broadly correlative with the Jibalah group (Bandel and Shinaq, 2003). $^{87}Sr/^{86}Sr$ values measured in some limestones are between 0.704 and 0.706, well below the range of reported Ediacaran marine values and suggesting significant Sr contribution from igneous rocks recently extracted from the mantle (Miller et al., 2008). Carbon isotopes in the carbonates, on the other hand, with $\delta^{13}C_{carb}$ near 2‰, are consistent with a marine environment (Miller et al., 2008). Nicholson et al. (2008) interpret Jibalah limestone in the Al 'Ula area as a distal marine deposit. Cloud et al. (1979) comment that the brecciated and micro-channeled appearance of fossiliferous rock in the Rubtayn basin, in the northwestern Arabian Shield, its locally dolomitic nature, and the prevalence of cryptalgalaminate favor a very shallow, locally turbulent, and perhaps episodically exposed marine or marginal marine setting. Diamictite and dropstone as well as the geochronology of the group are consistent with deposition during or sometime after the Gaskiers (~580 Ma) Ediacaran glacial event.

Two contrasting depositional models are proposed for the Jibalah group. One envisages that the group was continuously deposited over a large part of the northern Shield as the result of a shallow marine incursion, and is now preserved in younger grabens, having been eroded in other places. Based on recent mapping and sampling, Nicholson et al. (2008) recognize the same stratigraphy in several of the Jibalah basins on the Arabian Shield consistent with the interpretation that the unit was originally widespread. The facies recognized by Nicholson et al. (2008) indicates deposition within a single, laterally continuous basin that evolved from proximal fluvial conditions at its base to a marine shelf setting at the top. The other model envisages that the Jibalah group was never regionally extensive but was deposited syntectonically in fault-controlled basins under fluvial to shallow-marine or lacustrine conditions (e.g., Delfour, 1977; Husseini, 1988; Al-Husseini, 2000; Kusky and Matsah, 2003; Nettle, 2009). In terms of a fault-controlled basin model, the Al Jifn basin (north-central Arabian Shield) is inferred to have developed at a releasing bend along the Halaban-Zarghat fault during a period of dextral shear (Matsah and Kusky, 2001; Kusky and Matsah, 2003). The Al Kibdi (eastern Arabian Shield) basin is located between two left-stepping strike-slip splays of the Ar Rika fault and is a pull-apart basin that formed during sinistral shear. The Antaq basin (eastern Arabian Shield) is a half-graben that appears to have formed as a result of normal dip-slip movement on the hanging wall, perhaps during E–W-directed extension. The Rubtayn basin (NW Arabian Shield) consists of fault blocks and grabens depressed as a result of subsidence along boundary faults (Hadley, 1974).

4. Late Cryogenian–Ediacaran magmatism

Igneous activity was very important in the Late Cryogenian-Ediacaran evolution of the ANS, and included both intrusive and extrusive events. Neoproterozoic plutonic rocks form 42% of the exposed surface in the Arabian Shield (Fig. 11) (15% monzogranite and syenogranite, 4% alkali-feldspar granite, and 8%, 7%, 6%, and 2%, respectively, granodiorite, tonalitic rocks, dioritic rocks, and gabbro) (Stoeser, 1986). The basement of the Egyptian Eastern Desert consists of between 40% and 80% plutonic rock, mainly granite (Hussein et al., 1982; Stern and Hedge, 1985) (Fig. 9). A particular feature of the ANS is an abundance of A-type granitoids (A for anorogenic), especially alkali granite; in fact it is said that the region contains one of the largest fields of alkali granite in the world (Stoeser, 1986). A-type granites have mildly alkaline geochemistry, and are interpreted to have crystallized under low water fugacities. They have high Fe/Mg, (K + Na)/Al, and K/Na, abundant F, Zr, Nb, Ga, REE, Y, and Zn, and low Mg, Ca, Al, Cr, and Ni (Collins et al., 1982; Creaser et al., 1991). Among these rocks, alkali granite is characterized by containing alkali (sodic and sodic–calcic) amphibole and/or pyroxene (Streckeisen, 1976), the presence of such minerals being evidence that the parental melt was peralkaline in composition. On the IUGS QAP diagram (Streckeisen, 1976), alkali-feldspar granite contains about 90% or more (on a normalized feldspar scale) alkali feldspar, including plagioclase with anorthite content less than An_{05}. In practice, difficulties and ambiguities were found when applying the name "alkali granite" to granitoids in the Arabian Shield, but guidelines used for many of the granite

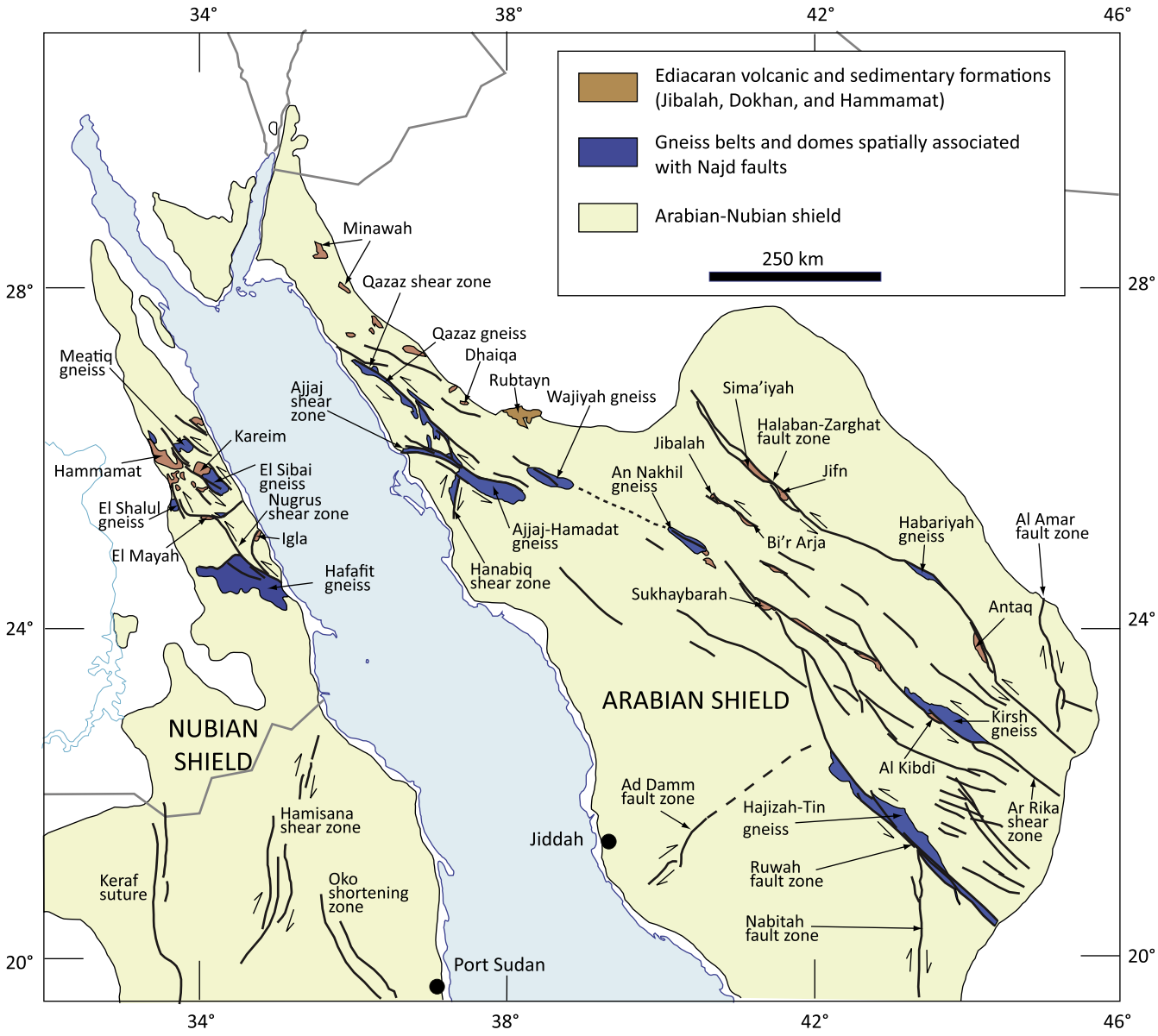

Fig. 10. Simplified map showing the spatial and genetic(?) relationships in the northern part of the Arabian–Nubian Shield between: (1) northwest-trending faults of the Najd fault system; (2) broadly contemporary shear zones of other orientations; (3) Ediacaran volcanic and sedimentary deposits of the Jibalah, Dokhan, and Hammamat groups; and (4) antiforms, domes, and linear belts of strongly deformed metasedimentary, metavolcanic, and metaplutonic rocks (paragneiss and orthogneiss). Names refer to fault zones, shear zones, depositional basins, and bodies of gneiss (compiled from Johnson and Woldehaimanot (2003), Abdelsalam and Stern (1996) and Shalaby et al. (2006)). Arrows show sense of shear.

studies conducted in the shield in the 1980s are set out by Ramsay et al. (1986).

The ANS late Cryogenian–Ediacaran intrusion styles range from sills, dikes, and stocks to plutons and batholiths, and the intrusions range from those with homogeneous compositions, to nested complexes, and to ring complexes. They were emplaced at mid- to high-levels in the crust, and some granitic intrusions can be seen in the field to have breached the surface and to be flanked by coeval lavas, such as in the east-central part of the Arabian Shield where the Wasit formation forms a volcanic pile of felsic tuffs and rhyolite overlying a posttectonic syenite (Pellaton, 1985). The late Cryogenian–Ediacaran plutons are typically discordant with respect to already deformed and metamorphosed country rocks, mostly lack penetrative deformation fabrics, and have the general character of late- to posttectonic intrusions. Exceptions are bodies of late Cryogenian–Ediacaran orthogneiss along Najd faults in the Arabian Shield, and in and around gneiss domes in the Eastern Desert that were syntectonically intruded during shearing and thrusting. Many plutons, particularly alkali-feldspar granites, weather out as prominent positive topographic features, elevated as inselbergs and enormous massifs above the surrounding rocks (Fig. 12); other plutons, particularly granodiorite and monzogranite, weather more readily and crop out as low-relief surfaces covered in grus.

4.1. Granitoids

Geographically, late Cryogenian–Ediacaran plutonic rocks are most abundant in the north and northeast of the ANS (Fig. 13). The reason(s) for this distribution is uncertain. It may reflect greater recent erosion of the ANS in the south than in the north because of post-Oligocene uplift over the Afar hotspot or a

greater degree of end-Precambrian uplift and peneplanation in the south than the north, resulting in the removal of epizonal plutons in the southern ANS. Other comparable N–S contrasts are evident in the distribution of post-amalgamation basins (Fig. 8) and late Cryogenian–Ediacaran gneisses, and in the orientations and origins of shear zones and shortening zones (see Fig. 19).

On the basis of the geochronologic data shown in Fig. 7, it is evident that from the perspective of the ANS as a whole, late Cryogenian–Ediacaran magmatism was quasi-continuous, although punctuated by surges in activity as well as systematic increase in LILE abundances with time. A commonly accepted view of Cryogenian–Ediacaran ANS magmatism is that it evolved from arc-related tholeiite and calc-alkaline TTG assemblages, to collisional-related calc-alkaline TTG and granite assemblages, to post-collisional within-plate A-type granitoids that formed in extensional regimes during orogenic collapse (Stern and Hedge, 1985; Beyth et al., 1994; Moghazi et al., 1998; Garfunkel, 1999; Jarrar et al., 2003; Mushkin et al., 2003; Moussa et al., 2008). The transition from collision to extension, manifested by the emplacement of granites in association with dike swarms and volcanic rocks extruded in molasse-type basins, is commonly dated about 610 Ma (Beyth et al., 1994).

Such a transitional model of magmatism has a long history, reflected in the Egyptian stratigraphic divisions of "Older granites" and "Younger granites" (Hume, 1934; El Ramly and Akaad, 1960; Akkad and Noweir, 1980; Bentor, 1985) and is, to some extent, supported by precise U–Pb zircon dating. In the Eastern Desert, for example, Youssef (2005) obtained SHRIMP U–Pb ages of ~755–655 Ma for "Older granites" at Gebel Gattar and 576 ± 6 Ma and 594 ± 3 Ma for the "Younger granites". Moussa et al. (2008) obtained SHRIMP U–Pb zircon ages of 652 ± 3 Ma for a granodiorite and ~595–605 Ma for later granitoids. Parts of the eastern Arabian Shield also provide evidence of a temporal change in granitoid type, with calc-alkaline assemblage of granodiorite, tonalite, trondhjemite, diorite, minor gabbro and local monzogranite, syenogranite and alkali-feldspar granite (Kishaybi and Idah suites) emplaced in the Afif terrane between 645–615 Ma and strongly fractionated peralkaline, peraluminous, and related leucocratic granites (Abanat suite) emplaced at 585–570 Ma (Cole and Hedge, 1986).

However, recent work challenges the traditional view of a straightforward temporal transition. Lundmark et al. (2011), using newly obtained U–Pb ID-TIMS ages and earlier U–Pb conventional, ID-TIMS and SHRIMP ages in the Central Eastern Desert (CED), Egypt, identify six pulses at: (1) 705–680 Ma; (2) ~660 Ma; (3) 635–630 Ma; (4) 610–604 Ma; (5) 599–590 Ma: and (6) 550–540 Ma. The first three pulses are synorogenic; pulses 4 and 5 record exhumation of mid-crustal gneisses, and pulse 6 postdates orogeny. In NE Sudan, Stern and Abdelsalam (1998) noted that plutons defined an early peak in LILE abundances at ~740 Ma followed by voluminous intrusion of ~690–720 Ma low-K TTG suites, and then by plutons that became increasingly LILE-rich with time. In Arabia, alkali granites as old as 686 ± 26 Ma, 678 ± 10 Ma, and 640 ± 3 Ma are reported from the Hijaz and Asir terranes in the Arabian Shield (Duyverman et al., 1982; Cooper et al., 1979; Johnson et al., 2001), whereas elsewhere calc-alkaline and alkaline suites are both coeval and younger. The Sabaloka area, SW of the ANS, contains post-collisional high-K 605 ± 4 Ma calc-alkaline granite as well as 591 ± 5 Ma shoshonitic granite. Late-tectonic magmatism in the Tokar/Barka terrane in Eritrea includes contemporary medium- to high-K, I-type calc-alkaline granodiorite and granite (622 ± 1 Ma) and alkaline to shoshonitic syenite dikes (628 ± 4 Ma) and small plutons (Teklay et al., 2001) and broadly coeval posttectonic granodiorite (606 ± 1 Ma) and granite (613 ± 1 Ma, 612 ± 6 Ma) are found in Ethiopia (Miller et al., 2003; Avigad et al., 2007). These results identify magmatic episodes in the southern ANS that encompass coeval intrusive rocks of different chemistry and modal compositions, and are EAO examples of the shift from high-K calc-alkaline to shoshonitic or alkaline–peralkaline magmatism recognized in the final stages of orogeny in the Neoproterozoic belts of West Africa (Liégois et al., 1998).

In the northern ANS, coeval as well as transitional late Cryogenian–Ediacaran magmatism is recognized in the northern Midyan terrane (Jordan) and Sinai (Egypt and Israel). In southern Israel, Beyth et al. (1994) dated an I- to A-type transition at ~610 Ma. In Jordan, Jarrar et al. (2003) noted a transition at about 600 Ma between calc-alkaline gabbro to high-silica granite belonging to the 640–600 Ma Aqaba complex and alkali-calcic to alkali rocks belonging to the 600–560 Ma Araba complex, yet the Aqaba complex itself includes both mafic and felsic assemblages. The mafic assemblage consists of quartz-diorite, quartz-monzodiorite, monzodiorite, and monzogabbro (the Araba Mafic to Intermediate Suite: 595–570 Ma); the felsic assemblage of microgranite, alkali-feldspar granite and syenogranite (the Humrat–Feiran Suite: 568 Ma), another evidence of coeval mafic and felsic magmatism during the closing stage of ANS evolution.

Coeval calc-alkaline and alkaline Ediacaran granitoids likewise dominate basement outcrops in Sinai (El-Shafei and Kusky, 2003; Be'eri-Shlevin et al., 2009b; Ali et al., 2009). Be'eri-Shlevin et al. (2009b) sampled slightly deformed to mostly undeformed calc-alkaline granodiorite, monzogranite and minor gabbro and quartz-diorite, referred to as a CA2 suite (~635–590 Ma) and alkaline and peralkaline granites and monzodiorite forming an AL suite (~608–580 Ma). Rocks within the CA2 suite show a change from mafic to felsic magmatism, with a peak in granodiorite to granite magmatism at 610–600 Ma. AL-suite magmatism started contemporaneously with the peak in the CA2 granitic magmatism at about 608 Ma and continued until ~580 Ma (Be'eri-Shlevin et al., 2009b). Ali et al. (2009) sampled discordant, posttectonic calc-alkaline as well as alkaline suites of monzogranite, syenogranite, and alkali granite elsewhere in Sinai, and discovered that they all date between 594 and 579 Ma and show no temporal progression.

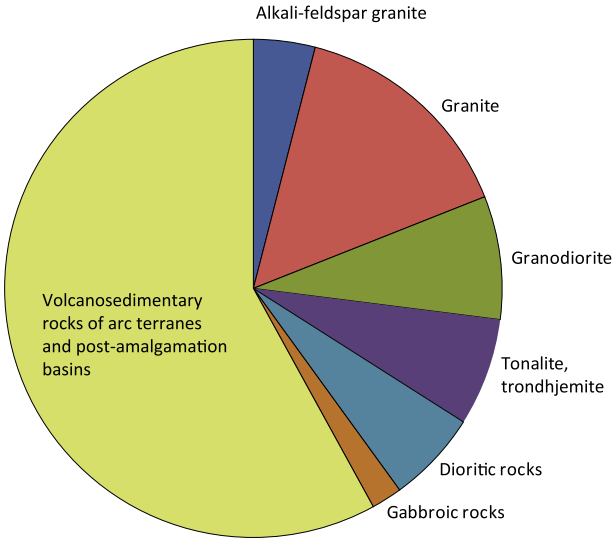

Fig. 11. Proportions of plutonic and other rocks in the Arabian Shield (after Stoeser, 1986). Orthogneiss does not figure as a separate category in this diagram because gneiss is calculated in terms of the protolith – thus dioritic gneiss is grouped with diorite; granite gneiss with granite, etc. Ultramafic rocks do not figure either, but amount to about 1%. The Nubian Shield has a similar composition except for a greater proportion of ultramafic rocks.

As these results indicate, the change from calc-alkaline to alkaline magmatism in the ANS was not instantaneous and cannot be neatly pinned at 610 Ma. Both types of magmatism occurred during the late orogenic extensional phase in the ANS and intrusions of both magma types are found juxtaposed in any given area. In places, the two magma types can be chronologically separated, with the calc-alkaline intrusions older than the alkaline, but in other places, the two overlap or are coeval. Similar associations between calc-alkaline and alkaline granitoids occur elsewhere in the world, because calc-alkaline magmatism is known to result from lithospheric extension in areas with a long history of previous subduction (Hooper et al., 1995), leading to the situation that both calc-alkaline and alkaline granitoids plot jointly in the post-collisional field on the Rb/Y + Nb discrimination diagram of Pearce (1996).

Late Cryogenian–Ediacaran magmatism in the Ar Rayn terrane in the eastern Arabian Shield reflects a different set of tectonic constraints (Doebrich et al., 2007). In this region, the plutonic rocks are divided into two partly coeval suites of (1) low-Al trondhjemite–tonalite–granodiorite (TTG suite) emplaced between 632 Ma and 616 Ma and (2) high-Al TTG/adakitic rocks emplaced between 689 and 617 Ma, and a suite of alkali-feldspar granite, two samples of which are dated at 607 ± 6 Ma and 583 ± 8 Ma (Doebrich et al., 2007). The TTG suites are arc-related and imply that subduction continued in the Ar Rayn terrane until at least about 615 Ma. The alkali-feldspar granite forms discordant plutons typical of a post-tectonic setting following the cessation of subduction.

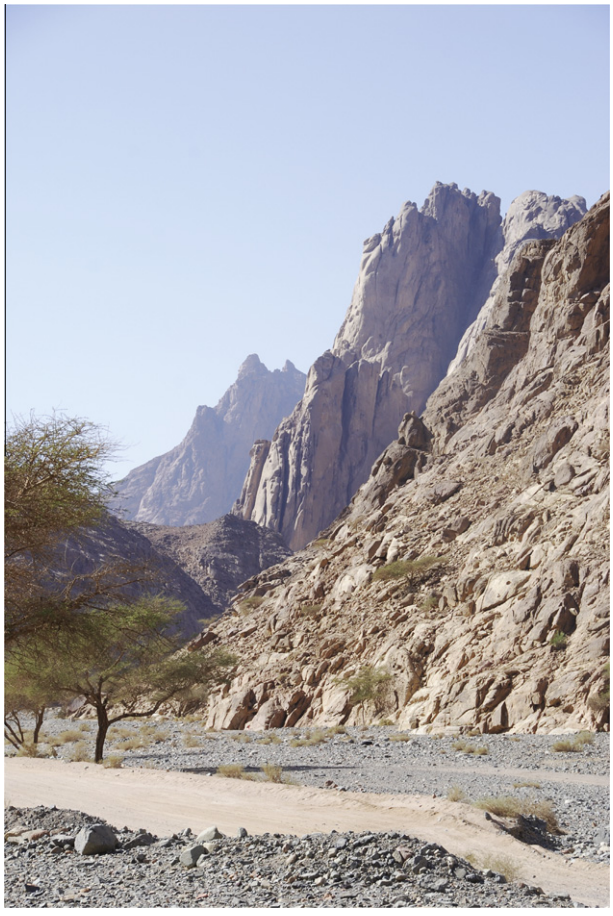

Fig. 12. View of the Dabbagh complex (577 ± 13 Ma: Aleinikoff and Stoeser, 1988), a typical alkali-feldspar granite in the northern part of the Midyan terrane that weathers out as a large granite massif rising high above the surrounding valleys.

4.2. Late Cryogenian–Ediacaran gabbro

Late Cryogenian–Ediacaran gabbro makes up a relatively small percentage of plutonic rocks in the ANS. Their geochronologic dataset (Appendix: five samples) is too small to draw a firm conclusion about their overall timing but the available data indicate a range of ~640 Ma to 540 Ma, implying that gabbro and granite magmatism overlapped in the ANS during the late Cryogenian–Ediacaran. Late- to posttectonic gabbros are commonly distinguished by prominent layering (Coleman et al., 1972; Sadek, 1994; Greiling et al., 1994). Wherever observed, they are strongly discordant and appear to be among the youngest rocks in any given region of the ANS.

Notable examples of gabbro intrusions include the Thalath complex in the central Arabian Shield (Al-Muallem and Smith, 1987). The complex crops out as gabbro intrusions as much as 50 km across; several are circular to ovoid. Most are isotropic, but some have prominent inward-dipping gabbro–dunite layering and at least one has a core of gabbro and rim of anorthosite suggestive of a ring dike. The Lakathah complex in the southwestern Arabian Shield (Martin et al., 1979) is a nearly circular ring dike 10 km across composed of a pyroxenite–hornblendite core, an intermediate zone of diorite–gabbro, and an outer ring of syenite. The Wadi Kamal complex, NW of Yanbu' al Bahr in the northwestern Arabian Shield, is an irregular body of gabbro, anorthosite, and subordinate norite and leucogabbro forming southern and northern lobes connected by a trail of scattered intrusions. The complex is a significant PGM exploration target. The Ad Dawadimi (Harrat al Ji'lani) gabbro intrudes granite in the Ad Dawadimi terrane as an oval ring structure 7 km across (Al-Shanti, 1976). It comprises inward dipping layers of norite, gabbro, and minor amphibolite, which add up to a thickness of more than 3 km. Plagioclase–pyroxene gabbro cumulate predominates. The complex contains minor chromite and hosts silver veins belonging to the Ad Dawadimi silver district, but has no reported titaniferous magnetite or other metallic minerals.

The Akrarem complex in the Eastern Desert is a concentrically zoned mafic–ultramafic intrusion in the Eastern Desert composed of dunite and an outer zone of lherzolite–clinopyroxenite and hornblendite (Helmy and Mogessie, 2001). The dunite contains Cu–Ni–PGE mineralization with net-textured and massive lenses of pyrrhotite, pentlandite, and chalcopyrite, as well as Cr-magnetite. The complex is inferred to be mostly posttectonic, but is locally sheared, and some of the mineralization has been remobilized. Other late- to posttectonic mafic–ultramafic intrusions in the Eastern Desert, which clearly postdate "late tectonic" granitoids, include complexes of leucogabbro, anorthosite, and diorite, and alkaline granitoid (Akad and Abu El-Ela, 2002). One such complex comprises the Umm Gheigh gabbro in the southern part of the Sibai area, Central Eastern Desert, Egypt, which has an ID-TIMS U–Pb zircon crystallization of ~545–540 Ma (Augland et al., 2011). It is intruded by a dike dated at ~540 Ma, and together the rocks represent some of the youngest undeformed and posttectonic plutonic rocks in the ANS. The gabbro may be unrelated to other, slightly older layered gabbros in the area (Augland et al., 2011). Other distinctive late- to posttectonic gabbros occur along the Allaqi-Heiana suture zone as circular intrusions as much as 10 km across characterized by layers dipping 10–65° inward (Greiling et al., 1994; Sadek, 1994; Abdeen and Abdelghaffar, 2011).

4.3. Chemical characteristics and tectonic discrimination

Late Cryogenian–Ediacaran granitoids have been studied in the ANS because (1) they are spatially and genetically related to gold, REE, Ta, and Nd mineralization: and (2) their chemistry and isotopic compositions give important insight into the origin and evolution of the ANS crust.

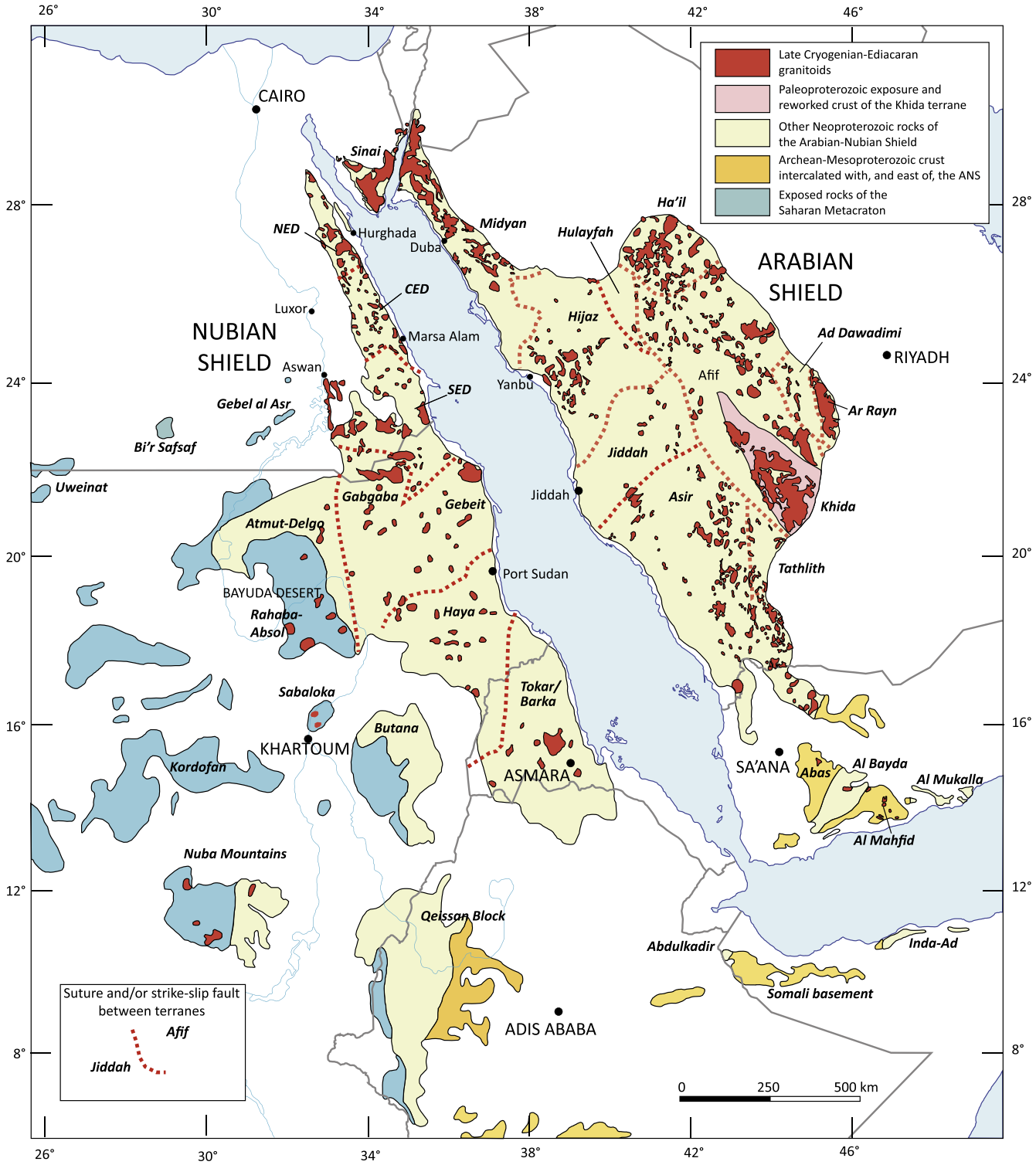

Fig. 13. Late Cryogenian–Ediacaran, late- to posttectonic, mostly discordant granitoids in the Arabian–Nubian Shield. Note the non-uniform distribution of the plutonic rocks with preponderance in the northern ANS.

Most ANS igneous rocks have lithologic associations (ophiolites, calc-alkaline igneous rocks, immature sediments) and isotopic compositions consistent with formation as juvenile continental crust. They have Nd model ages close to their crystallization ages (Stern, 2002; Stoeser and Frost, 2006; Moussa et al., 2008), mostly positive initial ε_{Nd}, and $^{87}Sr/^{86}Sr$ (Sr_i) close to that expected in evolving mantle of the same age (Fig. 14). This is particularly true for the TTG calc-alkaline rocks in the ANS. Initial $^{87}Sr/^{86}Sr$ above the standard mantle growth curves are found in middle to late Cryogenian and Ediacaran monzogranite, syenogranite, and alkali-feldspar granites and are notable, together with evolved Pb and Nd isotopes, in rocks from the Khida terrane (Stoeser and Frost, 2006) in which Paleoproterozoic crust was reworked during the Neoproterozoic.

An important recent study has established the magmatic O isotopic compositions of zircons in Ediacaran granitic rocks in Sinai. O isotopic compositions of granitic whole-rock samples are not reliable because hydrothermal and deuteric alteration is common, but O isotopic values determined from zircons are robust and preserve magmatic information because of the refractory character of zircon. Be'eri-Shlevin et al. (2009c) analyzed zircons from well dated granitic, post-collisional calc-alkaline (~635–590 Ma) and alkaline (~608–580 Ma) rocks from Sinai. Both suites have indistinguishable and restricted $\delta^{18}O$ values of 5.7 and 5.8‰, which points to dominance of mantle-like $\delta^{18}O$ sources in their formation, either because of anatexis in the lower crust or fractionation of mafic melts. Be'eri-Shlevin et al. (2009c) concluded that the granitic magmas were derived from mantle-like $\delta^{18}O$ reservoirs, with little evidence for involvement of altered juvenile crust, except in the northernmost Sinai basement.

With regard to trace-element geochemistry for late Cryogenian–Ediacaran granitoids in the ANS, data are not systematically available, but what are available show some differences in trace-element contents and REE patterns that help to distinguish between calc-alkaline I-type granitoids and A-type granitoids, although there is significant overlap and discrimination is not always clear. For example, most calc-alkaline ANS granitoids plot in the fields of volcanic-arc and syn-collisional granites on the Nb/Y and Rb/Y + Nb diagrams of Pearce et al. (1984), but many samples also plot in the post-collisional Rb/Y + Nb sub-field of Pearce (1996) and some extend into the within-plate field. Examples include the 630 Ma granitoids sampled by Teklay et al. (2001) in the Nakfa terrane in the southern part of the ANS, metaluminous and peraluminous CA2 granitoids as well as some CA1 granitoids studied by Be'eri-Shlevin et al. (2009b) in Sinai, and most granitoids in the Aqaba suite in Jordan (Jarrar et al., 2003). The Nakfa granitoids of Eritrea have slightly LREE-enriched REE patterns; some samples have negative Eu anomalies, others positive anomalies (Teklay et al., 2001). Calc-alkaline mafic and felsic plutons in Sinai show moderate REE enrichment and steep REE patterns, with no to slight Eu anomalies on chondrite-normalized REE plots (Be'eri-Shlevin et al., 2009b). Mafic members of the Aqaba suite (640–600 MA) in Jordan are enriched in LILE relative to HFSE and are moderately enriched in REE [$(La/Lu)n = 5–11$], traits typical of arc basalts. Granitoids of the same suite are high in Ba, Sr, and LREE, have low Y and have steep REE patterns [$(La/Lu)n = 20–25$]. They have low-initial $^{87}Sr/^{86}Sr$ (~0.70305) and high ε_{Nd} values (+2.3–5.0) and may have been generated by high degrees of partial melting (10–30%) of subducted oceanic crust, with or without a small proportion of ocean sediments (Jarrar et al., 2003).

Late Cryogenian–Ediacaran A-type granitoids in the North Eastern Desert (NED) (Moussa et al. (2008) include peraluminous granites that plot in the within-plate and post-collisional fields of Pearce et al. (1984) and Pearce (1996). Similar rocks in Sinai mostly plot as within-plate granites although some extend into the volcanic-arc field of Pearce et al. (1984) but are all within the post-collision field of Pearce (1996) and Be'eri-Shlevin et al. (2009b). The mafic end members of the younger Araba suite (600–560 Ma) are enriched in LILE compared to mafic members of the Aqaba suite, but have a similar REE pattern [$(La/Lu)n = 5–15$], despite being emplaced in a within-plate tectonic environment. The felsic, granite, end member of the Araba suite has chemical features typical of A-type granite. It is characterized by moderate enrichments in LREE $(La/Sm)_n \sim 2$, flat HREE patterns $(Gd/Lu)_n \sim 1$, and strong negative Eu anomalies ($Eu/Eu^* = \sim 0.07–0.53$) (Jarrar et al., 2003). A-type granitoids in the Aswan area of Egypt dating between 606 and 595 Ma have high Zr, Y, and LREE, and display affinities to shoshonitic magma series (Finger et al., 2008). These tendencies towards enrichments in some trace elements are important for mineralization, discussed in a later section.

The TTG arc-related suite in the Ar Rayn terrane is characterized by weakly fractionated REE patterns with moderately negative Eu anomlies (Doebrich et al., 2007). The high-Al calc-alkaline suite of diorite, granodiorite, and granite displays depleted HREE patterns and no, or positive, Eu anomalies. On average, these rocks are enriched in Rb and Sr, and depleted in Y and Yb relative to the low-Al TTG suite. Both suites plot in the volcanic-arc/syn-collisional granite field of Pearce et al. (1984) consistent with their inferred subduction-related arc setting. The alkali-feldspar granites are generally more evolved than the calc-alkaline rocks, and have strongly fractionated REE patterns with strongly negative Eu anomalies. Like the calc-alkaline rocks, they also plot in the volcanic-arc granite/syn-collisional granite field despite their posttectonic field characteristics, a feature that may have been inherited from the arc-related crust into which they were intruded.

Overall, the variation in REE patterns in the ANS indicates that older CA I-type granitoids formed in equilibrium with residual garnet and that feldspar fractionation played little role in magma genesis. These REE patterns could reflect subduction zone magmagenetic processes or lower crustal melting. In contrast, REE patterns for younger A-type granitoids indicate strong feldspar control and no evidence for residual garnet. These REE patterns strongly implicate low-*P* fractionation processes, perhaps in the upper to middle crust.

The mostly positive values of $\varepsilon_{Nd}(T)$ values of late Cryogenian–Ediacaran granitoids indicate that their magma sources were dominated by juvenile crust and(or) depleted mantle (Moussa et al., 2008). Although tectonic setting may be a fundamental control, as in the case of calc-alkaline melts generated during subduction, the coeval relationship of some calc-alkaline and alkaline suites indicates that calc-alkaline as well as alkaline magmas evolved in anorogenic, post-collisional settings. In these cases, the presence of suites with different chemical affinities may reflect different source rocks rather than different tectonic settings.

The term "A-type" granite originally applied to granite generated in extensional settings along continental rift zones (Loisell and Wones, 1979) but it is now known that A-type granites occur in a variety of settings ranging from within-plate, anorogenic environments to plate boundaries (Bonin, 2007). With regard to their magma origins, one proposal is that they derive from anhydrous high-grade metamorphic rock, for example, granulite that had previously yielded a granitic partial melt (Barker et al., 1975), although it is very hard to understand how such depleted material could generate such enriched melts. Another proposal is that they derive from mafic to intermediate calc-alkaline crust made up of diorite, tonalite, and granodiorite (Anderson, 1983). This model, as applied in the ANS, encompasses the melting of earlier arc rocks followed by anhydrous fractionation giving rise to magmas that retain a calc-alkaline signature (Kessel et al., 1998; Jarrar et al., 2003, 2008), such as the Ar Rayn alkali-feldspar granites, described above. A third model, one which is increasingly applied to Ediacaran ANS and West African granitoids, is that they derive from partial melting of phlogopite-bearing spinel lherzolite perhaps from OIB-type lithospheric–asthenospheric mantle (e.g., Liégois et al., 1998; Jarrar et al., 2008) present in subduction-modified mantle wedges under tectonothermal conditions created by slab break-off or delamination following cessation of subduction (Finger et al., 2008).

Whatever their origin, granites dominate late Cryogenian–Ediacaran magmatism in the ANS. They constitute the most abundant rock type of this period exposed at the surface and, on the basis of seismic refraction data, are inferred to be the main component of the upper 20 km of lithospheric crust in the Arabian Shield (Gettings et al., 1986). The Nubian crustal structure is presumably similar and the structure of both Arabian and Nubian Shields reflects a massive emplacement of granitic magma in the closing stage of evolution of the northern EAO.

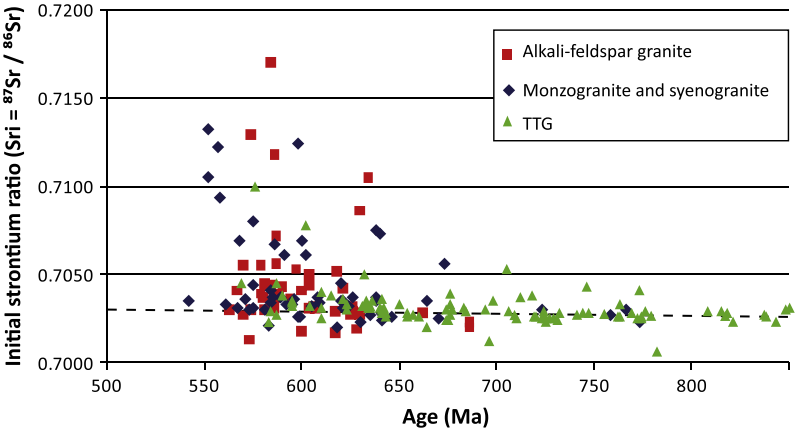

Fig. 14. Initial $^{87}Sr/^{86}Sr$ for plutonic rocks from the Arabian Shield, by general rock type. The TTG series includes diorite, tonalite, trondhjemite, granodiorite, and some gabbro. The data are taken from a table of geochronologic data for the shield compiled by Johnson and Kattan (2007), see for data sources. The dashed line is a Sr-evolution curve indicating a single-stage evolution of depleted mantle from initial $^{87}Sr/^{86}Sr$ of 0.699 at 4.6 Ga to the average modern island-arc value of 0.7037 (adapted from Fleck et al., 1980). The close fit of TTG values to the evolution curve is consistent with the juvenile character of ANS TTG plutonic rocks, which have initial $^{87}Sr/^{86}Sr$ expected for melts formed during the period 850–600 Ma in intraoceanic island arcs. The slightly elevated initial $^{87}Sr/^{86}Sr$ of younger granitic rocks suggests a contribution to the melts from more differentiated sources with higher Rb/Sr, perhaps reflecting partial melting of a thickened crust.

5. Gneiss domes and belts

Gneiss is not widespread in the ANS but is locally present in (1) high-grade parts of arc terranes and Neoarchean–Paleoproterozoic crust in the Abas and Al Mahfid terranes in Yemen (Windley et al., 1996), in the Khida terrane in Saudi Arabia (Stoeser et al., 2001), in the Barka terrane and along the western margin of the Red Sea in Eritrea (Ghebreab et al., 2005); (2) along early to middle Cryogenian sutures zones including the Bi'r Umq–Nakasib suture (Johnson et al., 2003; Hargrove, 2006), the Hulayfah–Ad Dafinah–Ruwah fault zone (Johnson and Kattan, 2001), and the Nabitah fault zone (Stoeser and Stacey, 1988); and (3) as belts and domes of late Cryogenian–Ediacaran gneiss along or close to NW- to WNW-trending fold structures and strike-slip faults in the northern part of the ANS, north-trending shear zones in the southern ANS, and north-trending shortening zones in the Nubian Shield (e.g., Sturchio et al., 1983a,b; El Ramly et al., 1984; Stern et al., 1989; Greiling et al., 1994; Fritz et al., 1996; Fowler and Osman, 2009; Al-Saleh, 2010; Andresen et al., 2010). The late Cryogenian–Ediacaran gneisses are particularly important and are the focus of attention here (Fig. 10).

Late Cryogenian–Ediacaran gneiss in the ANS is chiefly orthogneiss, but in places includes significant paragneiss. The gneiss reflects upper greenschist-amphibolite grade metamorphism under highly ductile to brittle–ductile conditions of deformation. It characteristically consists of mylonitic gneiss containing prominent mineral and stretching lineations and abundant microkinematic shear-sense indicators. Much of the gneiss is probably exhumed ANS middle crust, largely molten because of the magma mush pillow that made up ANS lower crust (Stern and Johnson, 2010), but some, particularly in the Arabian Shield, is likely made up of syntectonic intrusions. In the Arabian Shield, late Cryogenian–Ediacaran gneiss crops out as relatively narrow northwest-trending gneiss belts (Fig. 15). In the Nubian Shield, the gneiss bodies mainly crop out in the cores of structural highs spatially associated with thrust duplexes, strike-slip faults and extensional faults (Fig. 16), and are referred to as gneiss domes or metamorphic core complexes.

5.1. Gneiss belts in the Arabian shield

The longest single gneiss belt in the Arabian Shield is the Hajizah–Tin gneiss, located along the Ruwah fault zone in the eastern shield (Fig. 15B). A series of other belts—the Kirsh, An Nakhil, Wajiyah, and Ajjaj–Hamadat–Qazaz gneisses—form parts of an *en-echelon* Najd fault zone about 1300 km long (referred to as the Qazaz–Ar Rika shear zone) that extends NW across the entire Arabian Shield and continues into the Eastern Desert as the Meatiq, El Sibai, and Hafafit gneiss domes and associated Najd faults (Fig. 10). These gneisses reflect regions along the Najd faults affected by brittle–ductile deformation and greenschist-amphibolite metamorphism; intervening regions were affected by brittle deformation in low grade (greenschist or lower) rocks. This implies that along their strike, the Najd faults pass through several *P*/*T* amphibolite-to-greenschist transitions.

The *Kirsh gneiss belt* (Fig. 15A) consists of an antiform of strongly foliated biotite monzogranite orthogneiss (Al Hawriyah anticlinorium), a belt of steeply dipping kyanite-quartz schist and paragneiss, and subvertical zones of mylonite and ultramylonite (Al-Saleh, 2010). The monzogranite is located in a zone of extension between left-stepping faults along the sinistral Ar Rika shear zone. Left-stepping faults on the southwest side of the shear zone contain a down-faulted section of nonmetamorphosed Jibalah group sedimentary rocks in the Kibdi basin. The Kirsh gneiss has gently NW- and SE-plunging mineral and stretching lineations (Fig. 15A inset). The gneiss is mostly an LS-tectonite, suggesting flattening as well as simple shear, but locally is an L-tectonite, indicating a large component of constriction, or unidirectional stretching. The lineation orientation is replicated in all the Najd-fault gneiss belts in the Arabian Shield and in the gneiss domes in the Eastern Desert and is one of the over-arching structural features of the Najd fault system across the region.

The gneiss belt evolved between about 645 and 590 Ma. Its maximum age is possibly constrained by granite gneiss and pegmatite along the shear zone that have U–Pb SHRIMP crystallization ages of 647 ± 8 Ma (Kennedy et al., 2010) and 637 ± 2 Ma (Kennedy et al., 2005) (Table 3). If the granite is syntectonic, its age would suggest an onset of deformation toward the end of the Nabitah orogeny, during early Murdama deposition. The presence of elongated pebbles in Murdama-group conglomerate (in places, granite pebbles have long axes of 1–2 m) indicates, however, that major ductile deformation in the Kirsh gneiss belt postdated deposition of the Murdama group (~650–625 Ma). Zircon rim overgrowths in the 647 Ma granite gneiss and ~637 Ma pegmatite suggest hydrothermal events between 623 and 589 Ma (Kennedy et al., 2005), consistent with active shearing until about 590 Ma. An

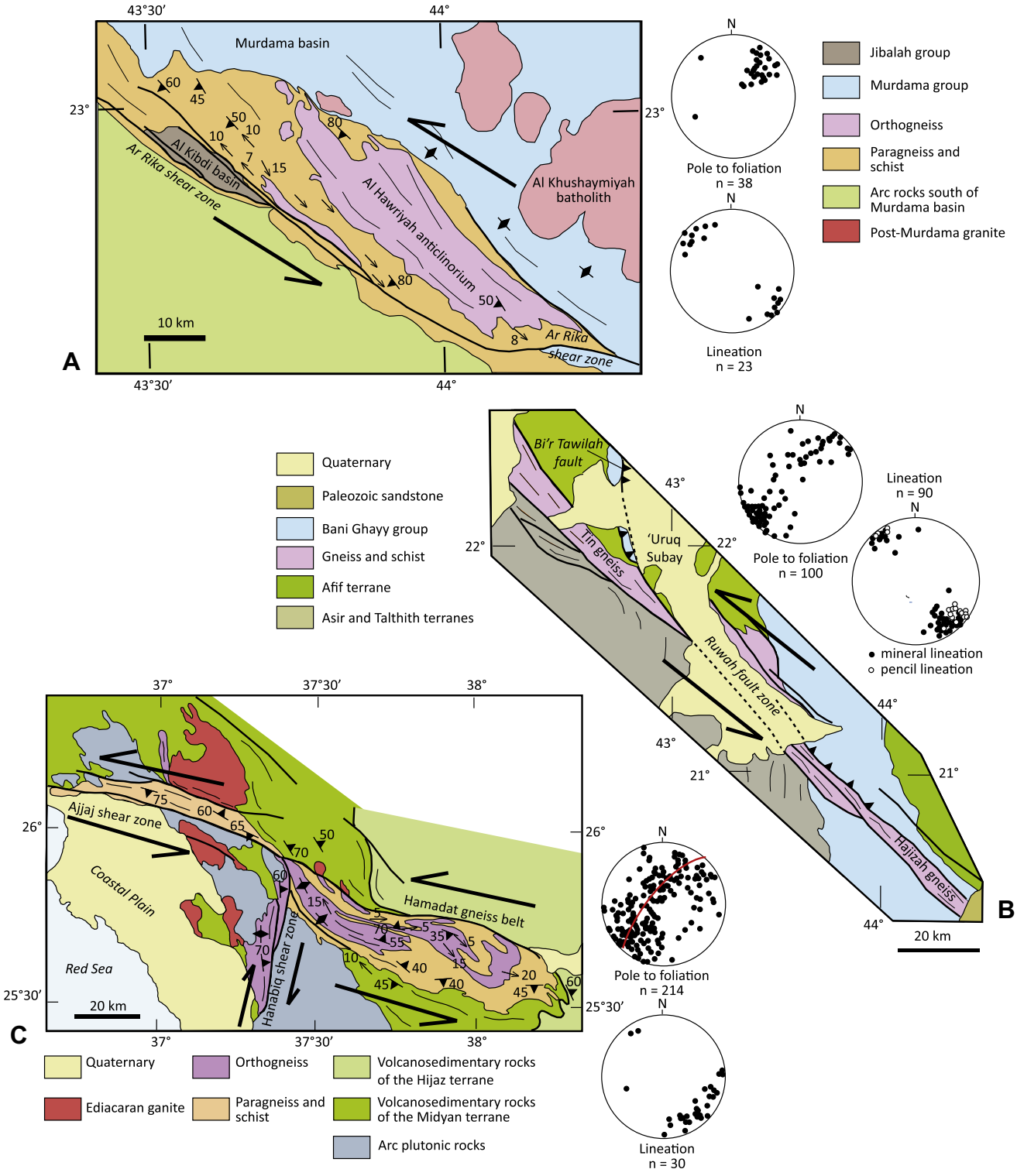

Fig. 15. Simplified geologic maps of selected gneiss belts in the Arabian Shield. A. Kirsh (Al Hawriyah) gneiss belt along the Ar Rika shear zone. B. Hajizah–Tin gneiss belts along the Ruwah fault zone. C. Hamadat gneiss belt and Ajjaj shear zone. Note the consistent NW–SE gentle plunge of lineations throughout the gneiss belts and the broad girdles shown by the plot of poles to foliations for the Hajizah–Tin and Hamadat gneisses suggesting folding of the gneisses. Antiformal structures are reported in the literature for the Al Hawriyah and Hamadat gneisses, but not for the Hajizah–Tin gneiss. See Fig. 10 for locations of these gneiss belts in the ANS.

$^{40}Ar/^{39}Ar$ age of 557 ± 15 Ma obtained from biotite paragneiss is interpreted as the time of cooling below the biotite closure temperature (Al-Saleh, 2010) and the cessation of deformation in the gneiss belt.

The *Hajizah–Tin gneiss belt*, 5–10 km wide and more than 160 km long (Johnson and Kattan, 2001) (Fig. 15B), consists of amphibolite-grade mylonitic orthogneiss, subordinate paragneiss, and minor serpentinite. It crops out along the Ruwah fault zone and may have a complicated history, having undergone initial ductile deformation during the Nabitah orogeny, when the Ruwah fault zone formed part of the Cryogenian suture between the Afif terrane and other terranes to the S, and having undergone

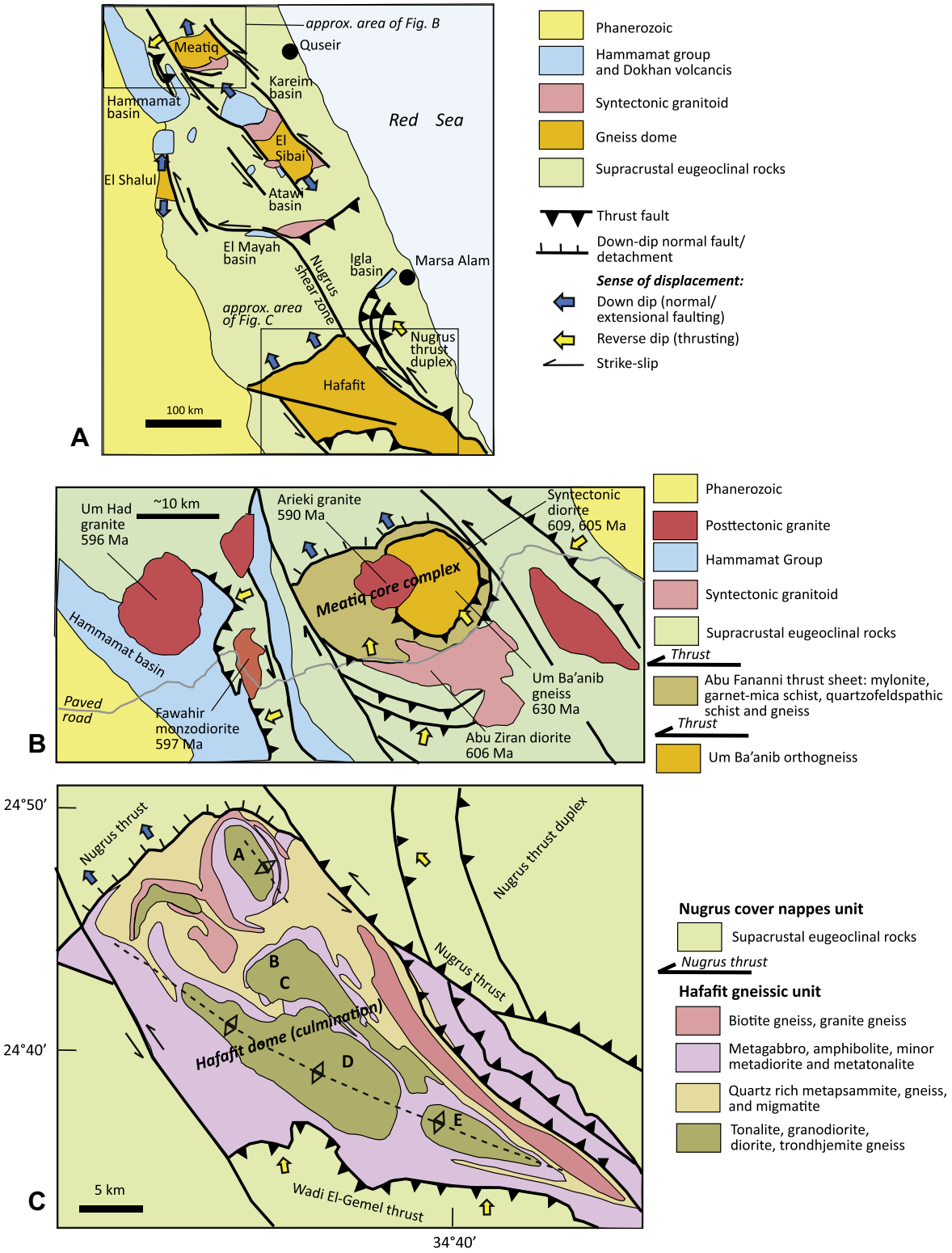

Fig. 16. Gneiss domes in the Eastern Desert, Egypt. (A) Regional structural setting (after Fritz et al. (1996)). (B) Meatiq Dome (after Fritz et al. (1996) and Andresen et al. (2009, 2010)). (C) Hafafit Dome (after Greiling (1997), Abd El-Naby et al. (2008), Shalaby (2010)).

remobilization during late Cryogenian–Ediacaran Najd faulting. Ultramafic rocks are present as lenses, altered by carbonate-rich fluids (listwaenite), along faults at the northern and southern margins of the gneiss belts. SW-verging thrust slices of barely metamorphosed Bani Ghayy group rocks overlie amphibolite on the northeastern side of the gneiss belt, and late- to posttectonic granite and gabbro and mafic and felsic dikes intrude the gneisses. Orthogneiss in the Hajizah gneiss belt is gray, fine-grained to very fine-grained, thinly layered trondhjemite gneiss, tonalite gneiss, quartz diorite, and hornblende diorite gneiss, all with well-developed mylonitic/ultramylonitic fabrics. The rocks are regionally metamorphosed to the almandine-amphibolite facies (Schmidt,

1981) and locally retrogressively metamorphosed along shear zones to epidote–biotite–hornblende assemblages representative of the upper-greenschist facies. The Hajizah gneiss was exhumed prior to overthrusting by the Bani Ghayy group. Both gneiss and overthrust Bani Ghayy group rocks are displaced by brittle sinistral Riedel faults oblique to the main trend of the gneiss belt and intruded by posttectonic dikes, signaling the cessation of brittle–ductile deformation along the Ruwah fault. L-tectonite is locally present, but LS-tectonite is the dominant rock type. Mineral and stretching lineations plunge gently to the NW or SE, comparable to those in the Kirsh gneiss. The maximum age of deformation in the Tin gneiss is constrained by a granodiorite gneiss protolith age of 683 ± 9 Ma (Stacey and Agar, 1985). An Rb–Sr age of 782 ± 26 Ma reported for orthogneiss in the Hajizah gneiss belt (Kröner et al., 1979) may reflect isotopic resetting of an even older protolith formed about 870 Ma. The minimum age of brittle–ductile deformation and metamorphism is constrained by an undeformed "Najd" granite dated 592 ± 4 Ma (Stoeser and Stacey, 1988) that intrudes the gneiss belt. An Rb–Sr potassium feldspar age of 530 ± 20 Ma and a K–Ar plagioclase age of 539 ± 20 Ma obtained from granite gneiss suggests that possible fault-induced isotopic disturbance on the gneiss belt continued as late as the early Cambrian (Kellogg et al., 1986), but such young ages require further confirmation before they are accepted as indicating that tectonic activity continued into Cambrian time. The broad girdle outlined on the plot of poles to foliation in Fig. 15B suggests large-scale folding of the gneiss belt but, unlike the Kirsh gneiss, no megascale antiformal or synformal structure has been observed in the field. Tight mesoscale folds in gneissic foliation are locally present, plunging gently SE and NW parallel to the observed lineations, but the belt as a whole has the appearance of a steeply dipping homocline.

High-grade rocks along the *Qazaz* and *Ajjaj shear zone* and *Hamadat gneiss belt* (Fig. 15C) include hornblende gneiss, tonalite gneiss, granodiorite gneiss, and granite gneiss. Strongly deformed volcanic and sedimentary rocks include quartzofeldspathic schist, amphibolite and amphibole schist, migmatite of alternating quartzofeldspathic and amphibole schist, garnet- and kyanite-bearing schist, and schistose volcanic rocks. Abundant S–C and S–C′ fabrics and rotated porphyroclasts consistently indicate a sinistral sense of shear. The maximum age of ductile deformation and high-grade metamorphism is not well constrained, but the presence of strongly elongated pebbles demonstrates that much searing postdated deposition of the Thalbah group (660–620 Ma). Ductile deformation continued until at least 575 Ma, the protolith age of granite gneiss on the northern margin of the Ajjaj shear zone, but ceased very shortly after that, prior to the intrusion of undeformed 573 Ma lamprophyre dikes (Kennedy et al., 2011). The Ajjaj shear zone and Hamadat gneisses are strongly foliated and lineated with lineations plunging gently SE and NW. L–S fabrics predominate but L-tectonites are locally present. Poles to foliation in the Hamadat gneiss (Fig. 15C) define a broad girdle, compatible with the map-scale anticlinorium that has been mapped in the gneiss, and broad antiformal structures are found in part of the Qazaz gneiss.

The northwest-trending Ajjaj shear zone is notable for its intersection with the north-trending *Hanabiq* dextral shear zone and *Baladiyah* gneiss (Fig. 15C), although the temporal and structural relationships between the gneisses and shear zones are yet to be fully established. Duncan et al. (1990) concluded that the Hanabiq shear zone is a continuation across the Red Sea of the Hamisana shear zone of the Nubian Shield (location shown in Fig. 10) and that the Ajjaj crosscuts the Hanabiq. Alternatively, the Hanabiq may form a "zipper" shear with the Ajjaj shear zone (Passchier, 2010). The Baladiyah gneiss has a protolith age of 676 Ma (conventional U–Pb zircon age; Hedge, 1984), indicating that the magmatic rock forming the gneiss was in place prior to movement on the Ajjaj shear zone. Overgrowth rims on zircons in the Baladiyah gneiss at 610 Ma may date metamorphism accompanying movement on the Ajjaj shear zone (Kennedy et al., 2010).

5.2. Late Cryogenian–Ediacaran gneisses in the Eastern Desert and Sinai

Gneisses on the Qazaz–Ajjaj shear zone continue into the Central and South Eastern Desert of Egypt as gneiss domes at Meatiq, El Sibai, and Hafafit (Fig. 16) (Sturchio et al., 1983a; Greiling et al., 1994; Fritz et al., 1996; Fowler and Osman, 2001; Bregar et al., 2002; Andresen et al., 2009). The gneiss domes are polydeformed, polymetamorphosed (Neumayr et al., 1998), and lithologically complicated. As a consequence, their origin, age, structure, and tectonic implications are debated. Nonetheless, all workers recognize that they are important to our understanding of ANS geology because they are windows into the structural infracrust and deeper part of the region and are at the heart of the debate about the presence or not of "older basement" in the region. In the early and "classical" Egyptian literature, the orthogneiss in the cores of the gneiss domes is considered to be an extension of the middle-Proterozoic crust exposed in the Western Desert of Egypt (e.g., El-Gaby et al., 1988, 1990) or derived by partial melting of such crust (Khudeir et al., 2008). However, there is a growing body of robust geochronologic and isotopic data that indicates the gneisses are variably deformed calc-alkaline Neoproterozoic intrusions and juvenile arc-related Neoproterozoic crust of the ANS (e.g., El Ramly et al., 1984; Greiling et al., 1984, 1988; Kröner et al., 1987; Andresen et al., 2009; Liégeois and Stern, 2010).

Many structural features of the Egyptian gneiss domes are similar to those in the gneiss belts exposed in the Arabian Shield. They have subhorizontal NW–SE-trending stretching lineations that are parallel in some cases to the overall dome axes. The dip of foliation is steep along the southwestern and northeastern dome margins and flat within the dome cores defining apparent antiforms (Fowler and Osman, 2001; Andresen et al., 2010). All of the domes are broadly aligned along a northwest-trending system of ductile to brittle shear/fault zones, referred to as the "Najd Corridor" (Fritz et al., 1996), which most workers correlate with the Najd fault system in the Arabian Shield. Both the Arabian Shield gneiss belts and the Eastern Desert gneiss domes evidence NW-directed extension. In the Arabian Shield, the evidence consists of pervasive stretching lineations and elongated sedimentary clasts (pebbles). In the Eastern Desert the evidence consists of normal faults and shear zones that developed predominantly along the northwestern and/or southeastern dome margins, and around depositional basins that evolved close to the domes, particularly adjacent to the bordering fault zones (Fritz et al., 2002). It should be noted, however, that the structural relationships of the gneiss domes are not always clear and are the subject of debate because different segments of the shear-extension system hosting the domes were affected by different amounts of displacement and strain partitioning (Fritz et al., 2002). As a consequence, some authors interpret the high-strain zones around the domes to be low-angle detachment faults; others consider the structural contacts to be the remnants of NW-directed thrusts (Andresen et al., 2010). Some authors envisage the domes to be controlled by extension in the "Najd-fault corridor" with normal faults representing extensional bridges or releasing steps between strike-slip Najd faults (Fritz et al., 2002). Still others treat the northwest-trending faults around the gneiss domes as due to later deformation superimposed on earlier high-strain zones.

Despite a lack of agreement about details, however, a general structural model for the evolution of the Egyptian gneiss domes has emerged. The model envisages an early phase of hanging wall displacement toward the northwest, possibly at the time of terrane accretion in the Eastern Desert, which emplaced ophiolite-bearing

Table 3
Geochronologic constraints on Najd faulting: a list of intrusive and(or) sedimentary and volcanic rocks that predate, postdate, are cut by, or are deformed by Najd faults and thereby help to constrain movements on the faults.

Age	Unit dated	Method	Fault zone affected	Comment	Source
591 ± 6	Undeformed "Najd granite"	U–Pb zircon Concordia method	Ruwah fault zone	A massive granite that intrudes the Ruwah fault; constrains cessation of movement on the fault	J.S. Stacey, written communication, 1983; cited by Kellogg et al. (1986)
Qazaz–Ajjaj shear zone					
705 ± 4	Zaam group paragneiss	U–Pb, SHRIMP	Qazaz–Ajjaj	Predates deformation on Ajjaj shear zone	Kennedy et al. (2010a, 2011)
670 ± 10	Hamadat diorite gneiss	U–Pb, SHRIMP	Qazaz–Ajjaj	Pre-dates Najd deformation	Kennedy et al. (2004)
630 ± 19	Raydan pluton	Rb–Sr	Qazaz–Ajjaj	Granite cataclastically deformed by Najd faulting: age probably reflects open isotopic system and perhaps the onset of active faulting	Kemp et al. (1980)
626 ± 4	Abu Suar complex; granite	U–Pb, SHRIMP	Qazaz–Ajjaj	Predates deformation on Qazaz shear zone	Kennedy et al. (2011)
609 ± 4	Ash Sha'b complex	U–Pb, SHRIMP	Qazaz–Ajjaj	Suspect syntectonic granite: massive immediately north of shear zone; altered to mylonitic gneiss within the shear zone: implies ductile deformation about or soon after 609 Ma	Kennedy et al. (2011)
599 ± 5 (core) 570 ± 5 (rim)	Jibalah group, Dhaiqa formation	U–Pb, SHRIMP	Qazaz–Ajjaj	Possible age of igneous zircon, implying deposition </= 599 Ma. Constrains brittle Najd deformation	Kennedy et al. (2011)
575 ± 10	Foliated granite on margin of Ajjaj shear zone		Qazaz–Ajjaj	Suspect syntectonic granite, synchronous with ductile deformation on Ajjaj shear zone	Kennedy et al. (2011)
573 ± 6	Undeformed lamprophyre dikes cross cutting Ajjaj shear zone gneiss		Qazaz–Ajjaj	Constrains cessation of ductile deformation on Ajjaj shear zone	Kennedy et al. (2011)
560 ± 4	Jibalah group, Dhaiqa formation		Qazaz–Ajjaj	Age of igneous zircon; constrains maximum deposition age and timing of brittle Najd deformation	Vickers-Rich et al. (2010)
Halaban-Zarghat					
624.9 ± 4.2	Murdama rhyolite: basement of Jifn basin	U–Pb	Halaban-Zarghat	Maximum age of formation of basin and initiation of dextral movement on Halaban-Zarghat fault	Kusky and Matsah (2003)
621 ± 8	An Nimriyah pluton: hornblende–biotite quartz monzodiorite	U–Pb	Halaban-Zarghat	Crystallization age: similar plutons in the area intrude Najd fault; implies onset of faulting predates 621 Ma	Cole and Hedge (1986)
621 ± 7	Mushrifah pluton: biotite–hornblende quartz diorite	U–Pb	Halaban-Zarghat	Pluton is cut by the Halaban-Zarghat fault; similar rocks exposed 10 km to the west on south side of fault: indicates right-offset after emplacement, and implies a <621 Ma period of dextral shearing	Cole and Hedge (1986)
620 ± 7	Al Asfah pluton: hornblende–biotite quartz monzodiorite (Idah suite)	U–Pb	Halaban-Zarghat	Truncates NW-trending splay faults that connect with Halaban-Zarghat fault: indicates offset on the splays had ended by about 620 Ma. Inferred that major transcurrent movement predates Idah suite, i.e. >620 Ma	Cole and Hedge (1986)
588 ± 12	Jabal Tukhfah granite	Rb–Sr	Halaban-Zarghat	May postdate Najd faulting; constrains cessation of movement	Fleck and Hadley (1982)
574 ± 28	Ar Rahadah pluton: alkalki-feldpsar granite	Rb–Sr	Halaban-Zarghat	Intrudes Murdama group and cut by Najd fault	Calvez et al. (1984)
576.6 ± 5.3	Undeformed felsite dike	U–Pb	Halaban-Zarghat	Intrudes Jibalah group in Jifn basin; gives a minimum age for movement on Halaban-Zarghat fault	Kusky and Matsah (2003)
573 ± 8	Habariyah monzogranite gneiss	U–Pb, SHRIMP	Halaban-Zarghat	Suspect syntectonic granite: 573 Ma is inferred main crystallization event: granite underwent hydrothermal alteration between 531–512 Ma. Constrains ductile deformation as 573 Ma or younger	Kennedy et al. (2005)
566 ± 8	Jibalah group (Antaq basin)	LA-ICP-MS	Halaban-Zarghat	Maximum deposition age; faulting active	Nettle (2009)
568 ± 11	Jibalah group (Antaq basin)	LA-ICP-MS	Halaban-Zarghat	Maximum deposition age; faulting active	Nettle (2009)
584 ± 10	Jibalah group (Antaq basin)	LA-ICP-MS	Halaban-Zarghat	Maximum deposition age; faulting active	Nettle (2009)
Ar Rika					
601 ± 4	Dahul granite	U–Pb	Between Ar Rika and Ruwah faults	Cut by brittle fault; implies brittle deformation as late as 601 Ma	Aleinikoff and Stoeser (1988)
579 ± 19	Kursh granite	Rb–Sr	Between Ar Rika and Ruwah faults	Cut by brittle fault; implies brittle deformation as late as 579 Ma	Calvez et al. (1983)
637 ± 2	Pegmatite in Kirsh granite gneiss	U–Pb, SHRIMP	Ar Rika	Possibly main crystallization event at ~637 Ma: subsequent recrystallization (metamorphic?) events between 623 and 589 Ma; constrains ductile deformation	Kennedy et al. (2005)
~600	Kirsh granite gneiss	U–Pb, SHRIMP	Ar Rika	A possible metamorphic age; consistent with ductile deformation at ~600 Ma	Kennedy et al. (2005)
~620–580	Kirsh granite gneiss	U–Pb, SHRIMP	Ar Rika	Possible crystallization age range	Kennedy et al. (2005)

(*continued on next page*)

Table 3 (*continued*)

Age	Unit dated	Method	Fault zone affected	Comment	Source
731 ± 8	An Nakhil gneiss: granite	U–Pb, SHRIMP	An Nakhil shear zone, part of Ar Rika-Qazaz system	Pre-dates Najd deformation	Kennedy et al. (2004)
567 ± 86	Abu Aris granite			Cut by Najd faults; implies brittle deformation as late as 567 Ma	Fleck and Hadley (1982)
632 ± 15	Haml suite: Awjah complex	U–Pb		Pluton cut by Najd fault; constrains maximum age of faulting	Stacey and Agar (1985)
632 ± 3	Hufayrah complex: alkali-feldspar granite	U–Pb		Pluton cut by Najd fault; constrains maximum age of faulting	Stacey and Agar (1985)
577 ± 21	Sanam pluton	Rb–Sr		Crystallization age is 607 ± 18 Ma: a younger age of 577 Ma reflects open isotopic system, consistent with active faulting	Calvez et al. (1983)
647 ± 8	Granite gneiss	U–Pb, SHRIMP	Ar Rika	Crystallization age about 647 Ma; subsequent thermal event about 600 Ma	Kennedy et al. (2011)
611 ± 3	Uwaiyjah complex	U–Pb	Ar Rika	Granodiorite immediately north of fault zone; If syntectonic, implies active faulting ~611 Ma; if posttectonic implies cessation of shearing and ductile prior to 611 Ma	Agar et al. (1992)

volcanosedimentary suites (supracrust) onto deeper parts of the crust (infracrust). The supracrustal rocks are part of the larger northwestward-verging thrust duplex of juvenile Neoproterozoic island-arc, sedimentary, and volcaniclastic rocks together with ophiolite fragments that make up most of the Eastern Desert. The infracrust contains calc-alkaline Neoproterozoic intrusions that underwent complex folding and thrusting and were transformed into gneiss that is exposed in dome cores. Other gneisses in the domes represent syntectonic intrusions emplaced during subsequent periods of northward displacement of the hanging wall. The juxtaposition of low-grade island-arc sequences of the hanging wall along a high strain zone against the intermediate and high-grade gneiss of the footwall indicates crustal scale thinning, best explained by extensional faulting, rather than thrusting (Fowler and Osman, 2009; Andresen et al., 2010). A distinctive recent interpretation is that the gneisses up-domed vertically through nappes of overthrust low-grade volcanosedimentary rocks of the Pan-African cover, having been previously emplaced during accretion of the nappes (Shalaby, 2010).

Ongoing convergence and Najd transpression buckled the infracrust and the high-strain zone between the infracrust and supracrust resulting in the emergence of domes with a general northwest-trending orientation. Along dome margins, oblique convergence partitioned into strike-slip and normal faults, most probably triggered by pronounced rheologic contrast between updomed gneissic infracrust and the rheologically weaker volcanosedimentary supracrust. Strike-slip faults developed preferentially on southwestern and northeastern dome margins (Fig. 16A and B), although this interpretation is subject to debate (Fowler and Osman, 2001; Andresen et al., 2010). In places, the domes are associated with oblique strike-slip thrust faults that evidence a significant vertical component of flow (Fig. 16C), and normal faults developed on northwestern and southeastern dome margins (Fig. 16A and B). This allowed for general NW–SE extension, causing dome exhumation and the development of intermontane basins such as the Kareim basin (Fig. 16A). Shear along strike-slip faults flanking the gneiss domes was generally sinistral. However, depending on specific local conditions and strain partitioning, different types of displacement may be observed such as shear reversal during dome exhumation, dextral shear, and normal (extensional) faulting (Andresen et al., 2010).

The initiation of extensional tectonics in the Eastern Desert may be determined by: (1) the ages of pre-, syn- and posttectonic plutons that intrude the gneiss domes; (2) the structural relations between the gneiss domes and sedimentary basins; and (3) direct dating of deformation, metamorphism, and general cooling of the domes. Although a diachronous evolution is suggested (Fritz et al., 2002), geochronologic work by Andresen et al. (2009) suggests, as a general model, that exhumation commenced around 620–606 Ma (oldest $^{40}Ar/^{39}Ar$ cooling ages and emplacement of extension related Abu Ziran granitoid), continued at intermediate crustal level for about 49 m.y., and ceased prior to emplacement of discordant posttectonic granitoids at about 580 Ma (see below for arguments from individual areas). It should be noted, furthermore, that most of the sedimentary rocks deposited within post-amalgamation Hammamat Group basins close to the gneiss domes are deformed, clearly indicating that shearing outlasted this sedimentation (Fowler and Osman, 2001; Abdeen and Greiling, 2005; Abdeen et al., 2008).

The geodynamic setting of the gneiss domes is a matter of discussion. Analogies have been drawn, on the one hand, with classic metamorphic core complexes, invoking gravitational collapse and extrusion tectonics (“extensional settings”) and, on the other hand, with an interplay between thick-skinned and thin-skinned thrusting (“compressional settings”). Aside from the fact that extensional and compressional settings may coexist during orogeny (in this case, Najd shearing), understanding the driving mechanism requires knowledge about the general state of the late Neoproterozoic lithosphere in the region of what is now the EAO. It is particularly important to understand: (1) the relative contribution of body (gravitational) forces versus boundary (plate) forces; (2) the configuration of plate boundaries, particularly the boundary of the entire EAO against paleoTethys and whether this was a zone of subduction or extension; and (3) the thermal state of the lithosphere. These issues will be considered in more detail in a forthcoming review of the EAO by H. Fritz and colleagues.

The *Meatiq Dome* (or core complex) (Sturchio et al., 1983a,b; Loizenbauer et al., 2001; Andresen et al., 2009, 2010) (Fig. 16B) consists of two units of quartzofeldspathic gneiss, schist, and mylonite—the Um Ba’anib orthogneiss and the Abu Fananni thrust sheet—structurally overlain by supracrustal rocks (island-arc volcanics, sedimentary rocks, and ophiolitic rocks) belonging to the typical juvenile crust of the Eastern Desert. Andresen et al. (2009) refer to the overlying rocks as a “eugeoclinal thrust sheet”. The dome is an oval outcrop about 25 km WSW–ENE and 15 km NNW–SSE comprising an asymmetric doubly plunging antiform trending NW–SE to NNW–SSE. The Um Ba’anib orthogneiss (630 Ma; Andresen et al., 2009), in the core and forming the lowest structural level of the dome, consists of recrystallized granitoid of possible granodiorite origin (Andresen et al., 2009). The overlying Abu Fananni thrust sheet consists of variably deformed and mylonitized intrusive and subordinate sedimentary rocks comprising garnet-mica schist and quartzofeldspathic gneiss and schist (Habib et al., 1985). The contact between the Um Ba’anib gneiss and Abu

Fananni thrust sheet is a zone of mylonite 100–200 m thick. The two may originally have had a quasi-depositional relationship, but kinematic indicators demonstrate that the Abu Fananni thrust sheet has been translated to the northwest over the Um Ba'anib orthogneiss (Loizenbauer et al., 2001; Andresen et al., 2009, 2010). The Um Ba'anib and Abu Fananni rocks contain conspicuous NW–SE to NNW–SSE-trending stretching lineations formed under conditions of amphibolite facies metamorphism and sparse kinematic indicators indicating top-to-the-NW displacement (Sturchio et al., 1983a,b; Andresen et al., 2009). The overlying ophiolitic and volcanosedimentary supracrustal rocks are separated from the underlying gneissic rocks by a high-strain zone referred to as the Eastern Desert Shear Zone (EDSZ) (Andresen et al., 2010). It is a top-to-the-NW shear zone (Fritz et al., 1996; Fowler and Osman, 2001; Fowler and El Kalioubi, 2004; Andresen et al., 2009). The EDSZ is intruded by the syntectonic Abu Ziran diorite (606 ± 1 Ma) (Andresen et al., 2009). Hammamat Group sedimentary rocks 20 km west of the Meatiq Dome are partly unconformable on and partly overthrust by the supracrustal rocks. Fritz et al. (1996) argue that the thrust-emplacement of supracrustal rocks over the Hammamat group reflects W- to SW-tectonic transport, which was contemporary with the NW-transport of the eugeoclinal thrust sheet at the Meatiq Dome itself, and is evidence of strong regional strain partitioning in this part of the Central Eastern Desert. It may, alternatively, reflect progressive deformation and a switch from NW-directed extension to transpression associated with bulk E–W shortening. The Hammamat rocks themselves were folded and overthrusted prior to intrusion of the posttectonic Um Had granite (596 ± 2 Ma) (Andresen et al., 2009) (Fig. 16B).

The Meatiq Dome is commonly viewed as being overprinted by northwest-trending strike-slip faults on the east and west and by gently dipping normal faults on the south and north (e.g., Fritz et al., 1996). Those on the east and west are steep, NW- to NNW-trending shears interpreted by most workers as a pair of sinistral Najd faults (e.g., Loizenbauer et al., 2001) that continue from the Arabian Shield as an extension of the Qazaz shear zone, and were active during exhumation of the dome. Andresen et al. (2010) report, however, that the shear zone on the northeastern flank of the dome is left lateral whereas that on the southwestern flank is right lateral, which is not compatible with the shear zones being part of a "Najd corridor". Instead, Andresen et al. (2010) argue that the shear zones are the effect of folding the EDSZ about a NW-trending axis. Either model, nonetheless, implies NE–SW shortening and NW–SE extension. In this context, the warning by Fowler and Osman (2001) is apposite, that "caution must be exercised in the recognition of transcurrent shears in the Eastern Desert since folded low-angle thrust-related mylonitic zones may be steepened by folding, producing steep shear zones with low-pitching slip lineations" (pg. 17). Lateral shear together with NW–SE extension is suggested from the intermontane Kareim basin, south of the Meatiq Dome (Fig. 16A). The basin is bound by northwest-trending steep shear zones and NW-dipping normal faults (Fritz and Messner, 1999), reflecting general NW–SE extension. NW–SE extension is viewed as causing the exhumation of high-grade infracrustal rocks into the core of the dome, concurrent with sinistral strike-slip shearing on the eastern and western margins, the emplacement of syntectonic granitoids, and NE–SW contraction (Fritz et al., 1996, 2002; Fritz and Messner, 1999). The southern Kareim basin is intruded by a posttectonic granitoid (Al Dabbah granodiorite: Fowler et al., 2007) causing contact metamorphism of basal strata of the sedimentary succession in the Kareim basin. This could narrow down the time of sedimentation but unfortunately this magmatic body is not dated.

Um Ba'anib gneiss protolith ages range from 779 ± 4 Ma ($^{207}Pb/^{206}Pb$ dating of an evaporated single zircon; Loizenbauer et al., 2001) to 626 ± 2 Ma (Rb–Sr whole-rock isochron; Sturchio et al., 1983b), but a recent ID-TIMS age of 630.8 ± 2.0 Ma obtained from dating of two fractions of zircon is possibly the most reliable crystallization age (Andresen et al., 2009). The 630 Ma age of emplacement of the Um Ba'anib orthogneiss protolith provides a maximum age for the ductile fabric recorded in the Um Ba'anib gneiss. The timing of ductile deformation in the Abu Fananni thrust sheet, which may reflect the time of northwestward displacement of the Abu Fananni thrust sheet (Andresen et al., 2009) or onset of younger extension, is constrained by syntectonic diorite dated at 609 ± 1.0 Ma and 605.8 ± 0.9 Ma (Andresen et al., 2009). The minimum age of the Um Ba'anib gneiss-forming event, as well as the minimum age for juxtaposing the Um Ba'anib and Abu Fananni gneisses, is constrained by the posttectonic Arieki granite (590.5 ± 3.1 Ma: Andresen et al., 2009) that intrudes the Um Ba'anib orthogneiss and Abu Fananni thrust sheet. The age of the main shearing in the region that emplaced the supracrustal rocks over the infracrustal gneisses in the Meatiq Dome is constrained by the interpretation adopted for the Abu Ziran diorite (606 ± 1 Ma). Andresen et al. (2009) interpret the diorite as a syntectonic intrusion into the mylonitic gneisses along the contact between the Abu Fannani thrust sheet and the supracrustal rocks and conclude that the supracrustal rocks were translated over the gneissic rocks prior to about 606 Ma. The Abu Ziran pluton, alternatively, has been interpreted as a magmatic body emplaced during extension and exhumation of the Meatiq Dome and coeval with southward displacement of its low-grade structural cover (Fritz and Puhl, 1997). The $^{40}Ar/^{39}Ar$ ages of white mica from the extensional shear zone at the southern margin of the Meatiq Dome indicate that NW–SE extension was initiated by 585 Ma (Fritz et al., 1996). The minimum age of sedimentation and deformation in the Hammamat basin west of and external to the Meatiq Dome is constrained by the posttectonic Um Had granite (596.3 ± 1.7 Ma) (Andresen et al., 2009), which intrudes the Hammamat and supracrustal rocks that were thrust westward over the Hammamat (Fig. 16B). Because the Um Had granite is not in contact with the Meatiq Dome, however, the age of the granite does not necessarily constrain the end of deformation in the internal part of the dome or in the "Najd corridor" flanking the dome. Taking the available geochronology into account, Andresen et al. (2009) concluded that the Meatiq Dome represents a young structural feature (<631 Ma) and that shearing and concurrent sedimentation and magmatism within and around the dome took place in a relatively short interval between 610 and 595 Ma. The timing of final exhumation of the Meatiq Dome is constrained by hornblende and white mica $^{40}Ar/^{39}Ar$ ages between 587 Ma and 579 Ma obtained from the Um Ba'anib orthogneiss (Fritz et al., 2002), close to the 590 Ma intrusion age of the posttectonic Arieki granite. The $^{40}Ar/^{39}Ar$ ages are interpreted as the time of cooling below the blocking temperatures for hornblende and white mica, respectively, and the timing of rapid exhumation of the dome.

Like the Meatiq Dome, the *Hafafit Dome* (or culmination) also comprises a structural high made up of high-grade orthogneiss and paragneiss flanked and structurally overlain by low-grade supracrustal rocks. The high-grade rocks, referred to as the Hafafit gneissic unit (Abd El-Naby et al., 2008; Shalaby, 2010), include (1) up to five separate small domes of tonalitic and trondhjemitic gneiss (lettered A–F in Fig. 16C); (2) a heterogeneous unit of metagabbro, massive and foliated amphibolite, minor metadiorite, and metatonalite; (3) quartz-rich metapsammite, metapsammitic gneiss, and migmatite; and (4) biotite-rich gneiss and granite gneiss. Structurally, the tonalitic and trondhjemitic domes and other rocks are a set of interference folds locally involving migmatites (Greiling et al., 1994; Fowler and El Kalioubi, 2002). The overlying low-grade supracrustal rocks, referred to as the Nugrus unit and equivalent to the supracrustal rocks flanking the Meatiq Dome,

consist of low-grade mica schist, metavolcanics, serpentinite, and metagabbro. They are separated from the high-grade rocks of the dome on the east by a steeply dipping shear zone (the Nugrus thrust) with a significant component of sinistral strike slip evidenced by a thick mylonitic zone (Greiling et al., 1988; El Ramly et al., 1984). Fowler and Osman (2009) model this mylonite zone as a folded low-angle extension-related normal shear. On the south and southwest, the Hafafit gneisses are bounded by the low-angle Wadi El-Gemel thrust, on the west by a NW-tending sinistral strike slip fault, and on the north by a low-angle normal fault. The granitic gneisses in the core of the Hafafit dome have been interpreted as pre-Neoproterozoic basement (El-Gaby et al., 1984, 1988) but U–Pb dating of zircons yield a crystallization age of 682 Ma or less (Stern and Hedge, 1985; Lundmark et al., 2011) demonstrating that the high-grade rocks are ANS juvenile crust. Whole-rock samples of biotite gneiss, hornblende gneiss, and amphibolite and garnet and plagioclase mineral separates yield Sm–Nd ages of 593 ± 4 and 585 ± 8 Ma, which are interpreted as the timing of cooling and exhumation following peak metamorphism (Abd El-Naby et al., 2008) consistent with $^{40}Ar/^{39}Ar$ ages of 586.1 ± 0.3 Ma and 584.2 ± 0.2 Ma obtained by Fritz et al. (2002) for hornblende separates from the dome. A slightly younger Sm–Nd age of 573 ± 6 Ma may reflect a later stage of cooling (Abd El-Naby et al., 2008). Garnet–biotite, garnet–amphibole, and amphibole–plagioclase geothermometry yields temperatures of 600–750 °C for metamorphism in gneiss and amphibolite within the Hafafit dome, and garnet-hornblende-plagioclase-quartz geobarometry suggests pressures of 6–8 kbar. Nd and Sr isotopic data also indicate that Hafafit gneisses represent juvenile Neoproterozoic crust (Liégeois and Stern, 2010).

In Sinai, late Cryogenian layered gneiss and associated syntectonic granodiorite referred to as the *Feiran–Solaf metamorphic belt* (Fowler and Hassen, 2008) crop out in the Wadi Feiran area as a series of northwest-trending anticlines overturned to the west and separated by northwest-trending thrust faults (El-Shafei and Kusky, 2003). The rocks are referred to in the literature as paragneiss (Akkad et al., 1967a,b) but low $^{87}Sr/^{86}Sr$ (0.7034–0.7039) suggests that the protoliths were very immature, volcanogenic wacke or lithic wacke interbedded with felsic tuffs (Stern and Manton, 1987). The gneiss has been dated using Rb–Sr whole-rock techniques at 643 ± 41 Ma (Bielski, 1982) and 614 ± 27 Ma (Stern and Manton, 1987), who also report a thin-layer Rb–Sr age of 610 ± 44 Ma. Conventional U–Pb dating of a single fraction of zircon yields an age of 632 ± 3 Ma (Stern and Manton, 1987). The U–Pb age may approximate the age of the protolith or the age of the crust sampled by protolith sediments, and the Rb–Sr ages may approximate the age of metamorphism and deformation that formed the gneiss (Stern and Manton, 1987). Clearly the Feiran gneiss formed in early Ediacaran times, as further indicated by a 591 ± 9 Ma (Rb–Sr whole-rock) posttectonic dike, which gives a minimum age for Feiran gneiss formation (Stern and Manton, 1987). The Feiran gneiss defines one of the most striking crustal boundaries in the ANS, separating early Cryogenian and latest Mesoproterozoic crust to the northeast from late Cryogenian and younger crust to the southwest, all intruded by Ediacaran igneous rocks. Evidence of much older crust was first recognized as relatively undeformed granodiorite with a discordant 3-fraction conventional U–Pb age of 782 ± 7 Ma that lies just to the east of the northwest-trending gneiss belt (Stern and Manton, 1987). Similar igneous rocks are recognized in this region, including the 844 ± 4 Ma Moneiga quartz-diorite (Bea et al., 2009). The ~610 Ma age of Feiran gneiss metamorphism, its NW trend, and subhorizontal lineations (Fowler and Hassen, 2008) and the fact that it separates an unusually old tract of early Cryogenian igneous rocks from younger Cryogenian basement to the west suggest that the Feiran gneiss belt is related to Najd deformation (Abu-Alam and Stüwe, 2009).

The Feiran–Solaf gneisses reflect relatively low *P*–high *T* amphibolite facies conditions. Eliwa et al. (2004) estimated $T \sim 638$–677 °C and *P* of 4–5 kbar for the Solaf zone biotite-hornblende gneisses, whereas Abu Alam et al. (2010) determined conditions of 7–8 kbar at $T \sim 600$–720 °C for the amphibolite-facies calc-silicate rocks. Overall, the Feiran gneisses originated during a single metamorphic cycle, with peak metamorphism at 700–750 °C and 7–8 kbar and subsequent isothermal decompression to ~4–5 kbar, followed by cooling to 450 °C (Abu-Alam and Stüwe, 2009). Cooling and structural shortening were synchronous and associated with Najd-related exhumation of the complex during an episode of oblique transpression. The *P–T* estimates for Feiran peak metamorphism indicate Ediacaran T gradients of several tens of °C/km, consistent with a partially molten mafic lower crust, at $T \sim 1100$–1300 °C. Gneissosity in the area developed during an early (D_1) phase of deformation (El-Shafei and Kusky, 2003) interpreted as an extensional tectonic event and underwent as many as three subsequent folding events (Fowler and Hassen, 2008).

Ninety km SE of the Feiran–Solaf area, the Sinai region contains a metamorphic core complex that is likewise interpreted as the result of extension during Ediacaran orogenic collapse (Blasband et al., 1997). Unlike the domes described above, however, the *Wadi Kid core complex*, as it is referred to, is identified by gently dipping mylonitic foliation and gently plunging mineral and elongation lineations in schistose metasedimentary rocks, not gneiss. The foliations defined a subhorizontal mylonitic zone as much as 1.5 km thick. Shear sense indicators give a consistent regional transport direction to the northwest, with local reversals to the southeast. Metamorphism in the mylonitic zone is of the LP/HT type (Shimron, 1987), and the foliated formations were formed at a depth of at least 10 km (Reymer et al., 1984). Two main periods of deformation are recognized in the rocks. The earlier, >620 Ma, D_1 event is related to compression associated with island-arc subduction. The D_2 event (620–580 Ma) was associated with extension and was responsible for development of the mylonitic foliation superimposed on D_1 structures. Non-coaxial deformation during D_2 indicates top-to-the-NW transport of the rocks overlying the mylonitic zone; reversal of movement to the SE was caused by subsequent upwarping due to the intrusion of late Ediacaran granitoids (560–530 Ma) (Blasband et al., 1997). The transition from D_1 compression to D_2 extension was due to orogenic collapse.

6. Middle Cryogenian–Ediacaran arc- and terrane-forming events

The distinctive geology of the Ad Dawadimi and Ar Rayn terranes located along the eastern edge of the Arabian Shield (Fig. 8) has been referred to earlier in this review (Section 4.3). The terranes are important because: (1) they are the youngest terranes in the ANS; (2) they provide evidence for subduction in the Ediacaran, well after other terranes had already amalgamated; (3) their mutual juxtaposition represents the youngest suturing event in the ANS; and (4) their juxtaposition with terranes to the west reflects the final closure of the Mozambique Ocean and the convergence of Neoproterozoic India with the African continents.

The Ad Dawadimi terrane comprises a thick sedimentary unit (the Abt formation), large plutons of syenogranite and alkali-feldspar granite, and minor layered gabbro, ophiolite, and serpentinite mélange. The Ar Rayn terrane comprises a continental-margin volcanic arc containing volcanic, volcaniclastic, and minor sedimentary rocks (Al Amar group), locally strongly metamorphosed, voluminous calk-alkaline TTG plutonic rocks, and a significant amount of granite. The two terranes are in contact along the serpentinite-decorated Al Amar fault, which is interpreted as a suture.

The Abt formation is entirely sedimentary, but because no base is observed it is treated as a terrane in its own right, not a post-amalgamation basin like other basins described in this review. The formation is exposed over an area of about 225 km N–S and 100 km E–W sandwiched between the Afif and Ar Rayn terranes but, on the basis of its subdued magnetic signature, is inferred to continue at least 300 km to the north beneath Phanerozoic cover (Fig. 17) (Johnson and Stewart, 1995). The formation is not directly dated but a maximum depositional age of ~620–615 Ma is provided by the U–Pb age of the youngest detrital zircon retrieved from five samples of the Abt Formation (618 ± 16 Ma; Cox et al., 2011) and the youngest age (621 ± 3 Ma) of detrital zircon cores reported by Kennedy et al. (2011) (Fig. 18).

The detrital zircons, overall, are Neoproterozoic with a major cluster of ages between 710 and 600 Ma, compatible with derivation, for example, from adjacent parts of the Ar Rayn or Afif terranes. Older zircons with near concordant Mesoproterozoic ages between 1805 Ma and 2120 Ma and early Paleoproterozoic ages form a minor, but significant component of the detrital grains (Cox et al., 2011). In addition, the Nd isotopes of the Abt formation yield Mesoproterozoic model ages, demonstrating that a significant amount of pre-Neoproterozoic material makes up the protolith of these rocks. On the basis of these observations, Cox et al. (2011) suggest that the Abt Formation was derived from the adjacent composite Afif terrane as this is the only terrane in the Saudi Arabian part of the Arabian Shield to contain pre-Neoproterozoic rocks.

$^{40}Ar/^{39}Ar$ plateau ages of metamorphic muscovite in the Abt formation (618 ± 6 Ma and 621 ± 4 Ma; using the constants of Renne et al., 2010) are evidence of Abt-basin metamorphism and deformation, presumably related to basin closure (Table 1) (Cox et al., 2011). Less precise hornblende $^{40}Ar/^{39}Ar$ ages between about ~616 and 601 Ma reported by Lewis (2009), Al-Saleh and Boyle (2001) and Al-Saleh et al. (1998) from the Abt formation, the At Tari window east of the Halaban ophiolite at the western margin of the Ad Dawadimi terrane, and the Ar Ridaniyah ophiolite mélange in the north-central part of the terrane are interpreted as metamorphic and cooling ages during further exhumation. Rims on detrital zircon cores in the Abt formation yield U–Pb SHRIMP ages between ~610 and 602 Ma (Kennedy et al., 2011), which probably reflect a later hydrothermal event. Following folding and metamorphism, the formation was intruded by undeformed syenogranite and alkali-feldspar granite dated with U–Pb SHRIMP zircon ages between 579 ± 3 Ma and 565 ± 2 Ma (Kennedy et al., 2005).

The Abt formation (Abt schist) is a monotonous assemblage of well-bedded fine- to medium-grained wacke, siltstone and shale. Bedding is mostly on the scale of a few centimeters to a few meters and sedimentary structures include cross bedding and grading. Delfour (1982) suggested that the formation is a sequence of turbidites but no rigorous sedimentological study of the formation has been published, and the tectonic setting of the formation is not clear. The formation has undergone greenschist-facies metamorphism, with mineral assemblages dominated by muscovite, chlorite, and variable amounts of quartz and feldspar. The formation is folded about north-trending folds. Folds are mostly open and upright, but become tighter in the east toward the Al Amar fault. Fold limbs are characterized by at least two generations of crenulations and crenulation cleavage. The crenulations are mutually co-axial and co-axial with the regional mesoscale folding but can be identified because the youngest crenulation affects the earlier cleavage and bedding (Lewis, 2009). In the Ar Ridaniyah area, in the central part of the Ad Dawadimi terrane, typical Abt formation rocks are structurally underlain by a volcanosedimentary sequence named the Ar Ridaniyah formation. The stratigraphic/depositional relationship between the Ar Ridaniyah and Abt formations is uncertain because they are in the footwall and hanging wall, respectively, of a west-vergent thrust. Al-Saleh and Boyle (2001) interpret the volcanosedimentary rocks as part of an ophiolitic mélange, probably part of the oceanic crust on which the formation was deposited whereas Elsass (1981) and Al-Shanti and Mitchell (1976) interpret the Ar Ridaniyah formation as a basal shelf facies that passes eastward and up-section into deep water facies of the typical Abt formation. Another ophiolitic complex is present at Jabal Tays, in the southern part of the basin (Al-Shanti and Gass, 1983). On Th/Sc vs. Cr and a Th/Sc vs. Zr/Sc diagrams, the Abt formation plots in the forearc and oceanic island-arc to continental-arc fields (Lewis, 2009).

The Al Amar arc (>690–615 Ma) is the main component of the Ar Rayn terrane. It consists of tholeiitic to calc-alkaline basaltic to rhyolitic volcanic and volcaniclastic rocks with subordinate tuffaceous sedimentary rocks and carbonates (Doebrich et al., 2007). They are variably deformed and metamorphosed and, in the eastern part of the terrane, crop out as amphibolite-facies paragneiss and schist. Metallogenetically, the terrane is distinctive as the host of epithermal gold, porphyry copper, and iron oxide-copper–gold occurrences (Doebrich et al., 2007). The Al Amar group is not dated, but some of the volcanic rocks in the arc have a minimum age of 689 ± 10 Ma, based on dates from trondhjemitic intrusions (Doebrich et al., 2007). The arc contains two TTG-suites comprising a low-Al suite (Group 1) (632–616 Ma; Stacey et al., 1984; Doebrich et al., 2007) and a high-Al or adakitic suite (Group 2) (689–617 Ma; Stacey et al., 1984; Doebrich et al., 2007). Both suites plot in the field of volcanic-arc granites (Doebrich et al., 2007) and are comagmatic with the volcanic rocks. A more evolved and younger phase of magmatism is represented by late- to post-tectonic alkali-feldspar granites (Group 3). They have strongly fractionated REE patterns with strongly negative Eu anomalies and Rb and Th peaks and plot on the Y–Nb diagram of Pearce et al. (1984) in the volcanic-arc granite/syn-collisional granite fields (Doebrich et al., 2007). Group-3 plutonic rocks are dated by the SHRIMP method at 607 ± 6 Ma and 583 ± 8 Ma (Doebrich et al., 2007) and by the Rb–Sr method at 581 ± 6 Ma (Abdel-Monem et al., 1982). Overall, the rocks of the Ar Rayn terrane range from >689 Ma (the minimum age for supracrustal rocks of the arc) to about 580 Ma. Subduction-related arc magmatism terminated about 615 Ma, the minimum age of TTG intrusions, making the arc the youngest in the ANS. Group 3 alkali-feldspar granites are interpreted as post-subduction intrusions.

The Al Amar arc has an Sr- and Nd-isotopic signature suggesting a mantle source that was less depleted than the sources of the juvenile oceanic terranes in the western shield, or a mixture of more depleted mantle with continental material (Stoeser and Frost, 2006). Its geology, structure, and metallogeny are characteristic of a continental-margin assemblage (Doebrich et al., 2007). The tectonic setting of the Ad Dawadimi terrane is less certain. Nonetheless, the parallelism of the Ad Dawadimi and Ar Rayn terranes indicated by the aeromagnetic data (Fig. 17) suggests that the two acted as a coherent tectonic unit during final assembly of the ANS. Whether the Abt formation is a forearc with respect to the Al Amar arc or a back arc is not established. Doebrich et al. (2007) interpret the Abt formation as deposited above a subduction zone dipping west beneath the Afif terrane. This model is supported by Cox et al. (2011) who link the provenance of the Abt formation to the Afif terrane. Al-Saleh and Boyle (2001) interpret the formation as deposited in a backarc between the Afif and Al Amar arc caused by easterly roll-back on a west-dipping subduction zone. Stacey et al. (1984) and Al-Husseini (2000), on the other hand, model easterly subduction, treating both the Abt formation and Al Amar arc as the leading edge of a crustal block beneath central Arabia separate from the rest of the ANS—the leading edge of the Rayn microplate of Al-Husseini (2000).

Pending further study in the area, it is inferred the Ad Dawadimi and Ar Rayn terranes were in contact and had jointly sutured with the Afif and other western terranes of the ANS by the time of emplacement of the alkali-feldspar-rich granites that intrude the two terranes. Those in the Ar Rayn terrane are somewhat older (~607–583 Ma) and those in the Abt formation younger (~579–565 Ma), but both sets of granites are undeformed and intrude already folded and metamorphosed rocks of the Al Amar group and Abt formation. They provide a minimum age for deformation in the easternmost part of the Arabian Shield and imply that terrane amalgamation and suturing had ceased by about 607 Ma.

7. Late Cryogenian–Ediacaran structure

Different parts of the ANS display different structural fabrics (Fig. 19), with northerly trends dominant in the south and northwesterly trends dominant in the north. This geographic difference

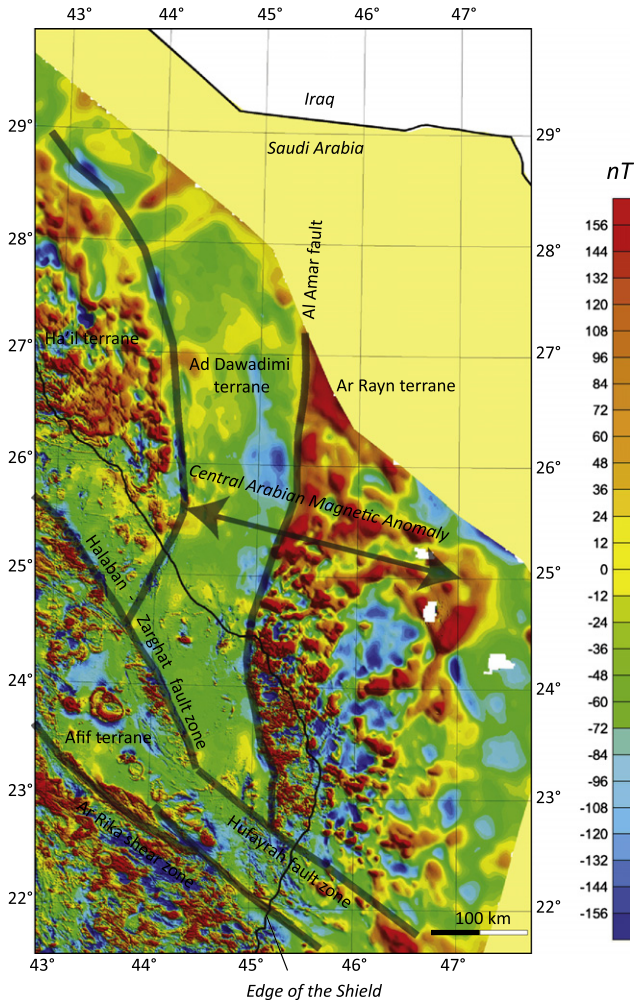

Fig. 17. Aeromagnetic-anomaly map (reduced to the pole) of central Saudi Arabia (after Zahran et al. (2003)) illustrating the continuation of the Ad Dawadimi and Ar Rayn terranes more than 300 km north of the edge of the Arabian Shield; their termination to the south at the Halaban-Zarghat and Hufayrah fault zones; and their discordant relationship with other, previously amalgamated terranes in the ANS to the west. The combined magnetic low of the Ad Dawadimi terrane and magnetic high of the Ar Rayn terrane constitutes the Central Arabian Magnetic Anomaly (CAMA) (Johnson and Stewart, 1995; Stern and Johnson, 2010). The CAMA is correlated with a fundamental crustal boundary (suture?) that extends north across the Arabian Plate to the Bitlis Zone. The magnetic data are strong evidence that the Ad Dawadimi and Ar Rayn terranes are structurally linked and, by implication, that deposition of the Abt formation is genetically associated with the Al Amar arc rather than with terranes to the west.

divides the ANS into southern and northern sections (Fig. 2) and is comparable to the differences in distribution of post-amalgamation basins and late- to posttectonic granitoids noted above. The difference is also consistent with radiometric ages north and south of the Cryogenian Bi'r Umq–Tharwah–Nakasib–Ariab suture, which separates mostly older (>750 Ma) Cryogenian basement in the south from mostly younger Cryogenian basement in the north (<750 Ma). As commented above, the distributions of post-amalgamation basins and granitoids could reflect differences in recent levels of erosion. However, because structural orientation was fixed during the Neoproterozoic deformation and is independent of erosion, a fundamental crustal difference in the ANS may be a factor in addition to recent erosional differences, applying to structure as well as post-amalgamation basins and granitoids.

Some of the principal late Cryogenian–Ediacaran shear zones and shortening zones are shown in Fig. 20. Late Cryogenian–Ediacaran shearing resulted in the reactivation or dislocation of earlier suture zones, the development of new faults, and the development of suture zones in the far west (Keraf suture) and far east (Al Amar fault). Shortening is expressed by folding that is more intense than in adjacent regions and in the refolding of earlier structures such as thrusts and sutures (Abdelsalam and Stern, 1996).

7.1. High-strain zones in the southern ANS

These structures, as much as 300 km long and 1–50 km wide, comprise north-trending brittle–ductile shear zones and belts of shearing and folding (shortening zones). In the Asir and Tokar terranes and the ANS in Ethiopia, the shear zones are mostly conformable with the dominant N–S trend of bedding and fold axes, and divide the terranes into discrete structural blocks (Greenwood et al., 1982; Abdelsalam and Stern, 1996; Tadesse, 1996; de Wall et al., 2001). Some are serpentinite decorated and possibly originated during the early to middle Cryogenian as sutures between crustal units within the Asir and Tokar composite terranes, but were reactivated during the late Cryogenian to Ediacaran contemporaneously with the final convergence of eastern and western Gondwana and long after peak orogeny in the Asir terrane (680–649 Ma). One of the high-strain zones, the Keraf shear zone, is the middle-late Cryogenian (~650–580 Ma) suture at the contact between the ANS and the Saharan Metacraton (Abdelsalam et al., 1998). Others, lacking serpentinite, are strike-slip shear zones of uncertain significance. Shortening zones, where recognized in the Nubian Shield, are orthogonal to the Nakasib and Sol Hamid suture zones and associated structures (Abdelsalam and Stern, 1996). They reflect a component of localized strong E–W compression expressed by north-trending folds superimposed on earlier, mainly easterly-trending folds and thrusts (Abdelsalam and Stern, 1996; de Wall et al., 2001).

The *Nabitah fault zone* (technically a brittle–ductile shear zone, but the term "fault zone" is established in the literature) is a north-trending zone of brittle–ductile anastomosing shears in the eastern part of the Asir terrane. It extends about 430 km from the Ruwah fault zone to the Yemen border and gives its name to the 680–640 Ma Nabitah orogeny and to the Nabitah orogenic (or mobile) belt (Stoeser and Camp, 1985; Stoeser and Stacey, 1988). The fault zone originated during the Nabitah orogeny (680–640 Ma) as a phase of ductile shearing associated with the emplacement of syntectonic, mylonitic orthogneiss (Stoeser and Stacey, 1988). It was subsequently reactivated following the peak of the Nabitah orogeny and the emplacement of ~640 Ma granites (Johnson et al., 2001) as a brittle–ductile shear zone associated with offsets of limestone beds and granite contacts, normal as well as strike-slip faulting, and folding and shearing of late Cryogenian sedimentary rocks in small basins along the fault zone (Al Junaynah group, <640 Ma: Table 2). The Nabitah fault zone is interpreted as a suture

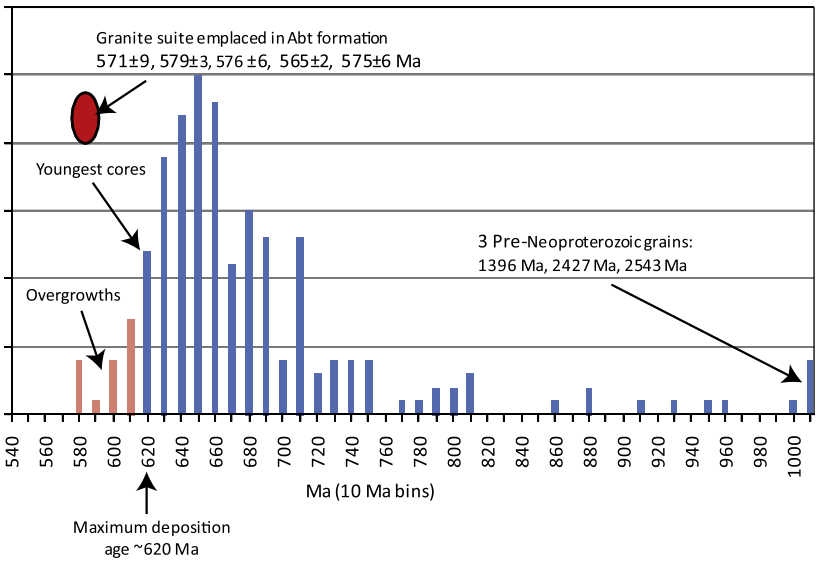

Fig. 18. Frequency plot of SHRIMP ages (±10% discordant) of zircons from the Abt formation. The youngest detrital grains with distinct cores suggest a maximum deposition age of about 620 Ma. Younger overgrowths possibly reflect hydrothermal events associated with metamorphism and later granite magmatism. The large grouping of grains dating 700–620 Ma is consistent with derivation from the Ar Rayn or other terranes to the west. Older ages indicate Tonian and Mesoproterozoic sources for some of the detrital grains, although the location of these sources is unknown. (Data from Kennedy et al. (2005, 2011), Lewis (2009) and Cox et al. (2011).)

in the north, where it separates greenschist-facies volcanosedimentary rocks of the Asir terrane from amphibolite-facies paragneiss and orthogneiss of the Tathlith terrane. In the south it is a ductile shear zone within the Asir terrane. The sense of shear on the fault zone is consistently dextral, indicated by abundant S–C and S–C′ fabrics, winged porphyroclasts, and flattened and rotated, sigmoidal conglomerate clasts. The unconformable contact between the Al Junaynah group and the ~640 Ma granites along the fault implies that the fault zone and granites underwent exhumation soon after emplacement of the granites and prior to deposition of the Al Junaynah sediments, followed by the resumption of dextral shearing.

The *Umm Farwah shear zone* extends about 200 km N–S across the central part of the Asir terrane. It is developed mostly in early Cryogenian volcanosedimentary and plutonic rocks and contains large lenses of serpentinite. At its northern end, it is the boundary between the Ablah group (640–615 Ma: Table 2) and arc rocks of the Asir terrane, and shearing here must be younger than 615 Ma. Umm Farwah shearing is also interpreted as the cause of crustal melting and emplacement of A-type granitoids (syenite; 617 ± 17 Ma; quartz-syenite and syenogranite; 605 ± 5 Ma) in the Ablah pluton (Moufti, 2001). If correct, these ages imply that brittle–ductile deformation occurred as late as 605 Ma, making the shear zone one of the youngest in the southern part of the Arabian Shield. The shear zone has S–C fabrics indicating both dextral and sinistral movements, and its overall sense of movement has not been determined. The shear zone is associated with moderate to strong folding in Ablah-group rocks about SSW-trending axes, which is consistent with transpressional sinistral shearing.

The *Muhayil* and *Sayayil shear zones* are curvilinear, northerly trending narrow zones of moderate to intense shearing in the southwest Asir terrane that continue to the north as the *Bidah shear zone*. The ages of the shear zones are unknown. The Bidah zone has a sinistral sense of movement. It is developed in the western part of the Asir terrane, in early Cryogenian volcanosedimentary rocks of the Bidah arc. Volesky et al. (2003) identified multiple episodes of deformation in the region. The earliest, D_1, episode is marked by E–W compression and the development of S_0/S_1 schistosity together with N-trending folds and mineral lineation. The D_2 episode was caused by transpressional deformation and resulted in the development of the brittle–ductile Bidah shear zone as a discrete structure. D_3 deformation comprises easterly trending, brittle, conjugate faults reflecting SE–NW shortening. D_2 and D_3 shearing postdated the early Cryogenian arc rocks of the Bidah area and sulfide mineralization (Volesky et al., 2003). The minimum age of shearing is determined by plutons of relatively undeformed biotite monzogranite and syenite and trondhjemite that intrude the sheared rocks. One of these plutons (muscovite-biotite granite) yields an Rb–Sr mineral age of 635 Ma (feldspar) (Aldrich, 1978), but it is unknown whether this is a crystallization or a metamorphic age. In summary, a lot of geochronologic work, both U–Pb zircon and Ar–Ar on hornblende and mica, is needed to resolve the ages of the N–S structures in the southern Arabian Shield.

Late Cryogenian–Ediacaran shear zones in *Eritrea* are exemplified by N-trending dextral strike-slip faults and low-angle mylonitic ductile shear zones that have both top-to-the-east and to-the-west senses of displacement (Ghebreab et al., 2005). The mylonites underwent progressive syn-deformation metamorphism at 593 ± 5 Ma (conventional U–Pb geochronology on monazite; Andersson et al., 2000) at peak *P–T* conditions of about 12 kbar and 650 °C, and have $^{40}Ar/^{39}Ar$ cooling ages for metamorphic hornblende and white mica of 579 ± 6 Ma and 567 ± 5 Ma, respectively (Ghebreab et al., 2005). The *P–T* and geochronologic data are evidence that the ductile shear zones in this part of the ANS are not merely an expression of N–S displacement associated with Ediacaran northward tectonic escape but also reflect E–W extension associated with orogenic collapse and exhumation of crustal rocks from depths of as much as 45 km (Ghebreab et al., 2005). N-trending shear zones in *southern Ethiopia* also contain a significant component of low-angle oblique normal slip manifesting regional gravitation tectonic collapse and extension, leading Tsige and Abdelsalam (2005) to conclude that N-trending belts in the southern part of the ANS are not necessarily the roots of northward expulsion of the ANS from the Mozambique Belt but are rather the expression of gravitational collapse involving detachment along low-angle shear zones.

In NE Sudan, the *Oko shortening zone* deforms rocks in the Gebeit terrane and warps the Nakasib suture, and the *Hamisana shortening zone*, the effective boundary betweeen the Gebeit and Gabgaba terranes, warps the Sol Hamid–Allaqi–Heiani suture and deforms

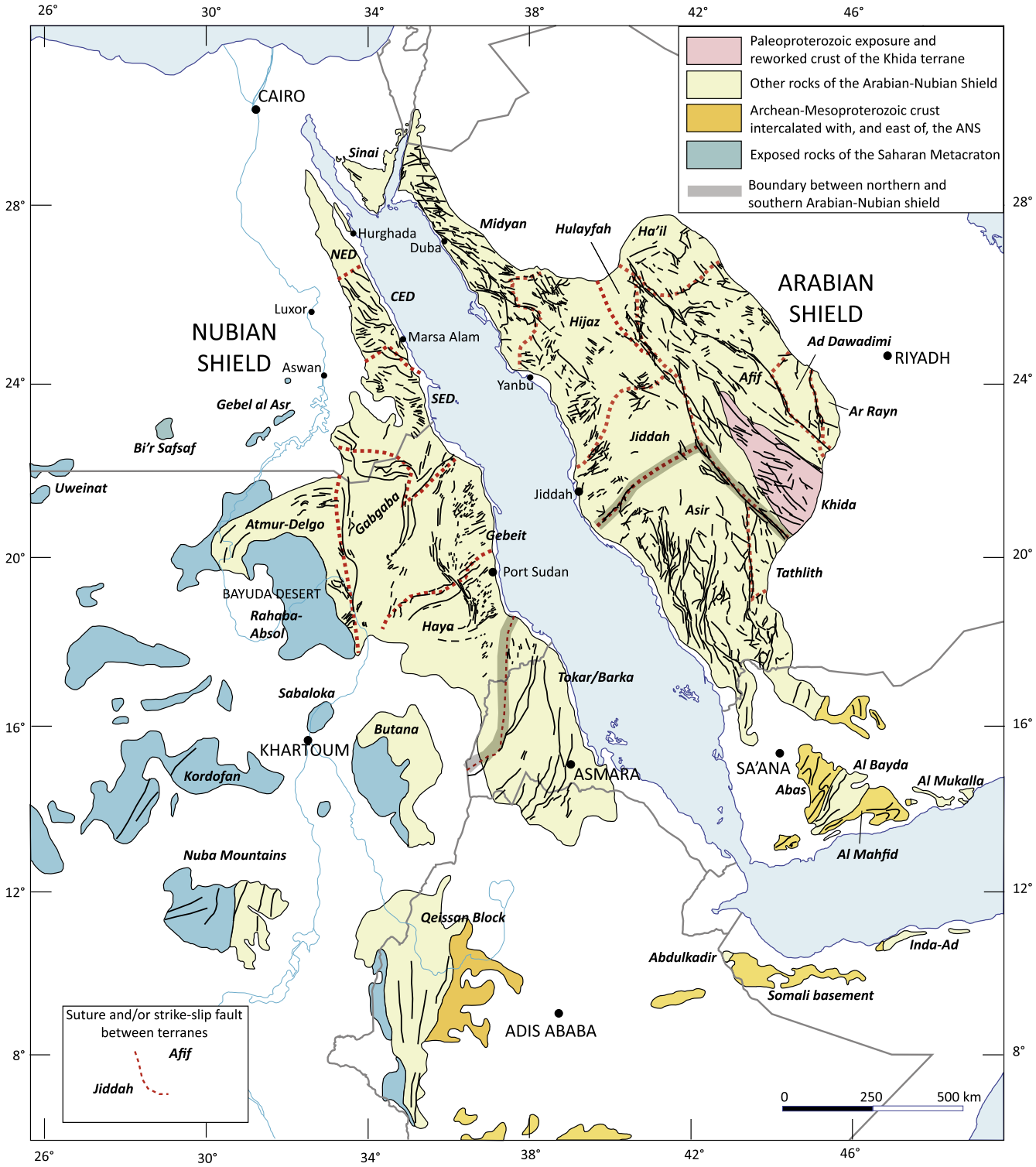

Fig. 19. Structural trends (shear zones and prominent foliation strikes) in the Arabian–Nubian Shield plotted on a base map showing the principal tectonostratigraphic terranes and suture zones (see Fig. 5B for the names and ages of the suture zones).

rocks in adjacent parts of the Gebeit and Gabgaba terranes. As noted above, the Hamisana shortening zone may continue into the Arabian Shield as the Hanabiq shear zone (Duncan et al., 1990). The shortening zones are chiefly zones of high strain that resulted in tight N–S folding rather than shearing, although a certain amount of horizontal shearing is displayed by both. Both zones are broadly sinuous and extend 200–250 km on strike and as much as 50 km across strike (Abdelsalam, 1994; Abdelsalam and Stern, 1996; Kusky and Ramadan, 2002). The Hamisana shortening zone has been variously interpreted as a suture zone, a regional shear zone, and a large-scale transpressional wrench fault. Magnetic anisotropy as well as field studies led de Wall et al. (2001) to conclude that deformation was dominated by pure shear but with a strong component of N–S extension consistent with earlier conclusions by Stern et al. (1989) and Miller and Dixon (1992). Extension was followed by minor NE–SW-trending dextral strike-slip. Thermal and tectonic activity on the zone is poorly constrained as having occurred ~660–550 Ma (Stern et al., 1989) and the zone is

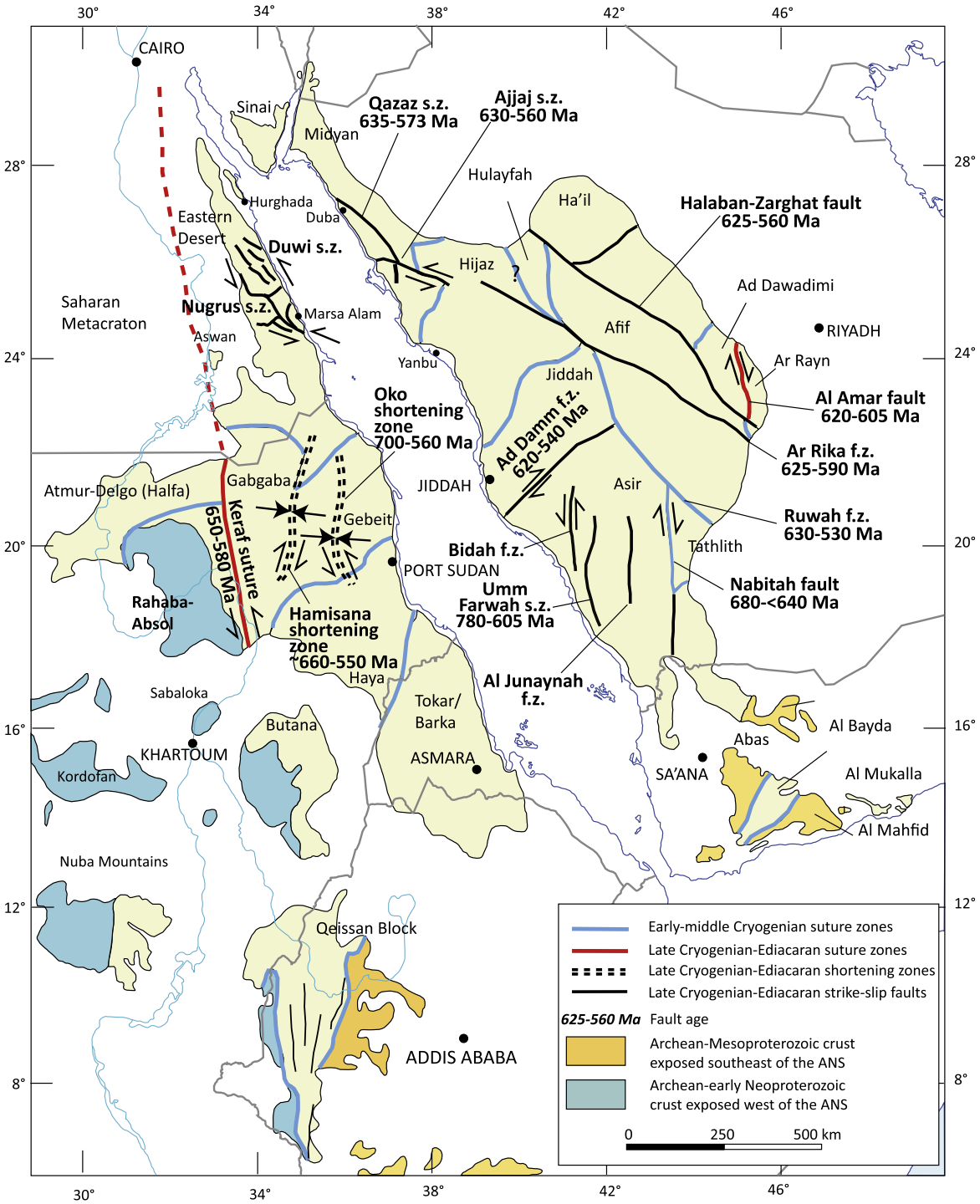

Fig. 20. ANS late Cryogenian–Ediacaran shear zones, shortening zones, and sutures.

interpreted to indicate significant middle Cryogenian–Ediacaran E–W compression.

The Oko shortening zone sinistrally offsets the 780–750 Ma Nakasib suture. It developed as an early phase of E–W compression resulting in NNW-trending tight upright folds and a later phase of subvertical NW-trending sinistral strike-slip faulting (Abdelsalam, 1994; Abdelsalam and Stern, 1996). Deformation is poorly constrained between 700 and 560 Ma.

The *Keraf suture* was broadly contemporary with the Hamisana and Oko shortening zones but has a fundamentally different tectonic significance. Rather than deforming preexisting arc assemblages and sutures, it is a major suture in its own right, comparable in age to the Al Amar suture in the Arabian Shield described below. The suture is ~500 km long and is up to 50 km wide but, as indicated in Fig. 5B, has a putative strike extension of more than 1000 km to the north, as an arc–continent suture at the border between reworked older crust of the Saharan Metacraton and juvenile crust of the ANS. Where exposed, the suture is superimposed on E- and NE-trending structures in adjacent parts of the Bayuda Desert and the Gabgaba and Atmur–Delgo terranes (Abdelsalam et al., 1998). In the north, the suture is dominated by N-trending upright folds; in the south by N- and NNW-trending sinistral strike-slip faults. The suture is interpreted to be caused by sinistral transpression along the western margin of the ANS, which

caused E–W compression as well as sinistral strike slip. The suture reflects closure of the Mozambique Ocean on the western margin of the ANS as already amalgamated terranes of the ANS converged and collided with the Saharan Metacraton. It is inferred that the suture began to develop during early oblique collision between ~650 and 600 Ma and underwent terminal collision at ~580 Ma (Abdelsalam et al., 1998). Hornblende and biotite separated from strongly deformed granite within one of the sinistral shear zones yield $^{40}Ar/^{39}Ar$ cooling ages of 577 ± 2 Ma and 577 ± 5 Ma (Abdelsalam et al., 1998). These ages are compatible with indications of orogenic activity obtained from K/Ar ages of 660 Ma for hornblende from granitoids and 560 Ma for biotite from high-grade gneiss and plutons (Bailo et al., 2003). The $^{40}Ar/^{39}Ar$ ages are evidence of very rapid cooling and exhumation following terminal collision and the cessation of ductile deformation.

7.2. Shear zones in the far eastern ANS

The Al Amar fault is a high-angle N-trending shear zone between the Ad Dawadimi and Ar Rayn terranes. It contains narrow lenses of ophiolites and carbonate-altered ultramafic rock (listwaenite and fuchsite-talc schist) (Al-Shanti and Mitchell, 1976; Nawab, 1979). The fault transects volcanosedimentary and associated plutonic rocks of the Al Amar arc (689–583 Ma), sedimentary rocks of the Abt formation ($\gtrsim$ 620 Ma), and sedimentary and volcanic rocks (Hamir group) (615–605 Ma) present in small deformed basins along the fault zone. The trajectory of convergence is unknown apart from limited observations of S–C shear fabric that suggest a component of dextral horizontal slip along the fault. The fault zone is conventionally interpreted as a suture between the Ar Rayn and Ad Dawadimi terrane, with the ultramafic rocks along the fault zone being remnants of ophiolitic crust. The timing of suturing is constrained by the observations that the Abt formation and Al Amar arc had already been deformed and metamorphosed at about 620 Ma and been uplifted at ~616 Ma prior to the emplacement of the 607–565 Ma posttectonic granites that intrude the two terranes. We therefore infer that suturing occurred between ~620–605 Ma, making the Al Amar fault the youngest suture in the Arabian Shield, broadly contemporary with the Keraf suture. As discussed in the following section, the Al Amar fault was also contemporary with the youngest movements on the Najd fault system.

7.3. Najd fault system

As originally defined (Brown and Jackson, 1960; Delfour, 1970), the Najd fault system consists of northwest-trending brittle–ductile shears in a zone as much as 300 km wide and over 1100 km long extending across the northern part of the Arabian Shield. The shears offset or reactivate middle to late Cryogenian sutures, offset Cryogenian volcanosedimentary and plutonic terrane-forming arc rocks, displace late Cryogenian–Ediacaran post-amalgamation basins, and transect late Cryogenian–Ediacaran intrusions. They are spatially associated with down-faulted blocks of the Jibalah group, gneiss domes, and gneiss belts (Fig. 10). The fault system is reported to have ~240 km cumulative displacement (Brown, 1972) but displacements of only tens of kilometers can be demonstrated for particular faults in the field. The fault zone continues NW into what, prior to Red-Sea spreading, were adjacent parts of the Nubian Shield, and is inferred, on the basis of magnetic and gravity data and paleogeographic reconstructions, to extend SE across the concealed basement of the Arabian Plate into parts of India and the Lut block of Iran that were adjacent to Arabia as Gondwanan components at the end of the Precambrian (Al-Husseini, 2000). Inferences that the Najd system extends into eastern Arabia are contested by Stern and Johnson (2010). Late Cryogenian–Ediacaran Najd-type northwest-trending transcurrent faults are present in the southern ANS and in the Mozambique Belt in Kenya and Madagascar (Raharimahefa and Kusky, 2010) and are inferred in the basement of southern Jordan, disrupted by much younger Cenozoic slip on the Dead Sea Transform (El-Rabaa et al., 2001). This extent of the fault system, if correct, would make the Najd fault system one of the largest shear systems known on Earth. Individual structures within the Najd system are brittle to brittle–ductile shears a few meters to several kilometers wide. The shears range from single, linear faults to broader sets of anastomosing shears. Movement was predominantly sinistral, although the offset of some plutons and inferences about the origin of some Jibalah group pull-apart basins suggest local dextral slip (Cole and Hedge, 1986; Agar, 1987; Matsah and Kusky, 2001; Kusky and Matsah, 2003). The shears chiefly trend NW to NNW, but a small number of NE-trending dextral shears such as the Ad Damm fault zone (Fig. 10) are believed to be conjugate shears for the Najd system (Davies, 1984).

Important features of the Najd faults include (1) transitions along strike from greenschist- to amphibolite-facies metamorphism and from brittle to ductile deformation; (2) the presence of belts and antiforms of mylonitic gneiss and schist with higher metamorphic grades than surrounding rocks; (3) the ubiquitous presence, in the high-grade rocks, of gently NW- and SE-plunging mineral and stretching lineations; (4) marker-bed offsets and microkinematic structures (S–C fabrics and rotated, winged porphyroclasts) indicating dominantly sinistral strike-slip displacement; (5) indications of local dextral strike slip during brittle faulting; (6) a juxtaposition, along some faults, of mylonitic gneiss domes, thrusts with a vergence orthogonal to the shear-zone strike, and fault-parallel and fault-oblique dikes; (7) the presence of fault-bounded basins filled by sedimentary and volcanic rocks of the Jibalah Group that either served as syn-fault, pull-apart depocenters or are younger extensional fault basins in which remnants of the Jibalah Group are preserved, or both; and (8) suspect syntectonic granitoids that form some of the orthogneisses along the fault zones (suspect because the fabric studies necessary to prove their structural setting have not yet been done). It is evident that Najd faulting involved a large component of oblique transpressional strike-slip shear, with constriction across and extension along the fault zones and vertical displacement of the sides of the fault zones relative to each other. The variations in metamorphic grade along strike indicate profound changes in *P*/*T* conditions at greenschist/amphibolite-grade interfaces of the type that are well known elsewhere to have implications for gold mineralization. The presence of suspect syntectonic intrusions (Table 3) indicates that the fault zones were favorable loci for intrusion and possibly involved feedback between intrusion and shearing. Intrusion would have thermally and hydrothermally weakened the crust; shearing would have opened up passage-ways for intrusion. An unknown structural element concerns the geometry of the Najd faults at depth. They may continue deep in the lithosphere, bottoming in horizontal detachments as envisaged by Lemiszki and Brown (1988), or flattening into listric faults. In the Arabian shield, the Najd faults have a strong magnetic and gravity expression (Fig. 21) (Mogren et al., 2008), in part reflecting an abundance of deep mafic intrusions along the faults (Gettings et al., 1986). The Najd faults are commonly modeled as a coherent structure, with an emphasis placed on features shared by individual faults, so that they are explained by a single regional cause (e.g., Moore, 1979). It should be recognized nonetheless that individual faults have distinctive structural and chronologic features (Table 3) indicating unique fault histories (Johnson and Kattan, 1999), and that the tendency to group all northwest-trending ANS faults as members of a common fault system may cause an oversimplification of interpretation of their origins.

Following interpretations by Tapponnier and Molnar (1976) and Molnar and Tapponnier (1977) for strike-slip faulting north of the Himalayas as a result of Eurasian collision with India, the Najd fault system was explained by Fleck et al. (1979) in terms of "indentor tectonics", with collision between the rocks in the Arabian Shield and a rigid block to the east. Stern (1985) pointed out discrepancies between an indentor model and the known orientations and slip directions of Najd faults, and alternatively proposed a significant role for extension in the northernmost ANS. Burke and Sengör (1986) introduced the concept of "tectonic escape" of continental material toward an oceanic free-face during collisional orogeny involving slip on transcurrent faults. In the ANS, the Najd faults are mostly modeled as transpressional structures that originated during late Cryogenian–Ediacaran oblique collision between eastern and western Gondwana, resulting in N-directed orogenic extension and escape of crust toward the paleo-Tethys ocean (Stern, 1994; Kusky and Matsah, 2003). A similar model of tectonic escape has been recently advocated for faulting in southern Africa (Jacobs and Thomas, 2004). Alternatively, the Najd system is interpreted as originating during Ediacaran–Cambrian extension associated with collapse of the East African Orogen and rifting of the Gondwana margin (e.g., Al-Husseini, 2000). A problem with the latter model is that Najd faults in the Arabian Shield predate deposition of lower Paleozoic sandstone that unconformably overlies the shield, implying that fault movement ceased by about 535 Ma, the age of the basal deposits as inferred by the youngest age of detrital zircons in the sandstone (Kolodner et al., 2006).

The principal throughgoing Najd-type structure in the Arabian Shield is the *Qazaz–Ar Rika shear zone*. It is an *en-echelon* set of shear zones that extends from the Qazaz–Ajjaj shear zone in the northwest to the Ar Rika shear zone in the southeast (Fig. 10). The Qazaz–Ajjaj shear zone hosts the Hamadat gneiss belt described above, the Ar Rika shear zone, and the Kirsh gneiss belt. Initial movements on the Ar Rika fault followed deposition of the Murdama group (~650–625 Ma) and subsequent movements followed emplacement of 611 Ma granitoids (Table 3). Gneiss and pegmatite in the Al Hawriyah antiform in the southeastern part of the Ar Rika fault zone have SHRIMP U–Pb ages indicating zircon growth at 623 Ma, 602 Ma, and 589 Ma, and possible metamorphism about 600 Ma (Kennedy et al., 2005, 2011). These results are consistent with slip on the Ar Rika fault zone between about 625 and 590 Ma. Movements on the Qazaz–Ajjaj shear zone are constrained to between ~635 and ~573 Ma (Calvez et al., 1984; Kennedy et al., 2010), bracketed by a cataclastically deformed granite with an inferred reset Rb–Sr age of 630 ± 19 Ma and the emplacement of an undeformed, post-shearing lamprophyre dike at 573 Ma that cuts paragneiss and schist along the shear zone.

The *Halaban-Zarghat fault zone* is a shorter Najd fault structure in the northern Arabian Shield. The Halaban part of the fault originated about 680 Ma as the suture at the eastern margin of the Afif composite terrane, but its trajectory deflected to the northwest during later strike-slip deformation, and the structure extended across the shield as the composite Halaban-Zarghat fault zone. Movement on the fault is predominantly sinistral and followed deposition of the Murdama group (Cole and Hedge, 1986), but subordinate dextral slip occurred after emplacement of Ediacaran diorite at 621 Ma. Along part of the fault, movement had ceased by the time of deposition of the Jurdhawiyah group (~595 Ma; Kennedy et al., 2004, 2005), but elsewhere the fault was active during and after deposition of the Jibalah group (~590–560 Ma) (Kusky and Matsah, 2003; Nettle, 2009).

As described above, the *Ruwah fault zone* is characterized by mylonitic orthogneiss, paragneiss, schist, and serpentinite of the Hajizah–Tin gneiss belt. The fault zone originated as part of the Hulayfah–Ad Dafinah–Ruwah suture zone at the western/southwestern margin of the Afif terrane, but was reactivated by Najd faulting. In the southeast, it is overthrust, along its northeastern margin, by Bani Ghayy group marble, in a region where brittle extensional fractures along the fault zone control gold-bearing quartz veins. To the northwest the Ruwah fault zone swings north and transitions into the Ad Dafinah and Hulayfah faults. The maximum age of deformation, the age of suturing, is constrained by a granodiorite gneiss protolith age of 683 ± 9 Ma (Stacey and Agar, 1985). Reactivation as a Najd fault followed deposition of the Bani Ghayy group (~650–620 Ma). Brittle–ductile deformation and metamorphism had ceased by the time of emplacement of undeformed "Najd" granite at 592 ± 4 Ma (Stoeser and Stacey, 1988; U–Pb zircon age from hornblende-biotite monzogranite).

The *Ad Damm fault zone* is a well developed NE-trending dextral strike-slip shear zone between the Jiddah and Asir terranes. It deforms the Numan complex—a granite of inferred Ediacaran age—creating mylonitic granite gneiss with very prominent rotated feldspar porphyroclasts. Fleck and Hadley (1982) suggest an age of approximately 620 Ma for the granite, which implies <620 Ma movement on the fault. Because of this age, Davies (1984) treats the fault as a conjugate dextral shear zone in the Najd system.

Although details are debated, it is widely accepted (e.g., Stern, 1985; Sultan et al., 1988) that the Najd fault system continues into the Egyptian Eastern Desert as the "Najd corridor" in the vicinity of the Hafafit, Sibai, and Meatiq gneiss domes (Fig. 16). El Ramly et al. (1990) challenged the correlation of the Najd faults across the Red Sea, arguing that claims of large-scale Najd strike-slip displacements on the margins of the Hafafit dome are not supported by the field evidence. The dispute partly reflects uncertainty as to the origin of the Meatiq and Hafatit gneiss domes. As mentioned above, some authors treat these domes as the product of exhumation associated with Najd faulting and extension, whereas others interpret the gneisses to be parts of pre-Najd thrust sheets that underwent subsequent folding or doming and were overprinted by Najd-style faulting.

The dominant shear zones around the Hafafit dome include the *Nugrus* and *Wadi Gemal thrusts* (El Ramly et al., 1984). The Nugrus thrust is a low-angle E- and N-dipping shear zone that wraps around the eastern and northern margins of the dome or is a low-angle extensional shear zone folded over the dome (Fowler and Osman, 2009). It has also been interpreted to form the base of a thrust duplex of low-grade supracrustal rocks transported to the northwest over high-grade infracrustal rocks (Greiling, 1997). The extent to which the Nugrus and Wadi Gemal thrusts were subsequently overprinted by Najd faulting is debated. El Ramly et al. (1984) and Greiling (1997), for example, show no NNW-trending strike-slip faults on their maps of the Hafafit dome. Fritz et al. (1996) infer sinistral strike-slip along the high-strain zone represented by the eastern part of the Nugrus thrust, as if the thrust was reworked by Najd strike-slip movements. Shalaby et al. (2006) show a system of linked thrusts and strike-slip faults extending from the Hafafit to the Meatiq Dome (illustrated in Fig. 16). Subsequent mapping of the northwestern end of the Nugrus shear (Fowler and Osman, 2009) however shows no further continuation of the Nugrus shear along a NW trend into the Central Eastern Desert.

The structural framework suggested by Shalaby et al. (2006) is an attractive interpretation for some Central Eastern Desert molasse basins as pull-apart basins formed at releasing bends in the shear system, accommodating orogen-parallel extension on the flanks of structural highs. There is doubt, however, about the extent of Najd faulting around the Meatiq Dome. As described above, all authors agree that the Meatiq Dome is a system of thrust stacks resulting from NW-directed tectonic translation that placed low-grade infracrustal rocks over high-grade supracrustal gneiss (Fritz et al., 1996; Loizenbauer et al., 2001; Andresen et al., 2010); but subsequent events are not agreed upon. Fritz et al. (1996, p. 311)

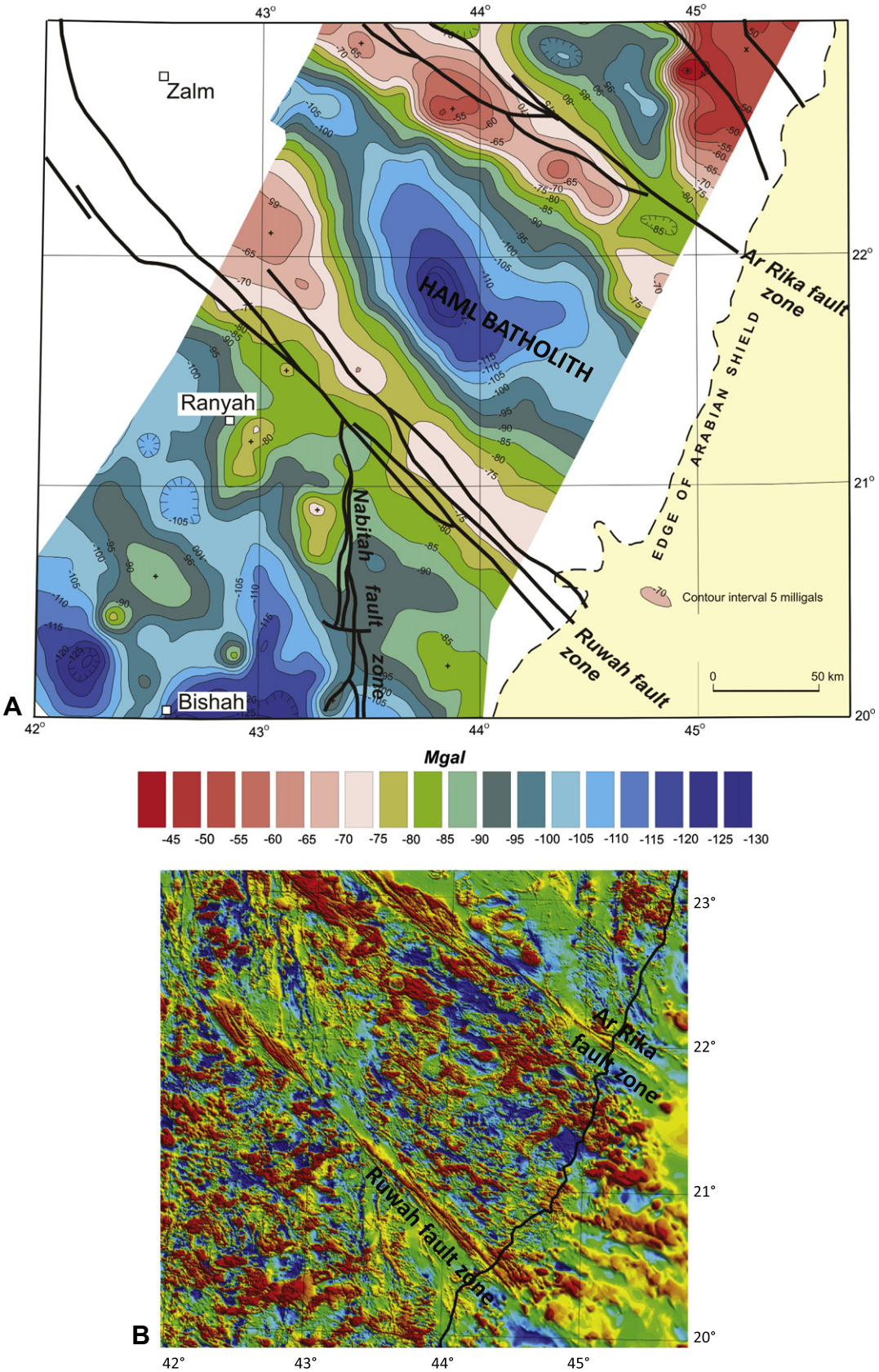

Fig. 21. Bouguer gravity (A) and aeromagnetic-anomaly maps (RTP) (B) of the eastern part of the Arabian Shield, showing the potential-field expression of Najd faults. Yellow dots on the magnetic-anomaly map are gold occurrences. The magnetic-anomaly map uses a conventional color scheme grading from red for high magnetic values through yellow and green, to blue for low values. Gravity data after Gettings et al. (1986); magnetic data after Zahran et al. (2003).

envisage that the dome was exhumed because of its setting within a "crustal-scale wrench corridor of the Najd fault system" interpreting steeply dipping, northwest-trending, high-strain zones on the east and west margins of the dome as sinistral Najd faults. Andresen et al. (2010), conversely, do not identify the bordering high-strain zones as Najd faults but interpret them as parts of the main EDSZ thrust between the infracrust and supracrust that dip steeply toward the east and west, respectively, because of folding about a NW-trending axis. This hypothesis was advanced earlier to explain the change from sinistral to dextral apparent senses on slip on the northeast and southwest flanks of a smaller gneissic culmination in the Um Had area to the west of Meatiq (Fowler and Osman, 2001).

7.4. Structural synthesis

It is well established that the ANS is part of an accretionary orogen, but as commented by Abdeen and Greiling (2005) "there is not yet any comprehensive study on the late Pan-African deformational pattern at the scale of the orogen" (p. 465). Many structural studies have been done of individual areas (e.g., Fritz et al., 1996; Worku and Schandelmeier, 1996; Blasband et al., 1997; Abdelsalam et al., 1998, 2003; Loizenbauer et al., 2001; Fowler and El Kalioubi, 2004; Abdeen and Greiling, 2005; Tsige and Abdelsalam, 2005; Fowler et al., 2006; Abdeen et al., 2008; Ghebreab et al., 2009; Andresen et al., 2010; Abdeen and Abdelghaffar, 2011) and preliminary syntheses have been done for the Central Eastern Desert (Greiling et al., 1994) and the Arabian Shield (Genna et al., 2002). Factors that currently inhibit consensus on the structural history of the ANS are a lack of systematic structural information for the region, conflicting or not-yet-resolved different interpretations, and a lack of dating of deformation and metamorphic events.

Using the Central Eastern Desert as an example of issues involved in making a structural synthesis, it is noted that the region consists of upper amphibolite-facies quartz-rich and quartzofeldspathic paragneisses and granitoid gneisses structurally overlain by (1) low-grade metamorphosed units of ophiolitic mélange (serpentinites, metagabbro, and metabasalt), island-arc mafic to felsic metavolcanics, calc-alkaline intrusive rocks, and metasediments; and (2) units of molasse (Hammamat Group) and calc-alkaline mafic to felsic volcanic rocks (Dokhan Volcanics). The high-grade rocks (variably referred to as Tier 1 and infrastructure) occupy the cores of dome-like structures. The lower-grade rocks (variously referred to as Tier 2, Pan-African nappe complex; ophiolitc nappes; and eugeoclinal rocks/eugeoclinal allochthon) form the flanks of the gneiss domes. High-strain mylonitic zones tens to hundreds of meters thick separate the high-grade and low-grade rocks and similar mylonitic zones occur within the high-grade rocks. This high-strain zone always seems to separate the high- and low-grade rocks, and it has been named the Eastern Desert Shear Zone (EDSZ) (Andresen et al., 2009, 2010). However, whether the shear zone extends as a continuous high-strain zone throughout the region or whether there are many shear zones of limited extent is not known. As commented above, despite earlier initial conclusions that the high-grade rocks are remnants of pre-Neoproterozoic continental crust (e.g., Habib et al., 1985; El-Gaby et al., 1988, 1990), the absence of significant geochemical, geochronologic, or isotopic differences between the high- and low-grade rocks strongly supports the view that they are correlative and all Neoproterozoic, belonging to the juvenile Neoproterozoic ANS crust.

The late Cryogenian–Ediacaran structural history of the CED is provisionally outlined in Fig. 22. The history illustrated extends from the end of the main collisional orogeny in the ANS, represented in the Nubian Shield by collision between the South Eastern Desert and Gabgaba terranes along the Allaqi-Heiana suture zone at 800–700 Ma (Abdeen and Abdelghaffar, 2011) and in the Arabian Shield by the Nabitah orogeny (680–640 Ma), to extension and exhumation of the ANS toward the end of the Neoproterzoic. Fowler and Osman (2001) describe bedding (S_0), gneissosity (S_g), and complex mesoscopic folds (F_g) in the high-grade rocks exposed in the core of the gneiss dome in Wadi Um Had and refer to the high-grade (garnet, cordierite, sillimanite) metamorphic event as M1. These structures and M1 metamorphism likely reflect the main collisional orogeny, and therefore date to about 700–640 Ma. S_g foliations bear a sillimanite lineation L_g. High-grade rocks in the core of the Meatiq Dome underwent a comparable early metamorphic event (referred to as M1) with peak temperatures exceeding 800 °C followed by M2 amphibolite-facies metamorphism ($T > 640$ °C, with P 6–8.5 kbar) that produced garnet-bearing assemblages (Neumayr et al., 1996a,b). It is important to note that all other, later structures (foliations, folds, lineations, thrusts, and transcurrent faults) affected the Hammamat Group and Dokhan Volcanics as well as the high-grade gneisses and low-grade eugeoclinal rocks. This imparts a common structural style to the entire region and means that, apart from the cryptic pre-640 Ma deformational event evidenced by the F_g folds in the high-grade rocks, the region has a common post-Hammamat and Dokhan structural history.

Following high-grade metamorphism, the region began to undergo orogenic collapse and extension resulting in subsidence and the development of basins that became the site of deposition of the Dokhan Volcanics and Hammamat Group (Abdeen and Greiling, 2005). Abdeen and Greiling (2005), and the authors cited by them in Table 1 in their paper (p. 460), infer general NW–SE to NNW–SSE extension. This must have occurred sometime between about 640 Ma and 630 Ma, prior to the onset of Dokhan/Hammamat deposition. Dokhan Volcanic extrusion continued until about 592 Ma and Hammamat Group deposition until 579 Ma, overlapping with subsequent deformation events and the emplacement of late- to posttectonic granites and dike swarms.

The earliest post-Hammamat structures (about or prior to 605 Ma) recognized throughout the region, reflect NNW–SSE to NW–SE shortening or northwestward gravitational collapse. Evidence for this comprises generalized ENE–WSW strikes and broad E–W-trending fold axes in several Hammamat Group basins (Abdeen and Greiling, 2005) and top-to-the-NW shearing in and around gneiss domes (Fowler and El Kalioubi, 2004). The Hammamat Group in the Hammamat basin shows an early phase of NW-directed low-angle thrusting associated with S- and SE-dipping cleavage and SE-plunging stretching lineations. Similar shortening is evidenced in other basins in the Central Eastern Desert (see Table 1 in Abdeen and Greiling, 2005). Thrusting resulted in the development of the EDSZ and its characteristic S_1 shear foliation in the Meatiq gneiss dome (Andresen et al., 2009, 2010) and the Um Had dome (Fowler and Osman, 2001). It is associated with rare F_1 folds that have axial planes parallel to S_1 (Fowler and Osman, 2001). The NW-direction of tectonic transport is evidenced by rare S–C structures, foliation"fish", shear-segmented veins (Fowler and El Kalioubi, 2004), and the intersection of S, C, and C′ surfaces (Andresen et al., 2010). In the Um Had domes, the thrust-related mylonitic fabric is associated with retrograde metamorphism (M2) of the earlier M1 metamorphic assemblages and the development of biotite-chlorite-mica schist (Fowler and Osman, 2001). The Um Had dome has a mineral-extension lineation (L_1) plunging gently NW and SE (Fig. 22) (Fowler and Osman, 2001); a similar lineation pattern is evident in the Meatiq Dome (Andresen et al., 2010). The timing of ductile deformation, and by implication the timing of the main period of NW-directed thrusting throughout the Central Eastern Desert, is constrained by the Abu Ziran syntectonic diorite (ID-TIMS age of 606 ± 1 Ma; Andresen et al., 2009).

There followed a period of NW-directed transpression associated with bulk E–W to ENE–WSW shortening. The effect of this was to develop NW–SE-trending F_2 folds, SW- and NE-dipping

thrusts, and northwest-trending transcurrent faults. In places these structures appear to be coeval as in the Wadi Queih Hammamat Group basin (Abdeen and Greiling, 2005); in other locations, such as between the Meatiq and Um Had Domes, folding and thrusting preceded transcurrent faulting (Fowler and Osman, 2001). F_2 folding is seen in the folding of the F_1 high-strain zones and S_1 foliations. The folding caused the broad girdles shown by the plots of poles-to-foliation in the Um Had area (Fig. 22), and created broad antiformal structures composed of curved outcrops of the EDSZ around the margins of the Meatiq and Um Had gneiss domes. In the Um Had area, west of the Meatiq Dome, the EDSZ is folded about a NW-trending and plunging axis (Fowler and Osman, 2001). The high-grade gneissic rocks are in the core of the antiform, creating the Um Had gneiss domes. The eastern flank of the dome is steeply dipping and here the EDSZ resembles a NW-trending sinistral transcurrent fault zone. On the western flank, the EDSZ resembles a dextral shear zone. Importantly, the folded EDSZ can be traced from the eastern to the western flanks around the northern tip of the dome, demonstrating that the margins indeed comprise a fold in the EDSZ (Fowler and Osman, 2001). A similar structure is described for the Meatiq Dome (Andresen et al., 2010), where EDSZ can be traced around the southern margin of the dome. In both cases, the eastern and western margins of the domes consist of mylonitic zones resembling transcurrent shears. As noted above, the shears flanking the Meatiq Dome have been interpreted as sinistral Najd faults, with the dome being confined to a "Najd corridor" (Fritz et al., 1996), but the observations of Fowler and Osman (2001) and Andresen et al. (2010) indicate that, what look like transcurrent shears, are the result of folding of the EDSZ.

The same bulk E–W shortening also caused the development of a zone of W- to SW-directed thrust imbrication in eugeoclinal island-arc rocks and the Dokhan Volcanics and Hammamat Group between the Meatiq Dome and the Um Had Dome (Fritz et al., 1996; Fowler and El Kalioubi, 2004). NE-dipping thrusts place the Dokhan Volcanics over the Hammamat Group, and ophiolitic mélange over the Dokhan. Duplex structures are present, and S–C fabrics confirm the sense of displacement (Greiling et al., 1996). The eastern margin of the Hammamat basin has NE-dipping thrusts that were overprinted by NNW-directed sinistral strike-slip shearing (Fowler and Osman, 2001; Abd El-Wahed, 2009). Elsewhere, SW-dipping thrusts are exposed, placing serpentinite over metagabbro and slicing and re-stacking the Hammamat Group (Fowler and Osman, 2001). Bulk shortening caused the development of NE-directed thrusts and northwest-trending folds in the Wadi Queih Hammamat basin (Abdeen and Greiling, 2005).

The concurrent, or final effect of this transpressive phase of deformation, was the production of NW-trending sinistral transcurrent faults that overprint the earlier formed SW- and NE-dipping thrusts. These faults are developed throughout the CED and, as is widely accepted, are the northwest tip of the Najd fault system. In the Wadi Queih basin these faults are associated with sub-parallel high-angle reverse faults that form a positive (half) flower structure (Abdeen et al., 1992; Abdeen and Warr, 1998) The El Mayah basin is aligned along an E–W shear belt to the south of the El Sibai gneiss dome that turns, on its western end, into a NW direction. Steep sediments are aligned and sheared along this E–W-trending structure, and the structure itself has been interpreted as a fault/shear zone conjugate to the overall NW-trending strike-slip structures (Shalaby et al., 2005, 2006). The ages of individual structures that belong to this transpressional phase of deformation are not certain, but in general it would appear that they developed by 590 Ma. Evidence for this is that thrusting in the Hammamat Group rocks in the Um Had area had occurred by the time of emplacement of the posttectonic Um Had granite (596 ± 2 Ma) and deformation in the Meatiq Dome had ceased by the time of emplacement of the Arieki granite (590 ± 3 Ma; Andresen et al., 2009). A similar constraint is provided by intrusion of leucogranites with Rb–Sr ages of 594 ± 12 and 610 ± 20 Ma (Moghazi et al., 2004) into the Nugrus shear zone on the northeast flank of the Hafafit dome. Terminal events in the CED include N–S to NW–SE extension evidenced by the dike swarms that intruded the region between about 600 Ma and 565 Ma (see Section 9.1.1), and $^{40}Ar/^{39}Ar$ ages that defined a period of peak cooling and exhumation (see Section 9.2.2. and Fig. 25).

8. Late Cryogenian–Ediacaran mineralization

Late Cryogenian–Ediacaran mineralization in the ANS is dominated by gold, the refractory metals tantalum, niobium, and tungsten (Ta, Nb, W), rare earth elements (including Y), uranium, and tin. The gold occurrences typically developed between about 650 Ma and 615 Ma (Table 4). They consist of gold-bearing quartz-carbonate veins that are commonly associated with late- to posttectonic calc-alkaline diorite, granodiorite, or granite intrusions emplaced following the Nabitah orogeny (680–650 Ma). Because the refractory metals, rare earth elements, uranium and tin are commonly (although not exclusively) associated with specialized posttectonic A-type granites, their development is clearly a result of the widespread emplacement of posttectonic A-type magmas in the ANS from about 610 Ma. Other, less common late Cryogenian–Ediacaran mineralization includes silver in quartz-carbonate veins; chromite, nickel, PGM, and ilmenite in layered mafic–ultramafic plutons; and polymetallic gold-silver-zinc epithermal mineralization together with an unusual type of zinc sulfide mineralization in the Ar Rayn terrane. It should be notes that a number of well-known metallic mineral deposits and mines in the ANS, including some that are being currently developed or explored, are outside the time-frame of this review because they are hosted by early-middle Cryogenian island-arc rocks. Such deposits include VMS Cu–Zn–Au occurrences at Jabal Say'id in the Arabian Shield and Bisha in the Nubian Shield.

8.1. Gold-quartz-carbonate veins

Gold-bearing quartz-carbonate veins have been the explored and mined in the ANS for over 6000 years (Klemm et al., 2001; Amer et al., 2009; Gabr et al., 2010). They crop out at hundreds of ancient mine sites and are worked at some of the gold mines operating in the region (Fig. 23). The veins, a type of mineralization referred to nowadays as "orogenic gold" (Groves et al., 1998; Goldfarb et al., 2001), are concentrated in areas of transpressional shearing, strike-slip faulting, and thrusting. They are preferentially concentrated in the margins and adjacent wall rocks of plutons of intermediate compositions such as diorite, tonalite, and granodiorite. A major concentration is along the Nabitah mobile (orogenic) belt in the Arabian Shield (Stoeser and Stacey, 1988). Other occurrences are adjacent to shear zones and gneiss domes in the CED of Egypt (e.g., Gabr et al., 2010; Amer et al., 2010; Greiling and Rashwan, 1994) (Fig. 23), in sheared rocks south of the Allaqi suture zone (e.g., Kusky and Ramadan, 2002) and elsewhere in the Gabgaba terrane, in transpressive shear zones in the Asmara block, Eritrea (Ghebreab et al., 2009), and in highly sheared rocks in the Tokar terrane and Queissan Block of Ethiopia. In the south Eastern Desert of Egypt, NW–SE oriented veins originated during arc–arc collision (D_1) and were subsequently deformed by D_2 folding and D_3 sinistral shearing (Abdeen et al., 2008).

Gold in these occurrences is free or associated with sulfides (arsenopyrite, chalcopyrite, sphalerite) in low-sulfide veins or disseminated in wallrock alteration zones. Gold is typically the primary economic commodity but some deposits produce

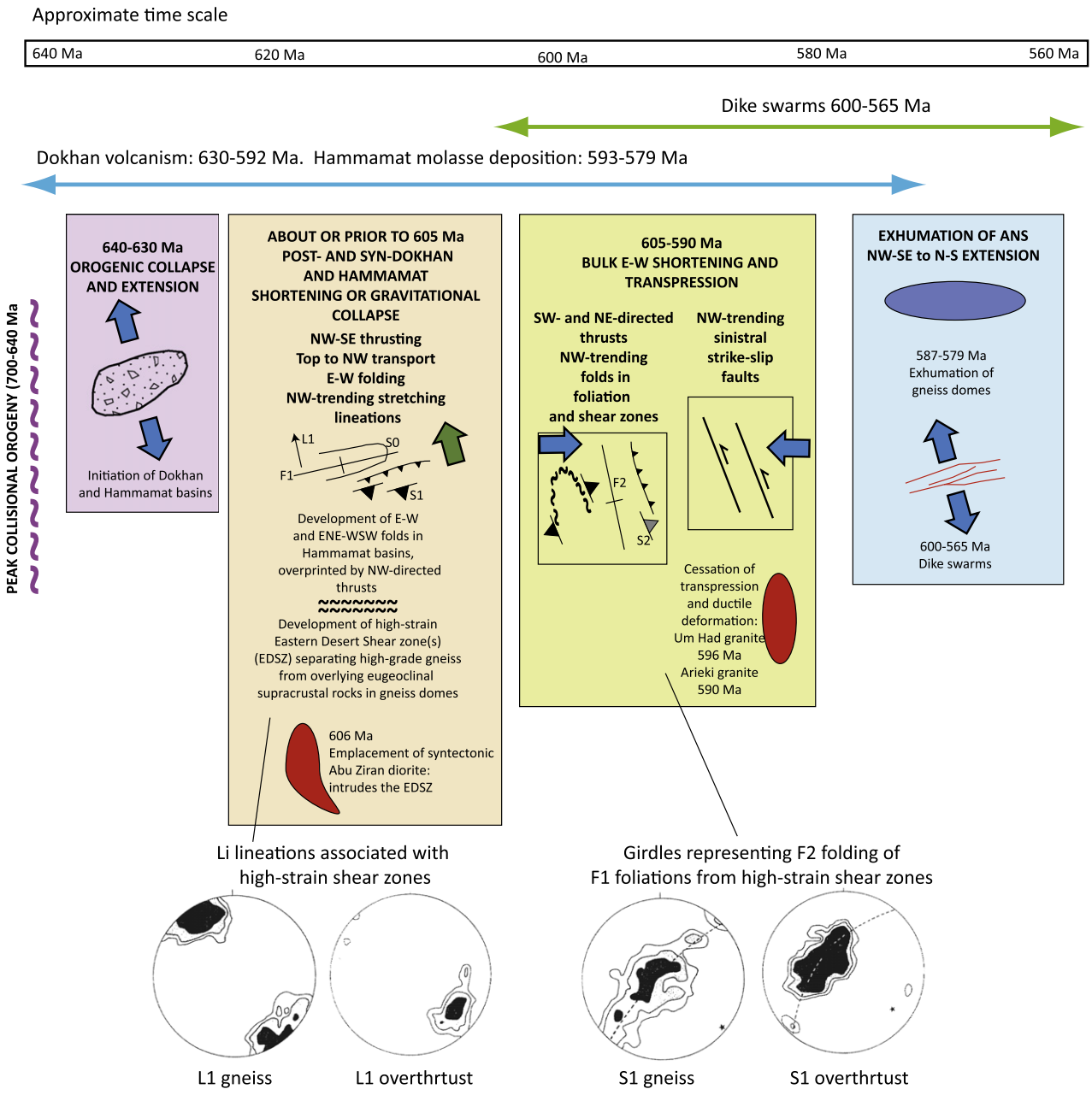

Fig. 22. Preliminary synthesis of late Cryogenian–Ediacaran structural events in the Central Eastern Desert events, largely after Abdeen and Greiling (2005), Fowler and Osman (2001), Fowler and El Kalioubi (2004), Andresen et al. (2010) and Fritz et al. (1996).

bi-product copper and zinc. Worldwide, the formation of orogenic gold reflects the passage of hot water in large volumes through permeable channel ways in a brittle structural environment or at the brittle–ductile transition at the base of the seismogenic zone (Sibson, 1987; Goldfarb et al., 2005, ref. therein). Such fluids tend to have a common composition with low salinity and high CO_2, and deposition tends to occur at a temperature of approximately 350 °C and depths of 4–12 km (Goldfarb et al., 2001).

The *Sukhaybarat–Bulghah* gold district is a large cluster of orogenic gold occurrences at the northern end of the Nabitah mobile belt in the Arabian Shield. It contains the Sukhaybarat Mine (now exhausted), the first orogenic-gold deposit developed in modern times in the ANS, which at the outset of mining in 1991 had a reserve of 17.6 t contained gold at a cutoff grade of 1.1 g/t (Al-Dabbagh and Dowd, 1996). Mineralization is hosted by sedimentary rocks of the post-amalgamation Murdama group and diorite, quartz diorite, and tonalite of the Idah suite (~620–615 Ma) (Albino et al., 1995; Al-Dabbagh and Dowd, 1996; Malmgren and Andersson, 1994). The deposit is located in a NNE-directed thrust (Malmgren and Andersson, 1994) or zone of shortening (Albino et al., 1995) at the margin of the host pluton. The veins are a few centimeters to about 1 m thick. They are low in sulfides, with arsenopyrite ± pyrite ± sphalerite ± galena ± chalcopyrite ± stibnite in the range of <1–5 wt.% (Albino et al., 1995; Lewis and Schull, 1994) and are flanked by arsenopyrite-gold-bearing alteration zones. Visible gold is not common in the Sukhaybarat–Bulghah district but individual veins at Sukhaybarat have grades of 30 g/t to as much as 200 g/t Au (Albino et al., 1995). The Sukhaybarat pluton is dated at 617 ± 2 Ma, implying that mineralization was <617 Ma (Table 4). Veins at an adjacent occurrence at An Najadi are significantly older, dated at 631 ± 12 Ma (D. Unruh, cited by Walker et al., 1994). Mineralization at the *Ad Duwayhi* prospect (31 Mt

containing 1Moz gold) (Doebrich et al., 2004), farther south along the Nabitah mobile belt, is older than Sukhaybarat. It is related to a late- to posttectonic granite (659 ± 7 Ma) and quartz porphyry (646 ± 11 Ma), and directly dated at 655.6 ± 2.7 Ma and 649 ± 2.3 Ma (Doebrich et al., 2004). The Ad Duwayhi mineralization consists of (1) gold-bearing quartz veins and breccia in and along the margins of a granite stock, and (2) a gold-bearing stockwork, sheeted quartz veins, and massive to banded quartz-rich tabular veins spatially associated with quartz porphyry.

The gold deposits of the *Nubian Shield* are more famous but less well-studied than those of Arabia. Klemm et al. (2001) concluded that Nubian gold mineralization formed when hot posttectonic granitoid plutons stimulated hydrothermal convection in the surrounding host rocks. Circulating water dissolved gold from slightly enriched mantle-derived rocks such as serpentinites and ophiolites, following joints and shear zones, altering the rocks and forming auriferous pyrite and/or arsenopyrite at 300–400 °C and 1–2 kbar. This scenario implies that most Nubian gold deposits are Ediacaran but radiometric dating is needed to test this model. The metallogenic overview presented by Botros (2002) recognizes different styles of gold mineralization at different stages in tectonic development. The island-arc stage is characterized by exhalative gold associated with BIF. The collisional-orogenic stage, just within the time-frame of this review, is associated with vein-type mineralization, the main target of gold exploration since Pharonic times, and lesser amount of gold associated with altered serpentinite (listawenite) and with the contact zones of gabbro and granite intrusions. The post-orogenic stage has small amounts of gold associated with disseminations, stockworks, and quartz veins of Sn–W–Ta–Nb.

Classic examples of vein-type, structurally controlled orogenic gold deposits in the Nubian Shield are the *Sukari mine*, 23 km SW of Marsa Alam in the Central Eastern Desert, Egypt (Arslan, 1989; Helmy et al., 2004) and the *Abu Marawat* deposit (Zoheir and Akawy, 2010). The Sukari deposit is hosted by an ophiolite and tonalitic to trondhjemitic pluton dated at 689 Ma (U–Pb ID-TIMS zircon age; Lundmark et al., 2011). The deposit is located in a NW-directed thrust duplex and is controlled by a local flower structure and extensional faults that accommodated NE–SW strike-slip deformation. Gold is present in low-sulfide (pyrite ± arsenopyrite ± sphalerite ± chalcopyrite ± galena) quartz veins and alteration zones. *P*/*T* conditions during initial vein formation were about 300 °C and 1.5–2 kbar, similar to the worldwide norms. The morphology of the veins indicates repeated veining and leaching, initiated by the intrusion of granodiorite, followed by sealing. The deposit has measured and indicated resources of 10.99 Mozs gold, inferred resources of 3.5 Mozs gold, and a reserve base of 9.1 Mozs gold (www.centamin.com.au January, 2011). The Abu Marawat deposit is interesting because it is hosted by a sequence of island-arc metavolcanic rocks and banded-iron formation. Mineralization is believed to have formed from ore fluids originating from possibly post-Hammamat granitoid intrusions leaching gold and base metals from the metavolcanics (Zoheir and Akawy, 2010). The deposit consists of sulfide-bearing quartz veins and hydrothermal breccia bodies displaying a complex history of shearing and crack-sealing quartz precipitation associated with a N-trending shear zone. Mineralization comprises pyrite–chalcopyrite ± pyrrhotite ± sphalerite ± galena. Gold is refractory in pyrite and chalcopyrite, and in rare visible gold/electrum and telluride specks.

Numerous gold-bearing quartz veins are known in western, northern and southern Ethiopia (Tadesse et al., 2003), and in several parts of Eritrea (Jelenc, 1966). In southern Ethiopia, the veins are hosted by shear zones along the contacts between low-grade volcanosedimentary rocks and high-grade gneisess. An example is the *Lega-Dembi Gold Mine* situated in the eastern boundary of the Megado zone/belt in southern Ethiopia (Ghebreab et al., 1992; Billay et al., 1997), which is currently in production. Mineralization occurred close to the peak of upper greenschist to lower-amphibolite metamorphism. Rb–Sr dating of sericite indicates an age of hydrothermal alteration and therefore of mineralization of about 545 Ma (Billay et al., 1997). This is considerably younger than gold mineralization in the main part of the ANS, and is closer to the age of orogenesis seen in the Mozambique Belt in Kenya and Madagascar—the Malagasy Orogeny of Collins and Pisarevsky (2005). Historically, hundreds of orogenic gold-bearing quartz veins were mined for gold in Eritrea, likewise in shear zones mostly within low-grade volcanosedimentary rocks (Ghebreab et al., 2009).

Table 4
Age of late Cryogenian–Ediacaran mineralization in the Arabian–Nubian shield.

Deposit name	Age of mineralization	Comment	Source
Orogenic gold			
Sukhaybarat gold	<617 Ma	Mineralization not directly dated, but must be younger than the Sukhaybarat pluton dated at 617 ± 2 Ma	Albino et al. (1995)
An Najadi gold	631 ± 12 Ma	Age of host pluton and inferred age of veining	Walker et al. (1994)
Ad Duwayhi gold	655.6 ± 12 Ma and 649 ± 2.3 Ma	Direct dating of veins; compare ages of associated plutons 659 ± 7 and 646 ± 11 Ma	Doebrich et al. (2004)
Lega-Dembi gold	545 Ma	Rb–Sr dating of sericite in hydrothermal alteration zone; constrains gold mineralization to about 545 Ma	Billay et al. (1997)
Refractory metals, Sn. W			
Kenticha tantalum	530 ± 2 Ma	Age of host pegmatite; associated with plutons dated between 550 and 520 Ma	Worku and Schandelmeier (1996) and Yibas et al. (2002)
Silsilah tin	587 ± 8 Ma	Deposit not directly dated; age inferred from that of host alkali feldspar granite	Du Bray (1984)
Ba'id al Jimalah tungsten	569 ± 16 Ma (age of granite host); ~575 Ma (age of quartz vein)	Age inferred from that of host microgranite and quartz vein	Cole and Hedge (1986) and Stacey and Stoeser (1984)
Kushaymiyah molybdenite–tungsten	<611 ± 3 Ma	Mineralization not directly dated; but must be younger than host granodiorite and quartz monzonite	Agar et al. (1992)
Ghurayyah REE	<577 ± 4 Ma	Ghurayyah stock has been dated but most zircons are about 660 Ma and probably inherited; the crystallization age of the stock is more reasonably constrained by the age of the adjacent Dabbagh pluton (577 ± 4 Ma) dated by Hedge (1984)	Hedge (1984)

8.2. Granitoid-associated refractory metals

Refractory-metals mineralization is not abundant in the ANS (Fig. 24) but, individually, some of the occurrences are of significant size and the region has the potential to become a major source of refractory metals (Küster, 2009). The host rocks are felsic intrusions, commonly referred to as "specialized granitoids" in discussions about refractory-metal mineralization in the ANS. They are chemically distinctive with K/Rb < 200, Ba < 200 ppm, Sr < 80 ppm, and Rb > 200 (Ramsay, 1986), may have peraluminous or peralkaline characteristics, and reflect extensive fractionation and geochemical evolution (Küster, 2009). The intrusions have I- and A-type affinities, and range in composition from granodiorite, monzogranite, syenogranite, to alkali-feldspar and alkali granite.

Defined by their extraordinary resistance to heat and wear, the refractory metals, strictly speaking, include niobium, molybdenum, tantalum, tungsten, and rhenium, but more generally include titanium, vanadium, chromium, zirconium, hafnium, ruthenium, osmium, and iridium. Because ANS occurrences of refractory metals commonly also include tin and(or) rare-earth elements, all these commodities are considered in this section.

In the ANS, distinctions can be recognized, depending on the composition of the host granitoids. Ta–Sn–Rb–Li–Be–Nb mineralization is mostly associated with peraluminous specialized granitoid; Nb–Zr–Y–REE–U–Th–Ta–Rb–Sn mineralization is associated with peralkaline specialized granitoids (Küster, 2009); and occurrences dominated by tin or tungsten are hosted by alkali-feldspar granite and subordinate granodiorite. The country rocks of the mineralized granitoids vary from previously deformed and metamorphosed arc terranes, to younger post-amalgamation, moderately deformed sedimentary assemblages, to serpentinite and other rocks in shear zones. The specialized granitoids themselves are posttectonic A-type intrusions. They may be strongly discordant small plutons or stocks, stocks within or on the margins of larger granitoid plutons, sheet-like bodies emplaced in tension gashes resulting from extension following the main phase of compressional deformation, or late pegmatites. As noted in a review of tin mineralization by Plimer (1987), but equally relevant to other special metals, these types of occurrences are associated with the last phase of posttectonic granites in extensional and/or shear tectonic regimes, and commonly occur in the apical parts of the intrusions.

8.2.1. Tantalum–niobium–REE–uranium mineralization

This type of mineralization is being mined at *Kenticha* in Ethiopia, is under development at *Abu Dabbab* in the Eastern Desert of Egypt, and is under exploration at *Ghurayyah*, in the Midyan terrane of northwestern Saudi Arabia.

Kenticha, in the Adola belt (south of the southern margin of Fig. 24) is a working mine with an indicated reserve ~17 Mt of ore grading 150 g/t Ta_2O_5. It is the largest known peraluminous pegmatitic rare-metal occurrence in the ANS (Küster, 2009). The deposit comprises a flat-lying, sheet-like body of peraluminous spodumene-albite pegmatite. in the midst of a 30-km long zone of pegmatites emplaced in sheared volcanosedimentary rocks, high-grade schist, and quartz-feldspar gneiss. The pegmatites and associated plutons of low-*P*, I-type biotite granite intrude a region with north-trending shears and thrusts but are posttectonic (Küster, 2009). They intruded post-collisional transtensional to extensional faults that reactivated the older structures. Plutons in the area are dated between 550 Ma and 520 Ma (Worku and Schandelmeier, 1996; Yibas et al., 2002); the Kenticha pegmatite has an emplacement age of 530 ± 2 Ma (U–Pb tantalite age; Küster et al., 2007). Other pegmatite-hosted occurrences in the ANS are at Laferug and Majayahan in Ethiopia (Küster, 2009).

Ghurayyah is hosted by a circular stock (0.9 km across) of porphyritic peralkalkaline arfvedsonite-alkali feldspar granite in the northwestern Midyan terrane (Küster, 2009). The stock is likely comagmatic with the adjacent larger Dabbagh granite, dated at 577 ± 13 Ma (Aleinikoff and Stoeser, 1988). Contacts of the stock dip steeply and wall rocks are only locally altered. Mineralization comprises disseminated columbite–tantalite, zircon, and thorite, and on the basis of limited drilling, constitutes a resource of nearly 400 Mt grading 245 g/t (0.024%) Ta_2O_5, 2840 g/t (0.28%) Nb_2O_5, 8915 g/t (0.89%) ZrO_2, and 1270 g/t (0.13%) Y_2O_3. Similar, but smaller, peralkaline-associated occurrences are at Jabal Hamra, Jabal Tawlah, Jabal Said, and Umm al Birak (Collenette and Grainger, 1994).

Abu Dabbab, in the Eastern Desert, is hosted by peraluminous granite, as is Nuweibi, and Nikrab in the Nubian Shield and Umm al Suqian in the Arabian Shield (Küster, 2009). The Abu Dabbab granitic body is a sheet- to stock-like intrusion as much as 300 m across, emplaced in early–middle Cryogenian ophiolitic mélange. The stock was probably intruded into tension gashes developed along a northwest-trending shear zone. The intrusion consists of strongly altered alkali-feldspar granite hosting disseminated Nb–Ta (columbite–tantalite) and Sn (cassiterite) minerals. Quartz and quartz–topaz veins occur in apical parts of the intrusion. The 44.5 Mt deposit is projected to produce more than 650,000 lb Ta_2O_5 per year over a mine life of 20 years as well as approximately 1530 tonnes of tin per year and may well become the world's largest supplier of tantalum feedstock (Gippsland Ltd., 2009, cited from company website February 2011 http://www.gippslandltd.com/). The Nuweibi prospect, 20 km S of Abu Dabbab, is an alkali-feldspar stock up to 2.2 km across. The stock has relatively high Ta content in its eastern part, where it contains indicated and inferred resources of 98 Mt ore grading 146 g/t Ta_2O_5 (Gippsland Ltd., 2007; cited by Küster (2009)).

A somewhat different type of mineralization consisting of U, Nb, Ta, and emerald is located along the Nugrus Shear Zone, in the Eastern Desert, Egypt. It is associated with alkaline pegmatites and granites (Lundmark et al., 2011). The mineralization is dated at 608 ± 1 Ma by ID-TIMS dating of a Nb–Ti oxide (Lundmark et al., 2011) tentatively identified as polycrase extracted from the Zabara orthogneiss. The orthogneiss has a protolith age of 633 ± 5 Ma. The Nb–Ti oxide has U contents in excess of 5% and also contains Y and Ta along with minor Ce, Th and Ca. It is proposed that the mineralization results from a hydrothermal flux associated with emplacement of highly fractionated syn- to post-kinematic leucogranites in the Nugrus Shear Zone (e.g. Abdalla and Mohamed, 1999; Lundmark et al., 2011). The leucogranites have Rb–Sr ages of 594 ± 12 and 610 ± 20 Ma (Moghazi et al., 2004), consistent with the Nb–Ti oxide age.

8.2.2. Tin and tungsten mineralization

Concentrations of tin and tungsten in the ANS are known in the northeastern Arabian Shield. The *Silsilah* tin prospect comprises low hills of greisenized granite in cupolas of an alkali-feldspar granite pluton (du Bray, 1984), surrounded by a large ring of alkali and alkali-feldspar granite (587 ± 8 Ma; Cole and Hedge, 1986) about 6 km in diameter. The mineralization is hosted by hydrothermally altered alkali-feldspar granite and comprises pods and disseminations of cassiterite in topaz–quartz and topaz–muscovite–quartz greisen. The deposit contains an estimated resource of some 1.5 Mt at an average grade of 0.19% Sn.

The *Ba'id al Jimalah* tungsten occurrence is located at a small intrusion of greisenized and quartz-veined porphyritic two-feldspar (perthitic microcline and albite) microgranite (569 ± 16 Ma; Cole and Hedge, 1986) emplaced in Murdama group sedimentary rocks about 100 km S of Silsilah. The occurrence is at the apex of an intrusion composed of interconnected and merging sills and

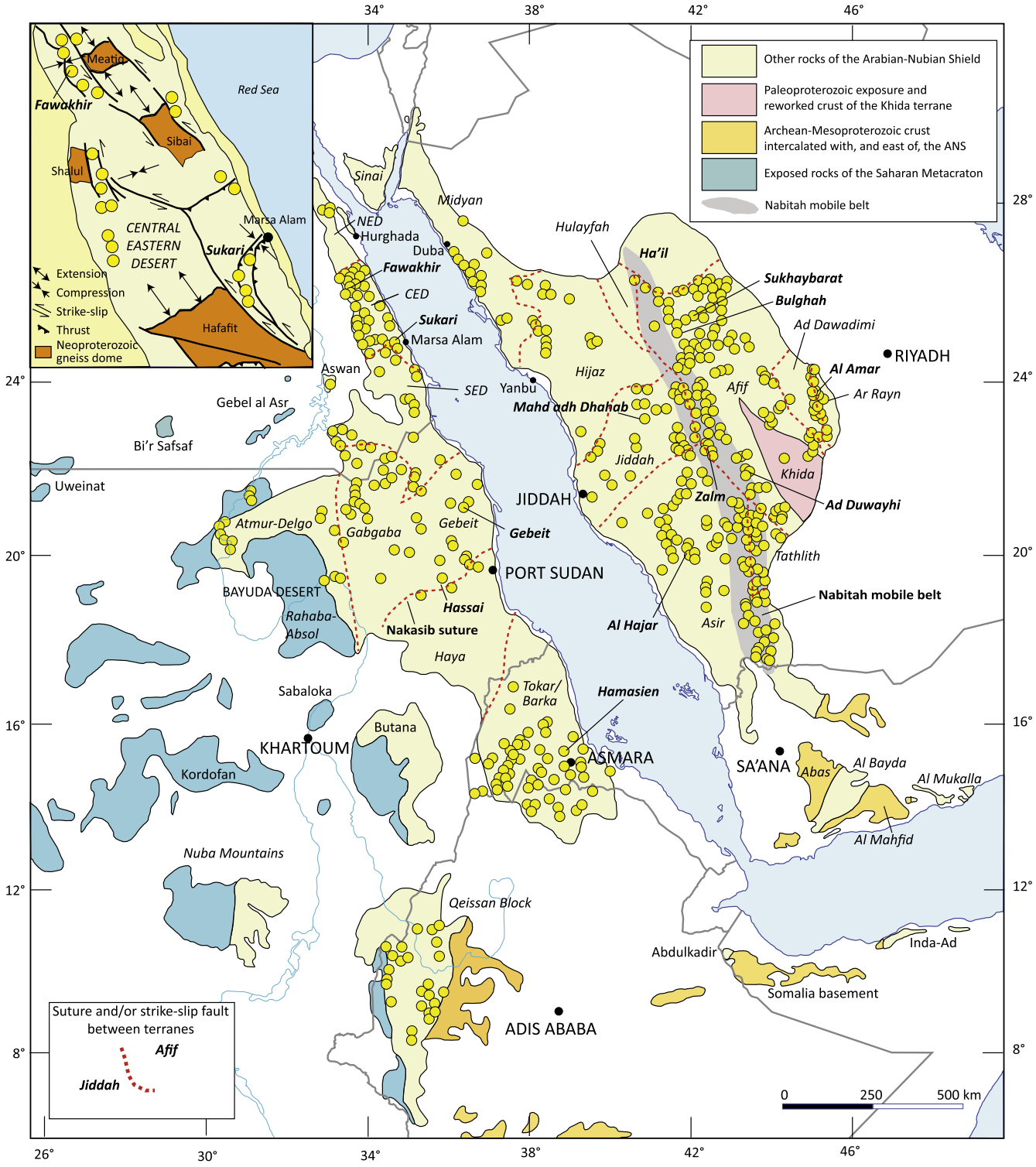

Fig. 23. Simplified plot of gold occurrences in the Arabian–Nubian Shield, showing their wide distribution throughout the region. The occurrences are predominantly late Cryogenian–Ediacaran orogenic-type gold in a variety of structural and lithologic settings, but include epithermal deposits (Mahd adh Dhahab, Al Amar), some VMS-gold, and carbonate-altered ultramafic-associated gold. After Saudi Arabian Mineral Occurrence Documentation System (for the Arabian Shield); Botros (2002) (for the Eastern Desert, Egypt); Klemm et al. (2001) (for northern Sudan); Tadesse et al. (2003) (for Ethiopia); Jelenc (1966) for Eritrea. Major deposits are named. Important orogenic-gold occurrences in Ethiopia, e.g., Lega-Dembi, are in the Adola Belt, at about 5°N, south of the present figure. Inset, after Helmy et al. (2004) as an example of the structural control on orogenic-type deposits.

dikes that connect with a larger sill about 100 m below the surface. Mineralization consists of wolframite, cassiterite, scheelite, and molybdenite in quartz veins and phyllic-altered microgranite and developed in three phases: early quartz-molybdenite stockwork veining; wolframite- and scheelite-bearing, greisen-bordered veining; and late quartz–carbonate–fluorite veining. U–Pb analysis of zircon from a quartz vein gives an approximate age of 575 Ma (Stacey and Stoeser, 1984), which is consistent with mineralization at

the time of granite emplacement. Fluid inclusions and oxygen isotope data indicate that the deposit formed over a temperature range of 120–550 °C, from low salinity magmatic and metamorphic fluids, and at a depth of about 4.2 km (Kamilli et al., 1993). Eighteen shallow percussion drill holes in the northern part of the occurrence outline a resource of 800,000 t of quartz-veined microgranite containing 0.090–0.117% WO_3 and 0.007–0.012% Sn, and the whole occurrence is estimated to be about 10 Mt.

8.2.3. Other types of granitoid-associated mineralization

Other types of late Cryogenian–Ediacaran granitoid-associated mineralization in the Arabian Shield include Ujaiyah (Khushaymiyah) (Mo–W–Bi), Bi'r Tawilah (W–Mo–Sn), and the Ad Dawadimi silver district (Pb–Zn–Ag), as well as a mineralized breccia pipe (Ablah-F), REE-bearing pegmatites and silexites, and contact Fe-replacement deposits associated with alkali-feldspar syenite, quartz alkali-feldspar syenite, quartz syenite, and particularly their fine-grained apical variants.

The *Ujaiyah* prospect is hosted by the Kushaymiyah batholith (611 ± 3 Ma; Agar et al., 1992) up to 50 km across, made up of as many as ten overlapping subcircular plutons of monzogranite and granodiorite, each 10–15 km in diameter. The batholith intrudes the Murdama group, and septa of Murdama rock are incorporated in the southeastern margin of the batholith. Mineralization is focused on the Thaaban pluton in the southeastern part of the batholith. The pluton is a ring complex with a core of quartz monzonite, an outer zone of granodiorite, and an outermost ring of younger quartz monzonite. The core is cut by a quartz vein swarm emplaced in pervasively sericitized and greisenized quartz monzonite. The veins carry disseminated pyrite, molybdenite, and scheelite with minor galena, chalcopyrite, and bismuthinite. The margin of the pluton has veins with Pb, Zn, Cu, and Ag. Metal values are low (averaging 80 ppm Mo in samples of quartz vein and host rock; and 430 ppm in veins alone), and no serious investigation has been conducted since early work by the USGS Saudi Arabian Mission (Dodge and Helaby, 1974).

The *Bi'r Tawilah* intrusion is a polyphase body of quartz leucodiorite, porphyritic biotite granodiorite, microgranodiorite, fine-grained porphyritic granite, and veins of albite microgranite (Collenette and Grainger, 1994). The intrusion was emplaced in sericite–quartz–chlorite schist immediately east of the Bi'r Tawilah thrust. Mineralization consists of aggregates and disseminations of wolframite, cassiterite, traces of base-metal sulfides, and pyrite in quartz veins in the intrusion and wall rock. Grades in the western part of the occurrence average 0.69% WO_3, 0.13% Sn, and 26 g/t Ag. Bi'r Tawilah tungsten was a primary focus of exploration in the area until a greater importance of gold was recognized.

The *Ad Dawadimi* silver district (Al-Shanti, 1976; Collenette and Grainger, 1994) comprises Pb–Zn–Ag mineralized quartz veins, which are similar to orogenic mesothermal gold veins in other parts of the shield but unique in that silver is the main economic metal. The district is in the heart of the Ad Dawadimi terrane in the eastern part of the shield centered on the town of Ad Dawadimi. The veins, many the site of ancient workings, crop out in an area of about 30 km N–S and 10 km E–W. Most of the mineralized veins, which trend either NW or NE, are in shear zones in a biotite monzogranite–granodiorite–quartz monzodiorite batholith or layered gabbro. The main silver minerals are polybasite, pyrargyrite, and freibergite, in association with galena and subordinate sphalerite. The wall rocks are extensively brecciated and pervasively affected by propylitic and weak phyllic alteration. The reason for such a concentration of silver-mineralized veins in this part of the shield is not known. Al-Shanti (1976) concluded that the mineralization was controlled by: (1) emplacement of the granite batholith; (2) Najd faulting which produced suitable host structures; and (3) the presence of Abt-formation argillaceous sedimentary inclusions in the batholith. During early investigations, only eight occurrences yielded results that justified drilling, and of the eight, only one (Samrah) is of any significance, with an estimated resource of 278,000 t grading 653 g/t Ag, 5.12% Zn, and 1.64% Pb.

Ablah, in the northwestern part of the Asir terrane, is the largest late Cryogenian–Ediacaran fluorite occurrence known in the ANS (Collenette and Grainger, 1994). It consists of massive fluorite and veins and pods of Cu-, Pb-, Zn-, and Ag-sulfides in a breccia pipe up to 22 m in diameter. The pipe is emplaced in a pegmatite–aplite breccia 300 m long and 130 m wide, which in turn is emplaced in a diorite host. *Jabal Hamra*, in the Hijaz terrane, is a lenticular vertical body of fine-grained silexite, an igneous rock composed essentially of primary quartz (60–100%), intruded into a quartz-alkali-feldspar syenite. The pipe carries disseminations of Nb-, Ta-, Sn-, REE-, Y-, Th-, U-, and Zr-bearing minerals and the host syenite contains pegmatite with Nb, Zr, Y, and REE minerals.

8.3. Late Cryogenian–Ediacaran arc-related mineralization

A distinctive suite of late Cryogenian–Ediacaran mineral occurrences are found in the Ar Rayn terrane in the easternmost ANS (Doebrich et al., 2007). They represent convergent-margin deposits of the type that elsewhere in ANS are associated with the older early-middle Cryogenian magmatic arcs but continued into the late Cryogenian–Ediacaran in the Al Amar arc because of ongoing >689–615 Ma subduction. The most notable occurrences are Al Amar, a polymetallic epithermal deposit, and Khnaiguiyah, a major Zn–Cu sulfide deposit (see references in Sangster and Abdulhay, 2005). Neither occurrence is dated, but mineralization is believed to be either approximately the same age or somewhat younger than the >689–615 Ma Al Amar-arc host rocks.

The *Al Amar* deposit comprises polymetallic and gold-bearing veins, subordinate massive sulfides, and beds and lenses of exhalative talc, barite, and Ca–Fe–Mn carbonates located a few hundred meters east of the Al Amar fault. The Al Amar host rocks include mafic to intermediate pyroclastic rocks and subordinate andesite flows; felsic volcaniclastic rocks and lava, subordinate red jasper, and polymict conglomerate; and felsic to intermediate tuffs and pyroclastic flows. The principal veins occur in two subvertical, northwest-trending zones referred to as the North and South Veins. They extend on the surface as much as 500 m along strike, discordant to the bedding, and to depths of at least 350 m. The veins are composed of quartz and subordinate Ca–Fe–Mn carbonates, barite, anhydrite, and sulfides (pyrite, sphalerite, chalcopyrite, and galena). Gold is locally free but mainly occurs as Au–Ag tellurides and electrum in the sulfides. Massive sulfide ore consists of sphalerite, barite, chalcopyrite, talc, carbonate, and chlorite, and probably originated during a period of volcanic quiescence. Doebrich et al. (2007) refer to the vein mineralization as epithermal, whereas Sangster and Abdulhay (2005) use the terms "structurally controlled, epigenetic". Pouit et al. (1984) interpret the massive sulfide mineralization as a volcanogenic exhalative deposit coeval with the formation of the Al Amar group. The deposit is in production, and as of mid-2007, had a reserve of 1.4 Mt ore grading 9.9 g/t Au, and total mineral resources comprising 2.0 Mt grading 11.2 g/t Au (SRK Consulting, 2007).

Khnaiguiyah is a sulfide deposit of uncertain origin in strongly sheared rocks in the northern part of the Ar Rayn terrane. It consists of four stratiform lenses of magnetite, hematite, pyrite, sphalerite, chalcopyrite, rhodochrosite, rhodonite, Ag-, Pb- and Bi-tellurides, and barite in carbonate-altered shear zones. The orebodies are hosted by discontinuous anastomosing bands of carbonatized rock in rhyolitic and subordinate andesitic rocks of

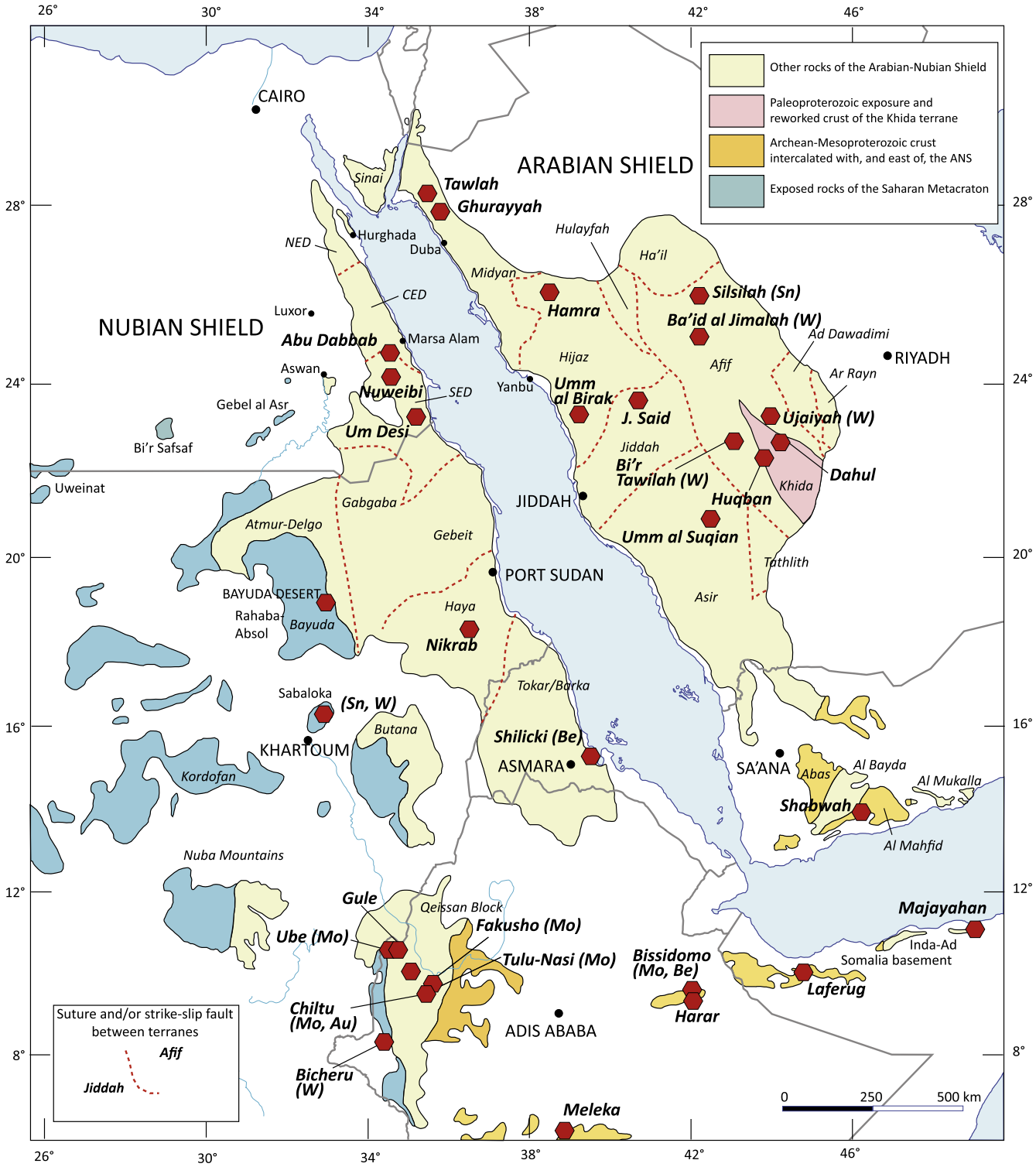

Fig. 24. Refractory and other special metal occurrences associated with late- to posttectonic, A-type granites, peraluminous granites, and localy pegmatites in the Arabian–Nubian Shield, after Saudi Geological Survey Mineral Occurrence Documentation System and Drysdall et al. (1984) (for the Arabian shield), Küster (2009) for Egypt, Sudan, and Somalia; and Jelenc (1966) and Tadesse et al. (2003) for Ethiopia and Eritrea. Occurrences are Ta–Nb–U rich unless otherwise indicated.

the Al Amar group. Alternative interpretations of the deposit are that it is a hydrothermal exhalation contemporary with the enclosing volcanic rocks—a type of VMS deposit (Testard, 1983), or that it is the result of hydrothermal alteration along post-metamorphic, posttectonic shear zones (BRGM Geoscientists, 1993). The Zn grades range between <5% and 33% and Cu grades range up to 1.5%. Resource figures published by BRGM Geoscientists (1993) indicate a "drill-measured total resource" of 24.8 Mt grading 4.11% Zn, 0.56% Cu.

8.4. Mafic-pluton associated mineralization

The *Lakathah* complex in the southwestern Arabian Shield (Martin et al., 1979) is a nearly circular posttectonic ring-dike

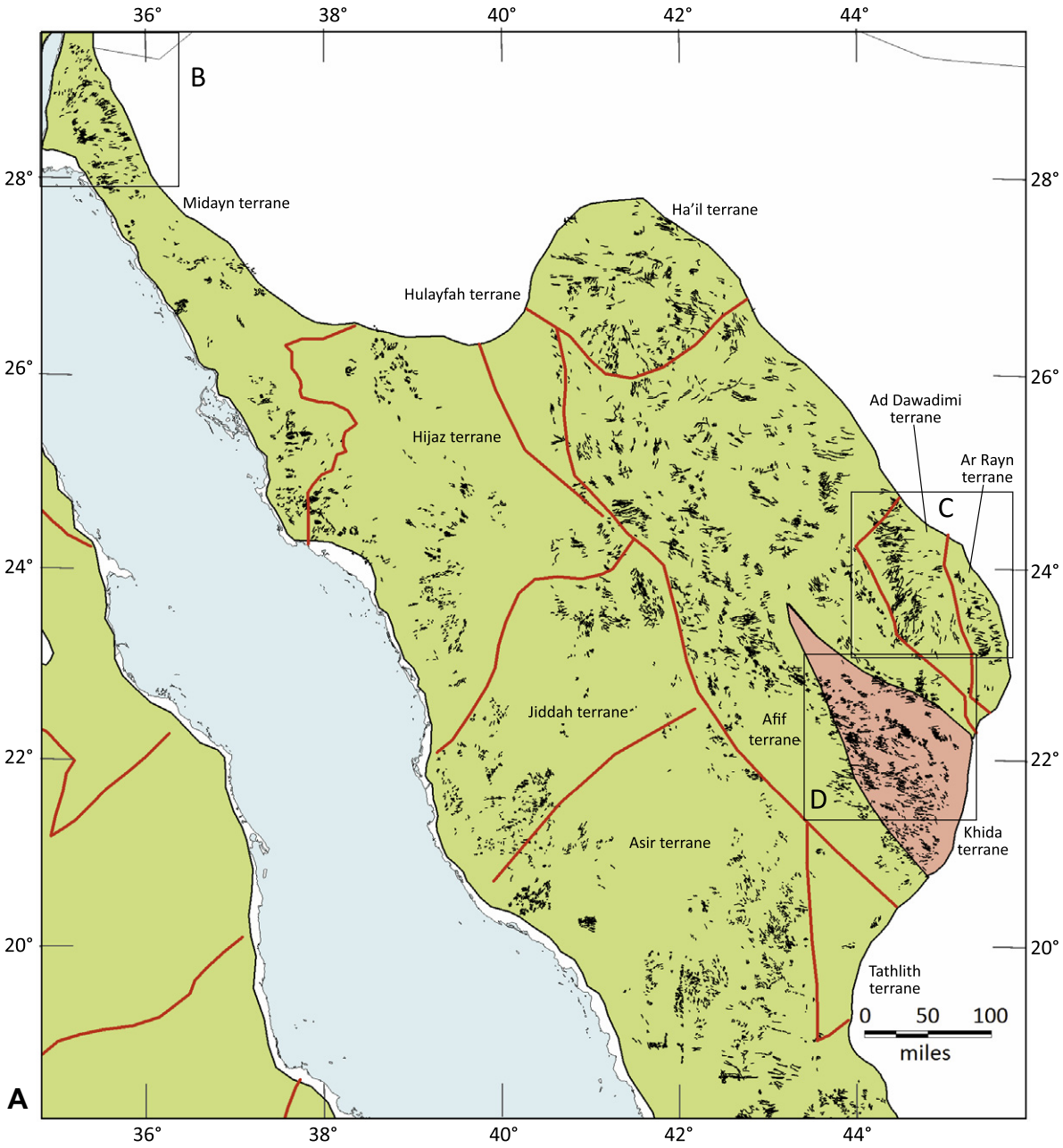

Fig. 25. Late Cryogenian–Ediacaran dikes swarms in the Arabian Shield. (A) A synoptic view showing the widespread distribution of dikes plotted on a simplified tectonic map of the shield. (B) Details of dikes in the Midyan terrane. Note the swing in orientation toward the Gulf of Aqaba reflecting rotation of Ediacaran dikes during Cenozoic sinistral strike slip on the Dead Sea transform. (C) Details of dikes in the Ad Dawadimi and Ar Rayn terranes. Note the change in prevailing dike orientation from north to south in the Ad Dawadimi terrane suggesting variation in the extension direction. (D) Detail of dikes in the Khida terrane and adjacent areas. Arrows shows schematic directions of extension implied by the prevalent strike-orientations of the dikes.

intrusion 10 km across composed of a pyroxenite–hornblendite core, an intermediate zone of diorite–gabbro, and an outer ring of syenite. Concordant lenses of titaniferous magnetite are present in the core ranging in thickness from a few centimeters to 3 m and as much as 50 m long. The *Wadi Kamal* complex, NW of Yanbu' al Bahr in the northwestern Arabian Shield, is an irregular body of norite, anorthosite, gabbro, and leucogabbro forming southern and northern lobes connected by a trail of scattered intrusions in surrounding schist and amphibolite. Gabbro and anorthosite predominate; norite forms an outer margin to the southern lobe. Samples of magnetite contain as much as 26% Ti and between 0.30% and 1.21% V_2O_5. A smaller body of dunite, amphibole-rich gabbro, and an ultramafic–mafic layered complex immediately S of the Kamal complex is a target for nickel and PGM mineralization. The concentrically zoned mafic–ultramafic *Akrarem* complex in the Eastern Desert contains Cu–Ni–PGE mineralization with net-textured and massive lenses of pyrrhotite, pentlandite, and chalcopyrite, as well as Cr-magnetite (Helmy and Mogessie, 2001). The ages of these intrusions, and their mineralizations, are not known, but they are undeformed massive plutons and, as suggested in Section 4.2, are likely to be late Cryogenian–Ediacaran.

9. Discussion

As schematically shown in Fig. 3, the final 100 million years of development of the Arabian–Nubian Shield is widely modeled in

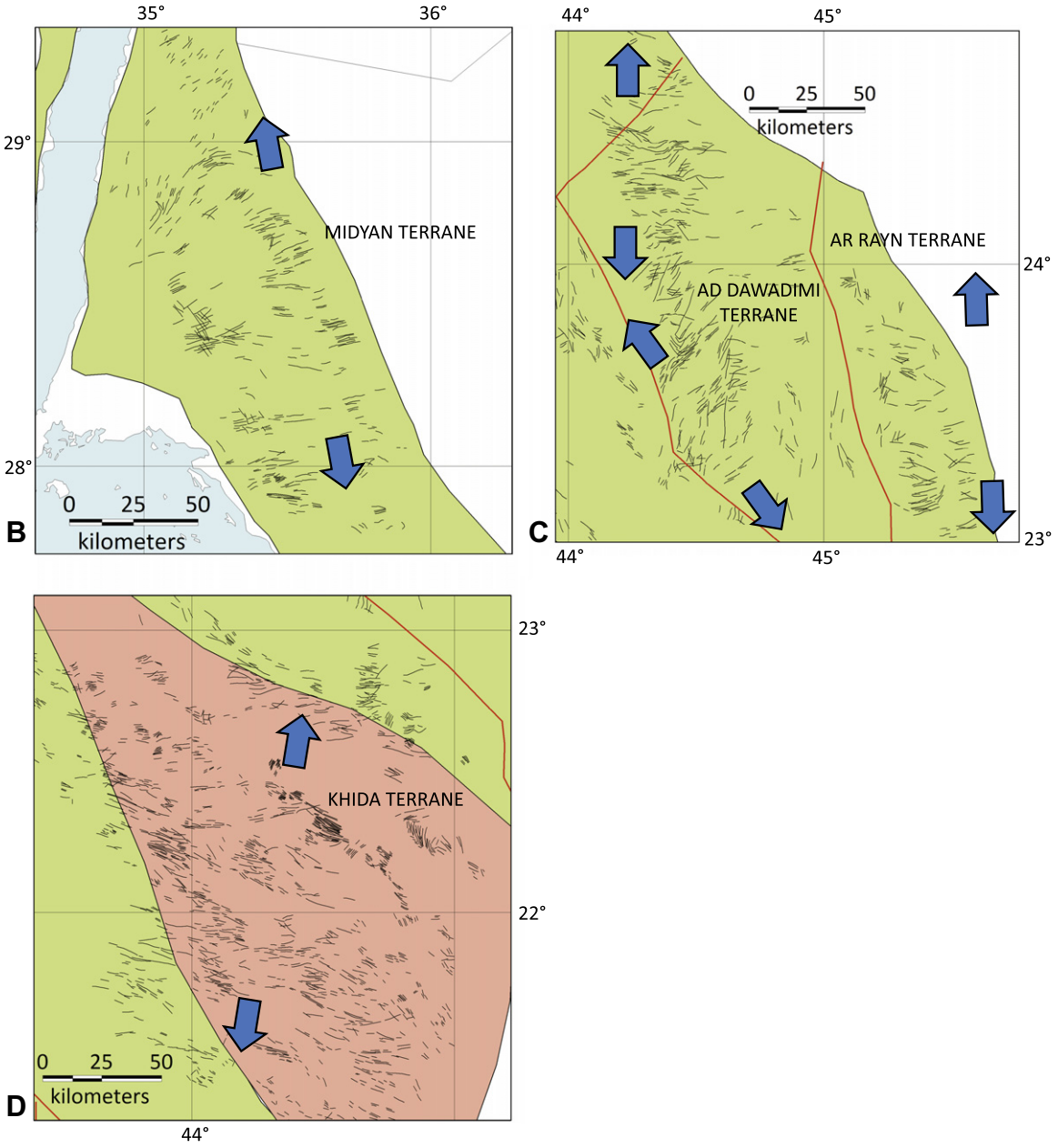

Fig. 25 (*continued*)

terms of crustal and lithospheric reworking. Elements in this process include transitions from peak orogeny to orogenic collapse, from lateral compression to pervasive lateral extension, from subduction-related magmatism and deposition to posttectonic/anorogenic magmatism and deposition, from the creation of intraoceanic juvenile arcs to the formation of a stable crust, and from periods of mountain-building and uplift to rapid and extensive erosional denudation.

Representative presentations of these transitions are by Stern (1994), Greiling et al. (1994), Abdeen and Greiling (2005), Blasband et al. (2000), Genna et al. (2002) and Johnson and Woldehaimanot (2003).

The model by Stern (1994), which is the background to the model shown in Fig. 3, and is widely accepted, initiates the formation of the ANS with seafloor spreading and the creation of arcs and backarcs following and during the breakup of Rodinia. Formation continued with the amalgamation of arc terranes and a few older continental fragments into new juvenile crust between about 870 Ma and 690 Ma. Continental collision and shortening first led to crustal thickening and uplift perhaps beginning about 750 Ma and continued with orogenic collapse and tectonic escape along strike-slip shear zones and faults until the end of the Precambrian.

The model of Greiling et al. (1994) and Abdeen and Greiling (2005) focuses on geologic events in the Eastern Desert of Egypt. They noted that the regional structure of the Eastern Desert mainly reflects post-collisional deformation characterized by extensional collapse, in some areas, and compression and (late) transpression, in other areas. Greiling and his colleagues noted the particular tectonostratigraphy of the Eastern Desert comprising suites of gneisses (Tier 1) structurally below low-grade supracrustal successions (Tier 2) (e.g., El Ramly, 1972; Bennet and Mosley, 1987; El-Gaby et al., 1988; Hermina et al., 1989; Shimron, 1990), but pointed out the lack of any difference between Tier 1 and Tier 2 rocks in terms of their protolith and geochemistry. They proposed that the two differ only in their degree of metamorphism and fabric and both represent juvenile Neoproterozoic crust, an

interpretation unequivocally supported by geochronologic and isotopic research over the past three decades, for example by work on the Meatiq and Hafafit domes (Andresen et al., 2009; Liégeois and Stern, 2010). In the Greiling and Abdeen-Greiling model, early Neoproterozoic igneous and metamorphic terrane-forming events occurred between 900 and 600 Ma. Collisional deformation of the terranes ended about 615–600 Ma, marked by a transition from Cryogenian compressional tectonics associated with calc-alkaline magmatism to an Ediacaran tectonic style that was dominated by A-type alkali granite magmatism. Greiling et al. describe extensional collapse occurring between 595 and 575 Ma, generating features such as molasse basins, normal faults, uplifted metamorphic core complexes flanked by low-angle normal faults, and high-angle strike-slip shear zones. A distinctive feature of their model is that the post-collisional extensional phase associated with NNW–SSE compression, NW-folding, and SE-dipping thrusts, was followed by a short period of shortening, mainly in a NNW–SSE direction, which led to folding and thrusting toward the NNW, and a subsequent period of transpressional wrenching related to Najd faulting. The Najd faulting resulted in northwest-trending sinistral faults and positive flower structures with NE-verging folds and SW-dipping thrusts. Regional compression after extension is interpreted as a continuation of plate convergence after an episode of extensional collapse.

Blasband et al. (2000) emphasize the presence of a widespread phase of Ediacaran crustal extension at the end of development of the ANS, but do not envisage a subsequent phase of compression. Formation of the ANS began with an oceanic phase represented by ophiolites and island arcs, followed by arc accretion, the development of sutures, and lithospheric thickening. The terminal events, triggered by gravitational instability leading to collapse of the ANS orogen, included pervasive NW–SE extension contemporary with the development of metamorphic core complexes, late-orogenic extensional basins, and large strike-slip shear zones.

Genna et al. (2002), discussing the Arabian Shield, refer to pre-Panafrican structures (>690 Ma) and Panafrican structures (690–590 Ma) that overprint and partly obscure the earlier structures. The pre-Panafrican structures developed in association with the formation, amalgamation, and accretion of oceanic volcanosedimentary terranes and the emplacement of diorite to granitic intrusions. These precratonic units were brought together by collision at about 690 Ma, which closed the oceanic domain and created sutures. Subsequent Panafrican tectonism (690–590 Ma) is represented by a complex web of structures referred to as the Nabitah Belt comprising anastomosing strike-slip shear zones, gneiss domes, and foreland and intracontinental molasse basins. Genna et al. infer that subsequent widespread intracontinental extension (590–530 Ma) caused crustal thinning, bimodal magmatism, the emplacement of significant dike swarms, and volcanism. A marine transgression toward the end of the extension phase led to deposition of the Jibalah group and effectively ended formation of the Arabian Shield. Further shield history belongs to the Phanerozoic passive-margin that developed along the margin of the shield.

In the tectonic model of Johnson and Woldehaimanot (2003), the Arabian Shield is considered to consist of Archean and Paleoproterozoic continental crust at its margins and in the Khida terrane, and a large swath of Neoproterozoic (*c.* 870–670 Ma) continental–marginal and juvenile intraoceanic magmatic-arc terranes that accumulated in the Mozambique Ocean. Subduction began about 870 Ma, and initial arc–arc convergence and terrane suturing occurred at about 780 Ma, marking the beginning of ocean-basin closure and Gondwana assembly. Terrane amalgamation continued until about 600 Ma, resulting in the juxtaposition of eastern and western Gondwana. Terrane amalgamation was associated with overlapping periods of post-amalagamation basin formation, rifting, compression, strike-slip faulting, and the creation of gneiss domes in association with extension and/or thrusting. Final assembly of Gondwana was achieved by about 550 Ma. Most post-amalgamation basins contain molasse deposits, but those in the eastern Arabian Shield and Oman have marine to glaciomarine deposits, which indicate that seaways penetrated the orogen soon after orogeny. The varied character of the post-amalgamation events reflects alternating periods of Late Neoproterozoic extension and shortening, uplift and depression, deposition and erosion.

These models have many elements in common, but differ in detail about the timing and significance of the events that went into the creation of the ANS. It is worth considering, therefore, the evidence for some of the key elements in these models within the late Cryogenian–Ediacaran timeframe of this review.

9.1. Extension

A common theme in many Ediacaran tectonic models of the ANS is upper crustal extension both in a broadly N–S or NW–SE direction parallel to the orogen, and an E–W direction transverse to the orogen. The principal evidence for extension derives from a set of interrelated structural features: (1) dike swarms; (2) low-angle normal faults or detachments; and (3) transcurrent faulting and extensional basins.

9.1.1. Dike swarms

Late Cryogenian–Ediacaran mafic, felsic, and composite mafic–felsic dikes are widespread in the ANS. They are well known in the northern part of the Nubian Shield, Sinai, and Jordan (Stern et al., 1984; Abdel-Karim and El-Baroudy, 1995; Jarrar, 2001; Jarrar et al., 1992, 2004). Similar, although less well known, dike swarms are present in the Arabian Shield (Fig. 25) (Genna et al., 2002). Such dikes are unambiguous evidence of extension during the final stages of shield development (Stern et al., 1984; Stern, 1985; Genna et al., 2002). The dikes are posttectonic. They represent some of the youngest Neoproterozoic rocks in any given area and cross cut most other rocks and structures. Several of these dikes have been dated, including lamprophyre dikes that intrude the Ajjaj shear zone in the Midyan terrane (573 ± 6 Ma; Kennedy et al., 2011), a 577 ± 5 Ma dike that intrudes the Jibalah group in the north-central part of the Arabian shield (U–Pb zircon age; Kusky and Matsah, 2003), a 591 ± 9 composite dike from Feiran, Sinai (Stern and Manton, 1987), a 591 ± 12 Ma dike in NE Egypt (Stern and Voegeli, 1987), dikes between 600 and 540 Ma in northernmost Sinai (Kessel et al., 1998), pegmatite dikes between 574 ± 11 and 564 ± 10 Ma in Jordan (Jarrar et al., 1983), and composite and mafic dikes in Jordan dated at 575 ± 6 Ma and 545 ± 13 Ma (Jarrar, 2001). In detail, Genna et al. (2002) recognize multiple generations of posttectonic dikes. They occur in linear or curved swarms varying from a few centimeters to meters in thickness and from several meters to several tens of kilometers in length. In a given area, the dikes may have a common strike direction or form a conjugate system with intersecting strikes. The dikes are mostly subvertical, commonly rhyolitic, but include basalt and andesite. Bimodal swarms are common, containing andesitic and rhyolitic dikes that display intrusive relationships indicative of synchronous emplacement of mafic and felsic magma (Stern et al., 1984) or consist of composite dikes that individually are bimodal with felsic cores and mafic external parts (Jarrar et al., 2004; Stern and Voegeli, 1987; Katzir et al., 2007). The orientations of the swarms vary across the region and no systematic quantitative analysis of their strikes has been published other than work by Genna et al. (2002). But on inspection (e.g., Fig. 25; Fig. 2 in Stern et al., 1984; Fig. 1C in Jarrar et al., 1992), it is evident that the dikes in many swarms trend in an easterly direction. For example, those in the North and Central Eastern Desert trend NE (Stern et al., 1984;

Greiling et al., 1988, 1994) as do those in the Ha'il (Fig. 25A) and Midyan and Ar Rayn terranes in the Arabian Shield (Fig. 25B and C). Dikes in the Khida terrane trend ESE (Fig. 25D), whereas those in the Elat and Amran area (southern Israel) include older calc-alkaline N–S-trending dikes, younger tholeiitic NE–SW-trending dikes, and a few basalt dikes trending NW–SE (Kessel et al., 1998). The orientations of these dikes are strong evidence of broad northerly extension in the northern ANS during the Ediacaran. Garfunkel (1999) estimates that intrusion of swarms of basaltic to rhyolitic dikes in the northern ANS was accommodated by ~20 km regional dilation. It should be noted however, that not all easterly trending dikes in the Arabian–Nubian Shield are Ediacaran. Greiling et al. (1988) describe a major swarm of ENE-trending basaltic dikes in the northern part of the Hafafit dome that are intruded by the Gabal Abu Khrug ring complex (~90 Ma; Lutz et al., 1978) and are believed to be about 104 Ma (Greiling et al., 1988).

9.1.2. Low-angle normal faults and shear zones

Late Cryogenian–Ediacaran low-angle normal faults or detachments are reported from many parts of the ANS, likewise implying crustal extension. The most widely publicized are in the North and Central Eastern Desert and Sinai, described from gneiss domes and structural highs. The Meatiq and Hafafit domes are flanked on the north and south by NNW- and SSE-dipping normal faults, comprising post-accretion low-angle ductile shear zones with top to NNW or top to SSE senses of slip (Fritz et al., 1996, 2002; Fowler and Osman, 2009; Rice et al., 1992). In Sinai, Blasband et al. (1997, 2000) describe moderately NW-dipping shear zones with top-to-the-NW sense of shear in Wadi Kid, and conclude that this is an extensional core complex, although Fowler et al. (2010) suggest that the low-angle shears are collision-stage thrusts. U–Pb SHRIMP zircon ages reported by Stern et al. (2010a) constrain extension in the Kid complex to have occurred between ~600 MA and 585 Ma. The constraint is provided by a concordant age of 598 ± 8 Ma obtained from a rhyodacite clast in the Beyda Formation (Heib Formation of Shimron, 1984), which predates development of the Wadi Kid core complex, and a concordant age of 585 ± 8 Ma obtained from the Kid granite, which postdates the core complex. In the southern ANS, low-angle shear zones are reported from the ~100 km-long 1–5 km-wide north-trending Chulul shear zone in the Bilbul belt of Ethiopia, containing moderately east-dipping mylonitic fabric displaying a top-to-the-SE sense of movement (Tsige and Abdelsalam, 2005). Pervasive subhorizontal to moderately west-dipping foliations in HP–HT amphibolite-facies gneiss and schists occur in the Ghedem Domain in eastern Eritrea (Ghebreab, 1999). A low-angle, top-to-the-E/SE brittle–ductile shear zone separates the Ghedem Domain in the footwall from lower grade metavolcanic and metasedimentary rocks of the Nakfa or Bizen Domain in the hanging wall (Ghebreab and Talbot, 2000; Beyth et al., 2003). Overall, these structures suggest that NW–SE extension prevailed in the northern ANS, with extensional fabrics dipping NW and(or) SE, whereas E–W extension prevailed in the south.

9.1.3. Transcurrent faulting

As described above, late Cryogenian–Ediacaran transcurrent faults of the Najd system are conspicuous in the ANS. The faults are oblique to the main N–S trend of the EAO. In detail, the faults are transpressional structures with components of vertical as well as horizontal slip, but the prevailing sinistral sense of movement implies overall N–S extension parallel to the axis of the EAO. Additional evidence of extension in association with the Najd faults is the presence of the Dokhan–Hammamat and Jibalah group pull-apart basins located between left-stepping faults or in strain-releasing bends.

9.2. Exhumation, uplift, and denudation

Exhumation, uplift, and erosion are another set of interrelated processes widely modeled by many authors for the final 100 million years of evolution of the ANS. Exhumation refers to the return of once deep-seated metamorphic rocks to the Earth's surface and, particularly, refers to the unroofing of a rock defined by the vertical distance traversed relative to the Earth's surface (Ring et al., 1999). The term "uplift" has two aspects: one refers to the vertical motion of Earth's surface relative to sea level (surface uplift); the other to the vertical motion of rock relative to sea level (rock uplift). Denudation refers to the removal of material on the Earth's surface.

The process driving ANS exhumation is debated. One school of thought invokes orogenic collapse following the development of an ANS crust thickened by orogeny. Avigad and Gvirtzman (2009), for example, argue that extension and orogenic collapse in the northern ANS were associated with the removal and replacement of thickened lithospheric mantle by delamination. They estimate that mantle delamination would cause more than 3 km uplift. This would trigger rapid erosional unroofing of a rock carapace about 10 km thick and cause extension as well as decompression leading to partial melting of the ANS upper mantle and lower crust; perhaps this was responsible for the flood of posttectonic magmas? Erosional denudation may be followed by an episode of isostatic uplift but erosion, as well as thermal subsidence, would ultimately lower the surface to sea level. Other authors (e.g., Fritz et al., 1996) argue that no substantial crustal thickening occurred, at least in the Eastern Desert of Egypt, and infer that exhumation of, in this case, core-complex gneisses, was achieved as the result of enhanced heat flow along fault systems during oblique NW–SE transpression and by extension on normal faults. The enhanced heat flow would have enabled the formation of syn-extensional plutonism and triggered the exhumation of hot middle crust. Garfunkel (1999) infers that the northern ANS underwent rapid erosion beginning about 610 Ma following the magmatic phase at the end of the orogenic period, during which the upper 8–12 km of crust was removed in about 20 million years, lowering the average relief by about 2 km. Later, the area was differentiated into basins and highs associated with sedimentation and concurrent emplacement of high-level alkali-rich plutons, and was eroded, which further reduced the relief.

Direct evidence of exhumation, uplift, and denudation in the ANS includes: (1) regional angular unconformities and nonconformities and deposition of clastic sedimentary rocks; and (2) post-metamorphic and(or) post-intrusion mineral cooling ages testifying to tectonic exhumation.

9.2.1. Unconformities

Angular unconformities and nonconformities are present in the ANS at the base of post-amalgamation basins. It is not always certain when these unconformities developed but it is likely they developed due to uplift and denudation at many different times. The oldest unconformity considered in this review is the middle Cryogenian erosion surface that truncates the 660 ± 4 Ma Imdan plutonic complex at the base of the Thalbah group. The group itself was deposited in a terrestrial basin at some unknown elevation above sea level. Erosional truncation of the plutonic complex indicates several kilometers of exhumation prior to deposition of the Thalbah group, and the thick sequence of conglomerate, sandstone, and shale in the group itself evidences a vast amount of denudation.

The Murdama group in the northeastern ANS was deposited at or below sea level on an erosion surface truncating diorite, quartz diorite, tonalite, granodiorite, and gabbro of the Suwaj domain (~680 Ma) (Cole and Hedge, 1986) as well as mafic granulite (Cole, 1988). The presence of granulite beneath the Murdama unconfor-

mity implies as much as 15–20 km exhumation prior to Murdama deposition. The unconformity developed sometime between emplacement of the Suwaj domain and the onset of Murdama deposition, namely in the interval between 680 and 650 Ma. During the course of deposition, the basement of the Murdama group must have undergone at least 10–15 km subsidence so as to accommodate the thick clastic Murdama succession. The merely local presence of conglomerate in the Murdama and the relatively small conglomerate-clast size (pebble to cobble; not boulder) suggest little differential uplift at the margins of the Murdama basin, implying that erosion of the hinterland kept pace with exhumation. The thick succession of marine carbonates close to the base of the Murdama group demonstrates that the surface of the basin was at or below sea level. Murdama group deposition overlapped and followed the 680–640 Ma Nabitah orogeny yet the depositional environments of the basin and other marine post-amalgamation basins described earlier in this review, suggest that a large area in the ANS on either side of the Nabitah mobile belt lacked great elevation within a relatively short period after orogeny. Either denudation was intense or the Nabitah orogeny did not produce a high mountain range, perhaps because the area underwent shortening and extensive magmatism rather than a great degree of thrust stacking. In the Timna area, Israel, a cryptic unconformity developed sometime after emplacement of ~630 Ma dikes (Katz et al., 2004), which were metamorphosed at amphibolite facies, and after intrusion of the epizonal Timna granite ~610 Ma (Beyth et al., 1994).

In Egypt, the unconformities at the base of the Dokhan Volcanics and Hammamat Group developed sometime after emplacement and exhumation of 620–610 Ma granitoids. The coarse clastic sediments of the Hammamat Group are evidence that exhumation and erosion developed a land surface with significant relief, with conglomerates deposited at the discharges of high-relief drainage basins (Eliwa et al., 2010). The basins themselves have no marine sediments, indicating elevations in the western part of the ANS at this time above sea level. In Arabia, the minimum age of unconformities beneath the Jibalah group is not well constrained. Jibalah rocks in the Jifn basin, for example, overlie 625 Ma rhyolite (Kusky and Matsah, 2003), but in the Antaq basin overlie rocks of the Suwaj domain (~680 Ma). Differential uplift across basin margins is considered to be the cause of fanglomerates in some of the terrestrial dominated Jibalah basins (Kusky and Matsah, 2003). Stromatolitic carbonates and carbonates with indications of a marine isotopic signature in other Jibalah basins suggest that the northern and northeastern parts of the ANS had locally subsided below sea level by 580–560 Ma.

The most profound unconformity in the ANS is the vast erosion surface represented by the contact between the shield and overlying Lower Paleozoic sandstone (Fig. 26). Wherever observed, Lower Paleozoic sediments overlie a saprolitized-lateritic weathered profile a few meters thick passing down into less weathered shield rocks. The erosion surface has mostly low relief (Fig. 26) and the basal Paleozoic rock is sandstone with only scattered matrix-supported pebbles, not conglomerate. The sandstone was deposited by a continental-wide braided stream system with a constant south-to-north (present configuration) flow direction over a very gentle slope (Kolodner et al., 2006). The sandstone now has mostly been removed from the ANS but is preserved around the margins of and in rare outliers on the Arabian Shield. This sandstone probably covered most of the ANS at the time of its deposition. Intense chemical weathering is considered to be important for the formation of the sub-Paleozoic erosion surface (Avigad et al., 2005; Angerer et al., 2011). Subsequent Phanerozoic burial vertically compacted laterite to about 75% of its original thickness (Angerer et al., 2011). Worldwide, the Ediacaran was a period of glaciation, at ~630 (Marinoan) and ~580 Ma (Gaskiers) (Smith, 2009). Evidence for Ediacaran glaciation is reported from Oman (e.g., Brasier et al., 2000), but apart from local exposures of possible Jibalah-age diamictite, the presence of Ediacaran glaciers in the ANS remains to be demonstrated. It is therefore uncertain whether glaciation helped carve the end-Precambrian peneplain.

The sub-Paleozoic erosion surface locally truncates the Jibalah group and 580–560 Ma alkali granites, and in such localities the unconformity has a maximum age of about 560 Ma. Elsewhere, the erosion surface truncates much older rocks, and may reflect erosion considerably older than 560 Ma. Cole and Hedge (1986) infer that the northeastern Arabian Shield underwent as many as three major periods of erosion prior to deposition of Lower Paleozoic sandstone. Erosion between 640 and 615 Ma truncated the Murdama group and older rocks and formed the surface on which the Hibshi (632 Ma) and Jurdhawiyah (612–594 Ma) groups were deposited. Further erosion may have followed emplacement of diorite, granodiorite, and granite of the Idah suite (620–615 Ma). It is possible that emplacement of this suite, as well as the volcanic rocks of the Hibshi and Jurdhawiyah groups, resulted from such extensive partial melting that the density structure and isostatic equilibrium of the crust was altered enough to cause epeirogenic uplift, leading to renewed erosion and the production of local high-relief surfaces flanking Jibalah-group basins (Cole and Hedge, 1986). The Jibalah group and broadly contemporary peralkaline, peraluminous, and leucocratic granites of the Abanat suite (580–570 Ma) were, in turn, exhumed and eroded prior to deposition of the Lower Paleozoic sandstone cover. It is interesting to note that in several locations in the northeastern Arabian Shield, only the apical parts of Abanat suite plutons are exposed and rhyolitic flow and pyroclastic rocks vented by Abanat plutons are preserved, implying that the Abanat plutons and associated volcanic rocks were little exhumed and denuded. Idah suite plutons (~620; Cole and Hedge, 1986), in contrast, are eroded to deeper levels. Because little-eroded Abanat suite plutons and deeply eroded Idah suite plutons are exposed in adjacent outcrops, Cole and Hedge (1986) concluded that most erosion in the northeastern Arabian Shield occurred after emplacement of the Idah suite but before intrusion of the Abanat suite, likely, between about 615 and 580 Ma. Abanat suite plutons were intruded into crust that had already been exhumed and denuded, but were themselves little eroded prior to deposition of the Lower Paleozoic sandstone. Similar multiple periods of erosion are suggested for the northernmost ANS in Sinai, Negev, and Jordan (Samuel et al., 2007). The northern ANS contains A-type granitoids and ~580–530 Ma alkaline rhyolite and volcanic-equivalents such as the Dokhan Volcanics of Egypt and Feinan volcanic succession in Jordan. As in the northeastern Arabian Shield, the presence of late Ediacaran–Cambrian(?) intrusives and extrusive equivalents implies relatively little denudation and exhumation after their emplacement. But Samuel et al. (2007) infer that emplacement of the A-type rocks was preceded by a phase of extensive erosion associated with lithospheric extension and crustal rupture.

The Lower Paleozoic sandstone flanking the ANS represents a fluviatile environment that grades laterally and vertically in Jordan and Israel into a marine environment represented by the Burg limestone. At the end of the Precambrian, therefore, the surface of the ANS was mostly close to or above sea level, passing below sea level to the north and northeast (present-day coordinates) where continental crust of the newly formed EAO had a free ocean face. High mountains, however, existed farther S in EAO, part of the >8000-km-long and >1000-km-wide mountain chain (the Transgondwanan Supermountain) that formed following the oblique collision between eastern and western Gondwana (Squire et al., 2006) and provided much of the clastic material of the Lower Paleozoic sandstone.

9.2.2. Cooling ages

Although unconformities are important indicators of exhumation and denudation, the timing of exhumation is best determined by cooling ages. It is well known that faulting, among other processes, is capable of unroofing mid-crustal rocks. A hallmark of such unroofing is the resetting of footwall rocks to a common isotopic age reflecting cooling as the hangingwall is stripped away. As a consequence, low-temperature thermochronometry is a fundamental tool in identifying and dating exhumation (Stockli, 2005). The principle is that the age determined reflects cooling below the thermal blocking temperature of the rock or mineral being dated, rather than the age of mineral growth during metamorphism or the age of thermal resetting. In some cases, Rb–Sr and Sm–Nd whole-rock or mineral ages are interpreted as cooling ages (see examples in Appendix A). Most commonly, however, for the purposes of research in the ANS, cooling ages are determined by $^{40}Ar/^{30}Ar$ dating of hornblende, white mica, and sometimes feldspar. Rapid cooling, the hallmark of exhumation, is inferred if two minerals (commonly hornblende and white mica) extracted from the same sample have similar cooling ages, the argument being that for two minerals with different blocking temperatures to have the same age means that the host rock rapidly cooled and was therefore rapidly exhumed. The present Arabian–Nubian Shield $^{40}Ar/^{30}Ar$ age dataset includes 23 cooling ages (Table 1); other $^{40}Ar/^{30}Ar$ ages reflect thermal resetting or prograde metamorphism. The cooling ages spread between about 620 and 555 Ma with peaks at 575–580 Ma and 595–600 Ma (note that the ages shown in Fig. 27 designate the age at the beginning of each 5 million-year bin).

As indicated in Fig. 27, the main period of cooling and exhumation in the ANS was between 600 and 575 Ma. However, some variation occurs by region. Beyth et al. (2003) and Ghebreab et al. (2005) determined that crust in northeastern Ethiopia and eastern Eritrea underwent rapid exhumation between 640 and 545 Ma. Gneisses in the Ghedem domain in eastern Eritrea have average plateau ages of about 579 ± 6 Ma for hornblende and 567 ± 5 Ma for white mica (Ghebreab et al., 2005) (Table 1). The gneisses underwent peak metamorphism when *P–T* conditions were near 12 kbar and 650 °C at a depth of as much as 45 km. They subsequently rose to about 30 km and cooled at about 570 Ma, and further rose and cooled at about 567 Ma (Ghebreab et al., 2005). Exhumation was accomplished by extension on the low-angle shear surfaces described above (Beyth et al., 2003; Ghebreab et al., 2005). Final exhumation of Ethiopian and Eritrean crust occurred during the Cenozoic due to deformation (rift-margin uplift) related to the opening of the Red Sea. The same process of rift-margin uplift affected crustal rocks of the ANS in Yemen, Saudi Arabia, and Sinai. The crest of the Red Sea escarpment on both flanks of the southern Red Sea, in Eritrea–Ethiopia, Yemen, and southern Saudi Arabia is 2500–3000 m above sea level, and Cenozoic uplift of this amount must be taken into consideration when estimating end-Precambrian exhumation of ANS crustal rocks.

Basement rocks in northern Sinai were rapidly exhumed at about 600 Ma (Cosca et al., 1999). Peak regional metamorphism occurred in the mid-crust at about 620 Ma under *P–T* conditions of 7 ± 1 kbar (20–25 km depth) and 650–700 °C. Muscovite and biotite from the Elat schist, Taba gneiss, Elat granite, and Elat granitic gneiss record rapid exhumation and cooling at ~600 Ma, synchronous with widespread A-type igneous activity and a transition from orogenic to post-orogenic tectonics reflecting large-scale extension and tectonic escape (Cosca et al., 1999).

In the eastern Arabian Shield, rapid cooling is recorded by hornblende $^{40}Ar/^{30}Ar$ plateau ages of 612 ± 3, 611 ± 8, 610 ± 2, and 596 ± 6 Ma obtained from amphibolite and metagabbro in the Ar Ridaniyah ophiolite mélange in the central part of the Ad Dawadimi terrane. The ages reflect reactivation of the Ar Ridaniyah fault and rapid exhumation of the mélange (Al-Saleh and Boyle, 2001). To the south, a $^{40}Ar/^{39}Ar$ isochron age of 557 ± 15 Ma obtained from biotite paragneiss in the Kirsh gneiss along the Ar Rika fault zone is interpreted as the time of cooling below the biotite closure temperature (Al-Saleh, 2010). The age reflects exhumation of the gneiss and by implication, constrains the minimum age of development of the Kirsh gneiss dome.

Regional cooling and exhumation in the Egyptian Central Eastern Desert is constrained by Sm–Nd and Rb–Sr ages obtained from biotite, hornblende gneiss, and amphibolite in the core of the Hafafit dome (Abd El-Naby et al., 2008) and by $^{40}Ar/^{30}Ar$ hornblende and muscovite ages obtained from the Hafafit, Sibai, and Meatiq Domes (Fritz et al., 2002). The available data indicate that granite gneiss in the *Hafafit Dome* with protolith crystallization ages of 682 Ma (Stern and Hedge, 1985), 698 Ma and 700 Ma (Kröner et al., 1994), underwent amphibolite-facies metamorphism under conditions of 600–750 °C and 6–8 kbar. Peak metamorphism was attained at about 600 Ma or slightly earlier (Abd El-Naby et al., 2008). Cooling after this peak is indicated by garnet, plagioclase, and whole-rock Sm–Nd ages of 593 ± 4 Ma and 585 ± 8 Ma. A Rb–Sr biotite and whole-rock age of 573 ± 6 Ma obtained from biotite gneiss and $^{40}Ar/^{39}Ar$ hornblende plateau ages of 586 Ma and

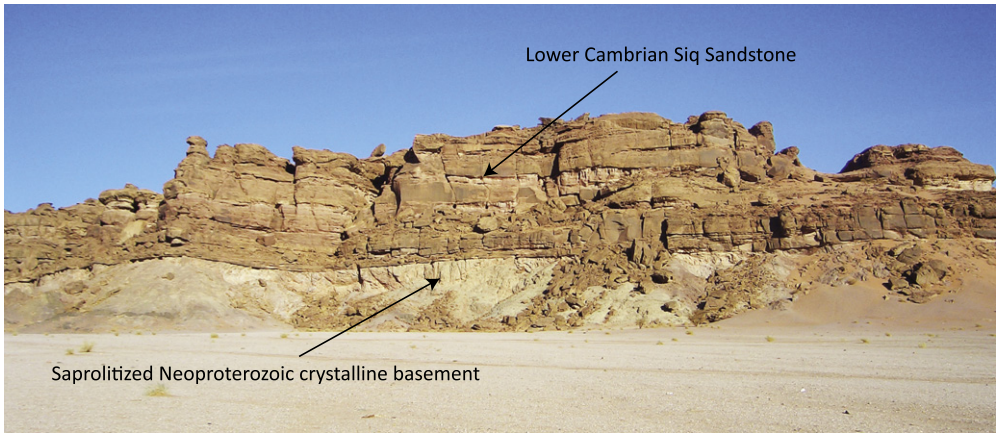

Fig. 26. Unconformity at the contact between the Arabian Shield and Lower Paleozoic sandstone, represented by a low-relief erosion surface exposed in a cliff about 50 m high about 25 km southwest of Al 'Ula at the northern margin of the shield in Saudi Arabia. At this locality, the shield rocks comprise Cryogenian greenstone and plutonic rocks belonging to the Midyan terrane. The Lower Paleozoic is sandstone and pebbly sandstone assigned to the Siq Sandstone. The shield rocks are deeply weathered for several meters beneath the unconformity, and present as saprolite.

584 Ma reflect further cooling and exhumation (Abd El-Naby et al., 2008) possibly localized along northeast-trending extensional faults (Fritz et al., 2002).

Hornblende $^{40}Ar/^{39}Ar$ plateau ages of 587 Ma, 583 Ma, 580 Ma, and 579 Ma from the Um Ba'anib gneiss indicates contemporary cooling and exhumation in the *Meatiq Dome*. Garnet-kyanite metapelite in the Meatiq Dome underwent peak metamorphism of ~750 °C and 8 kbar (about 27 km depth). This was followed by decompression to 4–5 kbar (13–17 km depth) (Neumayr et al., 1998) with a $^{40}Ar/^{39}Ar$ muscovite age suggesting rapid cooling and exhumation at about 583 Ma (Fritz et al., 2002). Muscovite from strike-slip and extension shear zones on the west and south of the Meatiq Dome yield plateau metamorphic ages of ~588 Ma and ~595 Ma indicating slip on the shear zones contemporary with 583 Ma exhumation within the dome (Fritz et al., 1996).

The *Sibai Dome*, in contrast, appears to have been exhumed 30 million years earlier at about 623 Ma with late cooling during exhumation and denudation after advective heating because of granite intrusion at 606 Ma (Fritz et al., 2002).

9.3. Orogenic collapse

It is common to refer to orogenic collapse in the closing stages of development of the ANS (Greiling et al., 1994; Fowler and El Kalioubi, 2004; Tsige and Abdelsalam, 2005; Ghebreab, 1999). Collapse occurs when lithostatic pressure exceeds rock strength limiting isostatically compensated elevation. The elevation of mountain belts (orogens) is determined by the balance between the force generated by plate convergence (collision), which causes the stacking of thrust sheets, buckling of rock sequences, crustal thickening, and the rise of mountains, and the force of gravity. With respect to the ANS, a pertinent question affecting the applicability of gravitational collapse concerns the amount by which the ANS was elevated above sea level at and after the peak of orogeny.

The *P–T* metamorphic conditions noted above suggest that a mountain belt existed in the southern ANS at about 650 Ma, and it is believed that this part of the ANS underwent rapid exhumation by orogenic collapse on low-angle shear zones between 640 and 545 Ma (Beyth et al., 2003). In contrast, the presence of marine post-amalgamation basins in the eastern ANS suggests that much of this part of the ANS was at or below sea level soon after the Nabitah orogeny peak deformation and metamorphism (680–640 Ma). The low elevations in the eastern ANS may reflect weak Ediacaran lithosphere due to largely molten lower crust (Stern and Johnson, 2010) but, whatever the cause, it is noteworthy that gravitational collapse has not been described from the eastern ANS.

Terrestrial Ediacaran deposits in the Eastern Desert and Sinai, conversely, suggest that the western ANS had greater elevation above sea level. It is therefore significant that published interpretations of gravitational collapse in the ANS are mostly reported from these areas. Fowler and El Kalioubi (2004), for example, describe the northwestward translation of intensely foliated ophiolite mélange and molasse deposits west of the Meatiq Dome as a gliding-spreading nappe caused by gravitational collapse following arc-collision and crustal thickening. Blasband et al. (2000) ascribe orogenic extension and collapse in the Wadi Kid area, Sinai, to gravitational instability created during the final stages of arc-accretion in the ANS.

A universal assumption of gravitational collapse in the ANS needs to be treated with caution however. Thus Fritz et al. (2002), discussing the same set of gneiss domes and molasse basins described by Fowler and El Kalioubi (2004) in terms of orogenic collapse, argue for exhumation of core complexes as the result of oblique island-arc collision zones associated with transpression and lateral extrusion. In this model, continuous magmatism weakened the crust and horizontal shortening was balanced by extension, creating a situation in which there was no major crustal thickening. It is envisaged that core complexes were continuously but slowly exhumed without creating significant relief, so there was no increase in potential energy and no gravitational collapse. In a similar vein, derivation of post-collisional magma from mantle sources is seen by Stern and Gottfried (1986) as indicating asthenosphere uplift and removal of upper mantle lithosphere, favoring orogenic extensional collapse (Dewey, 1988; Greiling et al., 1994).

9.4. Indentor and escape tectonics

Another topic commonly referred to in late Cryogenian–Ediacaran tectonic models for the ANS concerns orogenic collision or indentation and consequent lateral extrusion or tectonic escape. As described in Section 7.3 on the Najd fault system, the concept derives from work by Tapponnier and Molnar (1976) and Molnar and Tapponnier (1977) with regard to the indentation of Eurasia by the Indian craton and the creation of strike-slip faults in the Tibetan Plateau. The idea was subsequently discussed by Burke and Sengör (1986) who noted that buoyant continental or arc material in orogenic belts generally moves during collision along strike-slip shear zones toward a nearby oceanic margin or free face. The indentor concept was first applied to the Arabian Shield by Schmidt et al. (1979), who envisaged that the shield was indented from the east by a rigid block in eastern Arabia, which caused strike-slip deformation on the Najd fault system. Stern (1985) cautioned that predictions of the model with regard to specific structures in the ANS fail, but the concept has become a commonly accepted structural framework within which to analyze the

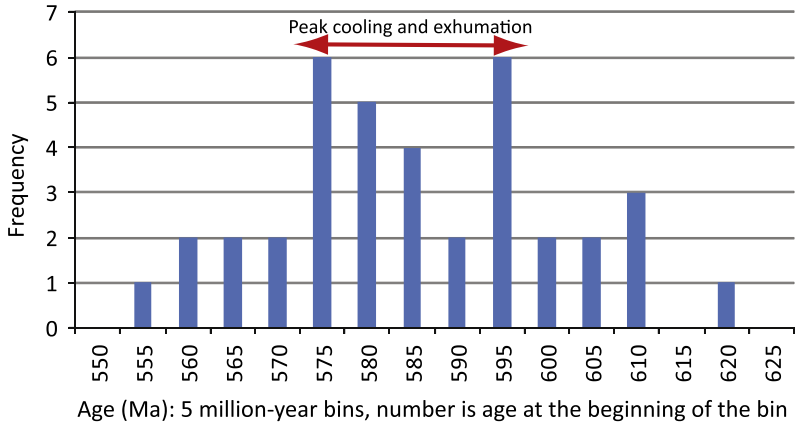

Fig. 27. $^{40}Ar/^{39}Ar$ cooling ages in the ANS. For sources of data, see Table 1.

processes of late Cryogenian–Ediacaran crustal shortening and orogen-parallel extension evident in the ANS. Berhe (1990) noted that northwest-trending strike-slip faults (i.e. the Najd system) exist throughout the ANS. It was inferred that they were the consequence of oblique collision although some of the kinematic assumptions were challenged by Abdelsalam and Stern (1991) in a discussion on the Berhe (1990) paper. In the context of the entire EAO, Bonavia and Chorowicz (1992) modeled the ANS as expelled northward from the Mozambique Belt because of indentation of East Africa by the Tanzanian craton. Jacobs and Thomas (2004) further developed this concept and proposed that indenter-escape tectonics on orogen parallel and orogen oblique shear zones occurred in both southern Africa and the ANS during collision of eastern and western Gondwana to form the East African–Antarctic Orogen. The existence of the East African–Antarctic Orogen as a continuous tectonic entity is disputed because East Africa and southern Africa are separated by an intervening E-trending orogenic belt (Hanson, 2003), and Collins and Pisarevsky (2005) pointed out that instead, the EAO appears to bifurcate south of Tanzania/Madagascar with one arm heading west into the Zambezi Belt and the other heading into India. However, the concept that ANS northward extrusion and southern African southward extrusion occurred during the final assembly of Gondwana is well grounded. A complication, of course, is that early models of the ANS being caught up in a hard collision between East and West Gondwana and extruding northward are simplistic because East Gondwana formed by a multiphase process of accretion and did not exist as a coherent single crustal block (Meert, 2002). Another complication is that not all orogen-parallel shear zones in the ANS necessarily reflect northward extension. Tsige and Abdelsalam (2005), for example, describe moderately E-dipping mylonitic zones in the ~100-km long north-trending Chulul shear zone in southern Ethiopia, the southern part of the Bulbul shear zone that have kinematic indicators showing top-to-the-SE tectonic transport. This sense of displacement is orthogonal to the trend of the EAO and is interpreted by Tsige and Abdelsalam (2005) in terms of easterly directed detachment and gravitation tectonic collapse rather than northward expulsion. The low-angle shear zones in Eritrea likewise reflect E–W gravity collapse between ~580–565 Ma rather than northward extension (Ghebreab, 1999; Ghebreab et al., 2005). Nonetheless, gross northward late Cryogenian–Ediacaran extension and, by implication, tectonic escape is inferred for the ANS on the basis of the sinistral sense of shear on the Keraf suture (Abdelsalam et al., 1998) indicating northward flow of the ANS relative to the Saharan Metacraton, the prevailing sinistral sense of shear on faults of the Najd fault system, and the widespread development of posttectonic dike swarms.

10. Gondwana assembly

Discussion about Gondwana assembly is not a prime objective of this review, and is more extensively covered in a pending companion review by Fritz and colleagues (this Journal). However, to contextualize our comments about indentor and escape tectonics, the development of the Abt formation and Al Amar arc, and the assembly of the ANS and its accretion to the Saharan Metacraton, we show a commonly accepted model of Gondwana assembly in Fig. 28 (Collins and Pisarevsky, 2005) and a cartoon of ANS assembly in Fig. 29, based on Fig. 28. The figures show that by 630 Ma, the core terranes of the ANS had already amalgamated forming the proto-Arabian–Nubian Shield (pANS), the Abt formation was being deposited on the flank of or close to the pANS, and the Al Amar arc was forming in what remained of the Mozambique Ocean. Marine and terrestrial post-amalgamation basins existed on the pANS, the region was being intruded by vast amounts of granitoids, and the pANS had begun to converge with the Saharan Metacraton. Between 620 and 580 Ma, the Al Amar arc and Abt formation accreted to the pANS, the pANS accreted with the Saharan Metacraton along the Keraf suture, and Ediacaran sedimentation ceased. Oblique collision resulting from convergence of Neoproterozoic India with the African parts of western Gondwana was focused in the southern part of the East African Orogen. This caused the development of orogen-parallel shear and shortening zones in the southern ANS, and transcurrent Najd faulting in the northern ANS, the general effect of which was northward tectonic escape. Exhumation of gneiss domes continued until ~580 Ma; granitoid magmatism continued until ~565 Ma. The crystalline basement of Eastern Arabia was in place by 540 Ma, prior to deposition of the lower Paleozoic sandstone that covered the entire region during the mid-Cambrian. Available evidence indicates that Eastern Arabia comprises juvenile Neoproterozoic rocks but as mentioned earlier in this review, the provenance of these rocks is uncertain—they may be an extension of the typical ANS or a separate crustal unit. We juxtapose it with the ANS in Fig. 29 at 620–550 Ma, and show the Al Amar arc, following Al-Husseini (2000), on the leading edge of the East Arabian crust, but we show its position at 630 Ma with a question mark because of the uncertainty of where Eastern Arabia formed in relation to the ANS.

11. Summary

We conclude this review by outlining, within the limits of available data, a chronology of Late Cryogenian–Ediacaran events in 10 million-year increments. We aim to highlight the fact that the end-Precambrian ANS continental crust was created by a large range of interacting depositional, magmatic, and structural events, and that any tectonic model for this period must account for contemporary subsidence, magma generation, shearing and shortening, exhumation, and erosion associated with the final amalgamation of the ANS terranes and collisional orogeny.

11.1. 650 Ma and earlier

By 650 Ma, most of the crust of the Arabian–Nubian Shield had formed, especially in the south. The western oceanic arc terranes had assembled along the Barka, Bi'r Umq–Nakasib, Yanbu–Sol Hamed–Allaqi–Heiani and Nabitah sutures, and had sutured with the Asir terrane along the Hulayfah–Ad Dafinah–Ruwah fault zone during the Nabitah orogeny (680–640 Ma). For convenience, we refer to this block of continental crust newly formed by terrane amalgamation as the proto-Arabian–Nubian Shield (pANS). Magmatism associated with the Nabitah orogeny was characterized by syntectonic gneisses emplaced along the Nabitah fault zone. The terrane assemblage existed east of, but not yet in contact with, the Saharan Metacraton (present coordinates), although oblique convergence between the two, along the eventual Keraf suture, was probably underway by 650 Ma. The northeastern margin of the pANS was marked by the Halaban ophiolite (emplaced ~680 Ma) and was flanked by an ocean basin. Active subduction in this oceanic basin was forming the Al Amar group (>689 Ma) and associated magmatic rocks (689–617 Ma) and oceanic sedimentation was forming the Abt formation, but the Abt formation and Al Amar arc did not accrete to the rest of the ANS for another 30 million years. Subduction beneath the pANS had probably largely ceased as a consequence of terrane amalgamation and suturing although some subduction, evidenced by continued convergence, shortening, and orogeny continued for another 100 million years during final assembly of the ANS. It is possible that delamination and sinking of detached subducted slabs, following peak orogeny, perturbed the mantle beneath the ANS crust facilitating the production of

magmas and the phases of granitoid magmatism that characterized the remaining late Cryogenian–Ediacaran history of the ANS. Within the newly formed continental crust of the pANS, exhumation, uplift, and erosion followed by subsidence formed post-amalgamation depositional basins, the oldest of which, within the time frame of this review, comprised the terrestrial, intermontane Thalbah group (660–620 Ma).

11.2. 650–640 Ma

During this period, the northeastern part of the pANS was exhumed and eroded, revealing deep levels in the crust, and the crust subsequently subsided, forming post-amalgamation basins, which were filled by the Murdama group (650–625 Ma), in a foreland-type of basin, and Bani Ghayy group (~650–620 Ma), in a fault-controlled (graben?) basin. These rocks were deposited on a profound regional unconformity that was developed across a large part of the northeastern ANS and accumulated in shallow-marine environments because of a late Cryogenian marine incursion. The Murdama and Bani Ghayy basins developed on the flank of and east of the Nabitah mobile belt; a small intermontane basin developed along the axis of the mobile belt in the south, filled by the Atura formation (<650 to >640 Ma). To the northwest, active terrestrial deposition continued in the Thalbah basin. In the 650–640 Ma period, furthermore, large parts of the eastern pANS (Arabian Shield) were intruded by calc-alkaline magma exemplified by suites of TTG and granite plutons such as the Laban complex (650 ± 7 Ma) in the Ha'il terrane, early phases of the Haml batholith, intrusions in the Siham arc (Jidh suite), and monzogranite–syenogranite plutons in the Asir terrane. Few plutonic rocks of this age are known in the Nubian shield. The plutons are largely undeformed and reflect the onset of posttectonic magmatism that characterized the remaining history of the pANS. Exceptions include a ~649 Ma biotite granite in Ethiopia, a ~647 Ma granite along the future Ar Rika shear zone, and a ~640 Ma granite and diorite in Sinai that were subsequently deformed and converted into gneiss (Bielski, 1982; Kröner et al., 1990). Minor late syntectonic magmatism along the Nabitah fault zone marked the waning Nabitah orogeny (e.g., the Makhdhul quartz diorite gneiss 641 ± 3 Ma and the Tathlith gneiss 639 ± 6 Ma). This period witnessed the earliest orogenic gold mineralization in the ANS, with the formation of deposits at Ad Duwayhi (~650 Ma). Deposition of the Abt formation and on-going arc-magmatism in the Ar Rayn terrane were active in the oceanic domain east of the pANS. Deformation, reflecting bulk E–W shortening, commenced on the north-trending Hamisana (660–550 Ma) and Oko (700–560 Ma) shear zones and fold belts in the southern ANS. Oblique sinistral convergence continued along the Keraf suture.

11.3. 640–630 Ma

This period was marked by continuing subduction in the oceanic basin east of the pANS, with a peak in TTG magmatism in the Al Amar arc, and by ongoing oblique convergence between the pANS and the Saharan Metacraton along the Keraf suture (Fig. 27). Metamorphism and deformation continued along shortening zones in the southern ANS. Marine environments persisted in post-amalgamation basins in the eastern ANS until about 625–620 Ma with continued deposition of the Murdama and Bani Ghayy groups. Folding and uplift of these deposits may have started soon after 630 Ma, resulting in a period of erosion that formed the regional unconformities on which the terrigenous and volcanic successions of the Hibshi, Hadn, and Jurdhawiyah units were subsequently deposited. The Hibshi formation (632 Ma) was probably deposited in a fault-controlled basin at the northern margin of the Murdama basin; the Hadn and Jurdhawiyah were deposited some 15 million years later. Marine connections were maintained in the heart of the pANS however, as evidenced by thick limestone in the Ablah group (640–615 Ma) of southern Arabia. Exhumation and brittle reactivation, forming small terrestrial molasse basins along the Nabitah fault zone, followed the emplacement of ~640 Ma posttectonic granites. Voluminous calc-alkaline magmatism occurred in the northern and northeastern ANS (Aqaba complex 640–600 Ma and Marabit suite 635–580 Ma in the Midyan terrane; Khishaybi suite ~640 Ma in the Afif terrane). Protoliths of the Um Ba'anib gneiss (631 ± 2 Ma) were emplaced in what would become the heart of the Meatiq Dome. The age of the Um Ba'anib gneiss constrains the maximum age of ductile deformation and the onset of northwesterly thrusting and tectonic transport in the Eastern Desert. This was broadly contemporary with the onset of shearing on the Qazaz–Ajjaj shear zone, evidenced by thermal resetting of the Raydan pluton (630 ± 19 Ma) and ductile deformation in the Thalbah group (<620 Ma). Orogenic gold mineralization continued, forming the An Najadi deposit in the Afif terrane (~631 Ma), associated with the posttectonic calc-alkaline magmatism that was widespread in the northeastern Arabian Shield.

11.4. 630–620 Ma

Posttectonic A-type granites were emplaced in the ANS as early as the middle Cryogenian (Hamra and Bishah plutons, ~686 Ma and ~678 Ma), but the first major pulse of alkali magmatism occurred between 630 and 620 Ma, with the emplacement of plutons in the southern (Asir terrane) and northern (Afif and Midyan terranes) ANS. These granites marked the onset of highly fractionated intraplate, posttectonic magmatism and the beginning of a transition from convergent to extensional tectonics that characterized the remaining ANS history. The geographic spread of alkaline magma was limited, however, and there is no record of A-type magmatism at this time in the Eastern Desert or Sinai. Concurrent calc-alkaline magmatism in the Ar Rayn terrane reflected ongoing subduction in the oceanic domain east of the pANS. Within the pANS, subaerial volcanism occurred in the Shammar group (~630–625 Ma), spatially associated with and the possible extrusive equivalents of alkali-feldspar granites. Deposition of the Murdama and Bani Ghayy groups in the marine post-amalgamation basins in the eastern ANS ceased during this period. Oblique convergence along the Keraf suture occurred, as did deformation on shortening zones in the southern ANS and transcurrent shearing began on the principal Najd faults in the northern ANS—the Halaban-Zarghat, Ar Rika, and Ruwah fault zones, indicating that transpressive E–W shortening and N–S orogen-parallel extension was pervasive in the pANS at this time. The Sibai gneiss dome was exhuming and cooling by about 623 Ma, reflecting the onset of Najd-related extension in the Eastern Desert; other gneiss domes in the Eastern Desert were exhumed in the following 30 million years.

11.5. 620–610 Ma

Significant posttectonic calc-alkaline magmatism continued during this period in parts of the Afif (Idah suite: 620–615 Ma), Asir, Midyan, and Hijaz terranes in the Arabian Shield, in Sinai, and in the Eastern Desert of Egypt. The Idah suite was associated with gold mineralization at Sukhaybarat (617 Ma). Magmatism was followed by exhumation and erosion, particularly in the northeastern Arabian Shield. Transcurrent slip on the Halaban-Zarghat and Ar Rika fault zones and the Qazaz and Ajjaj shear zones continued, as did transpressional sinistral convergence on the Keraf suture and deformation on shear zones and shortening zones in the southern ANS. Metamorphism of the Abt formation between 621 and 618 Ma (indicated by $^{40}Ar/^{39}Ar$ dating) is evidence of faulting and exhumation in parts of Abt basin. These events likely marked

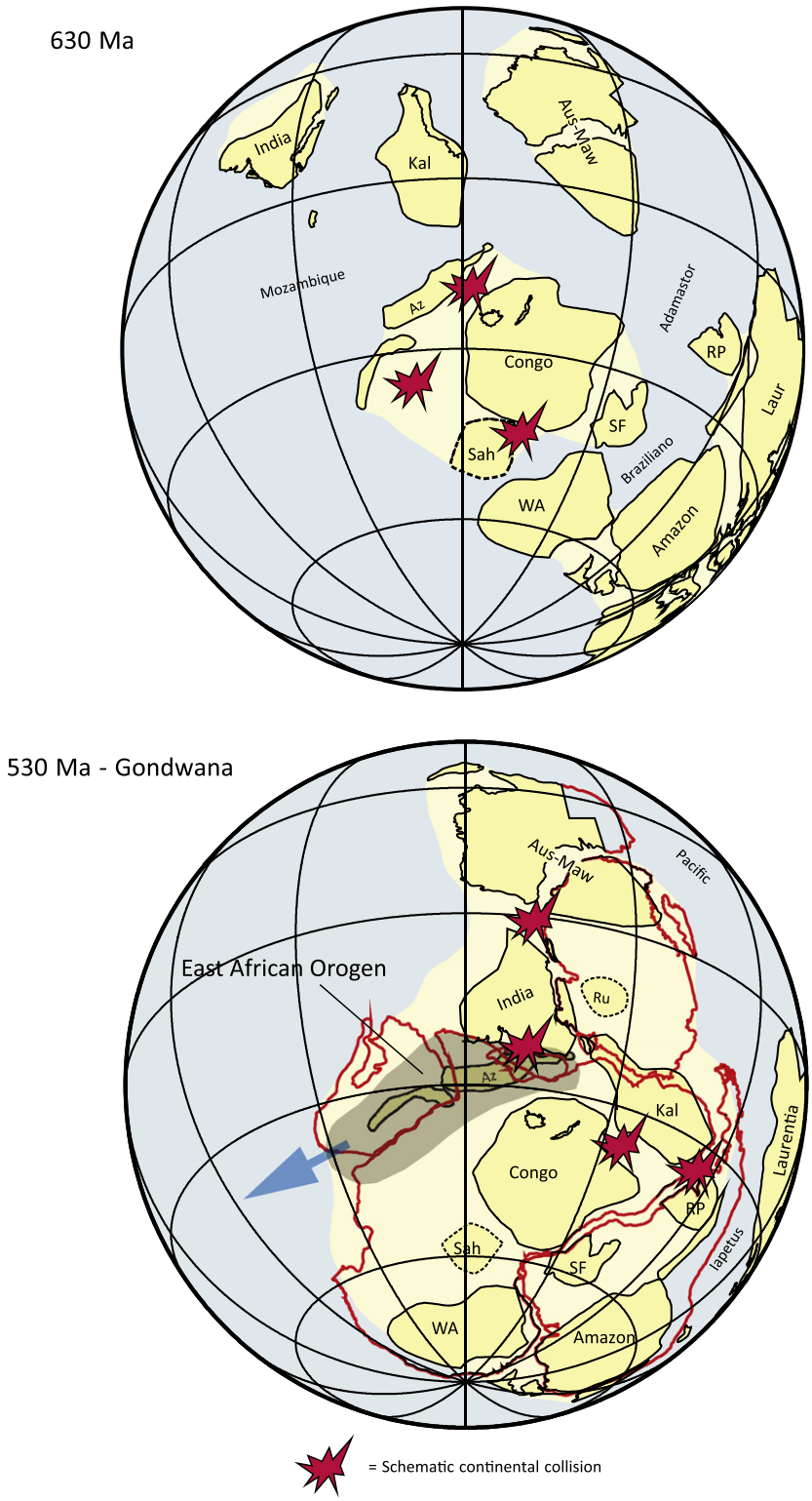

Fig. 28. Late Cryogenian–Ediacaran assembly of Gondwana, showing intense continent–continent collision between India and the Congo Craton in the East African part of the East African Orogen and the position of the Arabian–Nubian shield with an oceanic free face allowing tectonic escape (indicated by arrow). Modified from Collins and Pisarevsky (2005). Az = Azania; Kal = Kalahari craton; WA = West Africa; SF = Sao Francisco; Sah = Saharan Metacraton; RP = Rio de la Plata; Aus-Maw = Australia/Mawson block; Ru = Ruker Terrane.

the cessation of deposition in the basin, the onset of basin closure, and the beginning of the process that would eventually lead to the suturing of the Ad Dawadimi and Ar Rayn terranes and their amalgamation with the pANS. These tectonic events in the eastern ANS were contemporary with ongoing collision along the Keraf suture betweeen the ANS and Saharan Metacraton, and with tectonic escape in the core of the ANS. TTG calc-alkaline magmatism continued in the Al Amar arc until about 616 Ma, but following the

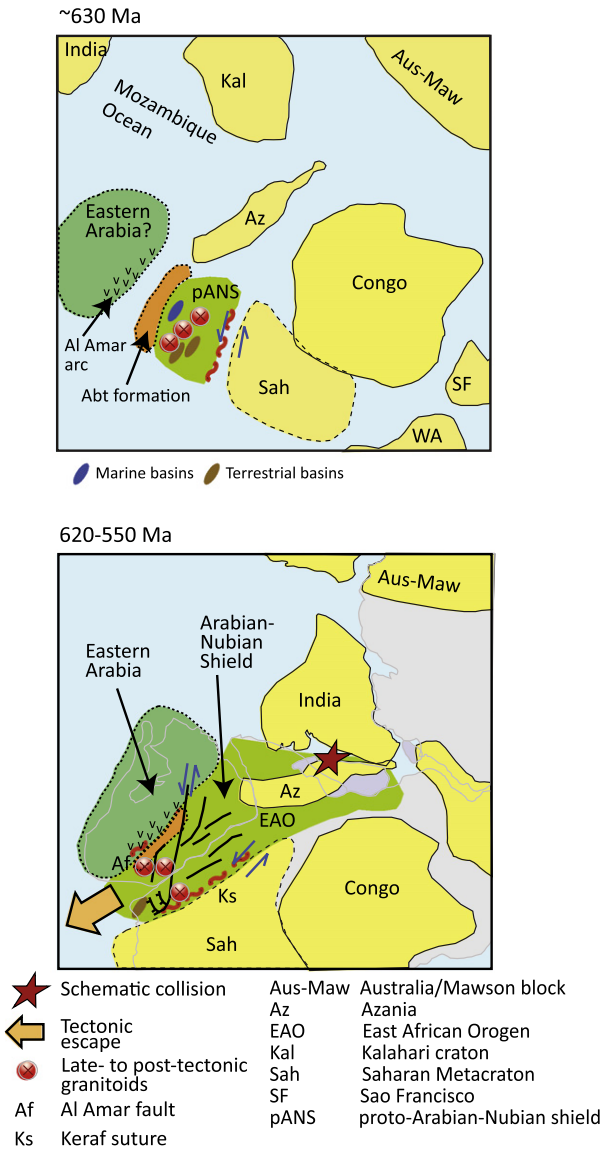

Fig. 29. Cartoon showing amalgamation and final accretion of the Arabian–Nubian Shield during the late Cryogenian and Ediacaran. Cartoon is based on the paleogeography illustrated in the Gondwana assembly model by Collins and Pisarevsky (2005) shown in Fig. 28.

waning or cessation of subduction beneath the arc, posttectonic alkali-feldspar granite magmatism became important. Intermontane molasse basins formed during this period in the western part of the pANS, filled by terrestrial sediments of the Hammamat Group and subaerial extrusives of the Dokhan Volcanics. The basins manifest extension and the formation of pull-aparts in a part of the ANS elevated above sea level and unaffected by marine influence. A major metamorphic event occurred in Sinai at about 620 Ma, followed 20 million years later by exhumation and cooling, further marking the transition from orogenic (compression) to post-orogenic (extension) tectonics.

11.6. 610–600 Ma

During this period, ductile deformation was active on the Qazaz, Halaban-Zarghat, Ar Rika, and Ruwah faults, concurrent with ongoing oblique convergence and orogen-parallel extension and tectonic escape throughout the pANS. At the same time, contact between the Saharan Metacraton and the pANS increased, with ongoing sinistral transpression on the Keraf suture. Thermal activity on the Hamisana and Oko shortening zones continued until ~550 Ma, indicating a persistence of E–W shortening, at least in the southern ANS, until virtually the end of the Precambrian. Further folding, low-grade metamorphism, and rapid exhumation and cooling in the Abt basin, recorded by $^{40}Ar/^{39}Ar$ ages of 616 Ma, 612, 611, and 610 Ma, and the onset of alkali-feldspar granite magmatism in the Al Amar arc (607–583 Ma) is believed to mark closure of the Abt marine basin and suturing between the Ad Dawdimi and Ar Rayn terranes. These events marked the elimination of the marine basin that had existed east of the earlier amalgamated pANS. Metamorphic rocks dating between 636 and 604 Ma, known from borehole intercepts east of the Ad Dawadimi and Ar Rayn terranes, in the basement of central Arabia (Al-Husseini, 2000, and references therein), were presumably also in place by this time but it is not clear whether the crust represents exotic material (part of eastern Gondwana?) or a continuation of juvenile Neoproterozoic material. Active deposition of Dokhan Volcanics and Hammamat Group rocks continued in terrestrial intermontane and molasse basins in western pANS and correlative terrestrial sedimentation and volcanism, represented by the Jurdhawiyah group (612–594 Ma), occurred at the eastern margin of the pANS. Further exhumation occurred in the Sibai gneiss dome and thrusting and ductile deformation occurred around the Meatiq Dome indicating major northwesterly tectonic transport at about 606 Ma. A different interpretation of the Abu Ziran diorite suggests significant extension. Voluminous posttectonic calc-alkaline magmatism occurred in much of the ANS, including Sinai (610–600), the Eastern Desert of Egypt, the Aswan area, Sabaloka, Ethiopia and Eritrea, and the Arabian Shield. A-type magmatism in Sinai and the Midyan and Eastern Desert terranes also occurred from about 608 Ma onward. The A-type magmatism, as well as evidence of rapid cooling and exhumation in Sinai at about 600 Ma, evidenced by $^{40}Ar/^{39}Ar$ dating, identifies pervasive post-collision extension and orogenic collapse in the northern ANS.

11.7. 600–590 Ma

A-type magmatism continued at this time in Sinai, the Central and Northern Eastern Desert, the Afif terrane, and Ar Rayn terrane. Concurrent calc-alkaline magmatism included the emplacement of monzogranite (~599 Ma) and monzodiorite (~598 Ma) in the Midyan terrane, hornblende–biotite granites (~599, 598 Ma) in the Saharan Metacraton; granites (~599–592 Ma) and quartz monzonite (~595 Ma) in Sinai; and granite and monzonite in the Sabaloka and Bayuda Desert area (~597, ~591 Ma). Bimodal alkali-calcic to alkali magmatism was represented by the Araba suite (~600–560 Ma), the result of melting of metasomatized mantle followed by shallow level feldspar-controlled fractionation in a rifting (extensional) environment. Emplacement of dike swarms constrained the cessation of metamorphism and ductile deformation and marked the onset of NW–SE directed extension in the northern ANS. Pre- to syntectonic granites with protolith ages of ~600 and ~597 Ma and a cooling age of ~600 Ma indicate the timing of peak metamorphism and deformation in the Atmur–Delgo terrane at the contact with the Saharan Metacraton and of major collision along the Keraf suture. Concurrent peak metamorphism at ~593 Ma occurred in Eritrea followed 15 million years later by exhumation and orogenic collapse. Ductile deformation and thrusting in the Meatiq Dome ceased by 590 Ma, constrained by emplacement of the posttectonic Arieki granite (590 Ma), concurrent with waning ductile deformation on Najd faults in the Arabian Shield. The Hafafit Dome underwent peak metamorphism at about 600 Ma or slightly earlier, followed by exhumation, cooling and extension between about 595 and 585 Ma. By ~590 Ma, ductile shearing on Najd faults in the Arabian Shield was ending; rapid exhumation and cooling occurred at the southern end of the Halaban-Zargaht

fault between ~601 and ~597 Ma, and the Ruwah fault zone was intruded by posttectonic granite at about ~592 Ma. Active deposition continued in intermontane basins in the western ANS, however, with formation of Dokhan Volcanic rocks until at least ~592 Ma and deposition of Hammamat sediments until ~585 Ma. The Hammamat Goup in the type Hammamat basin was folded and overthrust by middle Cryogenian supracrustal rocks prior to the emplacement of the posttectonic Um Had granite at 596 Ma. The thrusting reflected bulk NE–SW shortening in the Eastern Desert. A transition to brittle deformation on several of the Najd faults marked the initiation of Jibalah group depositional basins at extensional zones along the faults.

11.8. 590–580 Ma

During this period, ductile deformation in the ANS was confined to Najd faults in the northwestern part of the Arabian Shield and perhaps in Egypt. The Meatiq Dome was exhuming and cooling, constrained by $^{40}Ar/^{39}Ar$ hornblende and white mica cooling ages of 587 Ma and 579 Ma obtained from the Um Ba'anib Orthogneiss. Exhumation affected the Hafafit Dome at about the same time with $^{40}Ar/^{39}Ar$ cooling ages between 593 Ma and 584 Ma following peak metamorphism. Slip on much of the Halaban-Zarghat fault had ceased by 588 Ma although deposition in extensional basins along the fault persisted and the Jibalah group continued to accumulate until about 565 Ma. Felsite emplaced at 587 Ma in already folded Abt formation confirms that the Abt basin was fully closed. Alkali-feldspar magmatism ceased in the Ar Rayn terrane but emplacement of strongly fractionated peralkaline, peraluminous, and related leucocratic granites continued at high levels in the crust elsewhere in the northeastern ANS and Sinai. Granites locally vented as rhyolitic flows and pyroclastic rocks.

11.9. 580–570 Ma

Ductile deformation and sinistral shearing occurred on the Qazaz–Ajjaj shear zones until 575 Ma, but ceased by 573 Ma, the age of posttectonic mafic dikes that intrude the shear zone. A final ductile deformation event on the Halaban-Zarghat fault zone is indicated by granite gneiss emplaced at 573 Ma, and alkali-feldspar granites intruded into the Abt formation denote a late Ediacaran phase of A-type magmatism (579–55 Ma) in the eastern ANS. Rapid exhumation and cooling on the Keraf suture (577 Ma) is taken as evidence that the pANS was almost fully accreted, at this time, to the Saharan Metacraton; which implies that assembly of the ANS was virtually complete. Rapid exhumation in Ghedem domain, Eritrea ($^{40}Ar/^{39}Ar$ ages ~579 and ~567 Ma) denotes ongoing orogenic collapse.

11.10. 570–560 Ma

During this period, Jibalah group deposition came to an end. Much of the group was deposited in terrestrial environments, but a late Ediacaran marine incursion is evidenced in the northern part of the ANS.

11.11. 560–550 Ma

Terminal exhumation on the Ar Rika fault, shown by $^{40}Ar/^{39}Ar$ cooling ages, occurred about 557 Ma, and orognic activity on the Keraf suture ceased by 560 Ma. Thus, by 560–550 Ma, orogeny in the ANS had ceased. The ANS thereafter underwent pervasive extension, as is indicated by the widespread emplacement of dike swarms until at least 545 Ma. By the end of the Ediacaran, the entire ANS had been subjected to strong chemical weathering and erosion, possibly in part effected by glaciation, and formed a vast low-relief erosion surface on which Lower Cambrian sandstone was eventually deposited.

Acknowledgments

The review represents a major international collaboration among authors whose work in the ANS spans three decades. The views expressed are based on an extensive body of literature, insights developed during prolonged periods of field work, and understanding gained from discussions with colleagues, but are ultimately those of the authors and are presented here as a summary of their present interpretations and a stimulus to further research. This review is a JEBEL contribution: R.J.S., A.A., and P.R.J. acknowledge the JEBEL Project as a means of bringing them together in the field, and providing a venue for gathering new information and exchanging ideas. Support for R.J.S. and P.R.J. to participate in the meeting was provided by NSF Grant 08221257. P.R.J. thanks Dr. Zohair Nawab, President, and colleagues at the Saudi Geological Survey for the opportunity to work on the Arabian Shield. A.A. acknowledges with thanks the staff and faculty at the Geology Department, Assiut University, particularly Dr. M.M.A. Abu El-Rus and Dr. E.M.S. El-Gaby, for exposing him to the geology, history, and problems of the Eastern Desert of Egypt. A.S.C's contribution forms TRaX Record #164. H.F. thanks the Austrian Science Foundation for financial support of a number of grants related to African geology (P12375, P09703, P15599, P12836, T247-N10) and colleagues at the Universities of Assuit and Mansour, Egypt. Funds for T.K. were provided by the National Natural Science Foundation of China (Grants 91014992 and 40821061) and the Ministry of Education of China (B07039). We thank Mohammed Abdelsalam and an anonymous reviewer for valuable comments that improved our final text, and acknowledge the Elsevier Press, the Journal of African Earth Sciences, and Tim Horscroft (editor) for the invitation to contribute this review.

Appendix A. Supplementary material

Supplementary data associated with this article can be found, in the online version, at doi:10.1016/j.jafrearsci.2011.07.003.

References

Abd El-Naby, H., Frisch, W., Siebel, W., 2008. Tectonic–metamorphic evolution of the Wadi Hafafit culmination (central Eastern Desert, Egypt). Implication for Neoproterozoic core complex exhumation in NE Africa. Geologica Acta 6, 293–312.

Abd El-Wahed, M.A., 2009. The role of the Najd fault system in the tectonic evolution of the Hammamat molasse sediments, Eastern Desert, Egypt. Arabian Journal of Geosciences. doi:10.1007/s12517-008-0030-0.

Abdalla, H.M., Mohamed, F.H., 1999. Mineralogical and geochemical investigation of emerald and beryl mineralisation, Pan-African Belt of Egypt: genetic and exploration aspects. Journal of African Earth Science 28, 581–598.

Abdeen, M.M., Abdelghaffar, A.A., 2011. Syn- and post-accretionary structures in the Neoproterozoic central Allaqi-Heiani suture zone, Southeastern Egypt. Precambrian Research 185, 95–108.

Abdeen, M.M., Greiling, R.O., 2005. A quantitative structural study of late Pan-African compressional deformation in the Central Eastern Desert (Egypt) during Gondwana assembly. Gondwana Research 8, 457–471.

Abdeen, M.M., Warr, L.N., 1998. Late orogenic basin evolution, deformation and metamorphism in the Pan-African Basement, Wadi Queih, Eastern Desert of Egypt. In: Naim, G.M., Hussein, A.A., Greiling, R.O., Warr, L.N. (Eds.), International Cooperation Scientific Series, 42, 272 pp.

Abdeen, M.M., Dardir, A.A., Greiling, R.O., 1992. Geological and structural evolution of the Wadi Queih Area (N Quseir), Pan-African basement of the Eastern Desert of Egypt. Zentralblatt fur Geologie und Palaeontolgie Teil I, 2653–2659.

Abdeen, M.M., Dardir, A.A., Greiling, R.O., 1997. Rain drop prints, mud crack polygons, and pebbles as strain markers in a Pan-African molasse basin, Wadi Queihm, Arabian Desert, Egypt. Annals of the Geological Survey of Egypt 20, 185–191.

Abdeen, M.M., Sadek, M.F., Greiling, R.O., 2008. Thrusting and multiple folding in the Neoproterozoic Pan-African basemenet of Wadi Hodein area, south Eastern Desert, Egypt. Journal of African Earth Sciences 52, 21–29.

Abdel-Karim, A.M., El-Baroudy, A.F., 1995. Petrology and geochemistry of felsic dyke swarms in SW Sinai, Egypt. Arab Gulf Journal of Scientific Research 13, 239–257.
Abdel-Monem, A.A., Radain, A.A., Gazzaz, M.A., 1982. Rb–Sr dating and petrology of Jabal Bitran granite, Idsas area, Saudi Arabia (abstract). Precambrian Research 16, A3.
Abdel-Rahman, A.M., Doig, R., 1987. The Rb–Sr geochronologic evolution of the Ras Gharib segment of the northern Nubian shield. Journal of the Geological Society, London 144, 577–586.
Abdelsalam, M.G., 1994. The Oko shear zone: post-accretionary deformations in the Arabian Nubian Shield. Journal of the Geological Society, London 151, 767–776.
Abdelsalam, M.G., Stern, R.J., 1991. Discussion of ophiolites in Northeast and East Africa: implications for Proterozoic crustal growth. Journal of the Geological Society, London 148, 602–604.
Abdelsalam, M.G., Stern, R.J., 1996. Sutures and shear zones in the Arabian–Nubian Shield. Journal of African Earth Sciences 23, 289–310.
Abdelsalam, M.G., Stern, R.J., Schandelmeier, H., Sultan, M., 1995. Deformation history of the Keraf Zone in NE Sudan, revealed by Shuttle Imaging Radar. Journal of Geology 103, 475–491.
Abdelsalam, M.G., Stern, R.J., Copeland, P., Elfaki, E.M., Elhur, B., Ibrahim, F.M., 1998. The Neoproterozoic Keraf suture in NE Sudan: Sinistral transpression along the eastern margin of West Gondwana. Journal of Geology 106, 133–147.
Abdelsalam, M.G., Liégeois, J.-P., Stern, R.J., 2002. The Saharan Metacraton. Journal of African Earth Sciences 34, 119–136.
Abdelsalam, M.G., Abdeen, M.M., Dowaidar, H.M., Stern, R.J., Abdelghaffar, A.A., 2003. Structural evolution of the Neoproterozoic western Allaqi–Heiani suture, southwestern Egypt. Precambrian Research 124, 87–104.
Abu-Alam, T.S., Stüwe, K., 2009. Exhumation during oblique transpression: the Feiran–Solaf region, Egypt. Journal of Metamorphic Geology 27, 439–459.
Agar, R.A., 1986. The Bani Ghayy group; sedimentation and volcanism in "pull-apart" grabens of the Najd strike-slip orogen, Saudi Arabian Shield. Precambrian Research 31, 259–274.
Agar, R.A., 1987. The Najd fault system revisited: a two-way strike-slip orogen in the Saudi Arabian Shield. Journal of Structural Geology 9, 41–48.
Agar, R.A., Stacey, J.S., Whitehouse, M.J., 1992. Evolution of the Southern Afif terrane – a Geochronologic Study. Saudi Arabian Deputy Ministry for Mineral Resources Open-File Report DGMR-OF-10–15, 41 p.
Akaad, M.K., Abu El Ela, A.M., 2002. Geology of the basement tocks in the eastern half of the belt between latitudes 25°30′ and 26°30′N Central Eastern Desert. Geological Survey of Egypt Paper 78, 118 p.
Akkad, M.K., El Ramly, M.F., 1958. Seven New Occurrence of the Igla Formation in the Eastern Desert of Egypt. Geol. Surv. Egypt, 37 p (Paper No. 3).
Akkad, M.K., Noweir, A.M., 1980. Geology and lithostratigraphy of the Arabian Desert orogenic belt of Egypt between latitudes 25°35′ and 26°30′N. King Abdulaziz University, Jiddah. Institute of Applied Geology Bulletin 3 (4), 127–134.
Akkad, M.K., El-Gaby, S., Abbas, A.A., 1967a. Geology and petrology of the migmatites around Feiran Oasis. Journal of Geology UAR 10, 67–87.
Akkad, M.K., El-Gaby, S., Abbas, A.A., 1967b. On the evolution of Feiran Migmatites, Sinai. Journal of Geology UAR 11, 49–58.
Albino, G.V., Jalal, S., Christensen, K., 1995. Neoproterozoic mesothermal gold mineralization at Sukhaybarat East mine. Transactions of the Institution of Mining and Metallurgy (Section B: Applied Earth Science) 104, B157–B170.
Al-Dabbagh, M.H., Dowd, P.A., 1996. Sukhaybarat Gold Mine, Saudi Arabia. Mineral Industry International, July 16–21.
Aldrich, L.T., 1978. Geochronologic Data for the Arabian Shield. Section l, Radiometric Age Determinations of Some Rocks from the Arabian Shield. Saudi Arabian Directorate General of Mineral Resources Project Report 240, pp. 1–9.
Aleinikoff, J.N., Stoeser, D.B., 1988. Zircon Morphology and U–Pb Geochronology of Seven Metaluminous and Peralkaline Post-orogenic Granite Complexes of the Arabian Shield, Kingdom of Saudi Arabia. Saudi Arabian Directorate General of Mineral Resources Open-File Report USGS-OF-06-5, 32 p.
Al-Husseini, M., 2000. Origin of the Arabian Plate Structures: Amar collision and Najd rift. GeoArabia 5, 527–542.
Ali, B.H., Wilde, S.A., Gabr, M.M.A., 2009. Granitoid evolution in Sinai, Egypt, based on precise SHRIMP U–Pb zircon geochronology. Gondwana Research 15, 38–48.
Al-Muallem, M.S., Smith, J.W., 1987. Geologic Map of the Ar Rawdah Quadrangle, Sheet 21F, Kingdom of Saudi Arabia. Saudi Arabian Deputy Ministry for Mineral Resources Geoscience Map GM-85, Scale 1:250,000, 25 p.
Al-Saleh, A.M., 2010. The Kirsh gneiss dome: an extensional metamorphic core complex from the SE Arabian Shield. Arabian Journal of Geosciences. doi:10.1007/s12517-0101-0179-1.
Al-Saleh, A.M., Boyle, A.P., 2001. Structural rejuvenation of the eastern Arabian shield during continental collision: $^{40}Ar/^{39}Ar$ evidence from the Ar Ridaniyah ophiolite mélange. Journal of African Earth Sciences 33, 135–141.
Al-Saleh, A.M., Boyle, A.P., Mussett, A.E., 1998. Metamorphism and $^{40}Ar/^{39}Ar$ dating of the Halaban ophiolite and associated units: evidence for two-stage orogenesis in the eastern Arabian shield. Journal of the Geological Society, London 155, 165–175.
Al-Shanti, A.M., 1976. Mineralization of Ad Dawadimi District, Kingdom of Saudi Arabia. Saudi Arabian Directorate General of Mineral Resources Bulletin 14, 50 p.
Al-Shanti, A.M., Gass, I.G., 1983. The upper Proterozoic ophiolite mélange zones of the easternmost Arabian Shield. Journal of the Geological Society, London 140, 867–876.
Al-Shanti, A.M.S., Mitchell, A.H.G., 1976. Late Precambrian subduction and collision in the Al Amar–Idsas region, Kingdom of Saudi Arabia. Tectonophysics 30, T41–T47.
Amer, R., Kusky, T.M., Ghulam, A., 2009. Lithological mapping in the Central Eastern Desert of Egypt using ASTER data. Journal of African Earth Sciences. doi:10.1016/j.jafrearsci.2009.06.004.
Amer, R.M., Kusky, T.M., Ghulam, A., 2010. New methods of processing ASTER data for lithological mapping. examples from Fawakhir, Central Eastern Desert of Egypt. Journal of African Earth Sciences 56, 75–82.
Anderson, J.L., 1983. Proterozoic anorogenic granite plutonism of N America. In: Medaris, L.G., Byers, C.W., Mickelson, D.M., Shanks, W.C. (Eds.), Proterozoic Geology, vol. 161. Geological Society of America Memoir, pp. 133–154.
Andersson, U.-B., Ghebreab, W., Teklay, M., Whitehouse, M.J., 2000. Ages and character of crust-forming and metamorphic events in east-central and northern Eritrea: new conventional and SIMS U–Pb and mineral P–T data. Journal of African Earth Sciences 30, 7.
Andre, C.G., 1989. Evidence for phanerozoic reactivation of the Najd fault system in AVHRR, TM, and SPOT images of Central Arabia. Photogrammetry Engineering and Remote Sensing 55, 1129–1136.
Andresen, A., Abu El-Rus, M.A., Myhre, P.I., Boghdady, G.Y., Corfu, F., 2009. U–Pb TIMS age constraints on the evolution of the Neoproterozoic Meatiq Gneiss Dome, Eastern Desert, Egypt. International Journal of Earth Sciences. doi:10.1007/s00531-007-0276.
Andresen, A., Augland, L.E., Boghdady, G.Y., Lundmark, A.M., Elnady, O.M., Hassan, M.A., 2010. Structural constraints on the evolution of the Meatiq gneiss domes (Egypt), East-African Orogen. Journal of African Earth Sciences 57, 413–422.
Angerer, T., Greiling, R.O., Avigad, D., 2011. Fabric development in a weathering profile at a basement-cover interface, the sub-Cambrian peneplain, Israel: implications for decollement tectonics. Journal of Structural Geology 33, 819–832.
Arslan, A.I., 1989. Contribution to the geochemistry of the El Sukari granite pluton, Eastern Desert, Egypt. In: Proceedings of the 1st Conference on Geochemistry, Alexandria University, Alexandria, Egypt. pp 1–18.
Augland, L.E., Andresen, A., Boghdady, G.Y., 2011. U–Pb ID-TIMS dating of igneous and metaigneous rocks from the El-Sibai area: time constrains on the tectonic evolution of the Central Eastern Desert, Egypt. International Journal of Earth Sciences. doi:10.1007/s00531-011-0653-3.
Avigad, D., Gvirtzman, Z., 2009. Late Neoproterozoic rise and fall of the northern Arabian–Nubian shield: the role of lithospheric mantle delamination and subsequent thermal subsidence. Tectonophysics. doi:10.1016/j.tecto.2009.04.018.
Avigad, D., Sandler, A., Kolodner, K., Stern, R.J., McWilliams, M., Miller, N., Beyth, M., 2005. Mass-production of Cambro–Ordovician quartz-rich sandstone as a consequence of chemical weathering of Pan-African terranes: environmental implications. Earth and Planetary Science Letters 240, 818–826. doi:10.1016/j.epsl.2005.09.021.
Avigad, D., Stern, R.J., Beyth, M., Miller, N., McWilliams, M.O., 2007. Detrital zircon U–Pb geochronology of Cryogenian diamictites and Lower Paleozoic sandstone in Ethiopia (Tigrai): age constraints on Neoproterozoic glaciation and crustal evolution of the southern Arabian–Nubian Shield. Precambrian Research 154, 88–106.
Bailo, T., Schandelmeier, H., Franz, G., Sun, C.-H., Stern, R.J., 2003. Plutonic and metamorphic rocks from the Keraf suture (NE Sudan). A glimpse of Neoproterozoic evolution on the NE margin of W. Gondwana. Precambrian Research 123, 67–80.
Bandel, K., Shinaq, R., 2003. Sediments of the Precambrian Wadi Abu Barqa Formation influenced by life and their relation to the Cambrian sandstones in southern Israel. Freiberger Forschungshefte C 499, 78–91.
Barker, F., Wones, D.R., Sharp, W.N., Desborough, G.Z., 1975. The Pikes Peak batholith, Colorado Front Range, and a model for the origin of the gabbro–anorthosite–syenite–potassic granite suite. Precambrian Research 2, 97–160.
Basahel, A.N., Bahafzalah, A., Omara, S., Jux, U., 1984. Early Cambrian carbonate platform of the Arabian shield. Neues Jahrbuch für Geologie und Paläontologie, Monatshefte (N. Jb., Geol. Paläont. Mh.), 113–128.
Bea, F., Abu-Anbar, M., Montero, P., Peres, P., Talavera, C., 2009. The 844 Ma Moneiga quartz-diorites of the Sinai, Egypt: Evidence for Andean-type arc or rift-related magmatism in the Arabian–Nubian shield? Precambrian Research 175, 161–168.
Be'eri-Shlevin, Y., Katzir, Y., Whitehouse, M.J., Kleinhanns, I.C., 2009a. Contribution of pre Pan-African crust to formation of the Arabian–Nubian Shield: New secondary ionization mass spectrometry U–Pb and O studies of zircon. Geology 37, 899–902.
Be'eri-Shlevin, Y., Katzir, Y., Whitehouse, M., 2009b. Post-collisional tectonomagmatic evolution in the northern Arabian–Nubian Shield: time constraints from ion-probe U–Pb dating of zircon. Journal of the Geological Society, London 166, 71–85.
Be'eri-Shlevin, Y., Katzir, Y., Valley, J.W., 2009c. Crustal evolution and recycling in a juvenile continent: oxygen isotope ratio of zircon in the northern Arabian Nubian Shield. Lithos 107, 169–184.
Be'eri-Shlevin, Y., Katzir, Y., Blichert-Toft, J., Kleinhanns, I.C., Whitehouse, M.J., 2010. Nd–Sr–Hf–O isotope provinciality in the northernmost Arabian–Nubian Shield: implications for crustal evolution. Contributions to Mineralogy and Petrology 160, 181–201.
Bennet, J.D., Mosley, P.N., 1987. Tiered-tectonics and evolution, E. Desert and Sinai, Egypt. In: Matheis, G., Schandelmerier, H. (Eds.), Current Research in African Earth Sciences. Balkema, Rotterdam, pp. 79–82.
Bentor, Y.K., 1985. The crustal evolution of the Arabo-Nubian massif with special reference to the Sinai Peninsula. Precambrian Research 28, 1–74.
Berhe, S.M., 1990. Ophiolites in NE and east Africa: implications for Proterozoic crustal growth. Journal of the Geological Society, London 147, 41–57.

Beyth, M., Stern, R.J., Altherr, R., Kröner, A., 1994. The late Precambrian Timna igneous complex, southern Israel: evidence for comagmatic-type sanukitoid monzodiorite and alkali granite magma. Lithos 31, 103–124.
Beyth, M., Avigad, D., Wetzel, H.-U., Matthews, A., Berhe, S.M., 2003. Crustal exhumation and indications for Snowball Earth in the East African Orogen, N Ethiopia and east Eritrea. Precambrian Research 123, 187–201.
Bielski, M., 1982. Stages in the Evolution of the Arabian–Nubian Massif in Sinai. Ph.D. Thesis, Jerusalem, Hebrew University, 155 p.
Billay, A.Y., Kisters, A.F.M., Meyer, F.M., Schneider, J., 1997. The geology of the Lega Dembi gold deposit, southern Ethiopia: implications for Pan-African gold exploration. Mineralium Deposita 32, 491–504.
Bingen, B., Jacobs, J., Viola, G., Henderson, I.H.C., Skar, Ø., Boyd, R., Thomas, R.J., Solli, A., Key, R.M., Daudi, E.X.F., 2009. Geochronology of the Precambrian crust in the Mozambique belt in NE Mozambique and implications for Gondwana assembly. Precambrian Research 170, 231–255.
Blasband, B., Brooijmans, P., Dirks, P., Visser, W., White, S., 1997. A Pan-African core complex in the Sinai, Egypt. Geologie en Mijnbouw 76, 247–266.
Blasband, B., White, S., Brooijmans, P., De Broorder, H., Visser, W., 2000. Late Proterozoic extensional collapse in the Arabian–Nubian Shield. Journal of the Geological Society, London 157, 615–628.
Boger, S.D., Miller, J.M., 2004. Terminal suturing of Gondwana and the onset of the Ross–Delamarian Orogeny: the cause and effect of an Early Cambrian reconfiguration of plate motions. Earth and Planetary Science Letters 219, 35–48.
Bonavia, F.F., Chorowicz, J., 1992. Northward expulsion of the Pan-African of NE Africa guided by a reentrant zone of the Tanzania craton. Geology 20, 1023–1026.
Bonin, B., 2007. A-type granites and related rocks. Evolution of a concept, problems, and prospects. Lithos 97, 1–29.
Botros, N.S., 2002. Metallogeny of gold in relation to the evolution of the Nubian shield in Egypt. Ore Geology Reviews 19, 137–164.
Brasier, M., McGarron, G., Tucker, R., Leather, J., Allen, P., Shields, G., 2000. New U–Pb zircon dates for the Neoproterozoic Ghubrah glaciation and the top of the Huqf Supergroup. Oman Geology 28, 175–178.
Bregar, M., 1996. Exhumation History of the Gebel Sibai Dome (Eastern Desert of Egypt): Constraints from Evolution of Low-angle Normal Faults and Corresponding Footwall Units. M.Sc. Thesis, University of Graz, Austria (unpublished).
Bregar, M., Bauernhofer, A., Pelz, K., Kloetzli, U., Fritz, H., Neumayr, P., 2002. A late Neoproterozoic magmatic core complex in the Eastern Desert of Egypt: emplacement of granitoids in a wrench-tectonic setting. Precambrian Research 118, 59–82.
Breitkreuz, C., Eliwa, H., Khalaf, I., El Gameel, K., Bühler, B., Sergeev, S., Larionov, A., Murata, M., 2010. Neoproterozoic SHRIMP U–Pb zircon ages of silica-rich Dokhan Volcanics in the northeastern Desert, Egypt. Precambrian Research 182, 163–174.
BRGM Geoscientists, 1993. Khnaiguiyah Zinc–Copper Deposit Prefeasibility Study: Synopsis of Geology and Mineralization: Saudi Arabian Directorate General of Mineral Resources Technical Report BRGM-TR-13-4.
Brito Neves, B.B.de., Cordani, U.G., 1991. Tectonic evolution of S America during the Late Proterozoic. Precambrian Research 53, 23–40.
Brown, G.B., 1972. Tectonic Map of the Arabian Peninsula. Saudi Arabian Directorate General of Mineral Resources Map AP-2, Scale 1:4,000,000.
Brown, G.F., Jackson, R.O., 1960. The Arabian Shield. XIX International Geological Congress, Pt. 9, pp. 69–77.
Brown, F.B., Schmidt, D.L., Huffman Jr., A.C., 1989. Geology of the Arabian Peninsula: Shield Area of Western Saudi Arabia. US Geological Survey Professional Paper 560-A, 188 p.
Burke, K., Sengör, C., 1986. Tectonic escape in the evolution of the continental crust. In: Barazangi, M., Brown, L. (Eds.), Reflection Seismology, vol. 14. American Geophysical Union Geodynamics Series, pp. 41–53.
Calvez, J.Y., Kemp, J., 1987. Rb–Sr geochronology of the Shammar Group in the Hulayfah Area, Northern Arabian Shield. Saudi Arabian Deputy Ministry for Mineral Resources Open-File Report BRGM-OF-07-11, 22 p.
Calvez, J.Y., Alsac, C., Delfour, J., Kemp, J., Pellaton, C., 1983. Geologic Evolution of Western, Central, and Eastern Parts of the Northern Precambrian Shield, Kingdom of Saudi Arabia. Saudi Arabian Deputy Ministry for Mineral Resources Open-File Report BRGM-OF-03-17, 57 p.
Calvez, J.Y., Alsac, C., Delfour, J., Kemp, J., Pellaton, C., 1984. Geological evolution of western, central, and eastern parts of the northern Precambrian Shield, Kingdom of Saudi Arabia. King Abdulaziz University, Jiddah, Faculty of Earth Science Bulletin 6, 24–48.
Calvez, J.Y., Delfour, J., Feybesse, J.L., 1985. 2000-million-years Old Inherited Zircons in Plutonic Rocks from the Al Amar Region. New Evidence for an Early Proterozoic Basement in the Eastern Saudi Arabian Shield? Saudi Arabian Deputy Ministry for Mineral Resources Open-File Report BRGM-OF-05-11, 27 p.
Cawood, P.A., Kroner, A., Collins, W.J., Kusky, T.M., Mooney, W.D., Windley, B.F., 2009.Accretionary Orogens through Earth History. Geological Society of London, Special Publication 2009, vol. 318, pp. 1–36. doi: 10.1144/SP318.1.
Church, W.R., 1991. Discussion of ophiolites in NE and East Africa: implications for Proterozoic crustal growth. Journal of the Geological Society, London 148, 600–601.
Cloud, P., Awramik, S.M., Morrison, K., Hadley, D.G., 1979. Earliest Phanerozoic or latest Proterozoic fossils from the Arabian Shield. Precambrian Research 10, 73–93.
Cole, J.C., 1988, Geology of the Aban al Ahmar Quadrangle, Sheet 25F, Kingdom of Saudi Arabia. Saudi Arabian Deputy Ministry for Mineral Resources Geoscience Map GM 105, Scale 1:250,000, 45 p.
Cole, J.C., Hedge, C.E., 1986. Geochronologic Investigation of Late Proterozoic Rocks in the Northeastern Shield of Saudi Arabia. Saudi Arabian Deputy Ministry for Mineral Resources Technical Record USGS-TR-05-5, 42 p.
Coleman, R.G., Brown, G.F., Keith, T.E.C., 1972, Layered Gabbros in SW Saudi Arabia. US Geological Survey Professional Papers 800-D, pp. D143–D150.
Collenette, P., Grainger, D.J., 1994. Mineral Resources of Saudi Arabia, not including Oil, Natural Gas, and Sulfur. Saudi Arabian Directorate General of Mineral Resources DGMR Special Publication SP-2, 322 p.
Collins, A.S., 2006. Madagascar and the Amalgamation of Central Gondwana. Gondwana Research 9, 3–16.
Collins, A.S., Pisarevsky, S.A., 2005. Amalgamating eastern Gondwana: the evolution of the Circum-Indian Orogens. Earth Science Reviews 71, 229–270.
Collins, A.S., Windley, B.F., 2002. The Tectonic Evolution of central and northern Madagascar and its place in the final assembly of Gondwana. Journal of Geology 110, 325–340.
Collins, W.J., Beams, S.D., White, A.J.R., Chappell, B.W., 1982. Nature and origin of A-type granites with particular reference to southeastern Australia. Contributions to Mineralogy and Petrology 80, 189–200.
Collins, A.S., Kinny, P.D., Razakamanana, T., 2010. Depositional age, provenance and metamorphic age of metasedimentary rocks from southern Madagascar. Gondwana Research. doi:10.1016/j.gr.2010.12.006.
Coolen, J.J.M.M.M., Priem, H.N.A., Verdurmen, E.A.T., Verschure, R.H., 1982. Possible zircon U-Pb evidence of Pan-African granuilite facies metamorphism in the Mozambique belt of southern Tanzania. Precambrian Research 17, 31–40.
Cooper, J.A., Stacey, J.S., Stoeser, D.B., Fleck, R.J., 1979. An evaluation of the zircon method of isotopic dating in the southern Arabian craton. Contributions to Mineralogy and Petrology 68, 429–439.
Cosca, M.A., Shimron, A., Caby, R., 1999. Late Precambrian metamorphism and cooling in the Arabian–Nubian Shield. Petrology and $^{40}Ar/^{39}Ar$ geochronology of metamorphic rocks of the Elat area (southern Israel). Precambrian Research 98, 107–127.
Cox, G., Lewis, C.J., Collins, A.S., Nettle, D., Halverson, G.P., Foden, J., Kattan, F., Jourdan, F., 2011. Ediacaran Terrane accretion in the Arabian Nubian Shield. Gondwana Research.
Creaser, R.A., Price, R.C., Wormald, R.J., 1991. A-type granites revisited: assessment of a residual source model. Geology 19, 163–166.
Darbyshire, D.P.F., Jackson, N.J., Ramsay, C.R., Roobol, M.J., 1983. Rb–Sr isotope study of latest Proterozoic volcano-sedimentary belts in the central Arabian Shield. Journal of the Geological Society, London 140, 203–213.
Dardir, A.A., Abu Zeid, K.M., 1972. Geology of the basement rocks between latitudes 27°00′ and 27°30′N, Eastern Desert. Annals of the Geological Survey of Egypt 2, 129–158.
Davies, F.B., 1984. Strain analysis of wrench faults and collision tectonics of the Arabian–Nubian Shield. Journal of Geology 82, 37–53.
Davies, F.B., 1985. Geological Map of the Al Wajh Quadrangle, Sheet 26B, Kingdom of Saudi Arabia. Saudi Arabian Deputy Ministry for Mineral Resources Geoscience Map GM 83, Scale 1:250,000, 27 p.
De Wall, H., Greiling, R.O., Sadek, M.F., 2001. Post-collisional shortening in the late Pan-African Hamisana high strain zone, SE Egypt: field and magnetic fabric evidence. Precambrian Research 107, 179–194.
Delfour, J., 1970. Le groupe de j'balah une nouvelle unite du bouchlier Arabe. Bureau de Recherches Géologiques et Minières Bulletin 2 (4), 19–32.
Delfour, J., 1977, Geology of the Nuqrah quadrangle, Sheet 25E, Kingdom of Saudi Arabia: Directorate General of Mineral Resources Geological Map GM 28, Scale 1:250,000, 32 p.
Delfour, J., 1982. Geologic Map of the Halaban quadrangle, Sheet 23G, Kingdom of Saudi Arabia. Directorate General of Mineral Resources Geologic Map GM 46, Scale 1:250,000, 32 p.
Dewey, J.F., 1988. Extensional collapse of orogens. Tectonics 7, 1123–1139.
Dodge, F.C.W., Helaby, A.M., 1974. Mineralization in the Uyaijah–Thaaban area, West Central Part of the Uyaijah Ring Structure, Kingdom of Saudi Arabia. US Geological Survey Saudi Arabian Project Report No. 191. 43 p.
Doebrich, J.L., Zahony, S.G., Leavitt, J.D., Portacio Jr., J.S., Siddiqui, A.A., Wooden, J.L., Fleck, R.J., Stein, H.J., 2004. Ad Duwayhi, Saudi Arabia. Geology and geochronology of a Neoproterozoic intrusion-related gold system in the Arabian shield. Economic Geology 99, 713–741.
Doebrich, J.L., Al-Jehani, A.M., Siddiqui, A.A., Hayes, T.S., Saleh, Y., Wooden, J.L., Johnson, P.R., Kattan, F.H., Shaikan, B., Basahel, M., Zahran, H., Al-Shammari, A., 2007. Geology and metallogeny of the Ara Rayn terrane, eastern Arabain shield. Evolution of a Neoproterozoic continental-margin arc during assembly of Gondwana within the East African Orogen. Precambrian Research 158, 17–50.
Drury, S.A., De Souza Filho, C.R., 1998. Neoproterozoic terrane assemblages in Eritrea: review and prospects. Journal of African Earth Science 27, 331–348.
Drysdall, A.R., Jackson, N.J., Ramsay, C.R., Douch, C.J., Hackett, D., 1984. Rare element mineralization related to Precambrian alkali granites in the Arabian shield. Economic Geology 79, 1369–1377.
du Bray, E.A., 1984. Geology of the Silsilah Ring Complex, Kingdom of Saudi Arabia. Saudi Arabian Deputy Ministry for Mineral Resources Technical Record USGS-TR-04-19, 78 p.
Duncan, I.J., Rivard, B., Arvidson, R.E., Sultan, M., 1990. Structural interpretation and tectonic evolution of a part of the Najd Shear Zone (Saudi Arabia) using Landsat thematic-mapper data. Tectonophysics 178, 309–315.

Duyverman, H.J., Harris, N.B.W., Hawkesworth, C.J., 1982. Crustal accretion in the Pan-African. Nd and Sr isotope evidence from the Arabian Shield. Earth and Planetary Science Letters 59, 315–326.

El Ramly, M.F., 1972. A New Geological Map for the Basement Rocks in the Eastern and Southwestern Deserts of Egypt. Annals of the Geological Survey, Egypt, scale 1:1,000,000, vol. 2, pp. 1–18.

El Ramly, M.F., Akaad, M.K., 1960. The Basement Complex in the Central-Eastern Desert of Egypt between Latitudes 24°30' and 25°40' N. Geological Survey of Egypt Paper 8, pp. 1–35.

El Ramly, M.F., Greiling, R., Kroner, A., Rashwan, A.A., 1984. On the tectonic evolution of the Wadi Hafafit area and environs, Eastern Desert of Egypt. King Abdulaziz University, Jiddah, Bulletin of the Faculty of Earth Sciences 6, 114–126.e.

El Ramly, M.F., Greiling, R.O., Rashwan, A.A., 1990. Comment on ''Extension of the Najd shear system from Saudi Arabia to the Central Eastern Desert of Egypt based on integrated field and Landsat observations'' by M. Sultan, R.E. Arvidson, I.J. Duncan, R.J. Stern, and B. El Kaliouby. Tectonics 9, 535–538.

El-Bialy, M.Z., 2010. On the Pan-African transition of the Arabian–Nubian Shield from compression to extension: the post-collision Dokhan volcanic suite of Kid-Malhak region, Sinai, Egypt. Gondwana Research 17, 26–43.

El-Gaby, S., El-Nady, O., Khudeir, A., 1984. Tectonic evolution of the basement complex in the Central Eastern Desert of Egypt. Geologische Rundshau 73, 1019–1036.

El-Gaby, S., Khudeir, A.A., El-Taky, M., 1989. The Sokhan Volcanics of Wadi Queih area, central Eastern Desert, Egypt. In: Proceedings of the 1st Conference on Geochemistry, Alexandria University, Egypt, pp. 42–62.

El-Gaby, S., List, F.K., Tehrani, R., 1988. Geology, evolution and metallogenesis of the Pan-African Belt in Egypt. In: El Gaby, S., Greiling, R. (Eds.), The Pan-African Belt of NE Africa and Adjacent Areas, Tectonic Evolution and Economic Aspects. Vieweg, Braunschweig, Wiesbaden, pp. 17–68.

El-Gaby, S., List, F.K., Tehrani, R., 1990. The basement complex of the Eastern Desert and Sinai. In: Said, R. (Ed.), The Geology of Egypt. Balkema, Rotterdam, pp. 175–184.

Eliwa, H.A., Abu El-Enen, M.M., Khalaf, I.M., Itaya, T., 2004. Metamorphic evolution of Sinai metapelites and gneisses: constraints from petrology and K/Ar dating. Egyptian Journal of Geology 48, 169–185.

Eliwa, H.A., Kimura, J.-I., Itaya, T., 2006. Late Neoproterozoic Dokhan Volcanics, N Eastern Desert, Egypt: Geochemistry and petrogenesis. Precambrian Research 151, 31–52.

Eliwa, H., Breitkreuz, C., Khalaf, I., El Gameel, K., 2010. Depositional styles of Early Ediacaran terrestrial volcanosedimentary succession in Gebel El Urf area, N Eastern Desert, Egypt. Journal of African Earth Sciences 57, 328–344.

El-Nisr, S.A., 1997. Late Precambrian volcanism at Wadi Allaqi, south Eastern Desert, Egypt: evidence for transitional continental arc/margin environment. Journal of African Earth Sciences 24, 301–313.

El-Rabaa, S.M., Al-Shumaimri, M.S., Al-Mishwat, A.T., 2001. Fate of the Najd fault system in northwestern Saudi Arabia and southwestern Jordan. Gondwana Research 4, 164–165.

Elsass, P, 1981. Geology and Mineralization of the Ar Ridaniyah Area. Saudi Arabian Deputy Ministry for Mineral Resources Open-File Report BRGM-OF-01-19, 39 p.

El-Shafei, M., Kusky, T.M., 2003. Structural and tectonic evolution of the Neoproterozoic Feiran–Solaf metamorphic belt, Sinai Peninsula. Implications for the closure of the Mozambique Ocean. In: Kusky, T., Abdelsalam, M., Tucker, R., Stern, R.J. (Eds.), Precambrian Research, Special Issue on The East African and Related Orogens, and the Assembly of Gondwana, pp. 269–293.

Fairer, G.M., 1985. Geological Map of the Wadi Baysh Quadrangle, Sheet 17F, Kingdom of Saudi Arabia. Saudi Arabian Deputy Ministry for Mineral Resources Geoscience Map GM-77, 1:250,000, 23 p.

Fike, D.A., Grotzinger, J.P., Pratt, L.M., Summons, R.E., 2006. Oxidation of the Ediacaran ocean. Nature 444, 744–747.

Finger, F., Dorr, W., Gerdes, A., Gharib, M., Dawoud, M., 2008. U–Pb zircon ages and geochemical data for the Monumental Granite and other granitoid rocks from Aswan, Egypt. Implications for geological evolution of the western margin of the Arabian–Nubian Shield. Mineralogy and Petrology 93, 153–183.

Fleck, R.J., Hadley, D.G., 1982. Ages and Strontium Initial Ratios of Plutonic Rocks in a Transect of the Arabian Shield. Saudi Arabian Deputy Ministry for Mineral Resources Open-File Report USGS-OF-03-38, 43 p.

Fleck, R.J., Greenwood, W.R., Hadley, D.G., Anderson, R.E., Schmidt, D.L., 1979. Rubidium–Strontium Geochronology and Plate-tectonic Evolution of the Southern Part of the Arabian Shield. US Geological Survey Saudi Arabian Mission Report 245, 105 p.

Fleck, R.J., Greenwood, W.R., Hadley, D.G., Anderson, R.E., Schmidt, D.L., 1980. Rubidium-Strontium Geochronology and Plate-tectonic Evolution of the Southern Part of the Arabian Shield. USGS Professional Paper 1131, 38 p.

Fowler, A., El Kalioubi, B., 2002. The Migif–Hafafit gneissic complex of the Egyptian Eastern Desert: fold interference patterns involving multiply deformed sheath folds. Tectonophysics 346, 247–275.

Fowler, A., El Kalioubi, B., 2004. Gravitational collapse origin of shear zones, foliations and linear structures in the Neoproterozoic cover nappes, Eastern Desert, Egypt. Journal of African Earth Sciences 38, 23–40.

Fowler, A., Hassen, I., 2008. Extensional tectonic origin of gneissosity and related structures of the Feiran–Solaf metamorphic belt. Precambrian Research 164, 119–136.

Fowler, T.J., Osman, A.F., 2001. Gneiss-cored interference dome associated with two phases of late Pan-African thrusting in the Central Eastern Desert, Egypt. Precambrian Research 108, 17–43.

Fowler, A., Osman, A.F., 2009. The Sha'it–Nugrus shear zone separating Central and S Eastern Deserts, Egypt: a post-arc collision low-angle normal ductile shear zone. Journal of African Earth Sciences 53, 16–32.

Fowler, A.-R., Khaled, G.A., Omar, S.M., Eliwa, H.A., 2006. The significance of gneissic rocks and synmagmatic extensional ductile shear zones of the Barud area for the tectonics of the North Eastern Desert, Egypt. Journal of African Earth Sciences 46, 201–220.

Fowler, A., Khamees, H., Dowidar, H., 2007. El Sibai gneissic complex, Central Eastern Desert, Egypt: folded nappes and syn-Kinematic gneissic granitoid sheets—note a core complex. Journal of African Earth Sciences 49, 119–135.

Fowler, A., Hassen, I.S., Osman, A.F., 2010. Neoproterozoic structural evolution of SE Sinai, Egypt: II. Convergent tectonic history of the continental arc Kid Group. Journal of African Earth Sciences 58, 526–546.

Fritz, H., Messner, M., 1999. Intramontane basin formation during oblique convergence in the Eastern Desert of Egypt: magmatically versus tectonically induced subsidence. Tectonophysics 315, 145–162.

Fritz, H., Puhl, J., 1997. Granitoid emplacement in a shear-extensional setting: A semiquantitative approach from physical parameters (Eastern Desert, Egypt). Zentralblatt fur Geologie und Palaeontolgie Teil 1, 257–276.

Fritz, H., Wallbrecher, E., Khudeir, A.A., Abu El Ela, F., Dallmeyer, D.R., 1996. Formation of Neoproterozoic metamorphic core complexes during oblique convergence (Eastern Desert, Egypt). Journal of African Earth Sciences 23, 311–329.

Fritz, H., Dallmeyer, D.R., Wallbrecher, E., Loizenbauer, J., Hoinkes, G., Neymayr, P., Khudeir, A.A., 2002. Neoproterozoic tectonothermal evolution of the Central Eastern Desert, Egypt: a slow velocity tectonic process of core complex exhumation. Journal of African Earth Sciences 34, 137–155.

Gabr, S., Ghulam, A., Kusky, T., 2010. Detecting areas of high-potential gold mineralization using ASTER data. Case study. Ore Deposit Reviews. doi:10.1016/j.oregeorev.2010.05.007.

Garfunkel, Z., 1999. History and paleogeography during the Pan-African orogen to stable platform transition: reappraisal of the evidence from the Elat area and the northern Arabian–Nubian Shield. Israeli Journal of Earth Science 48, 135–157.

Genna, A., Guerrot, C., Deschamps, Y., Nehlig, P., Shanti, M., 1999. Les formations Ablah d'Arabie Saoudite (datation et implication géologique). Compte Rendue Acadamie Sciences, Paris 329, 661–667.

Genna, A., Nehlig, P., Le Goff, E., Guetrrot, C., Shanti, M., 2002. Proterozoic tectonism of the Arabian Shield. Precambrian Research 117, 21–40.

Gettings, M.E., Blank, H.R., Mooney, W.D., 1986. Crustal structure of southwestern Saudi Arabia. Journal of Geophysical Research 91, 6491–6512.

Ghebreab, W., 1999. Tectono-metamorphic history of Neoproterozoic rocks in eastern Eritrea. Precambrian Research 98, 83–105.

Ghebreab, W., Talbot, C.J., 2000. Red Sea extension influenced by Pan-African tectonic grain in eastern Eritrea. Journal of Structural Geology 22, 931–946.

Ghebreab, W., Yohannes, E., Woldegiorgis, L., 1992. The Lega Dembi gold mine: an example of shear zone-hosted mineralization in the Adola greenstone belt. Journal of African Earth Sciences 15, 489–500.

Ghebreab, W., Talbot, C.J., Page, L., 2005. Time constrains on exhumation of the East African Orogen from field observations and $^{40}Ar/^{39}Ar$ cooling ages of low-angle mylonites in Eritrea, NE Africa. Precambrian Research 139, 20–41.

Ghebreab, W., Greiling, R., Solomon, S., 2009. Structural setting of Neoproterozoic mineralization, Asmara district, Eritrea. Journal of African Earth Sciences 55, 219–235.

Goldfarb, R.J., Groves, D.I., Gardoll, D., 2001. Orogenic gold and geologic time: a global synthesis. Ore Geology Reviews 18, 1–75.

Goldfarb, R.J., Baker, T., Dube, B., Groves, D.I., Hart, C.J.R., Gosselin, P., 2005. Distribution, Character, and Genesis of Gold Deposits in Metamorphic Terrains. Society of Economic Geologists, Inc., Economic Geology 100th Anniversary Volume, pp. 407–450.

Grainger, D.J., Hanif, M.R., 1989, Geologic Map of the Shaghab Quadrangle, Sheet 27B, Kingdom of Saudi Arabia. Saudi Arabian Directorate General of Mineral Resources Geologic Map GM 109, Scale 1:250,000, 31 p.

Greene, R.C., 1993. Stratigraphy of the Late Proterozoic Murdama group, Saudi Arabia. US Geological Survey Bulletin 1976, 59 p.

Greenwood, W.R., Anderson, R.E., Fleck, R.J., Roberts, R.J., 1980. Precambrian Geologic History and Plate Tectonic Evolution of the Arabian Shield. Saudi Arabian Directorate General of Mineral Resources Bulletin 24, 35 p.

Greenwood, W.R., Stoeser, D.B., Fleck, R.J., Stacey, J.S., 1982. Late Proterozoic Island-arc Complexes and Tectonic Belts in the Southern Part of the Arabian Shield, Kingdom of Saudi Arabia. Saudi Arabian Deputy Ministry for Mineral Resources Open-File Report USGS-OF-02-8, 46 p.

Greiling, R.O., 1997. Thrust tectonics in crystalline domains: the origin of a gneiss dome. Proceedings of the Indian Academy of Science (Earth and Planetary Sciences) 106, 209–220.

Greiling, R.O., Rashwan, A.A., 1994. Large-scale shear zones and related mineral deposits: examples from the Nubian Shield (Proterozoic), Egypt. Africa Geoscience Review 1, 503–514.

Greiling, R.O., Kröner, A., El Ramly, M.F., 1984. Structural interference patterns and their origin in the Pan-African basement of the southeastern desert of Egypt. In: Kröner, A., Greiling, R.O. (Eds.), Precambrian Tectonics Illustated. Schweizerbart'sche Verlagsbuchhandlung, Stuttgart, pp. 401–412.

Greiling, R.O., Kroner, A., EI Ramly, M.F., Rashwan, A.A., 1988a. Structural and geological relationship between the southern and central parts of the Eastern Desert of Egypt. In: EI-Gaby, S., Greiling, R.O., (Eds.), The Pan-African Belt of NE Africa and Adjacent Areas. Vieweg, Braunschweig, Wiesbaden, pp. 121–145.

Greiling, R.O., Abdeen, M.M., Dardir, A.A., El-Akhal, H., El-Ramly, M.F., Kamal El-Din, G.M., Osman, A.F., Rashwan, A.A., Rice, A.H.N., Sadek, M.F., 1994. A structural synthesis of the Proterozoic Arabian–Nubian Shield in Egypt. Geologische Rundshau 83, 484–501.

Greiling, R.O., Naim, G.M., Hussein, A.A., (Eds.), 1996. Excursion across the Pan-African, Neoproterozoic basement Qena–Quseir Guide Book. Centennial of the Egyptian Geological Survey 1896–1996. Egyptian Geological Survey and Mineral Authority, Cairo, Egypt.

Grothaus, B., Eppler, D., Ehrlish, R., 1979. Depositional environments and structural implications of the Hammamat Formation, Egypt. Annals of the Geological Survey of Egypt IX, 564–590.

Groves, D.I., Goldfarb, R.J., Gebre-Mariam, M., Hagemann, S.G., Robert, F., 1998. Orogenic gold deposits: a proposed classification in the context of their crustal distribution and relationship to other gold deposit types. Ore Geology Reviews 13, 7–27.

Grunow, A., 1999. Gondwana events and palaeogeography: a palaeomagnetic review. Journal of African Earth Sciences 28, 53–69.

Habib, M.E., Ahmed, A.A., El Nady, O.M., 1985. Tectonic evolution of the Meatiq infrastructure, Central Eastern Desert, Egypt. Tectonics 4, 613–627.

Hadley, D.G., 1974. The Taphrogeosynclinal Jubaylah Group in the Mashhad Area, Northwestern Hijaz, Kingdom of Saudi Arabia. Saudi Arabian Directorate General of Mineral Resource Bulletin 10, 18 p.

Halverson, G.P., Wade, B.P., Hurtgen, M.T., Barovich, K.M., 2010. Neoproterozoic chemostratigraphy. Precambrian Research 182, 337–350.

Hanson, R.E., 2003. Proterozoic geochronology and tectonic evolution of southern Africa. In: Yoshida, M., Windley, B.F., Dasgupta, S., (Eds.), Proterozoic East Gondwana: Supercontinent Assembly and Breakup: Geological Society, vol. 206. London, Special Publication, pp. 427–463.

Hargrove, U.S., 2006, Crustal Evolution of the Neoproterozoic Bi'r Umq Suture Zone, Kingdom of Saudi Arabia. Geochronological, Isotopic, and Geochemical Constraints. Unpublished Ph.D. Thesis, University of Texas at Dallas, 343 p.

Hargrove, U.S., Stern, R.J., Kimura, J.-I., Manton, W.I., Johnson, R., 2006. How juvenile is the Arabian–Nubian Shield? Evidence from Nd isotopes and pre-Neoproterozoic inherited zircon in the Bi'r Umq suture zone, Saudi Arabia. Earth and Planetary Science Letters 252, 308–326.

Harms, U., Darbyshire, D.P.F., Denkler, T., Hengst, M., Schandelmeier, H., 1994. Evolution of the Neoproterozoic Delgo Suture Zone and crustal growth in northern Sudan: geochemical and radiogenic isotope constrains. Geologische Rundschau 83, 591–603.

Hassan, M.A., Hashad, A.H., 1990. Precambrian of Egypt. In: Said, R. (Ed.), The Geology of Egypt. Balkema, Rotterdam, pp. 201–248.

Hedge, C.E., 1984. Precambrian Geochronology of Part of Northwestern Saudi Arabia. Saudi Arabian Deputy Ministry for Mineral Resources Open-File Report USGS-OF-04-31, 12 p.

Helmy, H.M., Mogessie, A., 2001. Gabbro Akarem, Eastern Desert, Egypt: Cu–Ni–PGE mineralization in a concentrically zoned mafic–ultramafic complex. Mineralium Deposita 36, 58–71.

Helmy, H.M., Kaindl, R., Fritz, H., 2004. The Sukari gold mine, Eastern Desert-Egypt: structural setting, mineralogy and fluid inclusion study. Mineralium Deposita 39, 495–511.

Hermina, M., Klitzsch, E., List, F.K., 1989. Stratigraphic Lexicon and Explanatory Notes to the Geological Map of Egypt. Conoco, Cairo, Scale 1:500,000.

Hoffman, P.F., Kaufman, A.J., Halverson, G.P., Schrag, D.P., 1998. A Neoproterozoic snowball Earth. Science 281, 1342–1346.

Hooper, P.R., Bailey, D.G., McCarley Holder, G.A., 1995. Tertiary calc-alkaline magmatism associated with lithospheric extension in the Pacific NW. Journal of Geophysical Research 100, 10303–10319.

Hume, W.F., 1934. Geology of Egypt – Part I – the Metamorphic Rocks. Government Press, Cairo.

Hurtgen, M.T., Halverson, G.P., Arthur, M.A., Hoffman, P.F., 2006. Sulfur cycling in the aftermath of a Neoproterozoic (Marinoan) snowball glaciation: evidence for a syn-glacial sulfidic deep ocean. Earth and Planetary Science Letters 245, 551–570.

Hussein, A.A., Ali, M.M., El Ramly, M.F., 1982. A proposed new classification of the granites of Egypt. Journal of Volcanology and Geothermal Research 14, 187–198.

Husseini, M.I., 1988. The Arabian Infracambrian extensional system. Tectonophysics 148, 93–103.

Jacobs, J., Thomas, R.J., 2004. Himalayan-type indenter-escape tectonics model for the southern part of the late Neoproterozoic–early Paleozoic East African orogen. Geology 32, 721–724.

Jarrar, G., 2001. The youngest Neoproterozoic mafic dyke suite in the Arabian shield. Mildly alkaline dolerites from S Jordan – their geochemistry and petrogenesis. Geological Magazine 138, 309–323.

Jarrar, G., Baumann, A., Wachendorf, H., 1983. Age determinations in the Precambrian basement of the Wadi Arab area, SW Jordan. Earth and Planetary Science Letters 63, 292–304.

Jarrar, G., Wachendorf, H., Saffarini, G., 1992. A late Proterozoic bimodal volcanic/subvolcanic suite from Wadi Araba, SW Jordan. Precambrian Research 56, 51–72.

Jarrar, G., Stern, R.J., Saffarini, G., Al-Zubi, H., 2003. Late- and post-orogenic Neoproterozoic intrusions of Jordan: Implications for crustal growth in the northernmost segment of the East African Orogen. Precambrian Research 123, 295–320.

Jarrar, G., Saffarini, G., Baumann, A., Wachendorf, H., 2004. Origin, age and petrogenesis of Neoproterozoic composite dikes from the Arabian–Nubian Shield, SW Jordan. Geological Journal 39, 157–178.

Jarrar, G.H., Manton, W.I., Stern, R.J., Zachmann, D., 2008. Late Neoproterozoic A-type granites in the northernmost Arabian–Nubian Shield formed by fractionation of basaltic melts. Chemie der Erde 68, 295–312.

Jelenc, D., 1966. Mineral Occurrences of Ethiopia. Ministry of Mines, Addis Ababa.720 p.

Johnson, P.R., 2003. Post-amalgamation basins of the NE Arabian Shield and implications for Neoproterozoic tectonism in the northern East African Orogen. Precambrian Research 123, 321–337.

Johnson, P.R., 2006. Explanatory Notes to the Map of Proterozoic Geology of Western Saudi Arabia. Saudi Geological Survey Technical Report SGS-TR-2006-4, 62 p., Scale 1:1,500,000.

Johnson, P.R., Kattan, F., 1999. The Ruwah, Ar Rika, and Halaban-Zarghat fault zones: NW-trending Neoproterozoic brittle–ductile shear zones in west-central Saudi Arabia, In: De Wall, H., Greiling, R.O. (Eds.), Aspects of Pan-African Tectonics, vol. 32. Bilateral Seminars of the International Bureau, Schriften des Forschungszentrum Jülich, pp. 75–79.

Johnson, P.R., Kattan, F., 2001. Oblique sinistral transpression in the Arabian shield: the timing and kinematics of a Neoproterozoic suture zone. Precambrian Research 107, 117–138.

Johnson, P.R., Kattan, F.H., 2007. Geochronologic Dataset for Precambrian Rocks in the Arabian Peninsula: a Catalogue of U–Pb, Rb–Sr, Ar–Ar, and Sm–Nd ages. Saudi Geological Survey Open-file Report SGS-OF-2007-3, 21 p.

Johnson, P.R., Stewart, I.C.F., 1995. Magnetically inferred basement structure in central Saudi Arabia. Tectonophysics 245, 37–52.

Johnson, P.R., Woldehaimanot, B., 2003. Development of the Arabian–Nubian shield: perspectives on accretion and deformation in the northern East African Orogen and the assembly of Gondwana. In: Yoshida, M., Windley, B.F., Dasgupta, S., (Eds.), Proterozoic East Gondwana: Supercontinent Assembly and Breakup: Geological Society, vol. 206. London, Special Publication, pp. 290–325.

Johnson, P.R., Kattan, F.H., Wooden, J.L., 2001. Implications of SHRIMP and microstructural data on the age and kinematics of shearing in the Asir Terrane, southern Arabian shield, Saudi Arabia. Gondwana Research 4, 172–173.

Johnson, P.R., Abdelsalam, M.G., Stern, R.J., 2003. The Bi'r Umq-Nakasib suture zone in the Arabian–Nubian Shield: a key to understanding crustal growth in the East African Orogen. Gondwana Research 6, 523–530.

Johnson, P.R., Kattan, F.K., Al-Saleh, A.M., 2004. Neoproterozoic ophiolites in the Arabian shield: field relations and structure. In: Kusky, T.M. (Ed.), Precambrian Ophiolites and Related rocks, Developments in Precambrian Geology, vol. 13. Elsevier, pp. 129–162.

Johnson, S.P., Rivers, T., De Waele, B., 2005. A review of the Mesoproterozoic to early Palaeozoic magmatic and tectonothermal history of South-central Africa: implications for Rodinia and Gondwana. Journal of the Geological Society, London 162, 433–450.

Kamilli, R.J., Cole, J.C., Elliott, J.E., Criss, R.E., 1993. Geology and genesis of the Baid al Jimalah tungsten deposit, Kingdom of Saudi Arabia. Economic Geology 88, 1743–1767.

Kattan, F.H., Harire, A.R., 2000. Geology of the Ad Duwayah-B'ir Warshah Mineral Belt: Saudi Geological Survey Open-File Report USGS-OF-99-6, 33 p.

Katz, O., Beyth, M., Miller, N., Stern, R., Avigad, D., Basu, A., Anbar, A., 2004. A Late Neoproterozoic (630 Ma) boninitic suite from southern Israel: Implications for the consolidation of Gondwanaland. Earth and Planetary Science Letters 218, 475–490.

Katzir, Y., Litvinovsky, B.A., Jahn, B.M., Eyal, M., Zanvilevich, A.N., Valley, J.W., Vapni, Ye., Beeri, Y., Spicuzza, M.J., 2007. Interrelations between coeval mafic and A-type silicic magmas from composite dykes in a bimodal suite of southern Israel, northernmost Arabian–Nubian Shield: Geochemical and isotope constraints. Lithos 97, 336–364.

Kellogg, K.S., Janjou, D., Minoux, L., Fourniguet, J., 1986. Geological Map of the Wadi Tathlith Quadrangle, Sheet 20G, Kingdom of Saudi Arabia. Saudi Arabian Deputy Ministry for Mineral Resources Geologic Map GM 103, Scale 1:250,000, 27 p.

Kemp, J., 1996. The Kuara Formation (northern Arabian shield); definition and interpretation: a probable fault-trough sedimentary succession. Journal of African Earth Sciences 22, 507–523.

Kemp, J., 1998. Caldera-related volcanic rocks in the Shammar Group, northern Arabian Shield. Journal of African Earth Sciences 26, 551–572.

Kemp, J., Pellaton, C., Calvez, J.Y., 1980. Geochronological Investigations and Geological History in the Precambrian of Northwestern Saudi Arabia. Saudi Arabian Directorate General of Mineral Resources Open-File Report BRGM-OF-01-1, 120 p.

Kennedy, A., Johnson, P.R., Kattan, F.H., 2004. SHRIMP Geochronology in the Northern Arabian Shield. Part I. Data Acquisition. Saudi Geological Survey Open-File Report SGS-OF-2004-11.

Kennedy, A., Johnson, P.R., Kattan, F.H., 2005. SHRIMP Geochronology in the Northern Arabian Shield. Part II. Data Acquisition 2004. Saudi Geological Survey Open-File Report SGS-OF-2005-10.

Kennedy, A., Kozdroj, W., Kattan, F.H., Kodzroj, M.Z., Johnson, P.R., 2010, SHRIMP Geochronology in the Arabian Shield (Midyan Terrane, Afif Terrane, Ad Dawadimi Terrane) and Nubian Shield (Central Eastern Desert), Part IV. Data Acquisition 2008. Saudi Geological Survey Open-File Report SGS-OF-2010-10, 101 p.

Kennedy, A., Kozdroj, W., Johnson, P.R., Kattan, F.H., 2011. SHRIMP Geochronology in the Northern Arabian Shield. Part III. Data Acquisition 2006. Saudi Geological Survey Open-File Report SGS-OF-2007-9.

Kessel, R., Stein, M., Navon, O., 1998. Petrogenesis of late Neoproterozoic dikes in the northern Arabian–Nubian Shield. Implications for the origin of A-type granites. Precambrian Research 92, 195–213.

Khudeir, A.A., Abu El-Rus, M.A., El-Gaby, S., El-Nady, O., Bishara, W.W., 2008. Sr–Nd isotopes and geochemistry of the infrastructural rocks in the Meatiq and Hafafit core complexes, Eastern Desert, Egypt: evidence for involvement of pre-Neoproterozoic crust in the growth of the Arabain–Nubian Shield. Island Arc 17, 90–108.

Klemm, D., Klemm, R., Murr, A., 2001. Gold of the Pharaohs – 6000 years of gold mining in Egypt and Nubia. Journal of African Earth Sciences 33, 643–659.

Kolodner, K., Avigad, D., McWilliams, M., Wooden, J.L., Weissbrod, T., Feinstein, S., 2006. Provenance of N Gondwana Cambrian–Ordovician sandstone: U–Pb SHRIMP dating of detrital zircons from Israel and Jordan. Geological Magazine 143, 367–391.

Kröner, A., Sassi, F.P., 1996. Evolution of the northern Somali basement: new constraints from zircon ages. Journal of African Earth Sciences 22, 1–15.

Kröner, A., Roobol, M.J., Ramsay, C.R., Jackson, N.J., 1979. Pan African ages of some gneissic rocks in the Saudi Arabian Shield. Journal of the Geological Society, London 136, 455–461.

Kröner, A., Greiling, R., Reischmann, T., Hussein, I.M., Stern, R.J., Durr, S., Kruger, J., Zimmer, M., 1987. Pan-African crustal evolution in the Nubian segment of NE Africa. In: Kröner, A. (Ed.), Proterozoic Lithospheric Evolution, American Geophysical Union Geodynamics Series, vol. 17, pp. 235–257.

Kröner, A., Eyal, M., Eyal, Y., 1990. Early Pan-African evolution of the basement around Elat, Israel, and the Sinai Peninsula revealed by single-zircon evaporation dating, and implications for crustal accretion rates. Geology 18, 545–548.

Kröner, A., Krüger, J., Rashwan, A.A.A., 1994. Age and tectonic setting of granitoid gneisses in the Eastern Desert of Egypt and south-west Sinai. Geologische Rundschau 83, 502–513.

Kusky, T.M., Matsah, M.I., 2000. Evolution of a Neoproterozoic Dextral Pull-apart Basin (Jifn Basin), NE Arabian Shield: Relationships to the Halaban-Zarghat (Najd) Fault System and the Closure of the Mozambique Ocean. Geological Society of America, Annual Meeting 2000.

Kusky, T., Matsah, M., 2003. Neoproterozoic Dextral Faulting on the Najd Fault System, Saudi Arabia, preceded sinistral faulting and escape tectonics related to closure of the Mozambique Ocean. In: Yoshida, M., Windley, B.F., Dasgupta, S., Powell, C. (Eds.), Proterozoic East Gondwana: Supercontinent Assembly and Breakup, vol. 206. Geological Society, London, Special Publication, pp. 327–361.

Kusky, T.M., Ramadan, T., 2002. Structural controls on Neoproterozoic mineralization in the SE Desert, Egypt. An integrated field, Landsat TM, and SIR C/X approach. Journal of African Earth Sciences 35, 107–121.

Kusky, T.M., Abdelsalam, M., Stern, R., Tucker, R., 2003. Preface to special issue on the East African and Related Orogens, and the Assembly of Gondwana. Precambrian Research 123, 81–85.

Küster, D., 2009. Granitoid-hosted Ta mineralization in the Arabian–Nubian Shield: ore deposit types, tectono-metallogenic setting and petrogenetic framework. Ore Geology Reviews 35, 68–86.

Küster, D., Liégeois, J.-P., 2001. Sr, Nd isotopes and geochemistry of the Bayuda Desert high-grade metamorphic basement (Sudan): an early Pan-African oceanic convergent margin, not the edge of the East Saharan ghost craton. Precambrian Research 109, 1–23.

Küster, D., Romer, R.L., Tolessa, D., Zerihun, D., Bheemalingeswara, K., 2007. Geochemical evolution and age of the Kenticha tantalum pegmatite, southern Ethiopia. In: International Symposium on Granitic Pegmatites: The State of the Art, May 2007, Porto, Portugal, Abstracts Volume, pp. 50–51.

Küster, D., Liégeois, J.P., Matukov, D., Sergeev, S., Lucassen, F., 2008. Zircon geochronology and Sr, Nd, Pb isotope geochemistry of granitoids from Bayuda Desert and Sabaloka (Sudan). Evidence for a Bayudian event (920–900 Ma) preceding the Pan-African orogenic cycle (860–590 Ma) at the eastern boundary of the Saharan Metacraton. Precambrian Research 164, 16–39.

Le Guerroué, L., Allen, P.A., Cozzi, A., 2006. Chemostratigraphic and sedimentological framework of the largest negative carbon isotopic excursion in Earth history: the Neoproterozoic Shuram Formation (Nafun Group, Oman). Precambrian Research 146, 68–92.

Lemiszki, P.J., Brown, L.D., 1988. Variable crustal structure of strike-slip fault zones as observed on deep seismic reflection profiles. Geological Society of America Bulletin 100, 665–676.

Lewis, C.J., 2009. A Structural, Geochronological and Geochemical Investigation of the Abt Schist; Ad Dawdimi Terrane, Central Saudi Arabia. University of Adelaide, Tectonics, Resources and Exploration, 88 p.

Lewis, R.S., Schull, H.W., 1994. Geology and gold mineralization of the An Najadi mineral belt and comparison to the Sukhaybarat gold mine, Kingdom of Saudi Arabia. Saudi Arabian Deputy Ministry for Mineral Resources Technical Report USGS-TR-94-6, 54 p.

Li, Z.X., Powell, C.M., 1993. Late Proterozoic to early Paleozoic paleomagnetism and the formation of Gondwanaland. In: Findlay, R.H., Unrug, R., Banks, M.R., Veevers, J.J. (Eds.), Gondwana Eight. Balkema, Rotterdam, pp. 9–21.

Li, Z.X., Bogdanova, S.V., Collins, A.S., Davidson, A., De Waele, B., Ernst, R.E., Fitzsimons, I.C.W., Fuck, R.A., Gladkochub, D.P., Jacobs, J., Karlstrom, K.E., Lu, S., Natapov, L.M., Pease, V., Pisarevsky, S.A., Thrane, K., Vernikovsky, V., 2007. Assembly, configuration, and break-up history of Rodinia: a synthesis. Precambrian Research 160, 179–210.

Liégeois, J.-P., Stern, R.J., 2010. Sr–Nd isotopes and geochemistry of granite–gneiss complexes from the Meatiq and Hafafit domes, Eastern Desert, Egypt: no evidence for pre-Neoproterozoic crust. Journal of African Earth Sciences 57, 31–40.

Liégois, J.-P., Navez, J., Hertogen, J., Black, R., 1998. Contrasting origin of post-collisional high-K calc-alkaline and shoshonotic versus alkaline and peralkaline granitoids. The use of sliding normalization. Lithos 45, 1–28.

Loisell, M.C., Wones, D.R., 1979. Charcteristics and origin of anorogranic granites. Geological Society of America Abstracts with Programs 11, 468.

Loizenbauer, J., Wallbrecher, E., Fritz, H., Neumayr, P., Khudeir, A.A., Kloetzli, U., 2001. Structural geology, single zircon ages and fluid inclusion studies of the Meatiq metamorphic core complex: Implications for Neoproterozoic tectonics in the Eastern Desert of Egypt. Precambrian Research 110, 357–383.

Lundmark, A.M., Andresen, A., Hassan, M.A., Augland, L.E., Abu El-Rus, M.A., Baghdady, G.Y., 2011, Repeated magmatic pulses in the East African Orogen of Central Eastern Desert, Egypt: an old idea supported by new evidence. Gondwana Research.

Lutz, T.M., Foland, K.A., Friedman, I., Serencsits, C.M., 1978. Ages of Egyptian alkaline complexes and Sr and O isotope relations at the Abu Khruq Complex. U.S. Geological Survey Open-File Report 78-101, pp. 265–267.

Malmgren, K., Andersson, W., 1994. Sukhaybarat gold mine. In: Collenette, P., Grainger, D.J. (Compilers), Mineral Resources of Saudi Arabia. Saudi Arabian Directorate General of Mineral Resources Special Publication DGMR-SP-2, pp. 111–115.

Martin, C., Roberts, R.J., Stoeser, D.B., 1979. Titaniferous Magnetite in the Layered Intrusive Complex at Lakathah, Kingdom of Saudi Arabia. USGS Saudi Project Report 238, 36 p.

Matsah, M., Kusky, T.M., 1999. Sedimentary facies of the Neoproterozoic Al-Jifn basin, NE Arabian shield: relationships to the Halaban-Zarghat (Najd) faults system and the closure of the Mozambique Ocean. In: Greiling, R. (Ed.), Pan-African of northern Africa–Arabia. Forschungszentrum Jülich. Geologisch-Palaeontoloigsches Institut, Ruprecht-Karls-Universitaet, Heidelberg, Proceedings of a Workshop, October 22–23, 1998.

Matsah, M.I.M., Kusky, T.M., 2001. Analysis of Landsat ratio imagery of the Halaban-Zarghat fault and related Jifn basin, NE Arabian shield: implications for the kinematic history of the Najd fault. Gondwana Research 4, 182.

Meert, J.G., 2002. A synopsis of events related to the assembly of eastern Gondwana. Tectonophysics 363, 1–40.

Meert, J.G., Lieberman, B.S., 2008. The Neoproterozoic assembly of Gondwana and its relationship to the Ediacaran–Cambrian radiation. Gondwana Research 14, 5–21.

Miller, M.M., Dixon, T.H., 1992. Late Proterozoic evolution of the N part of the Hamisana zone, NE Sudan: constraints on Pan-African accretionary tectonics. Journal of the Geological Society, London 149, 743–750.

Miller, N.R., Alene, M., Sacchi, R., Stern, R.J., Conti, A., Kröner, A., Zuppi, G., 2003. Significance of the Tambien Group (Tigrai, N. Ethiopia) for Snowball Earth events in the Arabian–Nubian Shield. Precambrian Research 121, 263–283.

Miller, N.R., Johnson, P.R., Stern, R.J., 2008. Marine versus non-marine environments for the Jibalah group, NW Arabian Shield: a sedimentologic and geochemical survey and report of possible metazoan in the Dhaiqa formation. Arabian Journal for Science and Engineering 33, 55–77.

Moghazi, A.M., Andersen, T., Oweiss, G.A., El-Bouseily, A.M., 1998. Geochemical and Sr–Nd–Pb isotopic data bearing on the origin of Pan-African granitoids in the Kid area, SE Sinai, Egypt. Journal of the Geological Society, London 155, 697–710.

Moghazi, A.M., Hassanen, M.A., Mohammed, F.H., Ali, S., 2004. Late Neoproterozoic strongly peraluminous leucogranites, South Eastern Desert, Egypt – petrogenesis and geodynamic significance. Mineralogy and Petrology 81, 19–41.

Mogren, S., Al-Amri, A.M., Al-Damegh, K., Faihead, D., Jassim, S., Algamdi, A., 2008. Sub-surface geometry of Ar Rika and Ruwah faults from gravity and magnetic surveys. Arabian Journal of Geosciences 1, 33–47.

Mohamed, F.H., Moghazi, A.M., Hassanen, M.A., 2000. Geochemistry, petrogenesis and tectonic setting of late Neoproterozoic Dokhan-type volcanic rocks in the Fatira area, eastern Egypt. International Journal of Earth Sciences 88, 764–777.

Möller, A., Mezger, K., Schenk, V., 1998. Crustal age domains and the evolution of the continental crust in the Mozambique Belt of Tanzania: Combined Sm–Nd, Rb–Sr, and Pb–Pb isotopic evidence. Journal of Petrology 39, 749–783.

Molnar, P., Tapponnier, P., 1977. Relation of the tectonics of eastern china to the India–Eurasia collision: application of slip-line field theory to large-scale continental tectonics. Geology 5, 212–216.

Moore, J.M., 1979. Tectonics of the Najd transcurrent fault system, Saudi Arabia. Journal of the Geological Society, London 136, 441–454.

Moufti, M.R.H., 2001. Age, geochemicstry, and origin of peraluminous A-type granitoids of the Ablah–Shuwas pluton, Ablah graben Arabian shield. Acta Mineralogica–Petrographica, Szeged 2001 42, 5–20.

Moussa, E.M.M., Stern, R.J., Manton, W.I., Ali, K.A., 2008. SHRIMP zircon dating and Sm/Nd isotopic investigations of Neoproterozoic granitoids, Eastern Desert, Egypt. Precambrian Research 160, 341–356.

Mushkin, A., Navon, O., Halitz, L., Heimann, A., Hartmann, G., Stein, M., 2003. The petrogenesis of A-type magmas from the Amram Massif, southern Israel. Journal of Petrology 44, 815–832.

Nawab, Z.A., 1979, Geology of the Al Amar-Idsas Region of the Arabian Shield. Evolution and Mineralization of the Arabian–Nubian Shield. King Abdulaziz University, Jeddah, Institute of Applied Geology Bulletin 3, v. 2, pp. 29–39.

Nettle, D., 2009. A Sequence Stratigraphic, Geochronological and Chemostratigraphic Investigation of the Ediacaran Antaq Basin, Eastern Arabian Shield, Saudi Arabia, Geology and Geophysics. University of Adelaide, p. 83.

Neumayr, P., Mogessie, A., Hoinkes, G., Puhl, J., 1996a. Geological setting of the Meatiq metamorphic core complex in the Eastern Desert of Egypt based on amphibolite geochemistry. Journal of African Earth Sciences 23, 331–345.

Neumayr, P., Hoinkes, G., Puhl, J., Mogessie, A., 1996b. Polymetamorphism in the Meatiq basement complex (Eastern Desert, Egypt): P – T variations and implications for tectonic evolution. Geological Survey of Egypt, Centennial Symposium Abstracts, pp. 139–141.

Neumayr, P., Hoinkes, G., Puhl, J., Mogessie, A., Khudeir, A.A., 1998. The Meatiq Dome, (Eastern Desert, Egypt) a Precambrian metamorphic core complex: petrological and geological evidences. Journal of Metamorphic Geology 16, 259–279.

Nicholson, P.G., Janjou, D., Fanning, C.M., Heaman, L.M., Grotzinger, J.P., 2008. Deposition, age and Pan-African correlation of late Neoproterozoic outcrops in Saudi Arabia. In: Geo 2008: 8th Middle East Geoscience Conference and Exhibition, Manama, Bahrain, March 2–5, 2008.

Passchier, C., 2010. The Al Wajh shear zone system, NW Saudi Arabia. In: Pease, V., Kadi, K.A., Kozdroj, W. (Eds.), JEBEL Project October 2009 Field Excursion to the Midyan Terrane, Kingdom of Saudi Arabia with Reports on Research by Participants of the JEBEL Project. Saudi Geological Survey Technical Report SGS-TR-2010-2, pp. 76–77.

Pearce, J.A., 1996. Sources and settings of granitic rocks. Episodes 19, 120–125.

Pearce, J.A., Harris, N.B.W., Tindle, A.G., 1984. Trace element discrimination diagrams for the tectonic interpretation of granitic rocks. Journal of Petrology 25, 956–983.

Pellaton, C., 1985. Geologic Map of the Miskah Quadrangles, Sheet 24F, Kingdom of Saudi Arabia. Saudi Arabian Deputy Ministry for Mineral Resources Geoscience Map GM-99, Scale 1:250,000, 23 p.

Pisarevsky, S.A., Murphy, J.B., Cawood, P.A., Collins, A.S., 2008. Late Neoproterozoic and Early Cambrian palaeogeography: models and problems. In: Brito Neves, B.B., Trouw, R.A.J., de Wit, M.J., Pankhurst, R.J. (Eds.), Western Gondwana: Pre-Cenozoic Geology Bordering the S Atlantic. Geological Society, London, Special Publication, pp. 9–32.

Plimer, I.R., 1987. Fundamental parameters for the formation of granite-related tin deposits. Geologische Rundschau 76, 23–40.

Pouit, G., Elsass, P., Ferrand, A., Milesi, J.P., Sabir, H., 1984. Metallogenic Base Metal Studies: Review of Activity during 1980–1983 AD (1400–1403 A.H.). Saudi Arabian Deputy Ministry for Mineral Resources Open-File Report BRGM-OF-04-11, 74 p.

Raharimahefa, T., Kusky, T.M., 2006. Structural and remote sensing studies of the southern Betsisimarka suture, Madagascar. Gondwana Research 10, 186–197.

Raharimahefa, T., Kusky, T.M., 2010. Temporal evolution of the Angavo and related shear zones in Gondwana. Constraints from LAMC-ICP-MS-U–PB zircon ages of granitoids and gneiss from central Madagascar. Precambrian Research 182, 30–42. doi:10.1016/j.precamres.2010.06.013.

Ramsay, C.R., 1986. Specialized felsic plutonic rocks of the Arabian Shield and their precursors. Journal of African Earth Sciences 4, 153–168.

Ramsay, C.R., Stoeser, D.B., Drysdall, A.R., 1986. Guide lines to classification and nomenclature of Arabian felsic plutonic rocks. Journal of African Earth Sciences 4, 13–20.

Renne, P.R., Mundil, R., Balco, G., Min, K., Ludwig, K.R., 2010. Joint determination of ^{40}K decay constants and $^{40}Ar/^{40}K$ for the Fish canyon sanidine standard, and improved accuracy for $^{40}Ar/^{39}Ar$ geochronology. Geochimica et Cosmochimica Acta 74, 5349–5367.

Ressetar, R., Monrad, J.R., 1983. Chemical composition and tectonic setting of the Dokhan Volcanic formation, Eastern Desert, Egypt. Journal of African Earth Sciences 1, 103–112.

Reymer, A.P.S., Matthews, A., Navon, O., 1984. Pressure–temperature conditions in the Wadi Kid metamorphic complex: implications for the Pan-African event in SE Sinai. Contributions to Mineralogy and Petrology 85, 336–345.

Rice, A.H.N., Greiling, R.O., Dardir, A.A., Rashwan, A.A., Sadek, M.F., 1992. Pan-African extensional structures in the area S of the Hafafit Antiform, Eastern Desert of Egypt. Zentralblatt fur Geologie und Palaeontolgie Teil I 11, 2641–2651.

Ries, A.C., Shackleton, R.M., Graham, R.H., Fitches, W.R., 1983. Pan African structures, ophiolites and mélange in the Eastern Desert of Egypt. A traverse at 26°N. Journal of the Geological Society, London 140, 75–95.

Ries, A.C., Shackleton, R.M., Dawoud, A.S., 1985. Geochronology, geochemistry, and tectonics of the NE Bayuda Desert, N. Sudan–implications for the western margin of the late Proterozoic fold belt of NW Africa. Precambrian Research 30, 43–62.

Ring, U., Brandon, M.T., Willet, S.D., Lister, G.S., 1999. Exhumation processes. In: Ring, U., Grandon, M.T., Lister, G.S., Willet, S.D. (Eds.), Exhumation Processes. Normal Faulting, Ductile Flow and Erosion. Geological Society, London, Special Publication, 154, pp. 1–27.

Sadek, M.F., 1994. A structural synthesis of the Proterozoic Arabian-Shield in Egypt. Geologische Rundschau 83, 484–501.

Samuel, M.D., Moussa, H.E., Azer, M.K., 2007. A-type volcanics in central eastern Sinai, Egypt. Journal of African Earth Sciences 47, 203–226.

Sangster, D.F., Abdulhay, G.J.S., 2005, Base metal (Cu–Pb–Zn) mineralization in the Kingdom of Saudi Arabia: Saudi Geological Survey (Jeddah), 128 p.

Schandelmeier, H., Abdel Rahman, E.M., Wipfler, E., Küster, D., Utke, A., Matheis, G., 1994. Late Proterozoic magmatism in the Nakasib suture, Red Sea Hills, Sudan. Journal of the Geological Society, London 151, 485–497.

Schmidt, D.L., 1981. Geology of the Jabal Yafikh Quadrangle, Sheet 23/43B, Kingdom of Saudi Arabia. US Geological Survey Saudi Arabian Mission Miscellaneous Documents 39, Scale 1:100,000, 99 p.

Schmidt, D.L., Hadley, D.G., Stoeser, D.B., 1979. Late Proterozoic crustal history of the Arabian shield, southern Najd province, Kingdom of Saudi Arabia. King Abdulaziz University, Jiddah. Institute of Applied Geology Bulletin 3 (2), 41–58.

Sengör, A.M.C., Natalin, B.A., 1996. Paleotectonics of Asia: fragment of a synthesis. In: Yin, A., Harrison, T.M. (Eds.), The Tectonics of Asia. Cambridge University Press, New York, pp. 486–640.

Shackleton, R.M., 1994. Review of Late Proterozoic sutures, ophiolite melanges and tectonics of eastern Egypt and NE Sudan. Geologische Rundschau 83, 537–546.

Shalaby, A., 2010. The northern dome of Wadi Hafafit culmination, Eastern Desert, Egypt: structural setting in tectonic framework of a scissor-like wrench corridor. Journal of African Earth Sciences 57, 227–241.

Shalaby, A., Stüwe, K., Makroum, F., Frtiz, H., Kebede, T., Klötzli, U., 2005. The Wadi Mubarak belt, Eastern Desert of Egypt: a Neoproterozoic conjugate shear system in the Arabian–Nubian Shield. Precambrian Research 136, 27–50.

Shalaby, A., Stüwe, K., Fritz, H., Makroum, F., 2006. The El Mayah molasse basin in the Eastern Desert of Egypt. Journal of African Earth Sciences 45, 1–15.

Sharland, P.R., Archer, R., Casey, D.M., Davies, R.B., Hall, S.H., Heward, A.P., Horbury, A.D., Simmons, M.D., 2001. Arabian Plate Sequence Stratigraphy. GeoArabia Special Publication 2, 371 p.

Shimron, A.E., 1984. Evolution of the Kid Group, SE Sinai Peninsula: thrusts, mélange and implications for accretionary tectonics during Late Proterozoic of the Arabian–Nubian Shield. Geology 12, 242–247.

Shimron, A.E., 1987. Pan-African metamorphism and deformation in the Wadi Kid region, SE Sinai Peninsula: evidence from porphyroblasts in the Umm Zariq Formation. Israel Journal of Earth Sciences 36, 173–193.

Shimron, A.E., 1990. The Red Sea line – a late-Proterozoic transcurrent fault. Journal of African Earth Sciences 11, 95–112.

Sibson, R.H., 1987. Earthquake rupturing as a mineralizing agent in hydrothermal systems. Geology 15, 701–704.

Smith, A.G., 2009. Neoproterozoic timescales and stratigraphy. In: Craig, J., Thurow, J., Thusu, B., Whitham, A., Abutarrama, Y. (Eds.), Global Neoproterozoic Petroleum Systems: The Emerging Potential in N Africa. Geological Society, vol. 326, London, Special Publication, pp. 27–54. doi: 10.1144/SP326.2.

Smith, M., O'Conner, E., Nasr, B.B., 1998. Transpressional flower structures and escape tectonics: a new look at the Pan-African collision in the Eastern Desert, Egypt. In: Greiling, R.O. (Ed.), Workshop on the Pan-African of Northern Africa–Arabia, Geologisch-Palaeontologiches Institut, Ruprecht-Karls Universitaet, Heidelberg Germany, October 22–23.

Squire, R.J., Campbell, I.H., Allen, C.M., Wilson, C.J.L., 2006. Did the Transgondwanan Supermountain trigger the explosive radiation of animals on Earth? Earth and Planetary Science Letters 250, 116–133.

SRK Consulting, 2007. An independent Mineral Experts' Report on the Gold Mining and Exploration Assets of Saudi Arabian Mining Company (Ma'aden). SRK Consulting Engineers and Scientists, Cardiff, 315 p (available on Ma'aden website).

Stacey, J.S., Agar, R.A., 1985. U–Pb isotopic evidence for the accretion of a continental micro plate in the Zalm region of the Saudi Arabian Shield. Journal of the Geological Society, London 142, 1189–1203.

Stacey, J.S., Hedge, C.E., 1984. Geochronologic and isotopic evidence for early Proterozoic crust in the eastern Arabian Shield. Geology 12, 310–313.

Stacey, J.S., Stoeser, D.B., 1984. Distribution of oceanic and continental leads in the Arabian–Nubian Shield. Contributions to Mineralogy and Petrology 54, 91–105.

Stacey, J.S., Doe, B.R., Roberts, R.J., Delevaux, M.H., Gramlich, J.W., 1980. Lead isotope study of mineralization in the Saudi Arabian shield. Contributions to Mineralogy and Petrology 74, 175–188.

Stacey, J.S., Stoeser, D.B., Greenwood, W.R., Fischer, L.B., 1984. U–Pb zircon geochronology and geologic evolution of the Halaban–Al Amar region of the eastern Arabian Shield, Kingdom of Saudi Arabia. Journal of the Geological Society, London 141, 1043–1055.

Stern, R.J., 1979. Late Precambrian Ensimatic Volcanism in the Central Eastern Desert of Egypt. Ph.D. Thesis, University of California, San Diego, 210 p.

Stern, R.J., 1985. The Najd fault system, Saudi Arabia and Egypt: a late Precambrian rift-related transform system? Tectonics 4, 497–511.

Stern, R.J., 1994. Arc assembly and continental collision in the Neoproterozoic East African Orogen: implications for the consolidation of Gondwanaland. Annual Reviews of Earth and Planetary Sciences 22, 315–319.

Stern, R.J., 2002. Crustal evolution in the East African Orogen: a neodymium isotopic perspective. Journal of African Earth Sciences 34, 109–117.

Stern, R.J., Abdelsalam, M.G., 1998. Formation of juvenile continental crust in the Arabian–Nubian shield: evidence from granitic rocks of the Nakasib Suture, NE Sudan. Geologische Rundschau 87, 150–160.

Stern, R.J., Gottfried, D., 1986. Petrogenesis of a Late Precambrian (575–600 Ma) bimodal suite in the N Eastern Desert of Egypt. Contributions to Mineralogy and Petrology 92, 492–501.

Stern, R.J., Hedge, C.E., 1985. Geochronologic and isotopic constraints on late Precambrian crustal evolution in the Eastern Desert of Egypt. American Journal of Science 285, 97–172.

Stern, R.J., Johnson, P.R., 2010. Continental lithosphere of the Arabian Plate: a geologic, petrologic, and geophysical synthesis. Earth-Science Reviews 101, 29–67.

Stern, R.J., Manton, W.I., 1987. Age of Feiran basement rocks, Sinai – implications for late Precambrian crustal evolution in the northern Arabian–Nubian Shield. Journal of the Geological Society, London 144, 569–575.

Stern, R.J., Voegeli, D.A., 1987. Geochemistry, geochronology, and petrogenesis of a late Precambrian (590 Ma) composite dike from the N Eastern Desert of Egypt. Geologische Rundschau 76, 325–341.

Stern, R.J., Gottfried, D., Hedge, C.E., 1984. Late Precambrian rifting and crustal evolution in the northeastern Desert of Egypt. Geology 12, 168–172.

Stern, R.J., Kröner, A., Manton, W.I., Reischmann, T., Mansour, M., Hussein, I.M., 1989. Geochronology of the late Precambrian Hamisana shear zone, Red Sea

Hills, Sudan and Egypt. Journal of the Geological Society, London 146, 1017–1029.
Stern, R.J., Ali, K.A., Andresen, A., Wilde, S., Abu-El-Ene, M., Hassan, I., 2010a. Results of Geochronological Investigations in Sinai Undertaken as Part of the 2008 JEBEL Field Trip. Saudi Geological Survey Technical Report – SGS-TR-2010-2, pp. 46–51.
Stern, R.J., Ali, K.A., Liégeois, J.-P., Johnson, P., Wiescek, F., Kattan, F., 2010b. Distribution and significance of pre-Neoproterozoic zircons in juvenile Neoproterozoic igneous rocks of the Arabian–Nubian Shield. American Journal of Science 310, 791–811.
Stockli, D.F., 2005. Application of low-temperature thermochronometry to extensional tectonic settings. Review in Mineralogy and Geochemistry 58, 411–448.
Stoeser, D.B., 1986. Distribution and tectonic setting of plutonic rocks of the Arabian Shield. Journal of African Earth Sciences 4, 21–46.
Stoeser, D.B., Camp, E., 1985. Pan-African microplate accretion of the Arabian shield. Geological Society of America Bulletin 96, 817–826.
Stoeser, D.B., Frost, C.D., 2006. Nd, Pb, Sr, and O isotopic characteristics of Saudi Arabian shield terranes. Chemical Geology 226, 163–188.
Stoeser, D.B., Stacey, J.S., 1988. Evolution, U–Pb geochronology, and isotope geology of the Pan-African Nabitah orogenic belt of the Saudi Arabian Shield. In: El-Gaby, S., Greiling, R.O. (Eds.), The Pan-African belt of NE African and Adjacent Areas. Friedrich, Viewig and Sohn, Braunschweig/Wiesbaden, pp. 227–288.
Stoeser, D.B., Whitehouse, M.J., Stacey, J.S., 2001. The Khida terrane – geology of Paleoproterozoic rocks in the Muhayil area, eastern Arabian shield, Saudi Arabia. Gondwana Research 4, 192–194.
Streckeisen, A., 1976. To each plutonic rock its proper name. Earth Science Reviews 12, 1–33.
Sturchio, N.C., Sultan, M., Batiza, R., 1983a. Geology and origin of Meatiq Dome, Egypt: a Precambrian metamorphic core complex? Geology 11, 72–76.
Sturchio, N.C., Sultan, M., Sylvester, P., Batiza, R., Hedge, C., El Shazly, E.M., Abdel-Maguid, A., 1983b. Geology, age, and origin of the Meatiq Dome – implications for the Precambrian stratigraphy and tectonic evolution of the Eastern Desert of Egypt. King Abdulaziz University, Faculty of Earth Sciences Bulletin 6, 127–143.
Sultan, M., Arvidson, R.E., Duncan, I.J., Stern, R., El Kaliouby, B., 1988. Extension of the Najd Fault System from Saudi Arabia to the central Eastern Desert of Egypt based on integrated field and Landsat observations. Tectonics 7, 1291–1306.
Tadesse, T., 1996. Structure across a possible intra-oceanic suture zone in the low-grade Pan-African rocks of northern Ethiopia. Journal of African Earth Sciences 23, 375–381.
Tadesse, S., Milesi, J.-P., Deschamps, Y., 2003. Geology and mineral potential of Ethiopia: a note on geology and mineral map of Ethiopia. Journal of African Earth Sciences 36, 273–313.
Tapponnier, P., Molnar, P., 1976. Slip-line field theory and large-scale continental tectonics. Nature 264, 319–324.
Teklay, M., Kröner, A., Mezger, K., 2001. Geochemistry, geochronology, and isotope geology of Nakfa intrusive rocks, northern Eritrea: products of a tectonically thickened Neoproterozoic arc crust. Journal of African Earth Sciences 3 (33), 283–301.
Tenczer, V., Hauzenberger, C.A., Fritz, H., Whitehouse, M.J., Mogessie, A., Wallbrecher, E., Muhongo, S., Hoinkes, G., 2006. ANosites in the Eastern Granulites of Tanzania—new SIMS zircon U–Pb age data, petrography and geochemistry. Precambrian Research 148, 85–114.
Testard, J., 1983. Khnaiguiyah, a Synsedimentary Hydrothermal Deposit Comprising Cu–Zn–Fe Sulfides and Fe Oxides in an Ignimbritic Setting. Saudi Arabian Deputy Ministry for Mineral Resources Open-File Report BRGM-OF-03-9, 106 p.
Tsige, L., Abdelsalam, M.G., 2005. Neoproterozoic–Early Paleozoic gravitational tectonic collapse in the southern part of the Arabian–Nubian Shield. The Bulbul Belt of southern Ethiopia. Precambrian Research 138, 297–318.
Vickers-Rich, P., Kozdroj, W., Kattan, F.H., Leonov, M., Ivantsov, A., Johnson, P.R., et al., 2010. Reconnaissance for an Ediacaran Fauna, Kingdom of Saudi Arabia. Saudi Arabian Geological Survey Technical Report SGS-TR-2010-8, 42 p.
Volesky, J.C., Stern, R.J., Johnson, P.R., 2003. Geological control of massive sulfide mineralization in the Neoproterozoic Wadi Bidah shear zone, southwestern Saudi Arabia, inferences from orbital remote sensing and field studies. Precambrian Research 123, 235–247.
Walker, B.M., Lewis, R.S., Al Otaibi, R. Ben Talib, M. Christian, R., Gabriel, B.R., 1994. An Najadi Gold Prospect, Kingdom of Saudi Arabia; Geology and Gold-resource Assessment. Saudi Arabian Deputy Ministry for Mineral Resources Technical Report USGS-TR-94-5, 89 p.
Wallace, C.A., 1986. Lithofacies and Depositional Environment of the Maraghan Formation, and Speculation on the Origin of Gold in Ancient Mines, an Najadi area, Kingdom of Saudi Arabia. Saudi Arabian Deputy Ministry for Mineral Resources Open-File Report USGS-OF-06-6.19 p.
Whitehouse, M.J., Windley, B.F., Ba-Bttat, M.A.O., Fanning, C.M., Rex, D.C., 1998. Crustal evolution and terrane correlation in the eastern Arabian shield, Yemen: Geochronologic constraints. Journal of the Geological Society, London 155, 281–295.
Whitehouse, M.J., Stoeser, D.B., Stacey, J.S., 2001. The Khida Terrane–Geochronological and isotopic evidence for Paleoproterozoic and Archean crust in the eastern Arabian shield of Saudi Arabia. Gondwana Research 4, 200–202.
Wilde, S.A., Youssef, K., 2000. Significance of SHRIMP U–Pb dating of the imperial Porphyry and associated Dokhan Volcanics, Gebel Dokhan, N Eastern Desert, Egypt. Journal of African Earth Sciences 31, 410–413.
Wilde, S.A., Youssef, K., 2002. A re-evaluation of the origin and setting of the Late Precambrian Hammamat Group based on SHRIMP U-Pb dating of detrital zircons from Gebel Umm Tawat, North Eastern Desert, Egypt. Journal of the Geological Society, London 159, 595–604.
Williams, P.L., Vaslet, D., Johnson, P.R., Berthiaux, A., Le Strat, P., Fourniguet, J., 1986. Geologic Map of the Jabal Hibshi Quadrangle, Sheet 26F, Kingdom of Saudi Arabia. Saudi Arabian Deputy Ministry for Mineral Resources Geoscience Map GM-98, Scale 1:250,000, 52 p.
Willis, K.M., Stern, R.J., Clauer, N., 1988. Age and geochemistry of late Precambrian sediments of the Hammamat series from the northeastern desert of Egypt. Precambrian Research 42, 173–187.
Windley, B.F., Whitehouse, M.J., Ba-Bttat, M.A.O., 1996. Early Precambrian gneiss terranes and Pan-African island arcs in Yemen: crustal accretion of the eastern Arabian Shield. Geology 24, 131–134.
Worku, H., Schandelmeier, H., 1996. Tectonic evolution of the Neoproterozoic Adola Belt of southern Ethiopia: evidence for a Wilson cycle process and implications for oblique plate collision. Precambrian Research 77, 179–210.
Yibas, B., Reimold, W.U., Armstrong, R., Koeberl, C., Anhaeusser, C.R., Phillips, D., 2002. The tectonostratigraphy, granitoid geochronology and geological evolution of the Precambrian of southern Ethiopia. Journal of African Earth Sciences 34, 57–84.
Yihunie, T., Tesfaye, M., 2002. Structural evidence for the allochthonous nature of the Balbul terrane in southern Ethiopia: A west-verging thrust nappe. Journal of African Earth Sciences 34, 85–93.
Youssef, K.M., 2005. The Age and Petrogenesis of the Major Rock Units at Gabal Gattar and Gabal El Dokhan, Northeastern Desert, Egypt. Unpublished PhD Thesis, Curtin University of Technology, 298 p.
Zahran A.M., Stewart, I.C.F., Johnson, P.R., Basahel, M.H., 2003. Aeromagnetic-anomaly maps of central and western Saudi Arabia. Saudi Geological Survey Open-File Report SGS-OF-2002-8, scale 1:2,000,000.
Zoheir, B.A., Akawy, A., 2010. Genesis of the Abu Marawat gold deposit, central Eastern Desert of Egypt. Journal of African Earth Sciences 57, 306–320.